FINAL REPORT ON NASA GRANT

NAGW-69

by

William Bernstein

Department of Space Physics & Astronomy

Rice University

Houston, TX 77251, USA

February 11, 1986

Final Report NAGW-69

Section I. Introduction

NAGW-69 grant to Rice University, with W. Bernstein as Principal Investigator, were initiated in early 1980 and has continued at a relatively constant funding level until the present. Initially the program had two basic objectives.

1. The simulation of some aspects of the perplexing past and planned flight electron beam injection experiments under controlled laboratory conditions. Although it was recognized that significant differences existed between the space and laboratory environments, we believed that these were not differences in the basic physical processes. Rather they arose primarily from the gross differences in boundary conditions and reasonable corrections for these differences could be made. It should be noted here that support for this laboratory work and for an accompanying modest theoretical effort was also provided by NSF under grant #ATM-8022550.

2. The participation in the planning, execution, data analysis and interpretation of rocket borne beam injection experiments including the E·B (April 1978), Canadian NBBV-06 (Winter 1980), SCEX 1 (Winter 1982) flights. Also studies of the acceleration of ion conics observed at low altitudes (>400 - 1000 km) during several rocket flights were continued in collaboration with B. A. Whalen.

Initially the laboratory research effort was planned to be carried out in the very large chamber at Johnson Space Center and several experimental series were possible prior to the shut down of the chamber in early 1981. Because of the long beam pathlength, the large chamber allowed operation at neutral gas densities, plasma densities, beam densities and magnetic field strengths

reasonably similar to those encountered in the ionosphere. It should be noted that this earlier laboratory work provided the framework for the TEBPP investigation proposed for future Spacelab flights. A committee effort, chaired by W. Bernstein and R. J. Jost, to develop support for restoration of the large chamber operation was not successful. However sufficient data had been obtained in the earlier large chamber experiments, which together with the data from the very extensive existing theoretical and experimental studies of beam-plasma interactions, indicated that scaling of the large experiment into a much smaller facility was possible without modifications of the basic physics.

Consequently, in collaboration with A Konradi, a 2-1/2 m long, 1 m diameter system was constructed at JSC. Although we employed the same electron gun as previously, the increased magnetic field strength, higher plasma density, and increased beam density required the construction of new diagnostic equipment including RF probes, Langmuir probes, energy analyzers, and scanning photometers. Essentially because of the dimensional scaling, the large instruments and their coarse positioning, which were adequate in the large chamber, had to be replaced with miniaturized instruments, operable in a 40G magnetic field, and a precision positioning system. Similarly, the scaling modified the wave frequencies from $<$ 30 MHz in the large chamber to $>$ 1 GHz in the small chamber.

In general, the objectives of the laboratory program have been successfully accomplished and include

a) The characteristics of the steady state beam-plasma interactions including both the beam plasma discharge, BPD, (avalanche ionization present) and the beam-plasma interaction, BPI, (ionization absent) have been catalogued and compared with theoretical predictions and other experimental studies. It

should be noted that the BPI state could not be produced with the existing laboratory parameters and the strong interaction always produced the BPD state. Our understanding of the BPI state has been derived primarily from the experimental work of Seidl et al. [1976] who used an externally produced ambient plasma rather than the beam produced plasma used in the present experiments.

b) The experiment parameters required for BPD ignition have been determined. Theory predicts that the thresholds for BPD ignition and BPI onset will occur when the conditions for strong wave growth are satisfied. If it were possible to contrive a state where the ambient plasma was still created by primary beam ionization alone, but ionization by suprathermal or heated electrons was suppressed, the BPD and BPI thresholds would be identical.

c) Theoretical models for BPD ignition when an electron beam traverses an initially neutral gas at low magnetic field strengths ($w_p > w_c$) in a finite length system were developed semi-independently by Papadopoulos [1985, 86] and by Llobet [1984]. Not only is there good functional agreement between the experiments and predictions, the agreement extends to the absolute magnitudes of the particular threshold parameter under study. The theoretical model allows extension of our understanding to experimental configurations not possible in the present experiment series.

The rocket flight experiments had two general objectives and significant results were obtained in both areas.

a) The study of the beam-plasma interaction physics was carried out through measurements of plasma waves, return energetic particle fluxes, vehicle potential, etc. Techniques were developed for the deployment of isolated subpayloads (TADS) for study of the perturbed local environment

without the complexities imposed by vehicle charging during beam emission.

b) One possible magnetospheric application for injected electron beams might be for the identification and characterization of the postulated electric fields, parallel to the geomagnetic field, associated with auroral arcs. Because of the desire to test this concept, all the flights were carried out in the presence of reasonably intense arcs. Rather surprisingly, because of a particularly favorable alignment of the injection-detection payloads in the SCEX 1 flight, hundreds of both prompt and delayed "echoes" were detected. During the first successful E∥B flight, only one such event was detected.

It was possible to interpret these injection-echo patterns in terms of reflection by a field aligned potential drop located at ~ 1 Re. An alternate explanation suggested that the delayed return flux is a consequence of the continuous instability of the propagating beam and that the echo pattern results from the passage of the detection payload through the return flux region.

Whatever the model (reflection or continuous backscatter) the experimental results are consistent with the imposition of severe energy and pitch angle diffusion on the incident beam. The prompt echoes, characteristic of all 3 flights, imply that these modifications are imposed near the injection point.

c) Although many of the secondary features of the BPD were observed on all these flights, the most striking characteristic of the BPD, the large local change in light emission (N_2, N_2^+) and the accompanying increase in plasma density were not observed even at lower altitudes on the downleg where the neutral density should have been sufficient for avalanche ionization. On the other hand, the light intensity for constant beam current decreased much

more slowly with altitude than the estimated N_2 abundance perhaps indicative of BPI rather than BPD. This discrepancy and others derived from other flights are discussed in detail in Section II. It seems clear now that the consistency between flight and laboratory results and between them both and theory is still rather poor. Section III is a portion of the final report for NSF grant ATM-8022550 and provides a brief description of the laboratory research program. Finally Section IV contains a) reprints of all papers published in referred journals, b) a tabulation of papers published in non-referred books and proceedings and c) Abstracts of the Ph.D. and M.S. thesis produced during this program.

It should be emphasized that both the large chamber and flight programs represented large scale group efforts. Among the various collaborators were A. Konradi, H. R. Anderson, P. J. Kellogg, K. Wilhelm, F. H. Linbach, T. J. Hallinan, E. P. Szuszczewicz, K. Papadopoulos, L. Linson, B. A. Whalen, H. Cohen, D. S. Evans, H. Koons, R. Holzworth, R. J. Jost, and S. Cuperman. All collaborators provided their own funding. With the closing of the large chamber only collaboration with A. Konradi continued in the small chamber research.

A Comparison of Laboratory Experiment and Flight Observations of Beam-Plasma Interactions

Both laboratory and flight experimental studies of non-relativistic but energetic electron beam-plasma interactions are by now mature fields. The laboratory work dates back to Langmuir, with temporary peaks in the 50's centered on " wave devices and in the 60's centered on the possible application to fusion. The final theoretical understanding including finite size effects, absolute versus convective instability, the role of nonlinear effects (soliton-caviton structures), the oscillating two stream instability, etc., appeared during the 1970's).

Flight experiments to study the injection of such beams into the ionospheric plasma began with the experiments of Hess et al. [1971] and was rapidly followed by the ECHO program of J. R. Winckler's group, the Franco-Soviet Zarnitza-ARAKS program, the NASA-Canadian E∥B flight series and a variety of other Soviet, Norwegian, and US flights. At the present time, similar experiments have been implemented on the Spacelab I and II flights and are planned for future shuttle and rocket flights.

In general, these flight experiments have had two primary objectives: (1) the use of such beams as probes for the overall electric and magnetic field configuration of the distant magnetosphere and (2) the simulation of natural beam phenomena (aurora, Type III radio bursts, etc.) under controlled conditions. Secondary objectives have included 3) the study of beam-plasma interactions for beams of finite radius immersed in an infinite, homogenuous plasma, 4) controlled stimulation of light emission, etc. In particular several pairs of extreme conditions are possible:

A) System Length

1) The axial length of the beam-plasma system is infinite so that finite length effects are unimportant.

2) The axial length of the beam plasma system can be very short as considered by Maltsev (1983); the length is determined by the effective pulse duration rather than by finite boundaries, as in the laboratory experiment, because of the vehicle motion transverse to B.

B) Ambient Plasma Density

1) The ambient plasma may be predominantly generated by a non-beam related source such as the ionosphere.

2) Collisional beam produced ionization represents the primary source of ambient plasma.

C) Avalanche Ionization by Energized Electrons

1) The time, t_i, required for ionization by either collisionlessly accelerated (superthermal) or collisional heated (thermal) electrons is < than their lifetime, τ_s, in the system ($t_i < \tau_s$). This is the condition for avalanche ionization characteristic of the BPD and exists for altitudes < ~ 200 km. The transition between the collisional & collisionless BPD occur at ~ 140 km. Lastly, at altitudes < ~ 90 km, the collision frequency > instability growth rate so that the interactions do not occur.

2) The neutral density is so small that $t_i > \tau_s$; i.e., the suprathermal electrons escape without producing new ionization. This is simply known as the Beam-Plasma Interaction (BPI state) and typically should occur at altitudes > 200 kms.

These different configurations are somewhat coupled as followed:

1) Flight vehicles may represent local sources of neutral gas because of outgassing, off gassing, and leakage processes. Sometimes large releases of

neutral gas are deliberately imposed. Clearly these releases can modify both the local gas density and composition particularly at altitudes > 200 km where the natural density is small.

2) Gradients in neutral density (which must arise when the vehicle is the neutral gas source) will result in gradients in ambient plasma density if collisional ionization represents the primary ambient plasma production method. Such gradients will convert an infinite length system into one of finite length and possibly inhibit growth of the interaction to large amplitudes.

3) For neutral densities where beam ionization would produce $t_i > \tau_s$, but with an ambient plasma density comparable to ionospheric densities (10^5 cm^{-3}), the criterion for BPD may also be satisfied. Thus it seems unlikely that the BPI can be produced in flight or in the laboratory if beam produced ionization is the only source of ambient plasma.

The flight experiments have yielded a variety of confusing results which could not be interpreted within the bounds of the existing laboratory experiments or theory. However, because of the gross differences in system length, radial boundaries, ambient plasma and neutral densities, magnetic field strength, etc. between the laboratory and flight experiments, signficant questions were raised about the applicability of the results from one configuration carried to the other. New laboratory experiments were therefore initiated, particulary those within the very large NASA environmental test chambers at the Johnson Space Center and Plum Brook; because of their large pathlength (> 20 m) and radius (> 10m), experiments could be performed at plasma and neutral densities + low magnetic field strength much closer to the absolute values of these parameters found in the ionosphere. In parallel with this experimental program, a new theoretical effort was initiated with the

objective of a general understanding of beam plasma interactions over very wide parameter ranges.

The peculiar inconsistencies between laboratory and flight experiments have continued to be apparent despite the broadened parameter range of the new laboratory experiments. In fact, the most striking consequence of the laboratory beam plasma interactions, the beam-plasma discharge, has been unambiguously observed in flights in only a few cases [Sasaki et al. 1985, Managadze et al., 1983, Kawashima 1982] whereas the most striking flight result, the anomalous backscatter flux returning from higher altitude, has not been observed in the laboratory at all [Wilhelm et al. 1985, Winckler et al. 1975, Llobet et al. 1985]. Similar inconsistencies exist for a large range of other diagnostics. It should be noted, however, that except for a few special cases, the new theoretical treatment provides a consistent description of laboratory results for one particular set of initial conditions - the interaction of the beam with an initially neutral gas. The purpose of this report is to summarize the apparent discrepancies between laboratory and flight experiments and between laboratory experiment and theory and to provide possible explanations of these differences where feasible.

II. Discrepancies Between Laboratory and Flight Experiments

a. The Beam Plasma Discharge

In all the recent laboratory experiments where the beam is injected into neutral gas alone (no ambient plasma present) the final steady-state beam-plasma configuration (in general) is either the BPD or a marginally stable configuration in which only minor modifications to the beam velocity distribution occur (single particle behavior) and little energy is transferred from the beam to the plasma other than by collisions. At very low neutral densi-

ties, an intermediate unstable but less dynamic state exists with specific wave and optical characteristics [Bernstein et al. 1979]. In particular, sharp thresholds for BPD ignition are observed in each of the experiment parameters (I_b, E_b, N_o, B, L) as shown in Figure 1. The BPD can be thought of as analogous to an RF discharge except that the RF waves are generated internally by the beam-plasma interaction rather than by an external oscillator. It is a true discharge in the sense that ignition is characterized by an avalanche increase in the ionization rate and therefore in the intensity of the optical emissions.

Typical experimental signatures for both the BPD and BPI interactions and possible measurement methods include

1) modifications of the beam velocitity distribution so that features charcteristic of stable (single particle) behavior such as the refocus modes or helical trajectory disappear. Either TV observations of the trajectory or direct measurements of the velocity distribution are possible techniques.

2) acceleration of ambient electrons to produce suprathermal tails or heating of the ambient electrons

3) intense waves at the local f_p or f_{UH} ($f_p \approx f_{UHF}$ when $f_p >> f_c$), in the Whistler region, $f < f_c$, and in the VLF region, $f < f_{LHF}$. Some conversion (10^{-4}) of the HF electrostatic wave power to EM waves will occur so that remote measurements are possible. The HF ES waves will be restricted to the beam region.

4) ion effects are unclear

5) sharp thresholds in the onset parameters for these interactions.

In addition, because of enhanced ionizstion associated with the BPD, it is additionally characterized by

1) the increased ionization rate is associated with a large increase in

the emission light intensity.

2) the increased ionization rate results in a locally increased plasma density as measured with probes or in an increased frequency of the f_p or f_{UHF} emissions.

3) the increased plasma density may even perturb telemetry transmissions etc.

The BPD has only been observed (unambiguously) during a few rocket flights. For example, it was apparently only produced during the entire ECHO series of flights in association with a large release of neutral gas [Winckler 1982]; without the gas release, the dependence of the λ 391.4 nm optical emission intensity on altitude tracked the N_2 abundance at constant beam current. Although this dependence broke down at the highest altitude where vehicle outgassing may have produced a modification of the small natural N_2 abundance; the BPD characteristic increase/decrease in light intensity at a critical altitude was not observed. Similarly, at constant altitude, the light intensity was proportional to the beam current and a non linear increase in light intensity with I_b was not observed. Because of the high beam energy used in the ECHO program, the gun perveance (perveance = $I_b V^{-3/2}$) did not exceed 1×10^{-7} amp volt$^{-3/2}$. Those flights, during which at least some specific BPD signatures (light + density) have been observed, used gun perveances in the range $1 \times 10^{-7} - 2 \times 10^{-6}$ amp volt$^{-3/2}$.

The joint US-Canadian EⅡB program has provided definitive evidence for BPD ignition by the flight beams in laboratory tests but not in flight based on optical measurements. During the laboratory test of the NBBV-06 payload at JSC, optical evidence (increase in light intensity and dissappearance of single particle features) for the BPD using 10 ma, 2KV and 100 ma 2+4KV beams was clearly observed in TV and photometric data [Bernstein et al. 1980]. This

optical evidence for ignition was not apparent in the subsequent flight of this payload [F. Harris private comm.]; i.e., no abrupt change in the N_2^+ or N_2 light intensity was observed with variation of either altitude or I_b. The light data from the earlier 27.010 AE flight [Bernstein et al. 1982] showed some features perhaps consistent with BPD ignition in the sense that the light emission region is best described as a field aligned cylinder extending both below and above the payload; the payload is located near or at the radial boundary of the emission region. However, as with NBBV-06, no abrupt change in light intensity with altitude or current was apparent. The SCEX I flight did not produce much useful optical data.

The Norwegian flight [Grandal et al. 1982] carried out extensive optical measurements as shown in Figure 2. These results showed an exponentially decreasing N_2^+ intensity with increasing altitude up to 140 kms; above this altitude the light intensity remained relatively constant despite the decreasing N_2 abundance. Thus at high altitudes, the measured λ391.4 nm intensity was much higher than predicted from the beam current and $+N_2$ abundance derived from the model atmospheres. Thus, either additional ionization sources or local N_2 densities must have been present; the latter was believed to be unlikely because of the mother-daughter payload configuration. These results were interpreted to be consistent with strong interaction phenomena because the decreasing frequency of electron-neutral collisions with increasing altitude could allow the more efficient production of suprathermal electrons and hence a relatively constant ionization rate. Similarly direct measurements, see Figure 3, of the suprathermal electron flux by Arnoldy et al. [1985] clearly show that this flux increases with increasing altitude in the range 150-240 km. However, below 140 km the absolute intensity of the N_2^+ light and its altitude dependence appear to be consistent with collisional

effects and the atmospheric N_2 abundance alone, with no evidence for unknown ionization sources in this altitude range. Yet, this is within the altitude range for BPD occurrence [Mishin and Ruzhin 1980, Kofsky et al. 1984, Managadze et al. 1983]. Like the E∥B results, there is no evidence for an altitude (neutral density) dependent threshold in this data set but rather just a slow transition from beam collisions alone to major light production by super thermal electrons.

Although Bernstein et al. [1983] report similar dependences of the N_2^+ and N_2 light intensities with decreasing neutral density in their laboratory experiment as reported by Grandal et al. [1981] in their flight experiment, all the laboratory measurements were made under known BPD conditions. The flight density and wave measurements seem more consistent with a BPI configuration because of the absence of any obvious density increase.

Lastly, Kofsky et al. [1984] have interpreted the EXCEDE data in terms of a collision dominated, rather than collisionless BPD because of the low altitude. Because of the limited altitude and current range of the experiment, no indications of gross non linearlities in the parameter dependences could be observed.

The only clear cut optical observations of the BPD are (1) the large increase in light produced when the ECHO beam was injected into the dense gas release [Winckler 1982] (2) the detection of a large increase in light when the high altitude SPURT rocket reached an altitude of approximate 160 km on the down leg [Managadze et al. 1983] and (3) the rocket measurements described by Kawashima [1982] and further by Sasaki et al. [1985a] when high current (80 ma) beams were emitted. Sasaki et al. (1985b) also report TV evidence for BPD ignition during the Spacelab 1 flight, but in the presence of a neutral gas release.

Other data provides far more impressive evidence for BPD ignition by the injected beam. The most important of these was the ground based detection of 75 and 50 MHz EM waves in association with beam injection during the ARAKS flights. If these frequencies corresponded to local plasma frequencies, plasma densities of 7×10^7 and 3×10^7 cm^{-3} were present; this represents an almost 200 fold increase in the nighttime F region density. This large density increase would have been indicative of BPD ignition. Waves of approximately this frequency were also observed with a vehicle borne receiver during the SPURT flight during periods for which the optical observations indicated the BPD [Managadze 1983]. Distortions of the telemetry patterns, particularly those observed during the Zarnitza flight, could be interpreted in terms of spatially localized high plasma density regions generated by the beam. On the other hand, the ground received signals observed by Monson and Kellogg [1978] have failed to identify similar super high frequency [$2f_c$ seems to be the highest frequency] waves during beam emission for both the ECHO and E$\parallel$B flight experiment series. In fact, with the exception of the results from the Soviet programs [Zarnitza, ARAKS, SPURT], none of the wave measurements both near and remote from the injection point have provided any evidence for the density increases characteristic of BPD; in fact, various probe measurements may indicate density decreases in the active regions as expected from plasma heating effects [Duprat et al. 1983]. Both Boswell and Kellogg (1984) and Llobet et al. (1985) suggest that these apparently very high frequency waves may be an artifact produced by large amplitude lower frequency waves and their harmonics and not be indicative of a greatly increased density.

The fundamental question to be answered is "Why is the BPD so difficult to identify in flight experiments even at altitudes where the natural neutral

gas densities should be sufficient for the collisional BPD whereas it is always easily observed in the laboratory simulation experiments?

b. Instability thresholds in the laboratory and flight

The BPD ignition - BPI threshold for each of the experimental variables in the laboratory experiments is sharp. Because the distinction between BPD [avalanche ionization ($t_i < \tau_s$)] and BPI [no ionization ($t_i > \tau_s$)] configurations lies simply in the probability of ionization of the ambient neutrals by the electrons heated in the wave-particle interactions and not in the interactions themselves, we believe, but have not demonstrated, that similar thresholds appear for both cases, i.e., we have assumed that the BPD or BPI threshold occurs when conditions for large wave growth are satisfied. In flight experiments (if the behavior were similar to that in the laboratory), typical threshold single parameter dependences which might be encountered include (1) altitude (N_o); (2) beam current; and (3) beam energy.

Basically, for the laboratory experiments, Seidl et al. (1976) and later Papadopoulos [1984, 1986] and Llobet [1984] have shown that in such finite length systems, the beam-plasma interaction which produces the required large wave growth, must almost always be an absolute instability. The convective growth usually possible in such short systems is much less than required for significant energy transfer from non-linear effects. The critical length (the length of the experimental system must exceed this length for occurrence of the absolute mode) is given by the simple requirement

$$L^2 \equiv \frac{|v_{g1} v_{g2}|}{\gamma^2} \qquad (1)$$

where v_{g1} and v_{g2} are the group velocities of the forward and backward (fast and slow) waves and γ is the instability growth rate. Because both v_{g1} and

v_{g2} are forward waves for $\omega_p < \omega_c$, only the convective instability occurs for this particular condition but if L is sufficiently large, wave growth to large amplitude can also occur.

Basically eqn. (1) can be rewritten as

$$L = \frac{2\sqrt{2}}{(n_b n_a)^{1/2}} \Omega_e v_b \quad \frac{\sin\theta}{R^{1/2}}$$

R ranges from 1 - 0.1 (see later discussion), or L $[(n_b n_a)^{1/2} > C_{crit}$ after appropriate substitutions for v_{g1}, v_{g2} and γ. Substitution of the experiment parameter dependences for n_a and n_b gives the various threshold ignition scaling laws [Bernstein 1979]. Obviously specification of L and n_a prescribes a critical value of n_b (I_b) for ignition. Similarly presciption of L and n_b (I_b) determines the critical value of n_a for ignition; for a selfmade plasma this condition in turn specifies N_o and I_b.

The effectively infinite pathlength available in the space experiments coupled with the presence of the uniform ionospheric plasma should greatly modify these parameter interdependences. As long as collisional effects remain unimportant ($\gamma >> (\nu_{(en)b}, \nu_{(en)a}$ the infinite available pathlength should eliminate all the described parameter threshold criteria because the condition $L(n_a n_b)^{1/2} >$ crit can always be satisfied. Threshold effects may still result from other criteria, such as the condition for nonlinear effects [the ratio of wave energy density to thermal energy density, $E^2/nkt \approx 1$], but these have not been theoretically or experimentally identified in these experiments to date. Yet, Ingsoy et al. [1985] have shown that a beam current threshold exists for the strong BPI interaction (identified by the presence of low energy suprathermal electrons but without an increase in ambient density) and that the I_b threshold scales about linearly with decreasing neutral

density (increasing altitude) precisely as observed in the finite length laboratory experiments [Bernstein et al. 1979] as shown in Figure 4. Furthermore, Ingsoy et al. [1985] specifically show that the plasma density collisionally produced by the beam remains small compared to the local ionospheric density which was measured to be in the range 1-2 x 10^5 cm^{-3} in the altitude range of the measurements 160-180 km. Therefore collisional ionization could not play a key role in setting the altitude dependence of the I_b threshold similar to the N_o threshold in the laboratory.

Similar results have been reported by Managadze et al. [1983] from the very high altitude SPURT rocket flight. The BPD interaction was observed for altitudes < 600 km on the upleg and < 160 km on the downleg. The difference was attributed to enhancement of the local neutral gas density on the upleg because of outgassing of the payload. Figure 5 shows that not only did the beam current threshold increase with increasing altitude, but a hysteresis effect similar to that observed in the laboratory experiments is also evident. By hysteresis, we mean that the interaction once initiated ceases at a value of beam current < than the threshold value. The hysteresis effect can also be explained by the threshold dependences on n_b, n_a and L and the differences in the ionization and loss rates for BPD and beam alone condition [Llobet 1984]. As with the Norwegian Flight [Ingsoy et al. 1985], the measured ambient ionospheric density was in the range 1-3 x 10^5 cm^{-3} over the altitude range 200-600 km. Unless the neutral density in the rocket environment was very high, any collisional beam produced ionization would also be small compared to the ionospheric density. Thus it is difficult to understand not only the observed threshold altitude-I_b scaling in the two experiments, but the specific hysteresis effect in the SPURT experiments. Kawashima et al. [1982] also report an abrupt onset of the BPD when the beam current exceeds a

critical value between 40-80 ma at 1KV in the altitude range 170 km. Kellogg and Monson [1983] concluded that the strong interaction was produced by 10 ma and 100 ma beams during the NBBV-06 flight but not by 1 ma beams. Although the plasma wave spectrum extended to frequencies much higher than the ionospheric plasma and cyclotron frequencies they do not suggest the presence of an increased plasma density but rather the presence of the BPD 2 state.

Two basic questions must be answered here.

(1) Why should abrupt thresholds appear for specific values of the experiment parameters when the ambient plasma is homogeneous of and effectively infinite length with its density >> than the density possibly accumulated by collisions alone? Why should the absolute values of these thresholds be similar to those measured in the laboratory?

(2) Why should the parameter scaling relationships closely approximate those determined in the laboratory when the collisional production and loss processes of the ambient plasma should be unimportant in flight but critically important in the laboratory.

c. Return (Backscatter) Fluxes

From their family of phase space maps of returning energetic particles, Winckler et al. [1975] recognized as early as 1975 that the configuration of beam injection up the field line ($\alpha > 90°$) and detection of particles moving down the field line ($\theta < 90°$) usually indicated much larger detected fluxes than could be explained by collisional backscatter in the dilute neutral atmosphere above the injection point. The alternative configuration of injection down the field line ($\alpha < 90°$) and detection of upward ($\theta > 90°$) moving particles gave the expected large intensities because of atmospheric backscattering and/or mirroring effects at lower altitudes. Typically however, the detected ECHO fluxes were factors of ~ 100 times less than predicted by

Monte Carlo calculations of atmospheric backscattering, but surprisingly, as described by Winckler [1982], and as shown in Figure 6, this particle loss appears to be limited to the first backscattering. For the multiple echoes (bounces) the attenuation in each later echo was consistent with the collisional predictions. Winckler et al. [1975] also speculated that the high altitude backscatter might be the result of a strong instability but did not present further information. Both the atmospheric and high altitude backscatter processes are, in general, associated with severe energy diffusion of the initially monoenergetic beam toward lower energies. In fact, because the ECHO detection systems were not energy selective, the true particle energy must be assumed in their interpretation of the ECHO patterns. Usually, a severe energy degradation to $\sim E_{inj}/2$ gives the best fit between the derived magnetic field configurations and theoretical field models. Typically the ECHO group assumes that the degradation was imposed by collisional atmospheric back-scatter but it might also have been caused by plasma instabilities.

The most detailed studies of the flight backscattered return beams have been reported by Wilhelm et al. [1980, 1985]. In these experiments, the fluxes returning to the injection altitude were measured with detectors located on both the injection payload and several isolated subsidiary vehicles. Clearly the flux and energy spectrum of the electrons returning to the injection payload would be influenced by vehicle charging during emission whereas the return fluxes to a subsidiary payload (located outside the "charging" sheath) would be modified only to the extent the injected energy was decreased by the charging. However, no evidence for charging > + 200V was apparent in these experiments [Duprat et al., 1983]. It should be stressed here that the only inflight attempt to measure the characteristics of the propagating beam after traversal of a relatively large distance (400 m) from

the gun was made on the recent Spacelab II flight with, as yet, unreported results. Another attempt will be made on the forthcoming SCEX II flight in 1987 [Whalen, private communication].

Wilhelm et al. [1980, 1985] attempted to identify and characterize the high altitude E∥B configurations, believed to produce auroral arcs, from observations of beams injected up the field line and reflected at the potential drop. Further information could be obtained from the different time delays between injection and detection of the reflected beam for different injection energies. In general, they separated the echo patterns into (1) those with delays < 50 msec (prompt echoes), corresponding to total travel distances of several hundred kilometers and 2) echoes with delay times > 50 ms (delayed echoes. Because the prompt echoes must have originated close to the injection point, they almost surely could not have been E∥B reflections while the delayed echoes could have been produced by such reflection. The delay time for reflection at the conjugate point would have been very much larger. Wilhelm et al. [1985] were well aware that complete adiabatic behavior of the injected beam would render the experiment impossible with only a limited number of detection systems. They suggested that some deviation from adiabaticity could be tolerated so that a non idealized experiment might prove feasible and yield the desired measurements of E∥B. Although only 2 delayed echoes were observed in the first E∥B flight, more than 200 delayed echoes were observed during the second (SCEX I) flight because of a particularly fortuitous alignment of the trajectories of the injection-detection payloads. Prompt echoes were detected for all 10ma and 100ma pulses with the detectors on the injection vehicle and for about 15 sec after the release of the favorably aligned subsidiary payload.

Wilhelm et al. [1985] suggested that although one could account for the

delayed echoes as arising from reflection by an E∥B configuration, an alternative explanation was also consistent with some aspects of the data. The delayed echoes might simply have represented the continuation of the prompt echo process for longer times. The authors proposed that features of the echo pattern could be explained by the assumption that the injected beam was continuously unstable in its transit to high altitudes and generated the backward directed particle flux through, as yet unknown, wave-particle interactions. This return flux was then detected at the time the detection payload traversed the backscatter footprint in the ionosphere.

Wilhelm et al. [1985] and in an earlier flight, Duprat et al. [1982] were able to measure the characteristics of the prompt backscatter flux at several fixed energies for injected beams of 2, 4 and 8 keV. Typically 8 keV injected beams produced prompt echoes at 2, 4, and 8 keV but delayed echoes at only 2 and 4 keV; 4 keV beams produced prompt and delayed echoes at 2 and 4 keV; 2 keV beams produced prompt and delayed echoes only at 2 keV. Thus like Winckler [1975] they observed severe energy diffusion to lower energies; very intense fluxes extending up to a few hundred eV range were observed by Duprat et al., (1983) + Winckler (1980) for all prompt echoes.

Wilhelm et al. [1985] and Wilhelm [private communication] have proposed that the prompt echo energy spectrum and pitch angle distribution are in fact, characteristic of the propagating beam. During the SCEX I flight, the two distinct groups of delayed echoes shown in Figure 7 were observed to have apparently identical characteristics including scaled delay time, 2π isotropy, and absolute flux magnitude. Note that for each echo group the measured delay time shows an approximate linear extropolation to the release time of the detection pay load. The different slopes could simply have been the result of a changed E∥B drift velocity. More importantly, for one group, injection was

down ($\alpha_E < 90°$) the field line, almost surely within the loss cone, whereas for the second group, injection was up ($\alpha_E > 90°$) the field line. It seems reasonable to anticipate that a significant difference would be observed between the two echo groups where, in one case, atmospheric backscatter would be the source of the upward propagating flux. In the second case, the upward directed primary beam was directly injected from the accelerator without important collisional effects. The absence of any significant difference between the two echo patterns implies that a backward flux, comparable to the forward propagating flux, must be associated with the injection process itself. Thus atmospheric backscatter only represents a secondary process. The nominal injection of the beam in one direction results in a nearly identical (flux, energy spectrum, pitch angle distribution) electron injection in both directions. This hypothesis is confirmed by measurements of the prompt echoes by detectors on the injection payload shown in Figure 8. Data is shown for 2 and 8KV, 100ma injected beams for two configurations: 1) injection upward ($\alpha_E > 90^0$) and detection downard ($\alpha_D < 90^0$) and 2) injection downard ($\alpha_E < 90^0$) and detection upward ($\alpha_E > 90^0$). Note that the energetic particle characteristics are about identical. Almost surely, the measured upward directed flux for downward injections represents the particle source for the delayed echoes associated with downward injection shown in Figure 8.

The significant questions to be answered include 1) Does the energetic return flux represent newly accelerated electrons or degraded primaries?, 2) Is the propagating beam continuously unstable? and 3) Why are the characteristics of the return fluxes independent of the direction of beam injection?

Soliton-caviton structures accelerate electrons parallel and antiparallel

to the B field in a transit time like acceleration process. In general, such particles constitute a non-Maxwellian tail distribution (suprathermal electrons) with maximum energy gains to ~50-100 T_e or perhaps as high as 100-200 eV for $E_b \approx 2$, 4, and 8 kV. It seems doubtful whether energies as high as 0.25 E_b could be generated by this process. The observed energy diffusion to lower energies (> 200 eV) seems to arise from the degradation of beam electrons rather than the acceleration of ambient electrons. On the other hand, Llobet et al. [1985b] suggest that these electrons may, in fact, be newly accelerated electrons because the flux at lower energies varies inversely with energy as expected in a tail distribution.

Lastly, Wilhelm et al. [1984a] have reported detection of electrons with $E >> E_b$ during the SCEX I flight; similar observations were made during the Spacelab I flight [Wilhelm et al 1984b]. No super accelerated electrons have been observed in any of the ECHO series (Arnoldy et al. 1985).

"Super" accelerated electrons have been characteristic of high power BPD experiments carried out in mirror configurations with mirror ratios > 3 [Smullin and Getty 1966]. They have not been observed in short-length solenoidal geometry experiments such as the large and small chamber experiments in this program where only the modest (20-30%) acceleration associated with particle trapping is reported. It has been generally accepted that these features of the 'super' accelerated electrons imply that 1) the acceleration must be $\perp B$ and 2) it is a generally stochastic (very short correlation times) rather than resonant process. In these laboratory experiments, the BPD provided a useful method for the generation of high β plasmas for study of the confinement properties of various open magnetic field configurations. More recently Katz et al. [1985] and Maltsev [1983] have respectively suggested that vehicle charging and beam non-neutrality could each lead to the appear-

ance of super accelerated (2 E_b) electrons in flight experiments. In general, this acceleration would be parallel (or antiparallel to B) for injection $\parallel B$ rather than at large pitch angle. The very limited flight observations of these superaccelerated electrons have not provided sufficient data to identify the acceleration mechanism, let alone the reality of the process.

Large instability backscatter fluxes have not been observed in any of our laboratory simulation experiments. The backscattered flux from the axial termination of the beam has been detected only in the large chamber experiments but not in the small chamber. The only effort to minimize this termination flux has been the use of low z targets (Al, C); more complex beam catchers have not been employed.

III. Possible Inconsistencies Between Laboratory Experiments and the Absolute Instability Theory

(a) The Relationship Between Pulsed and Steady State Injection for a Self Generated Plasma.

An important verification of the absolute instability theory for BPD ignition has been the comparison of pulsed and steady state ignition characteristics. For the specific case of beam injection into an initially neutral gas ($n_a = 0$) the evolution of n_a is time dependent, determined by the production rate (collisional ionization by the beam) and various loss processes (axial and radial diffusion and recombination), until steady state conditons are achieved. Szuszczewicz et al. [1982] have shown that the behavior of n_a (neglecting recombination because of the small plasma density) can be written as

$$dn_a/dt = P - \frac{n_a}{\tau}$$

P is rate of ionization cm^{-3} given by $\frac{I_b}{A_b e} N_o \sigma$ (A_b is the beam area, N_o is the neutral density and σ is the ionization cross section at E_b) and τ is the plasma lifetime with the axial loss determined by ambipolar processes and the radial loss by Bohm diffusion. This equation can be integrated to give the temporal dependence of n_a as

$$n_a = P\tau \left[1 - e^{-t/\tau}\right);$$

for $t \ll \tau$, $n_a \approx Pt$ cm^{-3} and for $t \gg \tau$, n_a reaches the limiting value $P\tau$ cm^{-3}. From Equation 2, the pulsed and steady state current thresholds should occur when the quantities $L^2(I_b P)_1 t = L^2(I_b P)_2 \tau$. Szuszczewicz et al. [1982],

in general, experimentally verified this equivalence for the specific case where the ambient plasma, n_a, was collisionally produced by the beam itself and the plasma lifetime in the large chamber was taken to be 4 msec as shown in Figure 9.

Obviously, the motion of the injection vehicle across the geomagnetic field transforms a steady state injection into a pulsed injection. A typical pulse duration (t) would be given by the time required for an orbiting vehicle to transit the beam, $t = d/N_I \approx \frac{1m}{10^4 \text{ m sec}^{-1}} = 1 \times 10^{-4}$ sec. Because of their much lower transverse velocity, this reduction is far less severe for rocket beam experiments. Here we have assumed 5 kV beam energy, ± 5° gun divergene angle and parallel injection. Obviously an increase in beam width appears for larger injection pitch angles. If beam produced ionization was the only source of ambient plasma, then the requirement that the quantity ($L^2 I_b Pt$) exceed the critical value for ignition, either I_b or N_o or both would be required to be much larger than for steady state conditions. Studies of this plasma build up time in the large chamber experiments are described by Szuszczewicz et al. [1982].

(b) Behavior where generation of ambient plasma by an alternative method and the neutral density is small.

The theory predicts that the presence of an ambient plama produced by auxilliary or alternative means, would modify the threshold dependences on I_b and N_o. Typically, the strong interaction would then occur when the quantity (L^2 I_b n_a) > critical value (collisional ionization is neglected because of the assumed very low neutral density); only the BPI state would result. Although this latter assumption was never satisfied, some experiments were performed in the large chamber with an ambient plasma of $\sim 10^6$ cm^{-3} produced by a large ion thruster mounted at the side wall. The addition of the thruster

plasma to the ambient neutral gas produced no observable change in the beam current required for BPD ignition in steady state, [inconsistent with prediction] but reduced t (the formative delay observed in pulsed operation) to less than measurable with the existing diagnostics [consistent with prediction]. Fig. 10 taken from the paper by Kellogg et al. [1982] shows the large differences in the beam-ambient plasma spatial distribution in the absence and presence of the thruster plasma. The full width of the ambient plasma produced by collisions alone is ~2-4 m whereas the thruster plasma density is almost uniform across the chamber diameter ~14 m. Thus the ratio of beam diameter to ambient plasma diameter (b/a) is significantly changed by thruster operation. This parameter enters in an important way into the calculation of R, the geometric reduction factor (see Equation 2). The reduction in the instability growth rate, γ, because of the different radial extent of the beam and ambient plasma has been estimated by Manickam [1973]. $R \approx 1$ for a beam-plasma filled wave guide and decreases to a lower limit of 0.1 for a finite beam in a plasma of infinite radial extent. For the collisionally produced ambient plasma in the large chamber, R is probably > 0.1; for simplicity, Papadopoulos [1984, 1986] assumed R = 0.1 in his estimates of the absolute magnitudes of the critical currents predicted the large chamber experiments.

In addition, Seidl et al. [1976] have shown that the absolute instability occurs only when the axial ambient plasma density distribution is uniform within a few percent; the convective mode still occurs in the presence of much larger density gradients. At the present time we have no measurements of the axial uniformity of the thruster plasma. Because the plasma was produced as a divergent beam by the thruster mounted at the wall, axial density gradients > a few % appear likely. The effective result of such gradients is a reduction

in L; this has a similar effect as the decrease in R discussed earlier, i.e., an increase in beam current required for ignition.

The experiments described in this section have confirmed one important feature of the absolute instability model for BPD ignition, but have raised doubts about another key feature as follows:

1) For the specific case where the ambient plasma is produced by collisional ionization alone, the ignition conditions observed for steady state ($t > \tau$) and pulsed ($t < \tau$) operation appear to be internally consistent.

2) For the cases where the ambient plasma is produced both by beam collisions and by alternative means, the ignition conditions only appear to be consistent with theory when specific assumptions about the beam-plasma geometric configuration are made.

Arnoldy, R. L., C. Pollock and J. R. Winckler, "The energization of electrons and ions by electron beams injected into the ionosphere," J. Geophys. Res., 90, 5197, 1985.

Bernstein, W., H. Leinbach, P. J. Kellogg, S. J. Monson and T. Hallinan, "Further laboratory measurements of the beam plasma discharge," J. Geophys. Res., 84, 7271, 1979.

Bernstein, W., J. O. McGarity and A. Konradi, "Electron beam injection experiments: replication of flight observations in a laboratory beam plasma discharge," Geophys. res. Lett., 10, 1124, 1983.

Boswell, R. W. and P. J. Kellogg, "Characteristics of two types of beam plasma discharge in a laboratory experiment," Geophys. Res. Lett., 10, 565, 1983.

Duprat, G. R. J., B. A. Whalen, A. G. McNamara and W. Bernstein, "Measurements of the stability of energetic electron beams in the ionosphere," J. Geophys. Res., 88, 3095, 1983.

Grandal, B., E. V. Thrane, and J. Troim, "Measurements of the 391.4 nm light produced by an artificial electron beam in the upper atmosphere," Planet. Space Sci., 28, 291, 1980.

Hess, W. N., M. G. Trichel, T. N. Davis, W. C. Beggs, G. E. Kraft, E. Stassinopoulos and E. J. R. Maier, "Artificial aurora experiment: experiment and principal results," J. Geophys. Res., 76, 6067, 1971.

Ingsoy, P., M. Majewski, and J. Troim, "Plasma disturbance induced by a rocket borne electron accelerator," Norwegian Defense Research Establishment FFI/Rapport-84/7035, Kjeller, Norway, 1984.

Katz, I., G. A. Jongeward, D. E. Parks, D. L. Reasoner, and C. K. Purvis, "Energy broadening due to space-charge oscillations in high current electron beams," presented at "Charge Neutralizaton Systems Workshop" Southwest Research Institute, San Antonio, TX 14-16 Aug. 1985.

Kawashima, N., "Experimental studies of the neutralization of a charged vehicle," in Artificial Particle Beams in Space Plasma Studies, B. Grandal, editor, Plenum Press, New York, 1982.

Kellogg, P. J., H. R. Anderson, W. Bernstein, T. J. Hallinan, R. H. Holzworth, R. J. Jost, H. Leinbach, and E. P. Suszczewicz, "Laboratory simulation of injected particle beams in the ionospehre," in Artificial Particle Beam in Space Plasma Studies, B. Grandal, editor, p. 289, Plenum Press, New York, 1982

Kellogg, P. J. and S. J. Monson, "A second kind of BPD-rocket and laboratory results," in Active Experiments in Space, W. R. Burke, editor, Paris, 1983.

Kofsky, I. L., "Measurement and Theory of the spatial distribution of excitation by high current electron beams injected into the ionosphere," Geophys. Res. Lett., 10, 1011, 1984.

Llobet, X., "A model of th beam-plama discharge, Ph.D. Thesis, Rice Univ., Houston, TX, 1984.

Llobet, X., W. Bernstein, and A. Konradi, "The spatial evolution of energetic electrons and plasma waves during the steady state beam plasma discharge, J. Geophs. Res., 90, 5187, 1985.

Maltsev, Yu P., "Adiabatic motion of an electron bunch in the magnetosphere," Planetary and Space Sci., 31, 659, 1983.

Managadze, G. G., W. Riedler, B. M. Balebanov, M. Friedrich, T. I. Gagua, Z. Klos, N. A. Laliashvili, N. A. Leonov, S. B. Lyakhov, A. A. Martinson, and A. D. Mayorov, "Plasma processes in the region of electron beam injection from a high altitude payload," in Active Experiments in Space, W. R. Burke, editor, European Space Agency, Paris, 1983.

Manickam, J., W. Carr, B. Rosen and M. Seidl, "Convective and absolute instabilities in beam-plasma systems," Phys. Fluids, 18, 369, 1975.

Mishin, E. V. and Yu Ya Ruzhin, "The model of beam plasma discharge in the rocket environmental during an electron beam injection in the ionosphere," Ann. Geophys., 36, 423, 1980.

Monson, S. J., P. J. Kellogg, "Ground observations of waves at 2.96 MH_2 generated by an 8 to 40 KeV beam in the ionosphere," J. Geophys. Res., 83, 121, 1978.

Papadopoulos, K., "On the plasma physics of the beam plasma discharge," Comments on Plasma Physics and Controlled Fusion IX, 11, 1984.

Papadopoulos, K., "Scaling of the beam-plasma discharge for low magnetic fields," J. Geophys. Res., in press, 1986.

Sasaki, S., N. Kawashima, M. Yanagisawa, T. Okayoshi, W. T. Roberts, D. L. Reasoner, W. W. L. Taylor, P. R. Williamson, P. M Banks, and J. L. Burch, "Ignition of the beam plasma discharge in the electron beam experiment in space," Geophys. Res. Lett., 12, 647, 1985a.

Sasaki, S., K. I. Oyama, N. Kawashima, K. Hirao, A. K. Akai, T. Yokata, Y. Watanabe, S. Tei, F. Okayashi, W. J. Raitt, P. R. Williamson, W. F. Sharp, A. B. White and P. M. Banks, "Results from the series of tethered rocket experiments," submitted to AIAA Journal of Spacecraft and Rockets, 1985b.

Seidl, M., W. Carr, D. Boyd and R. Jones, "Non-linear development of absolute and convective instabilities," Phys. Fluids, 19, 75, 1976.

Smullin, L. D. and W. D. Getty, "Characteristics of the beam plasma discharge," in Proc. International Conf. Plasma Physics and Controlled Nuclear Fussion, 2 815, 1966.

Szuszczewicz, E. P., K. Papadopoulos, W. Bernstein, C. S. Lin and D. N. Walker, "Threshold criterion for a space simulatin beam-plasma discharge, J. Geophys. Res., 87, 1565, 1982.

Wilhelm, K., W. Bernstein and B. A. Whalen, "Study of electric fields parallel to the magnetic lines of fore using artificialy injected energetic electrons, Geophys. Res. Lett, 7, 117, 1980.

Wilhelm, K., W. Bernstein, P. J. Kellogg, B. A. Whalen, "Acceleration of electrons in strong beam-plasma interactions," Geophys. Res. Lett., 11, 1176, 1984a.

Wilhelm, K., W. Studeman and W. Riedler, "Electron flux intensity distributions observed in response to particle beam emissions from Spacelab 1, Science, 225, 186, 1984b.

Wilhelm, K., W. Bernstein, P. J. Kellogg and B. A. Whalen, "Fast magnetospheric echoes of energetic particle beams," J. Geophys. Res., 90, 491, 1985.

Winckler, J. R., R. L. Arnoldy and R. A. Hendrickson, "ECHO II: a study of electron beams injected into the high latitude ionosphere from a large sounding rocket," J. Geophys. Res., 80, 2316, 1975.

Winckler, J. R., "The use of artificial electron beams as probes of the distant magnetosphere," in Artificial Particle Beams in Space Plasma Studies, B. Grandal, editor, Plenum Press, New York, 1982.

Winckler, J. R., "The application of artificial electron beams to magnetospheric research," Rev. Geophys. Space Phys., 18, 659, 1980.

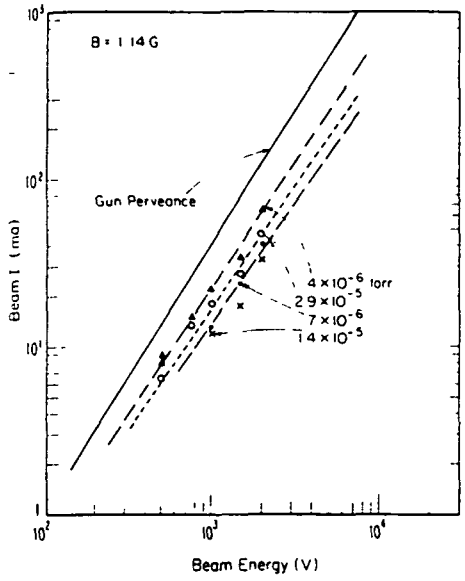

Dependence of the threshold current on beam energy for several neutral gas pressures The magnetic field strength is 1 14 G, beam injection is parallel to B, and interaction length is 20 m BPD operation could not be produced at $P < 2 \times 10^{-6}$ torr for $B = 1$ 14 G

$I_b - E_b$

P, B, L Constant

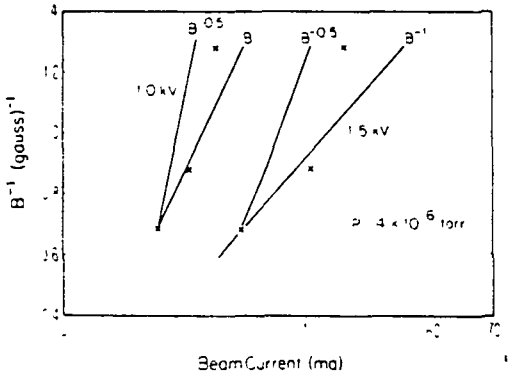

Dependence of the threshold current on magnetic field strength for 1 0- and 1 5-kV beams The pressure is 4×10^{-6} torr, injection is parallel to B and interaction length is 20 m Also shown are curves for $B^{-0.5}$ and B^{-1} dependences normalized at the experimental point at $B^{-1} = 0\ 68\ G^{-1}$ (1 48 G)

$I_b - B$

E_b, P, L, constant

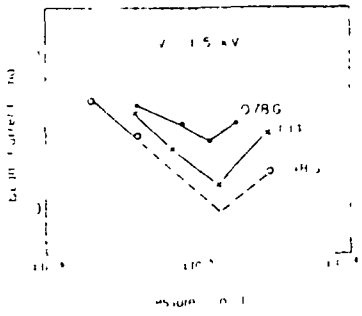

Dependence of the threshold current on neutral gas pressure for several magnetic field strengths The beam energy is 1 5 kV injection is parallel to B and interaction length is 20 m

$I_b - P$

E_b, B, L, constant

Figure 1

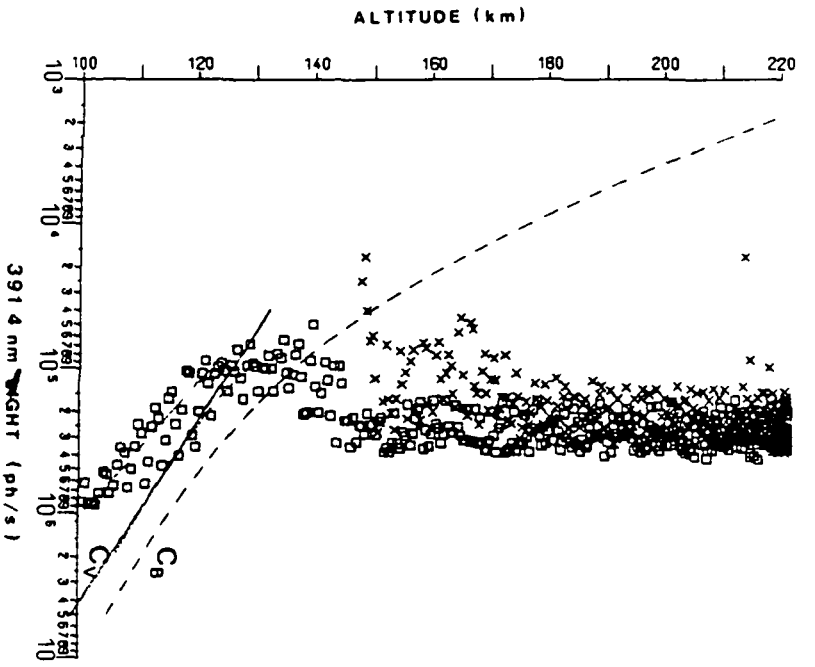

Observed beam induced luminescence as a function of altitude

Figure 2

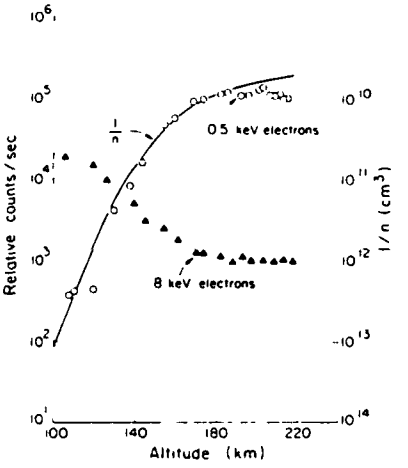

The altitude dependence of Echo 5 0.5-keV and 8-keV electrons measured during beam injection The curve $1/m$ is the inverse of the neutral density

Figure 3

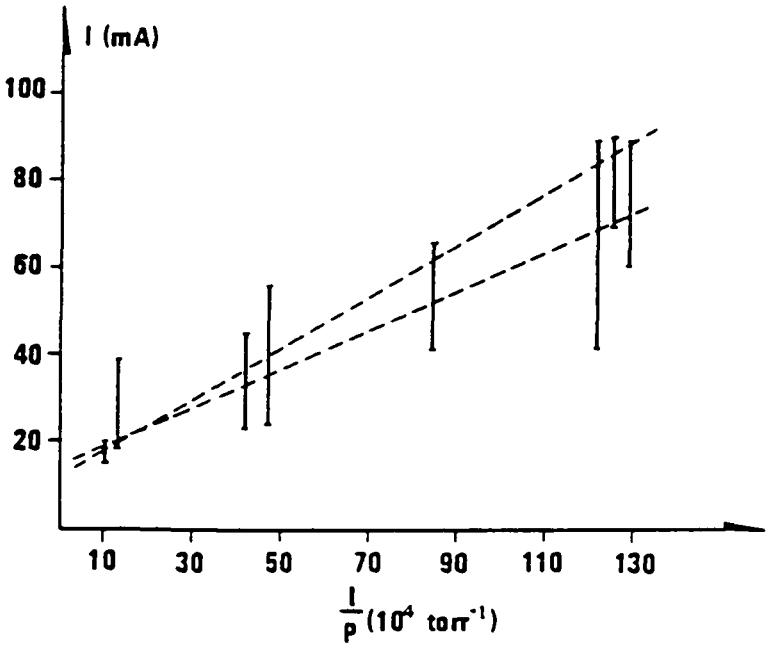

Estimates of the threshold current, I_c, plottes against the inverse neutral pressure. Each of the current intervals shown includes the threshold current.

Figure 4

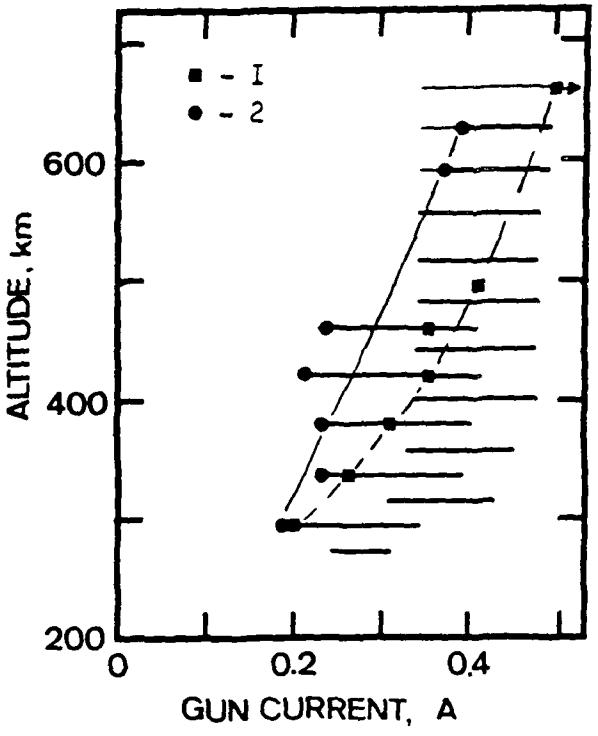

Record of HF-emissions in the frequency range 20 to 320 MHz of the receiver in the integral channel for successive injection pulses in the upleg. The injection current ranges where radiation is observed and the current where radiation begins (1) or stops (2) is indicated

Figure 5

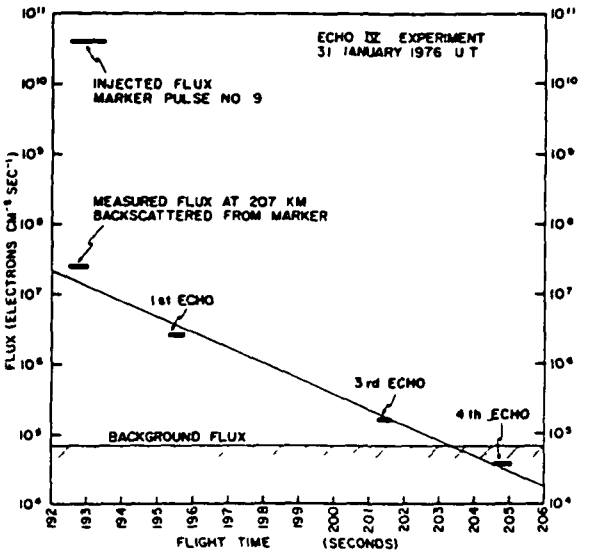

Time-Intensity history of the multiple-bounce event echoes a

Figure 6

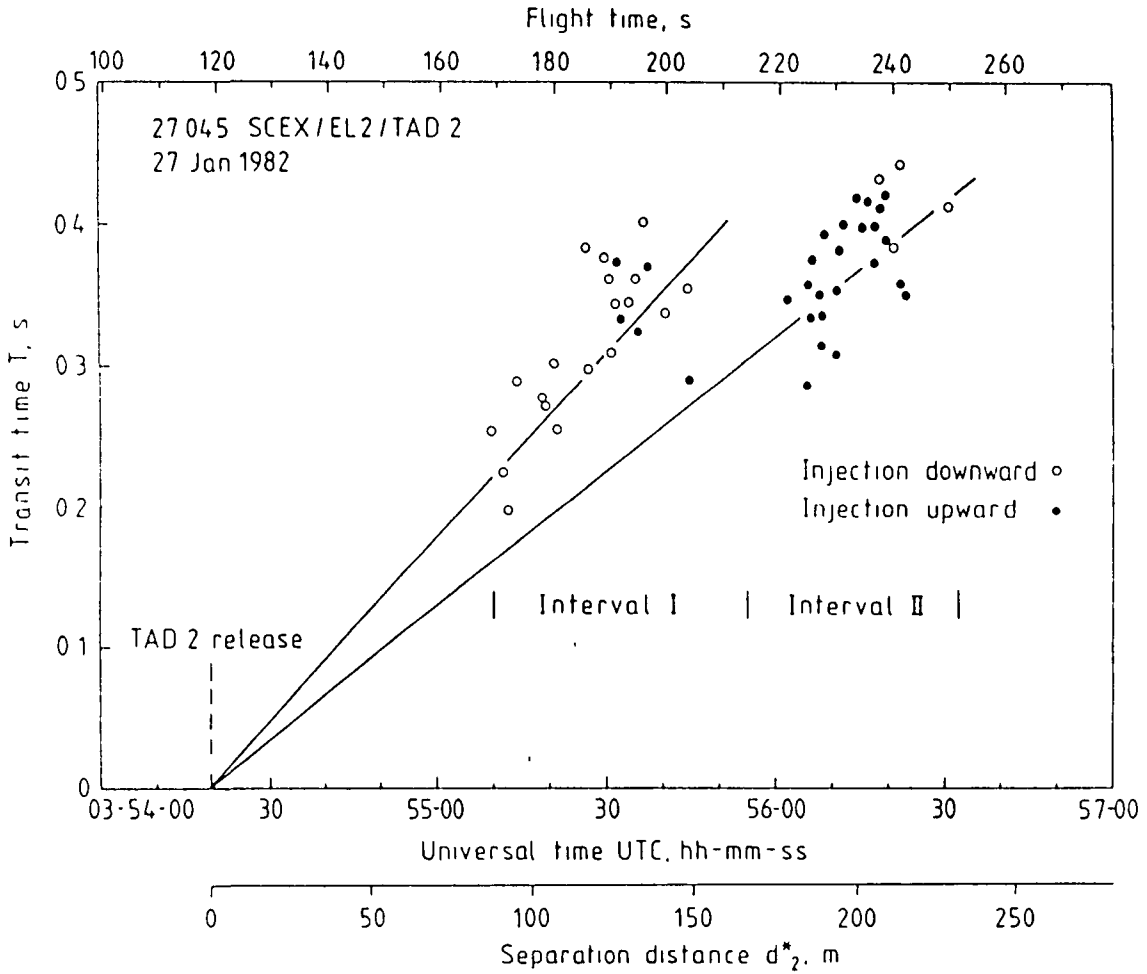

Figure 7. Transit times of 2 and 4 keV delayed echoes originating from 100-ma accelerator operations over flight time. Regression lines for each of the echo groups intercept the time of the detection payload release. Upward and downward injection directions are indicated.

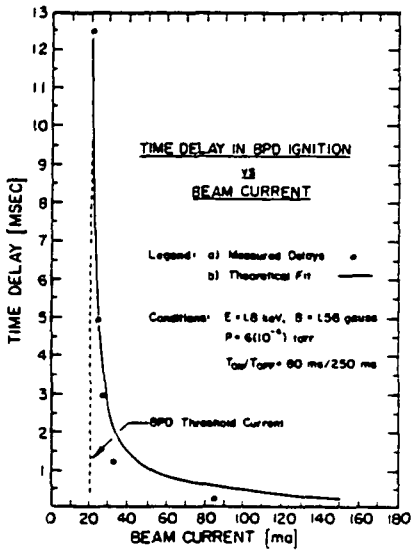

Time delay in the ignition of the beam-plasma discharge with threshold current at 20 ma. Electron gun operation was in the pulsed mode with T_{on}/T_{off} = 80 ms/250 ms

Figure 9

PRECEDING PAGE BLANK NOT FILMED

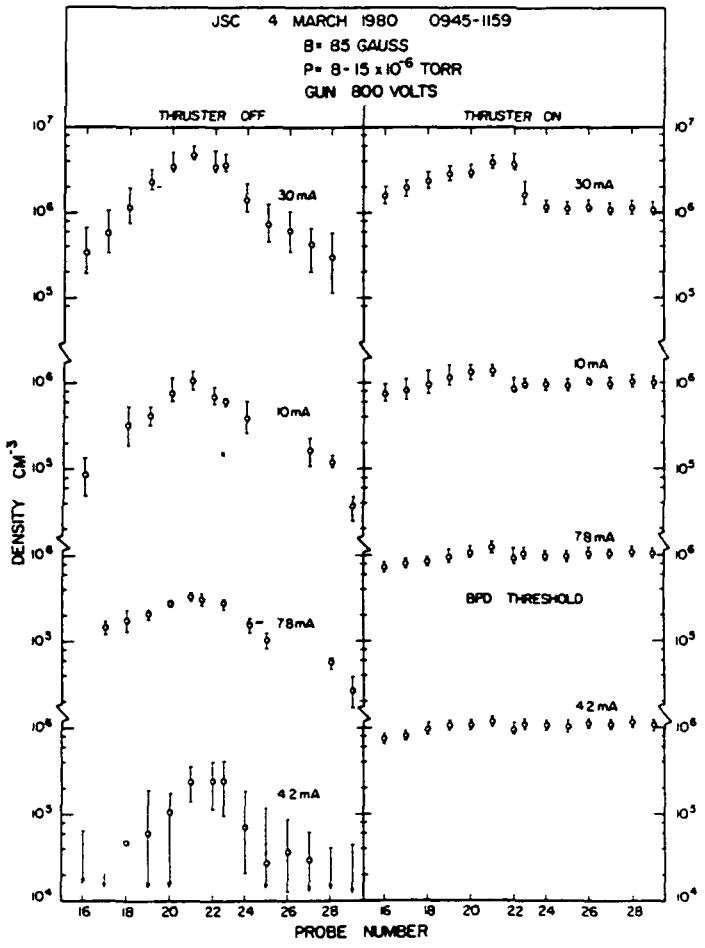

Plasma densities generated by the electron beam together with and without a background plasma generated by a Kaufman engine.

Figure 10

Final Report NSF Grant ATM 80-22550

I. Introduction

This material represents the final report for NSF grant ATM 80-22550. As will be apparent, many of the proposed objectives of this research program will have been accomplished including

(a) The observed characteristics of the steady state beam-plasma interactions including both the beam plasma discharge, (avalanche ionization present and the beam plasma interaction (BPI) (ionization absent) have been catalogued and compared with theoretical predictions and other experimental studies.

(b) The experiment conditions required for the initiation of the strong interaction (BPI or BPD) have been determined. In parallel a theoretical derivation of the ignition process was developed which allows extension of our understanding to experimental configurations not accessible in the present laboratory experiments.

(c) The important stages in the temporal evolution of the beam plasma system to the steady state (pulsed operation) have been measured and explained.

(d) In a parallel NASA supported program, considerable effort was devoted to the identification of both similarities and differences between the laboratory results and those from a variety of flight experiments.

(e) One Ph.D. and 3 M.S. theses were generated during the course of the program.

This report will be divided into several separate sections as follows:

Section II presents a general overview of the laboratory experiments and parallel theoretical research specifically supported by NSF grant ATM 80-22550

for the past 4 years. This text provides the basis for a review paper entitled "Beam Plasma Interactions - Laboratory Experiments and Theory" to be given at the URSI Meeting in Vancouver, Canada, June 17-21, 1985.

Section III contains reprints of the papers which primarily describe results of the laboratory experiment and theoretical research studies and which specifically appeared in referred journals. For continuity, the reprints are arranged in chronological order and begin with the initiation of NSF support.

Section IV contains reprints of papers which describe aspects of flight experiments which have appeared in refereed journals.

Section V contains a tabulation of non-refereed publications and presentations.

Section VI contains a tabulation of M.S. and Ph.D. thesis in this research area and abstracts of the theses.

Section II

BEAM-PLASMA INTERACTIONS - LABORATORY EXPERIMENTS AND THEORY

by

William Bernstein
Department of Space Physics and Astronomy
Rice University
Houston, TX 77251 USA

and

A. Konradi
Solar System Exploration Division
NASA/Johnson Space Center
Houston, TX 77058 USA

Talk presented by A. Konradi at the 1985 North American Radio Science Meeting, Vancouver CANADA, June 17-21, 1985

I wish to summarize the important results from an extensive theoretical and laboratory experiment program designed to study electron beam-plasma-neutral gas interactions under environmental conditions likely to be encountered in the E and F regions of the ionosphere. We believed such studies would provide a useful framework for the design of future flight experiments and the interpretation of existing flight data. In particular, although we were very much aware of important differences between the finite laboratory and infinite flight geometries, we expected that the development of a good theoretical understanding of the laboratory experiments would be applicable to the flight experiments and perhaps even to some "beam associated" natural processes. Although this ground based program has been included in the reviews given by E. P. Szuszczewicz at recent URSI and AIAA meetings, we hope you will find the present talk contains new data and new physical insights. Most of the work to be discussed represents the combined efforts of the TEBPP* group; we also draw heavily on the experimental and theoretical work of M. Seidl's group at the Stevens Institute of Technology.

We have employed two experimental configurations. In the initial work, the experiments were conducted in the very large vacuum chamber at Johnson Space Center [Bernstein et al., 1979]; the arrangement is shown schematically in Fig. 1. Following its deactivation in 1982, a smaller scaled configuration, shown schematically in Fig. 2, was constructed [Konradi et al., 1983]. A major improvement in the small facility was the addition of a precision diagnostic positioning system which covered the distance 26-52 cm from the gun. Table 1 gives the pertinent experimental parameters for the two configurations and also those employed by Seidl et al. [1976]. The most

* The TEBPP group includes H. R. Anderson, W. Bernstein, T. J. Hallinan, R. J. Jost, P. J. Kellogg, L. Linson, K. Papadopoulos, and E. P. Szuszczewicz.

important difference was that the ambient plasma (with which the beam interacts) was produced by an auxilliary discharge in the Seidl et al. experiments whereas it was collisionally produced by the beam itself in the JSC experiments.

Evidence for a strong collective interaction is readily apparent in the following beam photographs from the large chamber experiments. Fig. 3 shows the trajectory of a stable beam injected parallel to B; Fig. 4 shows a stable beam injected at a large pitch angle. The periodic refocussing of the beam in both cases together with the helical trajectory in Fig. 4 provide good evidence for the monoenergetic beam distribution. Fig. 5 shows the beam configuration when the beam current is increased above a critical level; similar thresholds are observed when P, B, L, E_b are individually varied for a constant I_b. The large increase in light (e.g. λ391.4 nm) indicates a greatly increased total ionization rate (as much as a factor of 30 above that produced by the primary beam alone); the disappearance of the refocus nodes and helical configuration implies a gross modification of the beam energy distribution. This particular configuration has been named the beam plasma discharge (BPD); in our experiment N_2 is the usual ambient gas although He, A, and Ne have been used. For the more general condition encountered in flight experiments, where the ambient plasma density is sufficient for the interaction, but the neutral gas density is very low, the enhanced ionization does not occur and this state is simply identified as the beam plasma interaction (BPI) state.

Our primary objectives in this program have been to determine

(1) the characteristics of the steady state strong beam plasma interaction (both BPD and BPI).

(2) the conditions required for the transition from stable to collective behavior.

(3) the time dependent evolution to the steady state system during pulsed injection.

I. Steady State Characteristics, $I_b > I_c$ (BPD)

In general for configurations where the ambient plasma is self (beam) produced, the condition $I_b > I_c$ always leads to BPD ignition. The BPI state has been studied in the configurations where the ambient plasma is produced by external or auxilliary means. During BPD, the important experiment parameters, n_b, n_a and N_o are coupled as shown in Fig. 6 and therefore these parameter dependences cannot be studied separately.

A. Optical Observations

(1) Configuration of the light emitting region [Hallinan et al., 1984; Bernstein et al., 1983]

As can be seen from Fig. 5, the optical emission intensity during BPD appears to be reasonably uniform axially; intensity gradients do exist at both axial terminations, but localized hot spots are not apparent, Fig. 7 shows radial profiles of the λ391.4 nm intensity for beams injected ∥B and at a large pitch angle measured about 10 m from the gun (midway) in the large chamber experiments. For parallel injection, the dependence of the FWHM of the emitting region on beam velocity and on magnetic field strength are shown in Fig. 8a and b. For the conditions of the measurement, the measured FWHM is approximately twice the estimated width at the antinode for a stable beam. The FWHM extrapolates to a finite intercept at 0 velocity but extrapolates to 0 width at large magnetic field strength. When injection is at large pitch angle, the double peaked intensity profile suggests that the emission region can be described as a hollow cylinder with its major radius given by the

cyclotron radius of the stable injected helix and its minor radius approximately twice that of the injected beam itself. Typically, both the first refocus node or a large portion of the first turn of the stable helix can be observed above the general BPD intensity suggesting that the significant modification of the beam electrons occurred at "some" axial distance from the gun. On the other hand the very limited changes in radial width imply that strong pitch angle and/or radial diffusion of the beam electrons does not occur within the pathlength. A reasonable model is that the beam electrons are modified primarily in the velocity $\parallel B$, and are immersed within a broader region of lower energy electrons (suprathermals) which produce the intense BPD light.

Neutral density also influences both the geometric configuration of the active region and the total λ391.4 nm light intensity as shown in Fig. 9. For neutral densities $> 3 \times 10^{12}$ cm^{-3} ($P \approx 1 \times 10^{-4}$ torr) the total intensity increases with increasing density while the FWHM of the emitting region remains constant. For densities $< 3 \times 10^{12}$ cm^{-3}, both the total light intensity and FWHM increase with decreasing density. Also, the Whistler mode wave amplitude remains small for $N_o > 3 \times 10^{12}$ cm^{-3}. These data imply that a significant change occurs in the coupling of energy from the beam to the plasma at $N_o \approx 3 \times 10^{12}$ cm^{-3}. Again, this transition neutral density is experiment dependent; qualitative data from the large chamber implies that $N_o \approx 3 \times 10^{11}$ cm^{-3} compared with 3×10^{12} in the small chamber but recall that ω_p has also been comparably increased.

(2) Beam Energy Dissipation [Hallinan et al., 1984]

It is possible to estimate the fraction of the input beam power ($E_b I_b$) dissipated in ionization of neutral gas from the λ391.4 nm total intensity measurements. Typical results lie in the range 1-4%. Because the total

λ391.4 nm intensity at high neutral density exceeds that at low density for $E_b I_b$ constant (see Fig. 9) the maximum efficiency for transfer of beam power to ionization occurs at high neutral density.

B Energetic Particle Measurements

1. Modifications in the Injected Beam Energy Distribution [Llobet et al., 1985; Jost et al., 1980]

Fig. 10 shows the evolution of the energy spectrum of a beam injected ∥B measured with a collimated detector also aligned ∥B, with increasing axial distance from the gun for E_b = 848 V, I_b = 16.9 ma and $N_o = 3 \times 10^{12}$ cm^{-3}. Even at only 26 cm from the gun, obvious beam heating has occurred; the heating increases with increasing distance. At larger distances, severe diffusion to lower energies occurs and the one dimensional velocity distribution approaches a stable plateau distribution. The locations of the regions of strong heating and energy diffusion tend to move closer to the gun with increasing I_b (n_b) and n_a, and farther from the gun with increasing E_b; the parameter coupling shown in Fig. 6 tends to obscure any quantitative measurements of the individual dependences. Fig. 11 demonstrates that the final spectrum measured near the collector is independent of the beam current ($I_b > I_c$); the scaling of the measured fluxes with beam current indicates the absence of any I_b dependent pitch angle scattering or radial diffusion of the beam electrons.

Direct electron measurements also show little evidence for strong pitch angle scattering or radial diffusion of the injected beam electrons despite the gross modification in the parallel energy. Fig. 12 shows the radial dependence of the integral fluxes, E_b > 300 eV together with the differential

energy spectra observed on the beam axis at distances of 52 cm (hot beam) and 191 cm from the gun (approximately plateau beam) at 0° pitch angle. The radial widths, measured at the 1/e intensity level, were 0.4 cm at 52 cm and 1.2 cm at 191 cm compared to the estimated antinode radius 0.91 cm for a stable beam. Because the beam was only heated at 52 cm, some residual features of the stable noding pattern were probably present at that position, at 191 cm the estimated and measured radii are consistent with the absence of gross radial diffusion. Similarly Fig. 13 shows the differential spectra observed at 0° pitch angle at 191 cm for stable (I_b - 5.8 ma) and BPD configurations (I_b = 7.2 ma); the ~8% FWHM for the stable beam is instrumental. Again the integral fluxes (E > 200 eV) are in agreement to approximately a factor of 2; any pitch angle scattering or radial diffusion should have resulted in the gross nonconservation of the energetic electron flux. Lastly measurements at different pitch angles show a decrease of approximately a factor of 30 in the integral flux (E > 300 eV) as the detector pitch angle is changed from 0° to 24°. Thus the direct energetic electron and optical measurements are consistent in indicating that the beam heating and energy diffusion is primarily in the ∥B component.

Also generally consistent with the optical results, a transition in the characteristics of the energy spectrum measured at a fixed distance from the gun also occurs at a neutral density $N_o \approx 3 \times 10^{12}$ cm^{-3} and is shown in Fig. 14. For $N_o < 3 \times 10^{12}$ cm^{-3}, the beam heating (FWHM) decreases with decreasing density consistent with movement of the heating region further from the gun with decreasing n_a. Surprisingly however, the heating also decreases with increasing density, $N_o > 3 \times 10^{12}$ cm^{-3}. At the higher densities, the severe diffusion to lower energies does not occur and the final state, as measured near the collector, represents a heated rather than plateau beam. The beam

energy loss characterized by a shift in peak position is not generally evident in this data probably because of the poor analyzer resolution.

(2) Beam Energy Dissipation [Llobet et al., 1985]

Because some beam electrons are energized to approximately 1.2 E_b in the heating stage, the near plateau distribution implies that the beam loses approximately 40% of its energy in traversal of the pathlength assuming the beam current is conserved. Obviously, at the higher neutral densities where the beam modification is terminated at the heating stage, the energy loss is much less and is not accurately determined with the poor resolution diagnostic, but is probably in the range of 10%. Yet the total λ391.4 Å intensity is higher at the highest neutral density implying that the smaller beam energy loss is more efficiently coupled to the ionization process at high density than at low density consistent with general dependences of the ionization mean free path, $\lambda \sim (N_o\sigma)^{-1}$. Clearly at low neutral densities, the large beam energy loss must appear at the experiment walls rather than as ionization.

(3) Super Accelerated and Backscattered Electrons

The acceleration of some beam electrons to approximately 1.2 E_b appears as a general characteristic of all computer simulation and laboratory experiments intended to study beam electron trapping by the plasma waves. In BPD experiments in $\geq$ 3:1 magnetic mirror configurations, injection of a 10 kV beam resulted in production of an approximately 100 keV T_e plasma - superacceleration. For smaller mirror ratios the flux of such particles decreased in intensity and energy and was not detectable when the BPD was produced in a solenoidal field configuration [Smullin 1980]. Consistent with these two results, the present solenoidal experiments only generated fluxes of electrons extending to approximately 1.2 E_b with no evidence for superacceleration. Similarly, any backscattered fluxes, generated in the interaction or even

experiment parameters (particularly the axial density gradient) as do other characteristics such as f_p, but the evolution is always completed within L.

II. BPD Ignition Studies with Steady State Beams [Bernstein et al., 1979]

A. Derivation of the Parameter Scaling Law for Ignition

The transition between the stable beam configuration (Figs. 3 and 4) and the BPD configuration (Fig. 5) with increasing beam current is abrupt; for these pictures the required change in beam current, ΔI_b, is only a few percent. Similar sharp transitions are observed when N_o, B, E_b and L were individually varied. On the assumption that each parameter represented an independent variable, Bernstein et al. [1979] formulated the following empirical ignition scaling relationship valid for low neutral densities

$$I_c \sim \frac{E_b^{1.5}}{LN_oB^{0.7}}$$

with the caveat that it was only valid for the specific experiment conditions as follows:

(a) All ambient plasma is produced by collisional ionization of the neutral gas by the beam for $I_b < I_c$.

(b) The beam source radius << antinode beam radius

(c) The gun, chamber walls and collector are electrically grounded

(d) The system length is long enough that the dominant ambient plasma loss process arises from radial diffusion rather than ambipolar axial loss and the density is low enough that recombination loss is unimportant [$n_a < (\alpha \tau)^{-1}$ where α is the dissociative recombination coefficient and is the lifetime given by diffusion]. Langmuir probe measurements by Szuszczewicz [1982] are consistent with this assumption for stable conditions. Thus the

term "stable" only refers to the beam-plasma configuration rather than that of the general plasma-magnetic field system.

Papadopoulos [1985] and Llobet [1984] have semi-independently developed theoretical derivations of this empirical parameter scaling for ignition; for simplicity we follow Papadopoulos' treatment here.

We assume that BPD ignition occurs when conditions for rapid wave growth are achieved; these correspond to the conditions required for the occurrence of the absolute instabilty [Seidl et al. 1976]. Note that this treatment does not specify anything with regard to the steady state BPD or BPI states. As given by Papadopoulos, several conditions must be satisfied for occurrence of the absolute instability; reflection from end boundaries and inhomogeneties can serve to convert a convective mode into an absolute instability but we do not consider this process here.

(a) The product $v_{g_1} \cdot v_{g_2} < 0$ where v_g is the wave group velocity. Typically $v_{g_1} \approx v_b$ and $v_{g_2} \approx -2v_b \frac{\omega_{ce}^2}{\omega_p^2} \cos^2\theta \sin^2\theta$. v_{g2} is the backward upper hybrid wave group velocity which provides the <u>energy feedback</u> for occurrence of the absolute instability. A necessary condition for the backward wave is $\omega_p > \omega_{ce}$.

(b) The linear growth rate $\gamma_0 = \frac{1}{2} \left(\frac{\omega_b^2 R^2 \cos^2\theta}{\omega_p^2}\right)^{1/2} \omega_p$ where R is a reduction factor arising from the small beam radius compared to the radius of the ambient plasma

$\gamma^2 > \nu_b \nu_a$ where $\nu_{b,a}$ = electron-neutral collision frequency for beam and plama electrons.

(c) $L > \frac{\left(|v_{g_1} v_{g_2}|\right)^{1/2}}{\gamma} \equiv L_c$ (critical length)

Thus in finite length systems, the length of the system L, must be $> L_c$ for the occurrence of the absolute instability. In an infinite length system the concept of a critical length appears uncertain.

Combining these equations with the following equations for n_b and n_a.

$$n_b = C_1 \frac{I_b B^2}{E^{3/2}} \text{ (conditions b + c)}$$

$$n_a = C_2 \frac{I_b N_o}{E_b^{\cdot 5} D} \text{ (conditions a b + c)}$$

where D is the diffusion coefficient for Bohm diffusion and is $\sim T_e/B$ and the ionization cross-section T scales as $\frac{1}{E^{\cdot 5}}$. Taking $\sin^2\theta/R = 1$ gives

$$I_c = \frac{C_3 E^{3/2}}{L\, N_o^{\cdot 5} B^{0\cdot 5}}$$

Note that in the original Bernstein et al. [1979] measurements, both the N_o and B dependence were only qualitatively determined so we do not consider the differences to be very significant. When the numerical values for C_3 are used, reasonable agreement in the calculated and measured I_c values are obtained.

B. Scaling Law Modifications for Modified Experimental Conditions

Very different scaling dependences will be observed when the experiment parameters create different dependences for n_b and n_a as follows:

(1) for the general case where the ambient plasma is produced by auxilliary means, n_a = constant independent of I_b and therefore

$$I_c \sim \frac{E_b^{5/2}}{n_a L^2}$$

(2) for strong magnetic fields or large source radius, $R_{antinode} < R_s$ so that the beam assumes only a rippled rather than noded configuration giving

$$n_b \sim \frac{I_b}{E_b^{1/2} R_s^2},$$

For a beam produced ambient plasma

$$I_c \sim \frac{E_b B^{1/2}}{L N_o^{1/2}} \text{ and}$$

for an externally produced plasma

$$I_c \sim \frac{E_b^{3/2} B^2}{L^2 n_a}$$

(3) for neutral densities sufficiently high that collisional rather than Bohm diffusion represents the dominant radial loss process and for a self generated ambient plasma

$$I_c \sim \frac{E_b^{3/2}}{BL}.$$

For still other cases, recombination or axial loss may be the dominant ambient plasma loss process requiring modified scaling laws.

A general confirmation of the theoretical model can be seen from the large differences (hysteresis) observed in the beam current required for BPD ignition and at which the BPD is extinguished [Bernstein et al. 1978] at low neutral densities and shown in Fig. 19. A simplistic model for hysteresis is that ignition occurs as the product $(n_a n_b)$ is increased above the critical value whereas extinction occurs as $(n_a n_b)$ is slowly decreased below the critical value. The grossly different ionization production rates for the

stable and BPD conditions cause the hysteresis effect. However, the disappearance of this hysteresis effect at higher neutral densities is not readily apparent in this interpretation of the scaling law physics because the gross difference in ionization rate between stable and BPD conditions is still present and presumably the plasma loss processes are unchanged. Rather it may be associated with the general change in BPD characteristics observed with increasing scaled neutral density and shown earlier in Fig. 9.

For some experimental conditions in both the large and small chamber experiments, an intermediate state is observed, over a small current range as the system evolves from the stable to the BPD state. As described by Bernstein et al. [1979] and shown in Figure 15a this state is characterized by narrow band emissions in the range $f_c < f < 1.5\ f_c$ and higher harmonics. Both the wave amplitude and frequency increase with increasing I_b. Optical measurements indicate that the total ionization rate during this stage is increased above that produced collisionally by the injected beam alone; however, because the ionization is distributed over a large cross-sectional area, the resultant enhancement in the plasma density is not large. Some recent measurements indicate that the maximum wave amplitude is observed near the collector indicating a convective instability. Clearly the absence of the absolute instability does not preclude the presence of a convective mode. The presence of this phase is also clearly evident in the studies of Getty and Sullin [1963]. However, we have not regarded it as critical in BPD ignition; in fact its existence was not apparent for the BPD at high neutral density in the large chamber experiments; thus the absence of this state and hysteresis effects occur together.

IV. Temporal Evolution of the Steady State Interaction - Pulsed Operation [Szuszczewicz et al., 1982]

Pulsed operation allows the study of temporal effects in BPD ignition for a variety of experimental conditions; as shown schematically in Fig. 20 for $I_b > I_c$, the temporal evolution may pass through the several phases discussed for steady state operation.

(A). Production of the Ambient Plasma

The accumulation of ambient plasma produced by collisional ionization alone is obviously a time dependent process. Assuming that time dependent density is given by the collisional production rate, P, (we neglect the increased ionization rate associated with the cyclotron waves and possible recombination loss) and a loss rate proportional to the density present gives

$$dn/dt = P - \frac{n_a}{\tau}$$

The plasma density at time, t, after initiating injection is given by

$$n_a = P\tau(1 - e^{-t/\tau}).$$

where τ is the ambient plasma lifetime. At short times ($t \ll \tau$), $n_a \sim Pt\ cm^{-3}$. At long times ($t \gg \tau$), n_a saturates $\sim P\tau\ cm^{-3}$. Because $P \sim I_b$, these equations can be reformulated in terms of the steady state values I_b and I_c for a fixed length system to give the plasma accumulation time (delay time for ignition)

$$t_d = \tau\ \ell n\ (I_b^2/I_b^2 - I_c^2);$$

for $I_b^2 \gg I_c^2$, t_d scales as $1/I_b^2$.

Fig. 21 shows the measured delay times together with predicted delay times, based on an assumed plasma lifetime of 4 msecs, for $I_b > I_c$. As can be seen, ignition times $t_d \lesssim 150$ μsec are possible for an electron gun perveance in the range 2×10^{-6} $AV^{-3/2}$ and a neutral density in the range 3×10^{11} cm^{-3}. Unfortunately the plasma lifetime of 4 msec is not grossly different from that estimated to arise from ambipolar axial loss processes for $T_e \approx 1$ eV; thus the assumption of dominant radial loss used in the derivation of the scaling law may only be qualitatively valid.

This model of ignition implies that the formative time delay would decrease as the ambient plasma density (produced by alternative means) at the start of injection increased and would disappear completely if the initial plasma density exceeded that required for occurrence of the absolute instability at the injected beam current employed. Experiments in which the pulse repetition rate and duration were adjusted so that beam injection was initiated at various times during the afterglow as the plasma density of the preceding pulse discharge decayed [Szuszczewicz and Lin, 1982] demonstrated the expected decrease of t_d with increasing initial plasma density. Similarly for conditions where an ion thruster provided approximately the required density, the formative delay time was reduced to the range < 50 μsec; in the absence of this plasma, t_d was ≈ 12 msec. In direct contradiction to the model however, no change in the magnitude of beam current required for ignition of the steady state BPD was observed in the presence or absence of the thruster plasma.

(B) Space Charge Expansion of the Beam

In the absence of initial plasma or subsequent beam produced plasma, the beam space charge will radially expand the beam across the magnetic

field until the beam density is reduced to satisfy the Brillouin condition $\omega_{pb}^2 \leq \frac{1}{2}\omega_c^2$. However because of the finite neutral gas density found in most laboratory experiments, collisional ionization produced by the beam causes the accumulation of positive ions which eventually neutralize the beam space charge. Thus the beam radius, observed at a fixed axial distance from the gun will appear to "collapse" with time. Beam neutralization occurs when the accumulated ion density equals the beam density or

$$t_n = [N_o \sigma_i v_b]^{-1} \approx 25 \text{ } \mu\text{sec for } E_b = 1 \text{ keV}$$

and $N_o = 3 \times 10^{11}$ cm^{-3}. Even at the best base pressure attained in the large chamber experiments (1×10^{-6} torr) $t_n = 0.25$ msec so that the steady state beam is always neutralized.

Steady state ($t \gg t_n$) optical measurements of the beam radial width for various beam currents with $I_b < I_c$ provide no evidence for a current dependent broadening. I_c was of sufficient magnitude that any space charge expansion would have been easily observed. However the space charge neutralization process does play a role in the temporal evolution of the system when the initial ambient plasma density $\omega_{pa} < \omega_{pb}$.

(C) Ion Effects

In the older computer simulation studies of the beam plasma interaction, ions were assumed to be stationary (infinite mass) and to simply provide overall charge neutrality. Even for collisionless conditions, the general quasi-linear evolution of the beam velocity distribution together with ambient plasma heating was the usual result. When the ions were given finite mass (no longer stationary) suprathermal electrons and soliton-caviton field and density structures were produced [Rowland, 1985]. Clearly, ion dynamics were

important, thus implying a time scale in the f_{p+} range, Bernstein et al. [1983] attributed the change in BPD characteristics, shown in Fig. 9, at $\sim 3 \times 10^{12}$ cm^{-3} neutral density to collisional effects on this time scale because $\nu_{en} \approx \omega_p \left(\frac{m}{2M}\right)^{1/2}$ at that neutral density. Typical ion frequencies in the large chamber experiments were $\omega_{p+} \approx 5 \times 10^5$ sec^{-1}

Seidl et al. [1976] have also shown that the HF instability occurs in bursts with typical duration in the range of the ion accoustic period; such modulation of the HF waves is clearly evident in the present experiments. They attributed this modulation to the periodic growth and quenching of different wave modes in the system.

(d) Relaxation Oscillations

A variety of LF oscillations have been observed and described in detail by Hallinan et al. [1984]. At times, the light intensity variations are as slow as a few Hz and are visually observable. Some of the measured time integrated frequency spectra show the presence of two distinct wave spectra, differing by ~10% in frequency and apparently indicating the relaxation between discrete plasma density states, but both with the enhanced density characteristic of the BPD. Sometimes the relaxation appears to occur simply between the unstable BPD and the stable (single particle) states.

Conclusions

The most important conclusion from the laboratory work is that in all three areas, (1) the characteristics of the steady state BPD, (2) the conditions required for BPD ignition and (3) the temporal development to ignition, the experimental results are in good agreement with the theoretical predictions of Papadopoulos [1985] and Llobet [1984] and the theoretical and experimental work of Seidl et al. [1976]. It seems reasonable to conclude

that the BPD and BPI are manifestations of the same basic physical process; for the finite length, self produced plasmas employed in the experiments, the strong interaction occurs when conditions for the absolute instability are satisfied. We therefore believe that we understand the ignition process reasonably well and can extrapolate the predictions to other experimental configurations including those in the ionosphere.

The theoretical models have allowed formulation of parameter scaling relations for BPD ignition for several different experimental conditions. In addition good agreement is observed between the theoretically predicted and experimentally observed temporal evolution to steady state conditions during pulsed operation. As always several gross discrepancies with the theoretical predictions have been described. Unfortunately these all have appeared at about the transition neutral density (typically 3×10^{11} cm^{-3} in the large chamber and 3×10^{12} cm^{-3} in the small chamber) where many changes in the BPD characteristics appear. Unfortunately the constraints imposed by the experimental facilities did not permit exploration of these inconsistencies at grossly different neutral densities.

Although all these factors may critically influence experiments in the ionosphere, we have not chosen to emphasize the relationship between flight and laboratory experiments in this talk. However it is believed that the sensible tabulation and explanation of the laboratory results will be useful to flight experiments.

TABLE 1

	Seidl	Large Chamber	Small Chamber
L	1.5 m	20 m	2.5 m
R	0.15 m	8 m	0.50 m
B	$\leq$ 3.5 Kg	0.5 - 2 G	5 - 39 G
N_o (typical) cm^{-3}	$6 \times 10^{12} < N < 3 \times 10^{13}$	$3 \times 10^{10} - 5 \times 10^{11}$	$1 \times 10^{12} - 2 \times 10^{13}$
na (max) cm^{-3}	$10^9 < na < 10^{12}$	3×10^7	$< 1.2 \times 10^{10}$
Na Production	external	beam, ion thruster	beam
Gas	He + A (Penning mix)	N_2	N_2, He, A
Injection Angle	0°	0 - 90°	$\approx$ 0°
E_b	$100V < E_b < 1$ KV	$400\ V < E_b < 2$ KV	$400\ V < E_b < 2$ KV
Source Radius	0.3 cm	0.15 cm	0.15 cm
Operation	Steady State	Pulsed and Steady State	Pulsed and Steady State

References

Bernstein, W., H. Leinbach, P. J. Kellogg, S. Monson, T. Hallinan, O. K. Garriott, A. Konradi, J. McCoy, P. Daly, B. Baker and H. R. Anderson, "The beam-plasma discharge at low pressures and low magnetic field strengths," Geophys. Res. Lett., 5, 127, 1978.

Bernstein, W., H. Leinbach, P. J. Kellogg, S. J. Monson and T. Hallinan, "Further laboratory measurements of the beam-plasma discharge," J. Geophys. Res., 10, 7271-7278, 1979.

Bernstein, W., J. O. McGarity and A. Konradi, "Electron beam injection experiments: replication of flight observations in a laboratory beam plasma discharge," Geophys. Res. Letts., 10, 1124-1127, 1983.

Getty, W. D. and L. D. Smullin, "Beam plasma discharge: buildup of oscillations, J. Appl. Phys., 34, 3421-3429, 1963.

Hallinan, T. J., H. Leinbach, G. Mantjoukis and W. Bernstein, "Measurements of the optical emission produced during the laboratory beam plasma discharge, J. Geophys. Res., 89 2335-2347, 1984.

Holzworth, R. H., W. B. Harbridge and H. C. Koons, "Plasma waves stimulated by electron beams in the laboratory and in the auroral ionosphere, in Artificial Particle Beams in Space Plasma Studies, edited by B. Grandal, pp. 381-391, Plenum Press, New York, 1982.

Jost, R. J., H. R. Anderson and J. O. McGarity, "Measured electron energy distributions during beam/plasma interactions, Geophys. Res. Letts., 7, 509, 1980.

Jost, R. J., H. R. Anderson, W. Bernstein and P. J. Kellogg, "Radial dependence of the HF field strength in the BPD column," in Artificial Particle Beams in Space Plasma Studies, edited by B. Grandal, pp. 431-437, Plenum

Press, New York, 1982.

Kellogg, P. J., H. R. Anderson, W. Bernstein, T. J. Hallinan, R. H. Holzworth, R. J. Jost, H. Leinbach and E. P. Szuszczewicz, "Laboratory simulation of injected particle beams in the ionosphere," in Artificial Beams in Space Plasma Studies, edited by B. Grandal, pp. 289-329, Plenum Press, New York, 1982.

Konradi, A., W. Bernstein, D. L. Bulgher, J. O. McGarity and J. L. Winkler, Jr., "Initial experimental results from a laboratory size beam-plasma discharge device," in Active Experiments in Space, European Space Agency Report ESA SP-195, Paris, 1983.

Llobet, X., "A Model of the Beam-Plasma Discharge," Ph.D. Thesis, Rice University, May 1984 (unpublished).

Llobet, X., W. Bernstein and A. Konradi, "The spatial evolution of energetic electrons and plasma waves during the steady state beam plasma discharge," J. Geophys. Res., accepted for publication, 1985.

Rowland, H., "Strong turbulence effects on the kinetic beam-plasma instability, Phys. Fluids, 23, 508, 1980.

Seidl, M., W., Carr, D. Boyd, and R. Jones, "Non-linear development of absolute and convective instabilties," Phys. Fluids, 19, 75-92, 1976.

Smullin, L. D., "A review of the beam plama discharge," in Relation Between Laboratory and Space Plasmas, edited by H. Kikuchi, pp. 45-65, D. Reidel, Dordrecht, Holland, 1980.

Stenzel, R. L. and D. A. Whelan, "Electromagnetic radiation from beam-plasma instabilities," in Artificial Particle Beams in Space Plasma Studies, edited by B. Grandal, pp. 471-480, Plenum Press, New York, 1982.

Szuszczewicz, E. P., K. Papadopoulos, W. Bernstein, C. S. Lin, and D. N. Walker, "Threshold criterion for a space simulation beam-plasma discharge," J. Geophys. Res., 87, 1565-1573, 1982a.

Szuszczewicz, E. P., C. S. Lin, "Time dependence plasma behavior triggered by a pulsed electron gun under conditions of beam plasma discharge, in Artificial Particle Beams in Space Plasma Studies, edited by B.Grandal, pp. 361-370, Plenum Press, New York, 1982.

Figure Captions

Fig. 1. Schematic representation of the experiment configuration in the large chamber.

Fig. 2. Schematic representation of the scaled small chamber experiment.

Fig. 3. Photograph of the trajectory of a stable beam in the large chamber - injection ∥B.

Fig. 4. Photograph of the trajectory of a stable beam in the large chamber - injection at large pitch angle.

Fig. 5. Photograph of unstable interaction in the large chamber.

Fig. 6. Coupling of experiment parameters n_b, n_a, N_o during BPD. Shown is the dependence of f_p^2 (where f_p is the fundamental RF frequency) on beam current (constant pressure) and pressure (constant beam current).

Fig. 7. Relative intensity profiles (λ391.4 nm) through the BPD for beams injected parallel and at large angle to B. The profiles are normalized to the same peak value; 2 R_c is the diameter of the helical beam and 4 R_L is the antinode diameter of a beam having a spread in pitch angle of ±5°. E_b = 1 keV, B = 0.9 G, I_b = 24 mA.

Fig. 8. (a) The inverse width of the BPD glow for a 1600-V, 40-mA beam varies linearly with magnetic field strength. (b) The width of the BPD at constant current, field strength, and pressure varies linearly with the velocity of the beam electrons.

Fig. 9. The variation of the FWHM and total intensity of the λ391.4 and greater than 618.5 nm emissions with pressure. Also shown is the simultaneously observed relative whistler wave amplitude greater than receiver noise.

Fig. 10. Energy spectra (0° detector pitch angle) measured at 26, 32, 38, 45, 52, and 191 cm from the gun for an 848 V, 16.9 mA beam at p = 1×10^{-4} torr; the energy spectrum observed for this energy beam under stable conditons (SP) is also shown.

Fig. 11. Energy spectra measured with the detector (0° detector pitch angle) located at 191 cm from the gun for various $I_b > I_c$; E_b = 848V, P = 1×10^{-4} torr. For these conditions, $I_c \approx$ 6-7 mA.

Fig. 12. Energy spectra (on axis and 0° detector pitch angle) and the dependence of the integrated flux > 300 V on radial position (0° detector pitch angle) measured at 52 and 191 cm from the gun. The beam energy was 862 V, beam current 27.4 mA and p = 3×10^{-5} torr.

Fig. 13. Energy spectra measured with the detector (0° detector pitch angle) located at 191 cm from the gun for pre BPD (I_b = 5.8 mA) and BPD (I_b = 7.2 mA); E_b = 600 V and P = 4.2×10^{-5} torr.

Fig. 14. The variation of the energy spectra (0° detector pitch angle) measured 52 cm from the gun with pressure measured in torr (neutral density) for a constant energy (851 V), constant current (16 mA) beam.

Fig. 15. RF noise spectrums in the low density (a) and high density (b) states. The beam current for the high density state has been reduced from the value required for ignition to illustrate the hysteresis effect (see Fig. 19).

Fig. 16. Radial confinement of HF waves to the primary beam region [from Seidl et al., 1976].

Fig. 17. RF spectra observed at 26, 52, 191 cm (top to bottom) from the gun for an 850 V, 27.4 mA beam; the corresponding energy spectra are

shown schematicaly. $P = 3.5 \times 10^{-5}$ torr.

Fig. 18. Axial location of the energy deposition region in an absolute beam-plasma interactions [from Seidl et al. 1976].

Fig. 19. The dependence of peak λ391.4 nm intensity on beam current showing the abrupt transition and subsequent hysteresis as the beam current is reduced from the value required for ignition. When the current is reduced to 26 mA, the high density state is extinguished and the beam returns to the low density condition.

Fig. 20. Schematic illustration of the temporal evolution of the BPD for pulsed injection ($I_b \gg I_c$) without an initial ambient plasma.

Fig. 21. The variation of the formative delay time, t_d, with beam current ($I_b > I_c$). The predicted data are calculated for an assumed plasma lifetime, $\tau = 4$ msec.

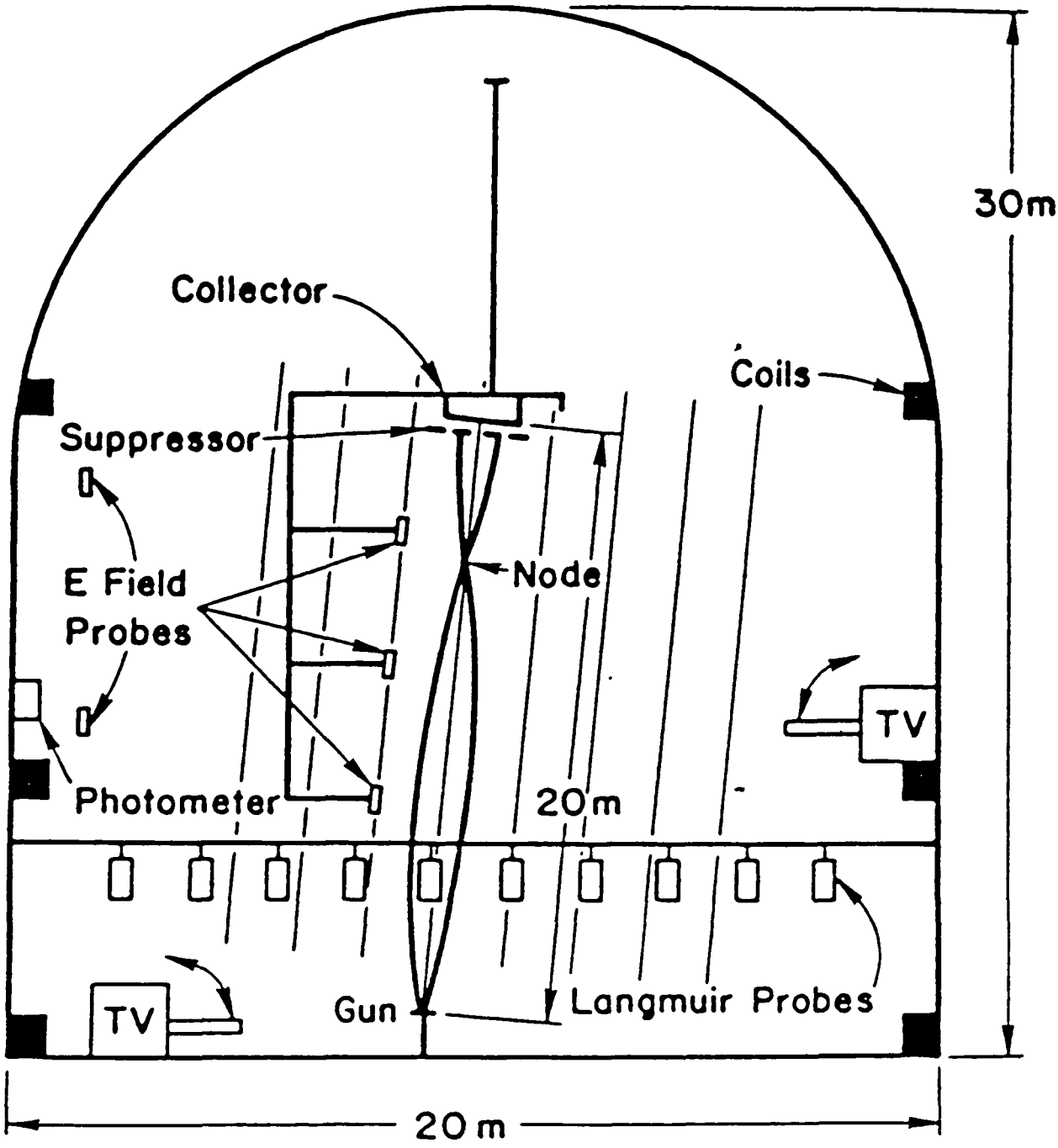
30m
Collector
Coils
Suppressor
E Field
Probes
Node
TV
Photometer
20m
TV
Gun
Langmuir Probes
20 m

Figure 1

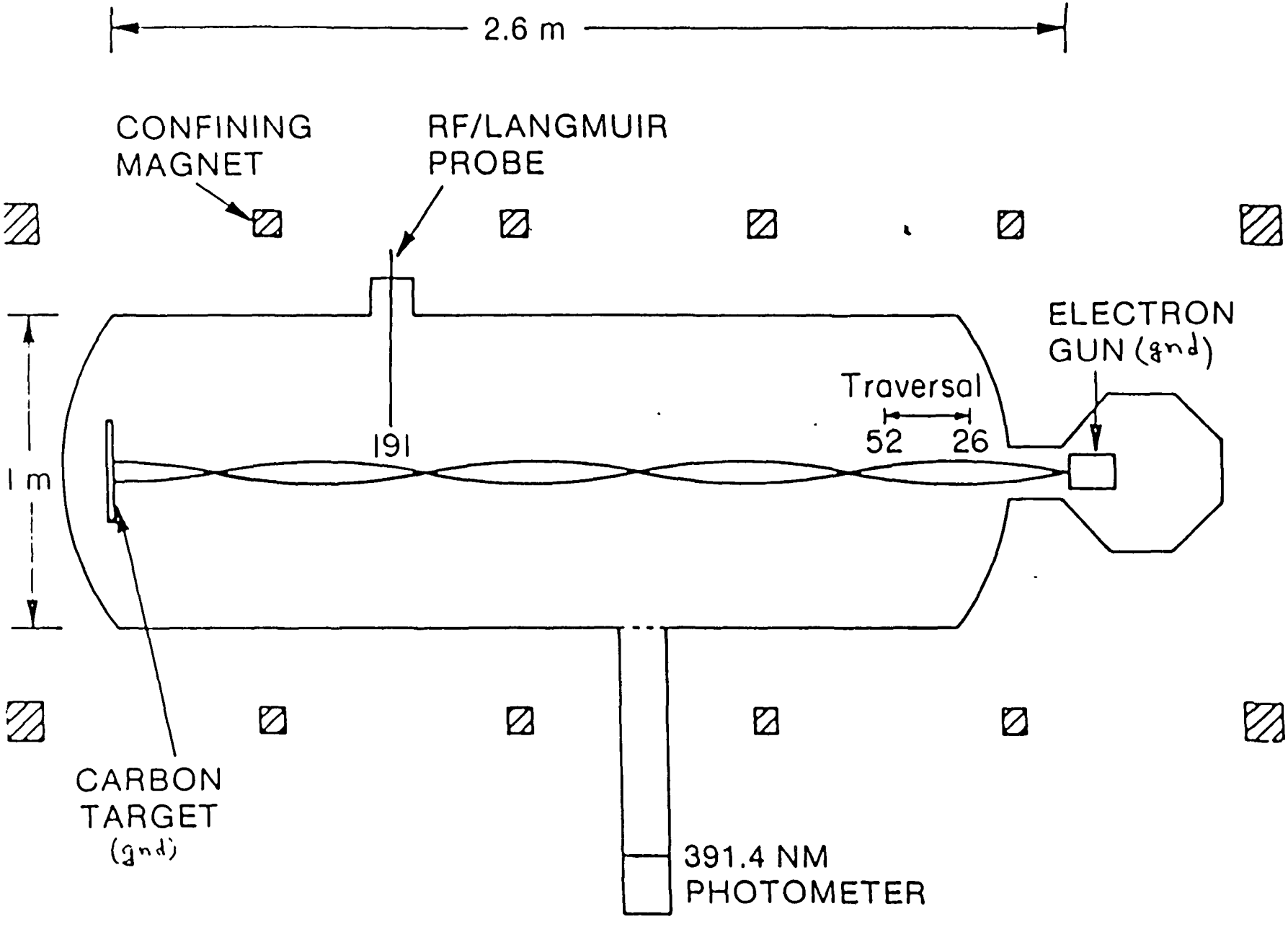
2.6 m
CONFINING MAGNET
RF/LANGMUIR PROBE
ELECTRON GUN (gnd)
Traversal
52
26
191
1 m
CARBON TARGET (gnd)
391.4 NM PHOTOMETER

Figure 2

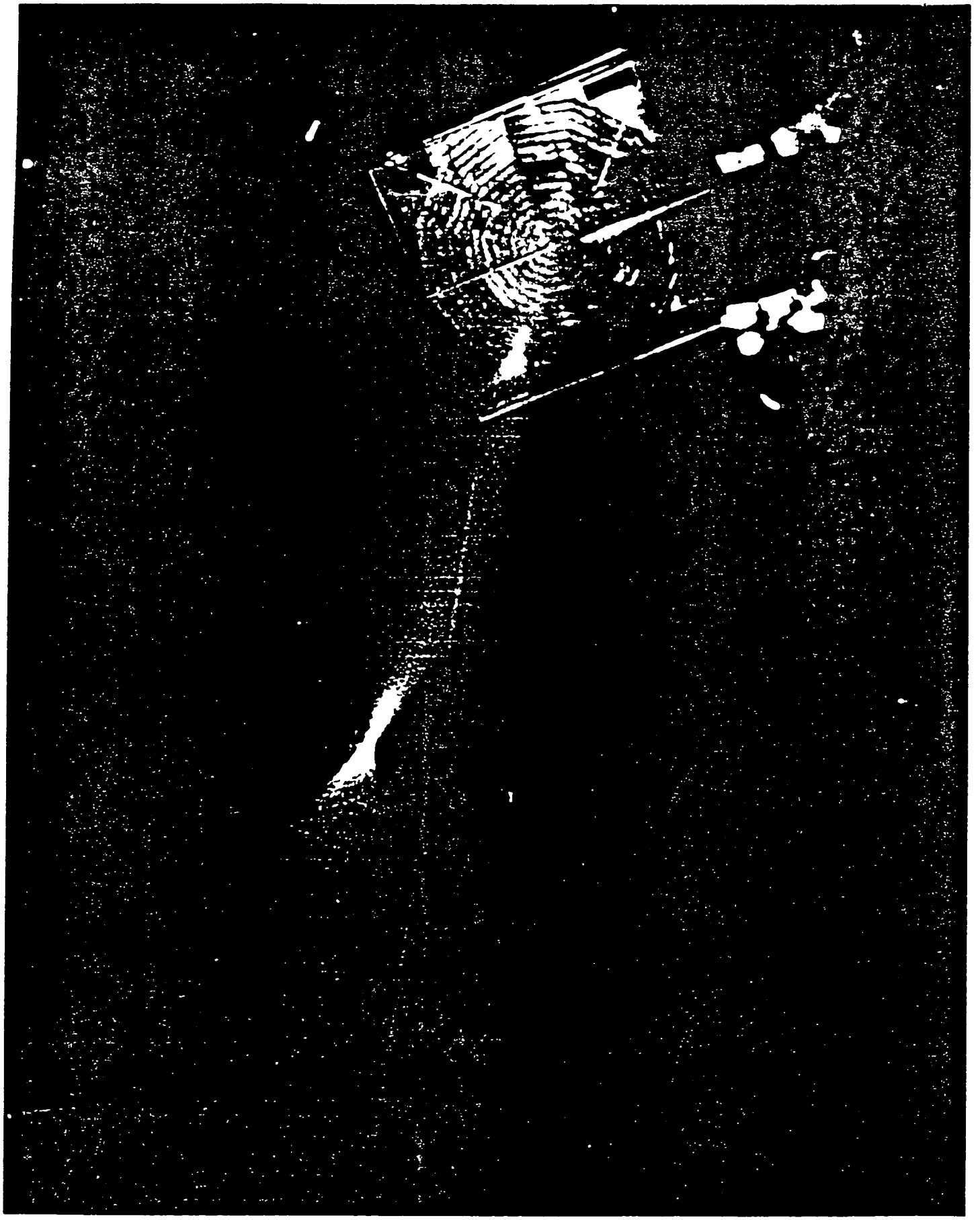

Figure 3

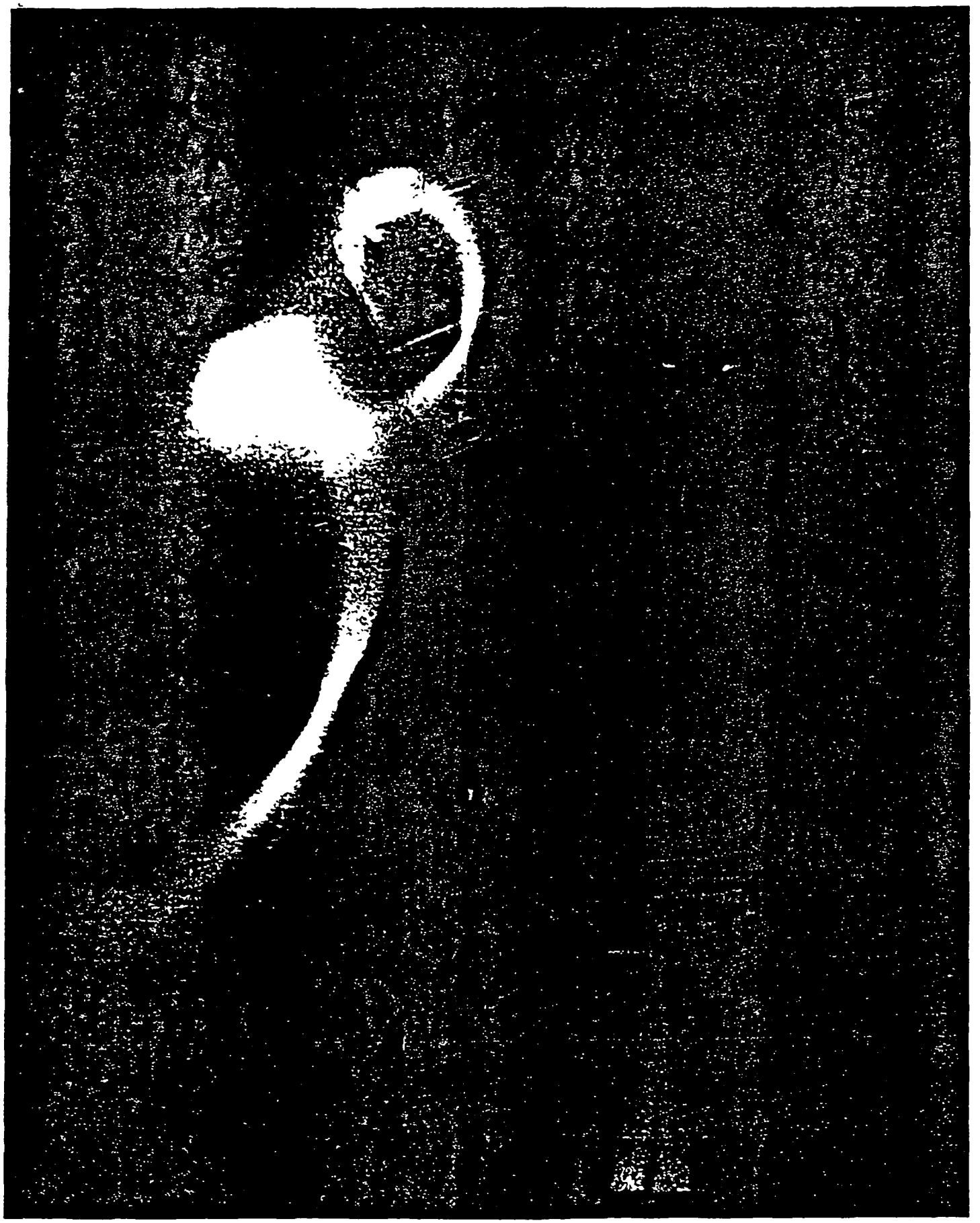

Figure 4

Figure 5

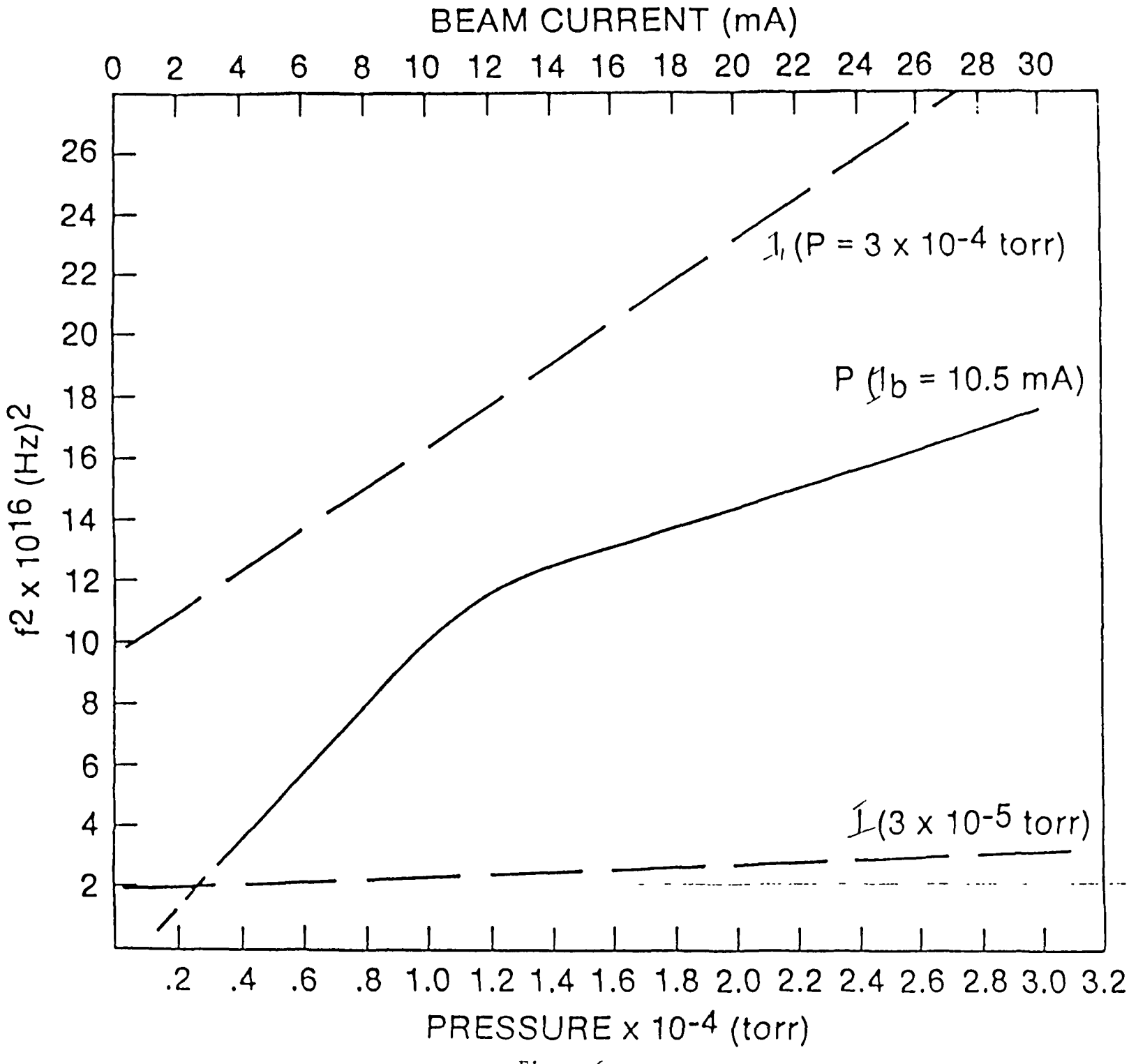
BEAM CURRENT (mA)
0 2 4 6 8 10 12 14 16 18 20 22 24 26 28 30
f2 x 10^16 (Hz)^2
26 24 22 20 18 16 14 12 10 8 6 4 2
I_i (P = 3 x 10^-4 torr)
P (I_b = 10.5 mA)
I (3 x 10^-5 torr)
.2 .4 .6 .8 1.0 1.2 1.4 1.6 1.8 2.0 2.2 2.4 2.6 2.8 3.0 3.2
PRESSURE x 10^-4 (torr)

Figure 6

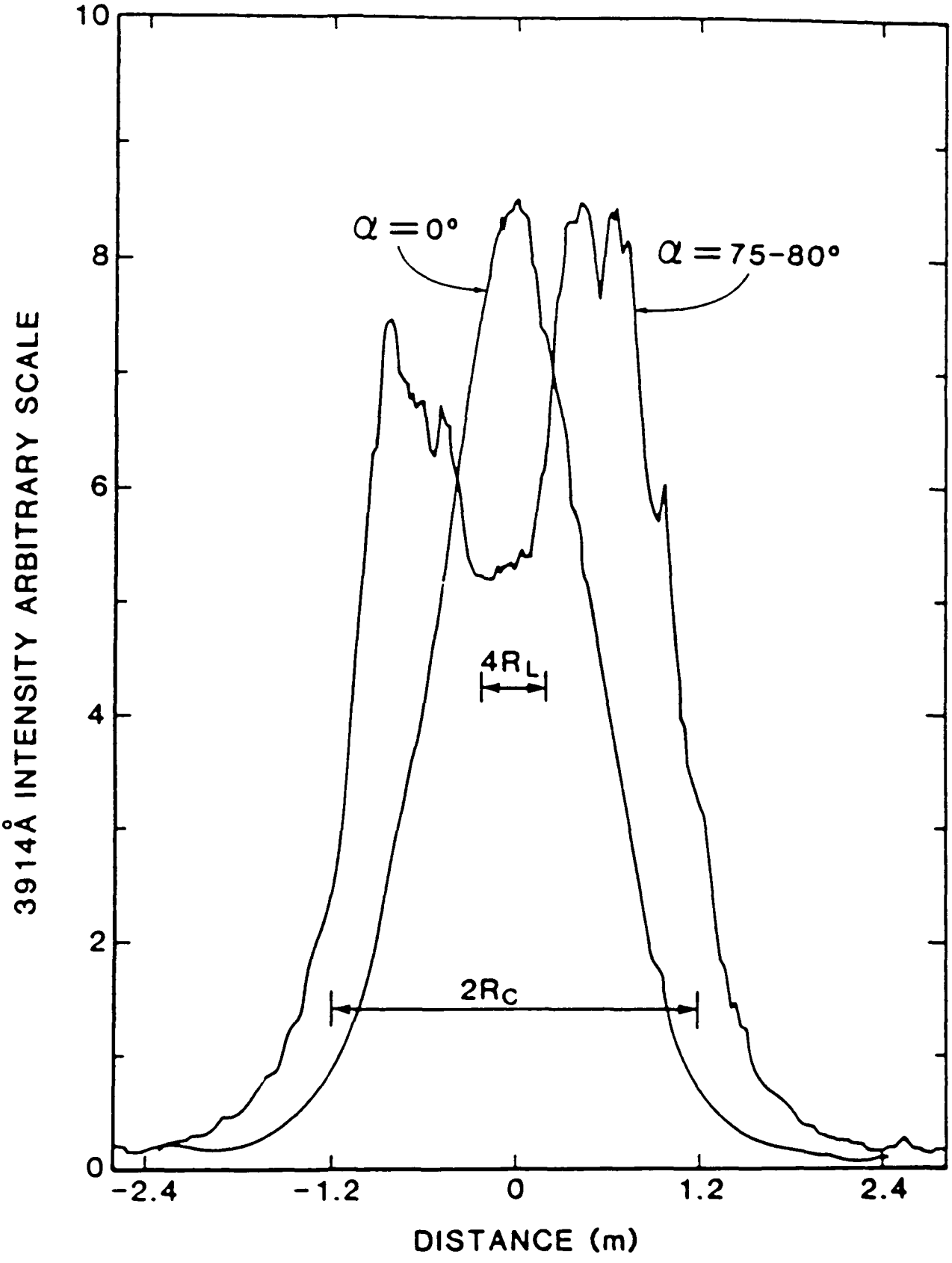
10
8
6
4
2
0
3914Å INTENSITY ARBITRARY SCALE
α = 0°
α = 75-80°
4R_L
2R_C
-2.4
-1.2
0
1.2
2.4
DISTANCE (m)

Figure 7

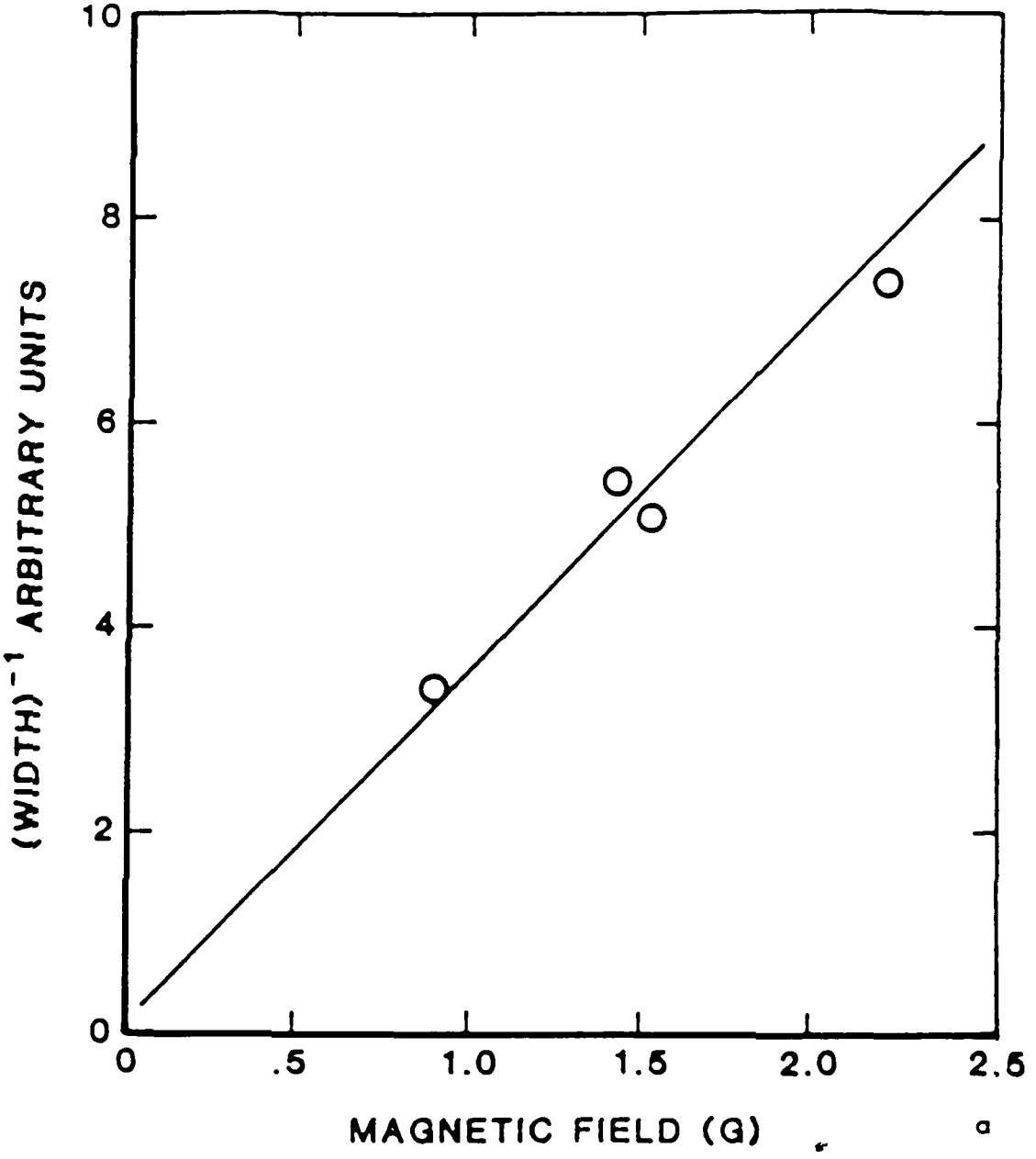

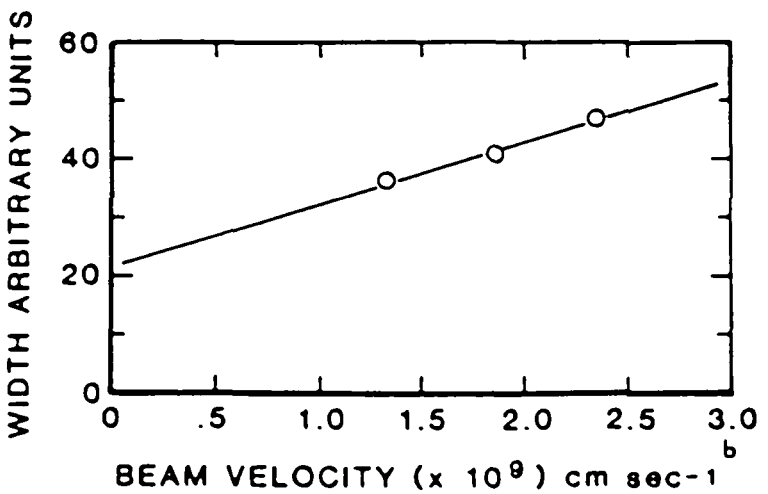

Figures 8a, 8b

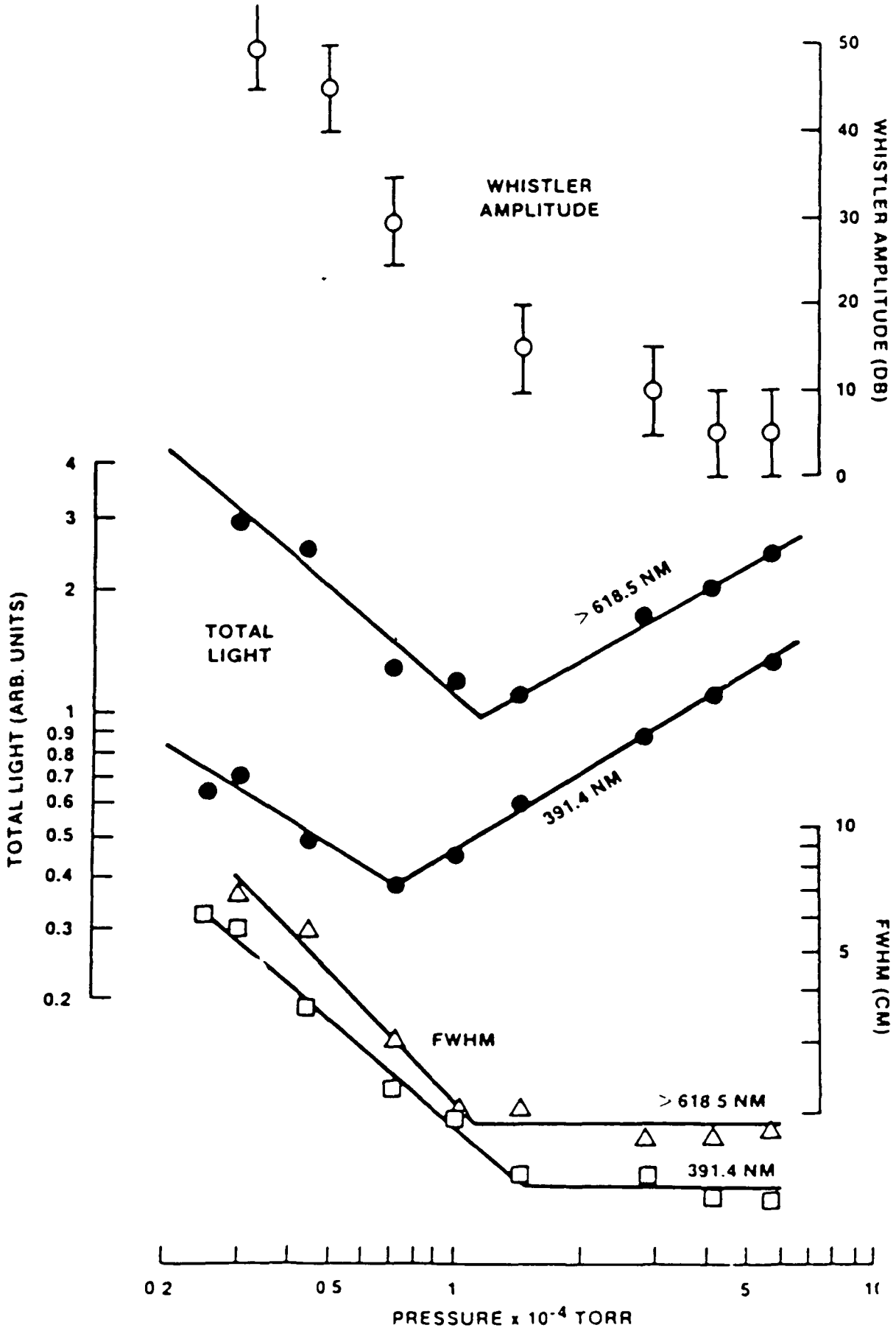
WHISTLER AMPLITUDE
WHISTLER AMPLITUDE (DB)
50
40
30
20
10
0
TOTAL LIGHT (ARB. UNITS)
4
3
2
1
0.9
0.8
0.7
0.6
0.5
0.4
0.3
0.2
TOTAL LIGHT
> 618.5 NM
391.4 NM
FWHM
FWHM (CM)
10
5
> 618 5 NM
391.4 NM
0 2
0 5
1
5
PRESSURE x 10⁻⁴ TORR

Figure 9

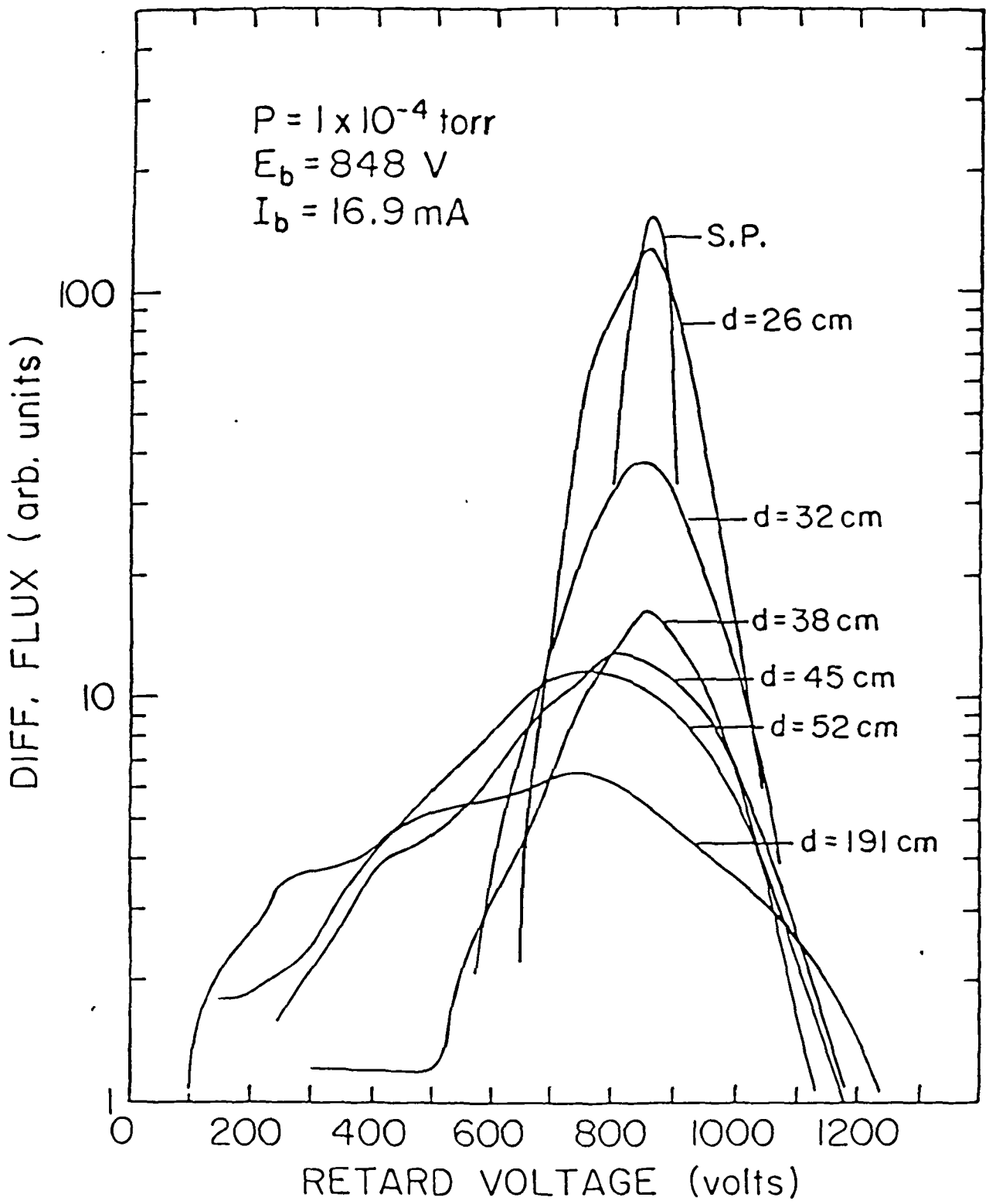
P = 1 x 10⁻⁴ torr
Eb = 848 V
Ib = 16.9 mA
S.P.
d = 26 cm
d = 32 cm
d = 38 cm
d = 45 cm
d = 52 cm
d = 191 cm
DIFF. FLUX (arb. units)
100
10
1
0
200
400
600
800
1000
1200
RETARD VOLTAGE (volts)

Figure 10

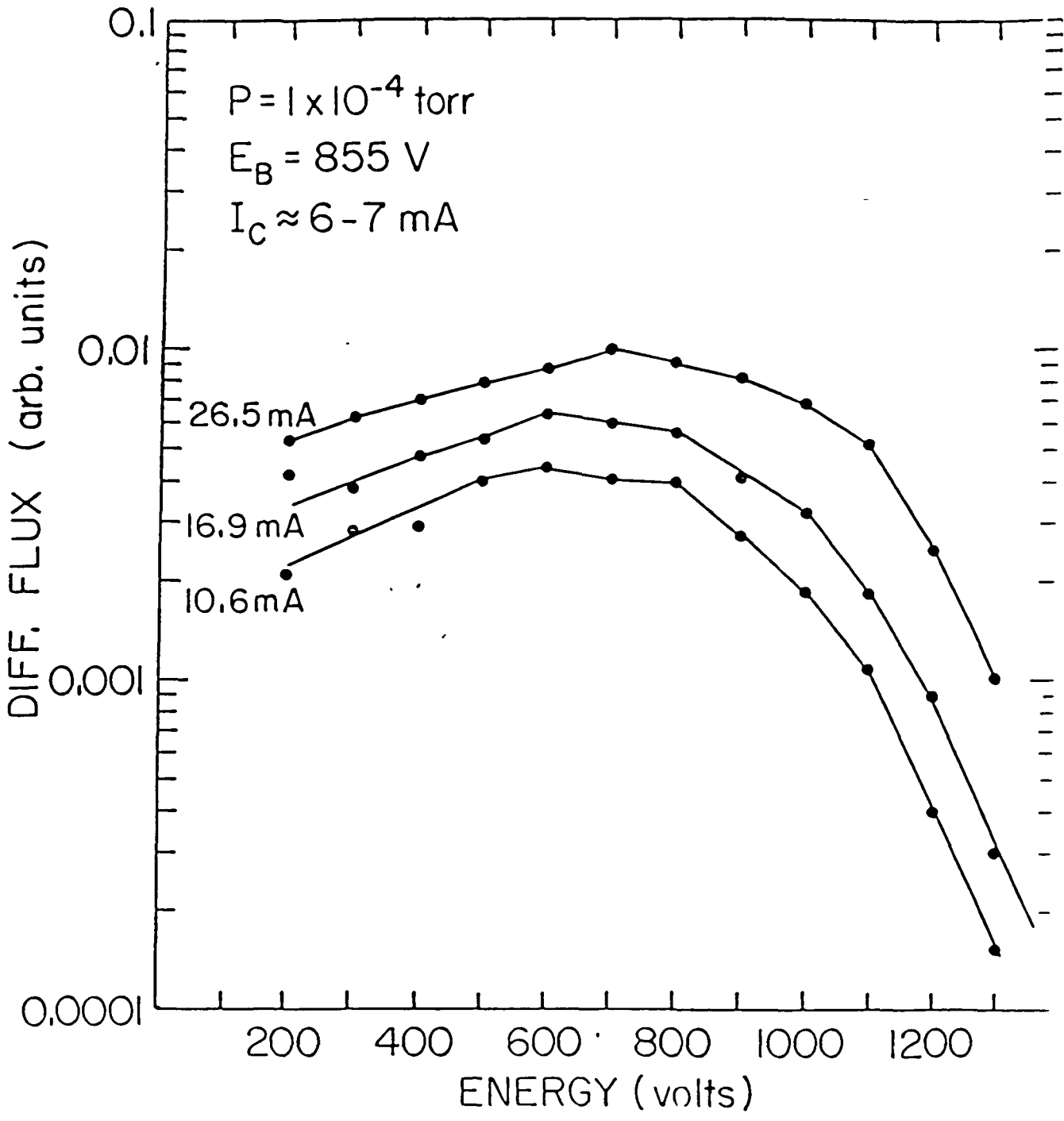
0.1
0.01
0.001
0.0001
DIFF. FLUX (arb. units)
P = 1 x 10^-4 torr
E_B = 855 V
I_C ≈ 6-7 mA
26.5 mA
16.9 mA
10.6 mA
200
400
600
800
1000
1200
ENERGY (volts)

Figure 11

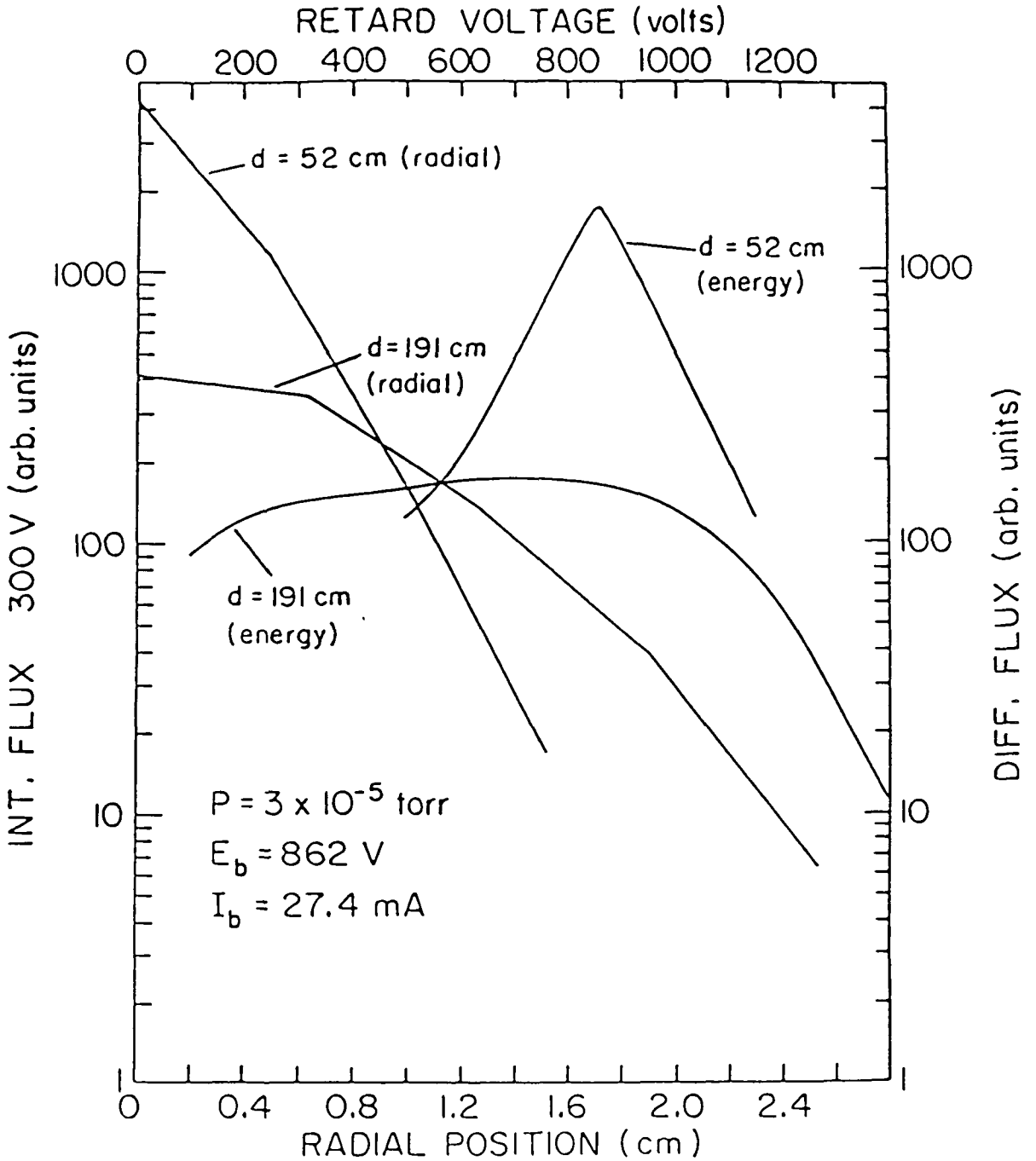
RETARD VOLTAGE (volts)
0
200
400
600
800
1000
1200
d = 52 cm (radial)
d = 52 cm
(energy)
d=191 cm
(radial)
d = 191 cm
(energy)
1000
100
10
1
INT. FLUX 300 V (arb. units)
DIFF. FLUX (arb. units)
P = 3 x 10⁻⁵ torr
E_b = 862 V
I_b = 27.4 mA
0
0.4
0.8
1.2
1.6
2.0
2.4
RADIAL POSITION (cm)

Figure 12

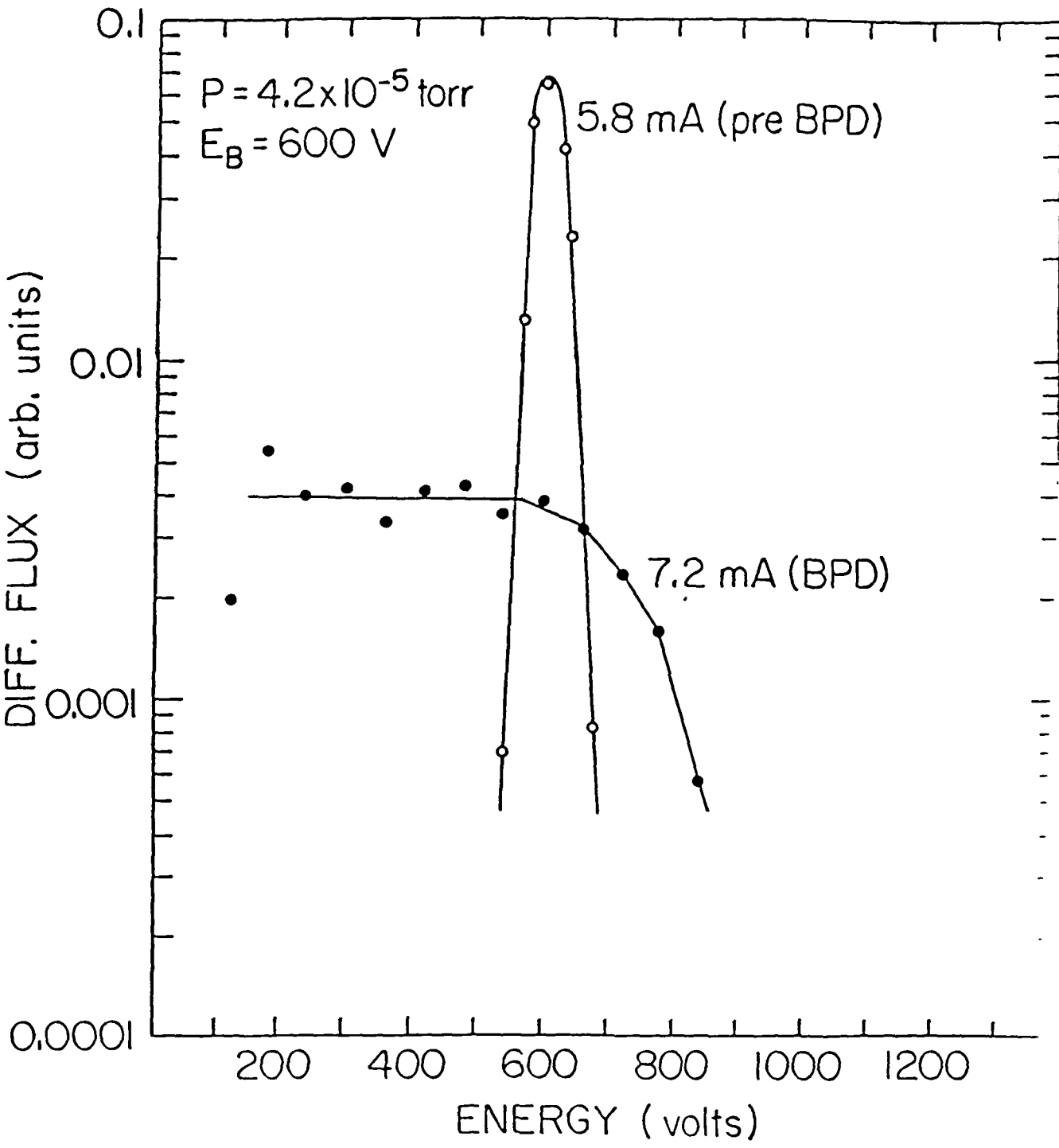
0.1
0.01
0.001
0.0001
DIFF. FLUX (arb. units)
P = 4.2x10⁻⁵ torr
E_B = 600 V
5.8 mA (pre BPD)
7.2 mA (BPD)
200
400
600
800
1000
1200
ENERGY (volts)

Figure 13

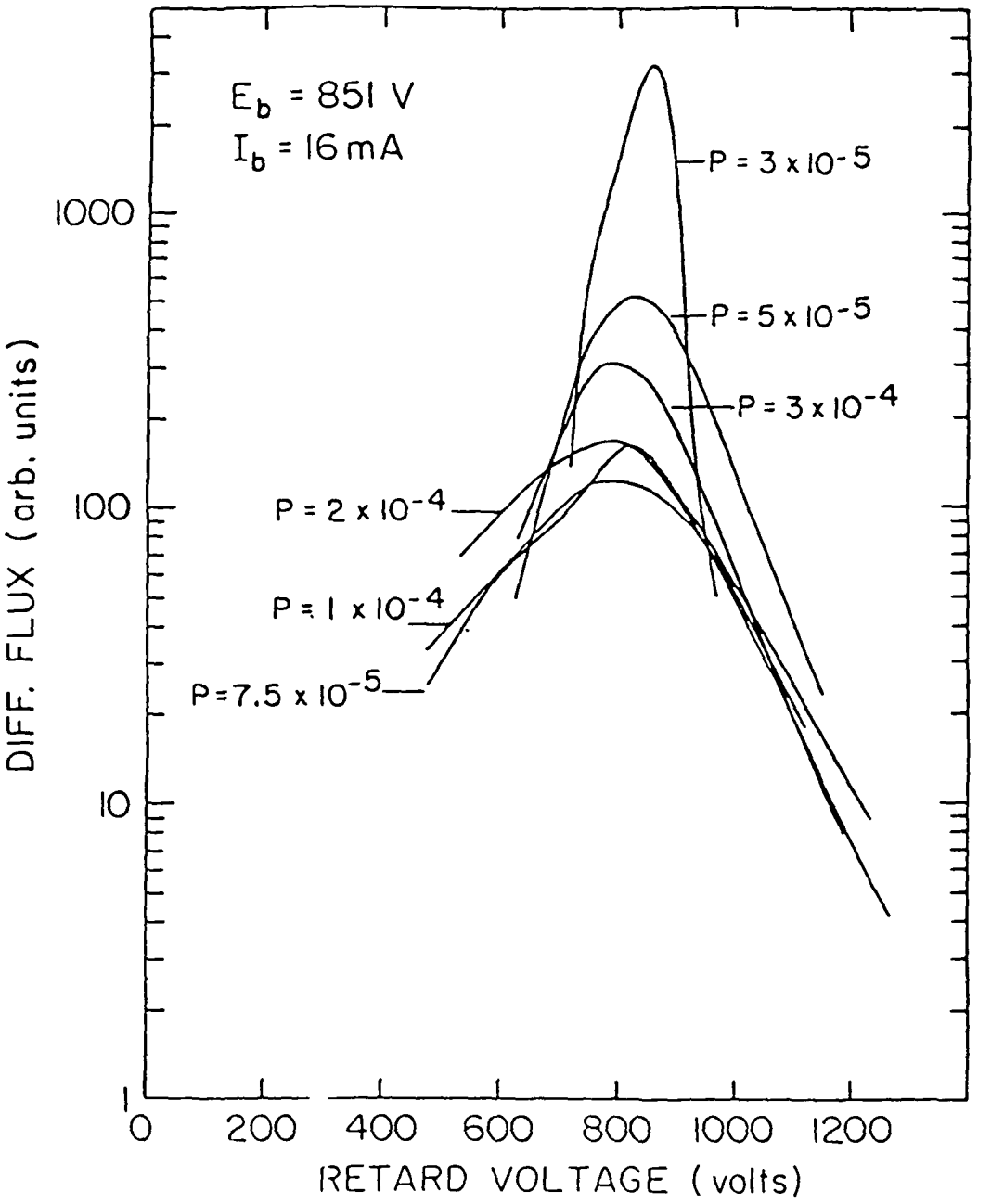
E_b = 851 V
I_b = 16 mA
P = 3 x 10-5
P = 5 x 10-5
P = 3 x 10-4
P = 2 x 10-4
P = 1 x 10-4
P = 7.5 x 10-5
DIFF. FLUX (arb. units)
1000
100
10
1
0
200
400
600
800
1000
1200
RETARD VOLTAGE (volts)

Figure 14

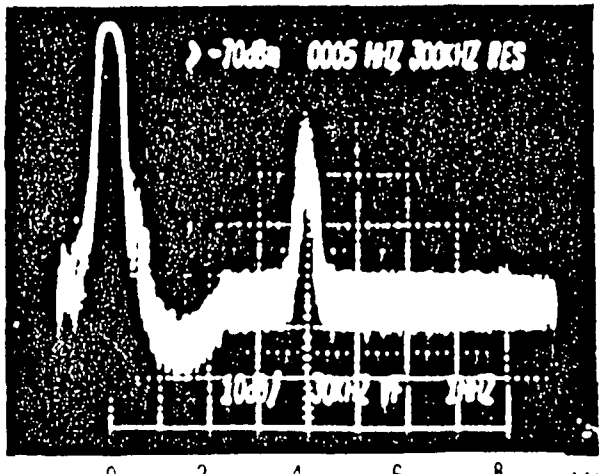

V_b = 10 kV, I = 35 ma, B = 1 23 G(max)
P = 10 x 10^{-6} Torr B = 1 07 G(min)

(a) LOW DENSITY

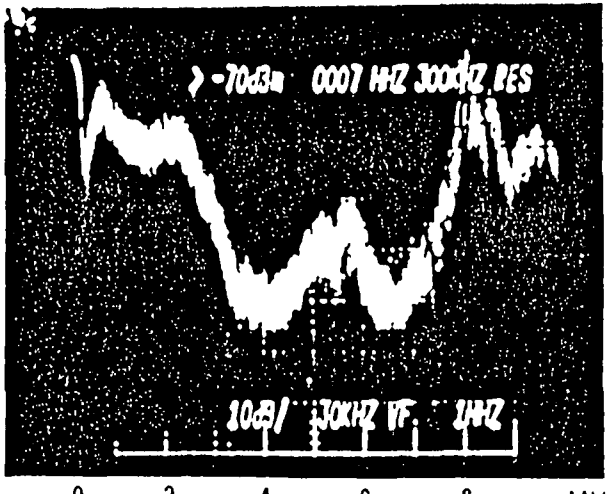

V_b = 10 kV, I = 33 ma, B = 1 23 G(max)
P = 10 x 10^{-6} Torr B = 1.07 G(min)

(b) HIGH DENSITY

Figure 15

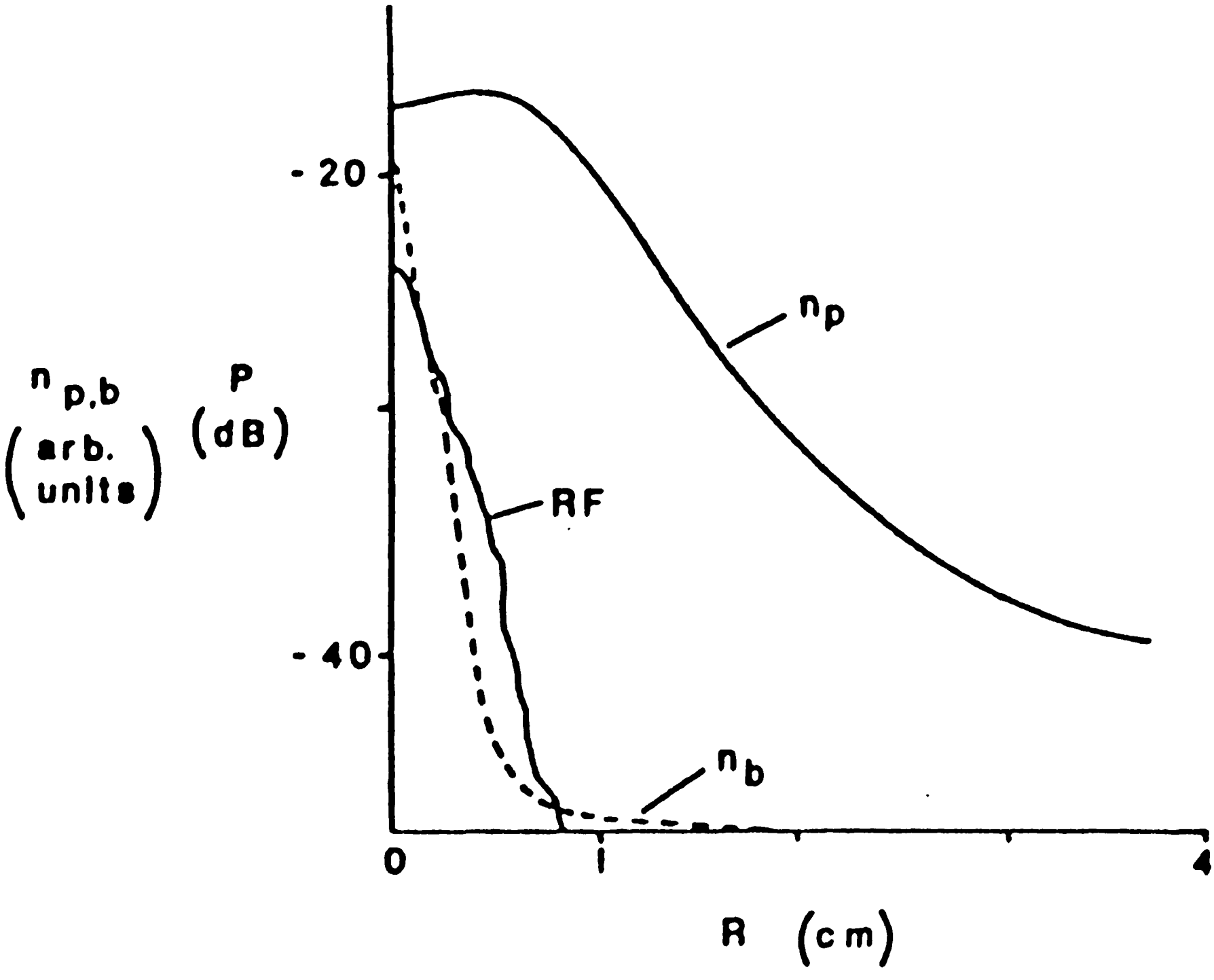

Figure 16

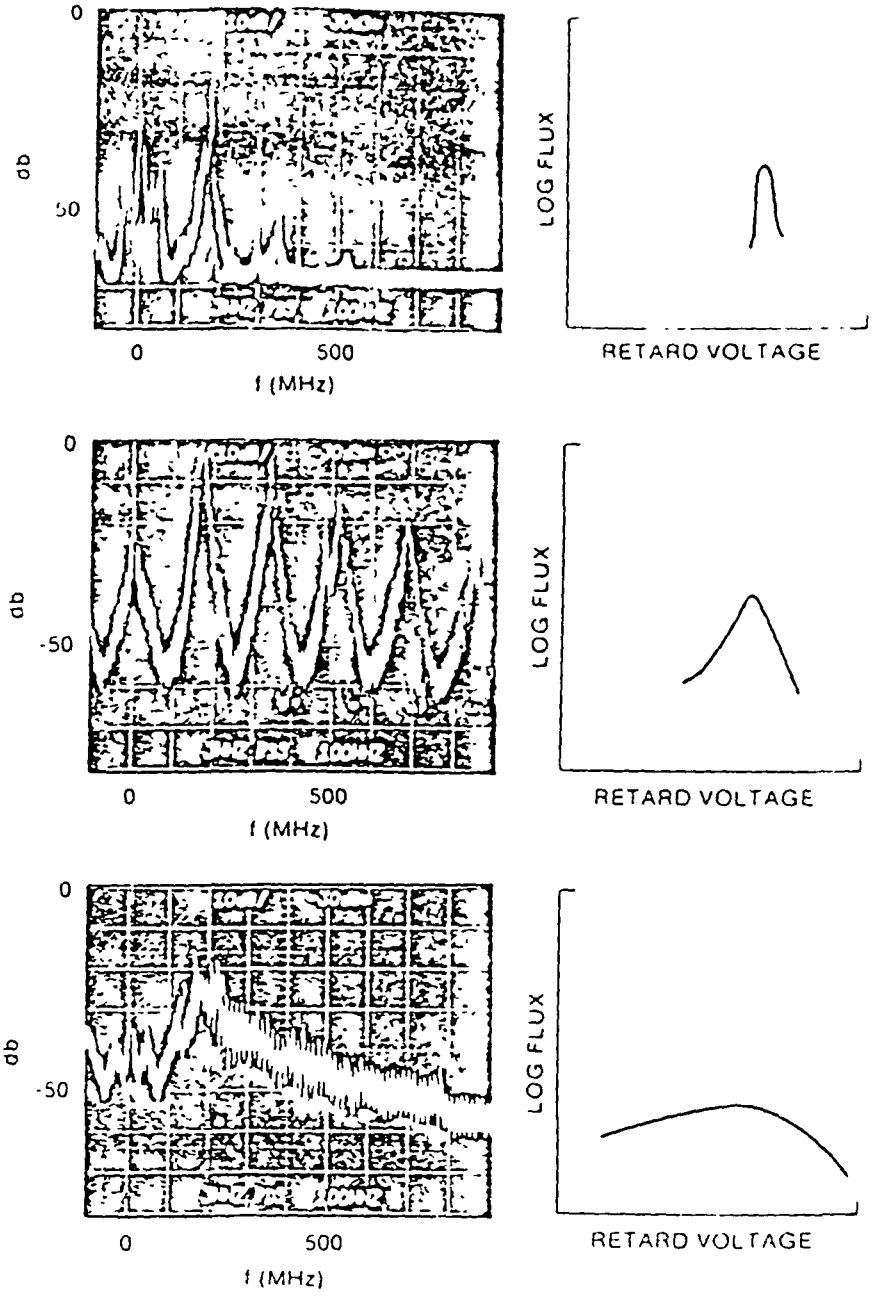

Figure 17

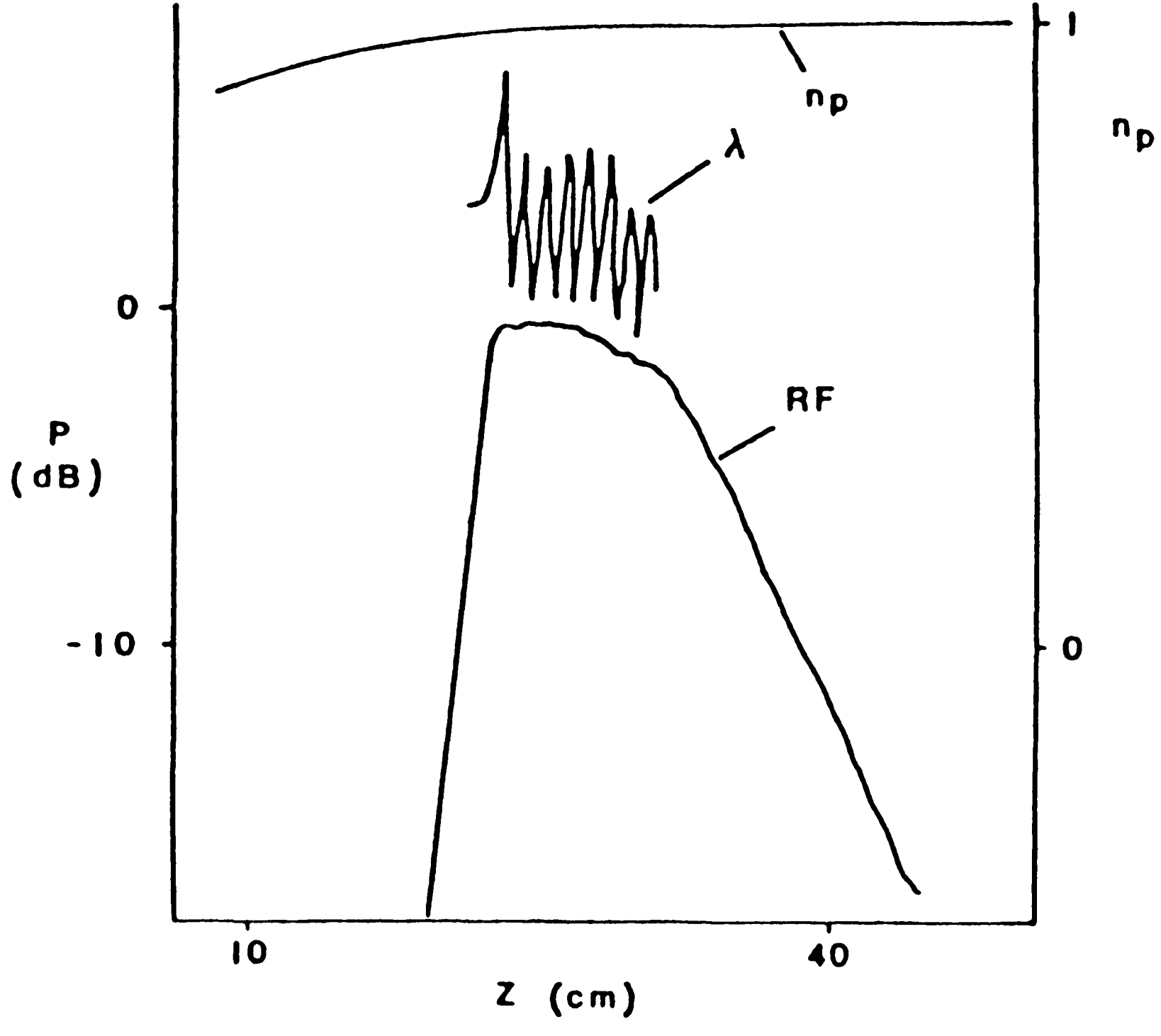

Figure 18

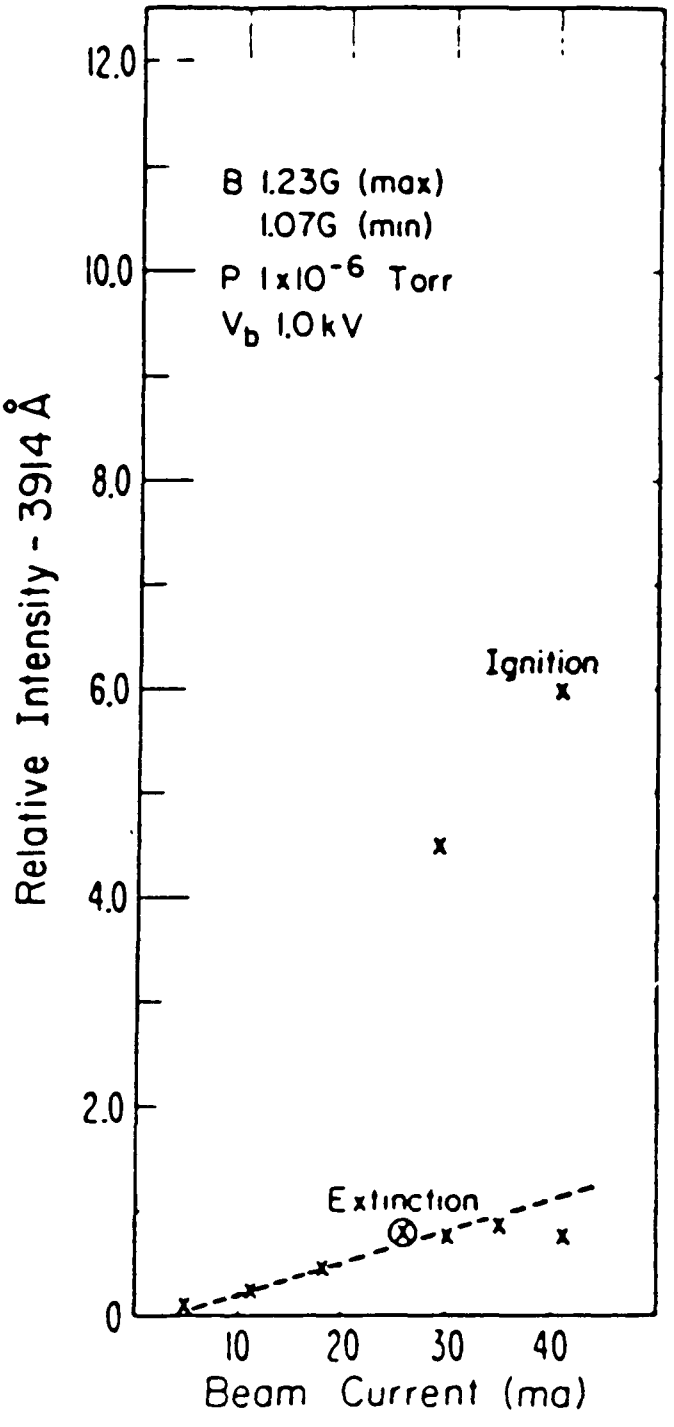
12.0
10.0
8.0
6.0
4.0
2.0
0
B 1.23G (max)
1.07G (min)
P 1x10⁻⁶ Torr
V_b 1.0kV
Ignition
Extinction
Relative Intensity - 3914 Å
10
20
30
40
Beam Current (ma)

Figure 19

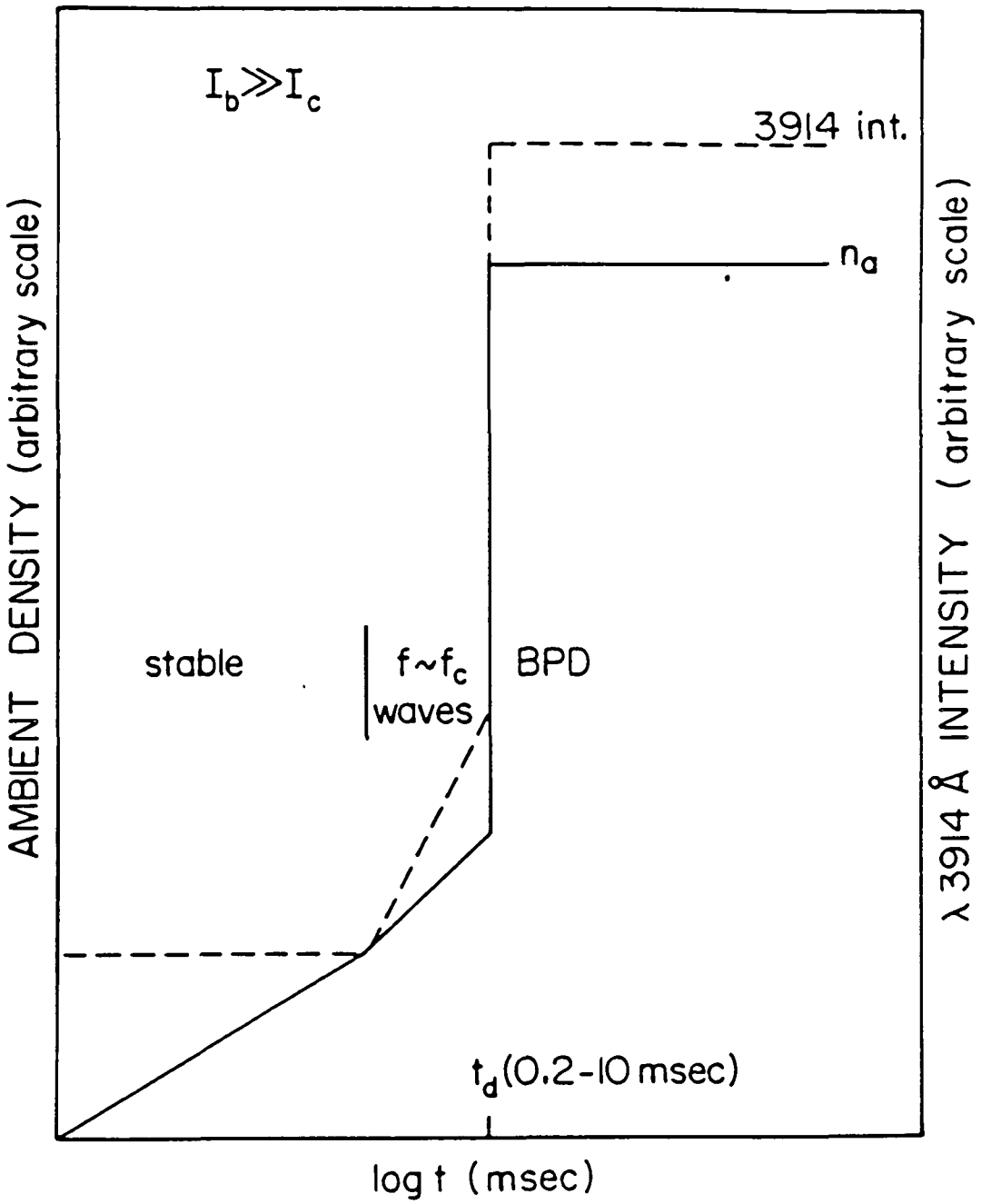
$I_b \gg I_c$
3914 int.
n_a
stable
$f \sim f_c$
waves
BPD
t_d(0.2-10 msec)
AMBIENT DENSITY (arbitrary scale)
λ 3914 Å INTENSITY (arbitrary scale)
log t (msec)

Figure 20

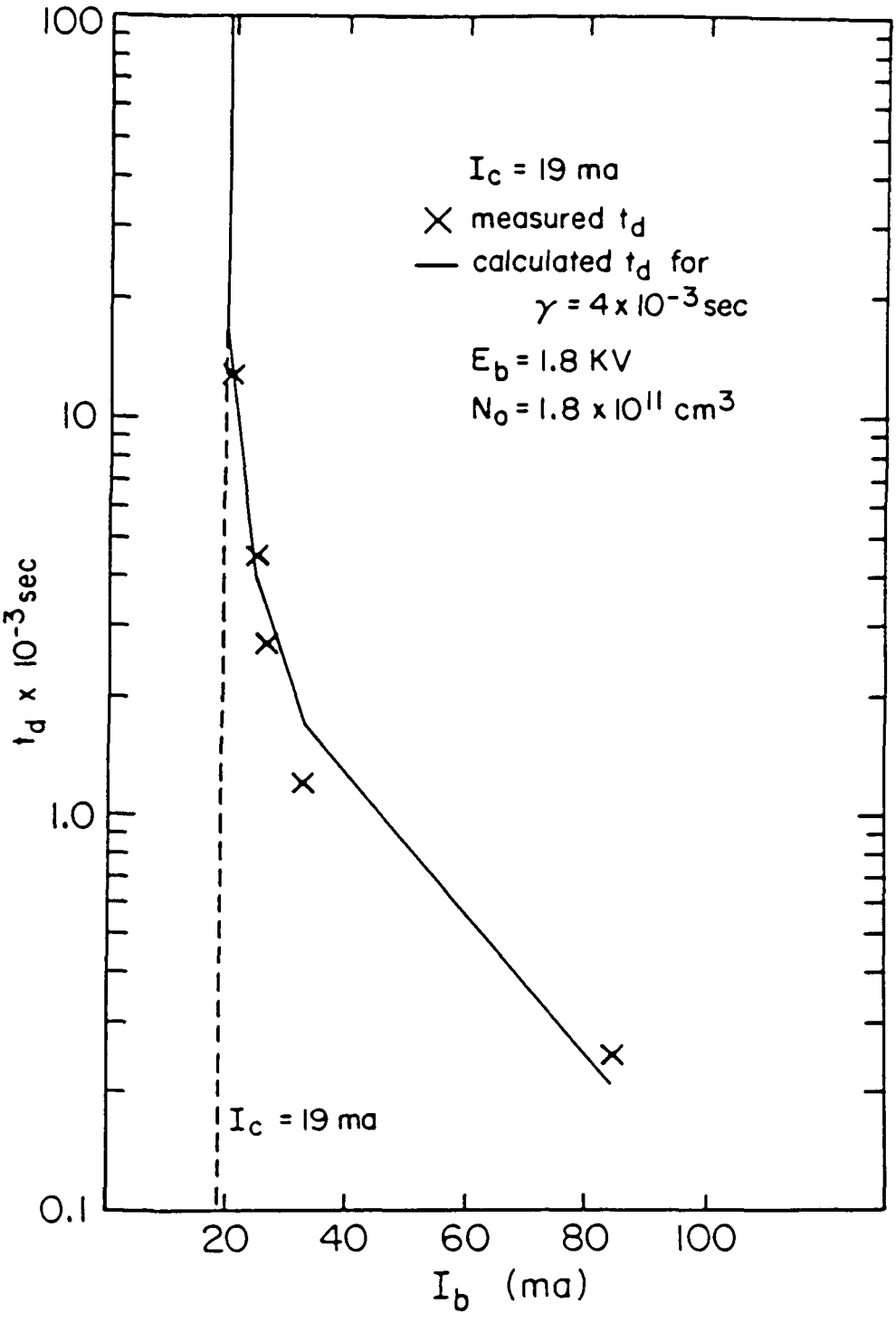
100
10
1.0
0.1
$t_d \times 10^{-3}$ sec
I_c = 19 ma
× measured t_d
— calculated t_d for
$\gamma = 4 \times 10^{-3}$ sec
E_b = 1.8 KV
$N_o = 1.8 \times 10^{11}$ cm^3
I_c = 19 ma
20
40
60
80
100
I_b (ma)

Figure 21

Section III - Laboratory Experiments

Bernstein W., H. Leinbach, H. Cohen, P. S. Wilson, T. N. Davis, T. Hallinan, B. Baker, J. Martz, R. Ziemke, and W. Huber "Laboratory observations of RF emissions at $\omega_{pe} + (n + 1/2)\ \omega_{ce}$ in electron beam-plasma and beam-beam interactions" J. Geophys. Res., 80, 4375, 1975.

Bernstein W., H. Leinbach, P. J. Kellogg, S. T. Monson and T. Hallinan "Further laboratory measurements of the beam-plasma discharge" J. Geophys. Res., 10, 7271-7278, 1979.

Bernstein W., B. A. Whalen, F. R. Harris, A. G. McNamara, and A. Konradi "Laboratory studies of the charge neutralization of a rocket payload during electron beam emission", Geophys. Res. Letters, 7, 93, 1980.

Szuszczewicz, E. P., K. Papadopoulos, W. Bernstein, C. S. Lin and D. N. Walker "Threshold criterion for a space simulation beam-plasma discharge", J. Geophys. Res., 87, 1565-1573, 1982.

Bernstein W., J. O. McGarity and A. Konradi, "Electron beam injection experiments: replication for flight observations in a laboratory beam plasma discharge," Geophys. Res. Letters, 10, 1124-1127, 1983.

Hallinan T. J., H. Leinbach, G. Mantjoukis and W. Bernstein, "Measurements of the optical emission produced during the laboratory beam plasma discharge," J. Geophys. Res., 2335-2347, 1984.

Llobet X., W. Bernstein and A. Konradi, "The spatial evolution of energetic electrons and plasma waves during the steady state beam plasma discharge," J. Geophys. Res., 90, 5187-5196, 1985.

JOURNAL OF GEOPHYSICAL RESEARCH, VOL. 87, NO A3, PAGES 1565-1573 MARCH 1, 1982

Threshold Criterion for a Space Simulation Beam-Plasma Discharge

E. P. SZUSZCZEWICZ,[1] K. PAPADOPOULOS,[2] W BERNSTEIN,[3] C S. LIN,[4] AND D. N. WALKER[1]

We have conducted an experimental and theoretical study of the threshold characteristics of a space simulation beam-plasma discharge with emphasis on density profiles and a density-dependent ignition criterion The study included various beam-plasma conditions covering beam currents from 8 to 85 ma, beam energies from 0.8 to 2 0 keV, and magnetic fields at 0 9 and 1 5 G The study included experimental determinations of radial profiles of electron density for each of the selected conditions extending from a low-density, pre–beam-plasma discharge state to a strong beam-plasma discharge condition. At beam-plasma discharge threshold it was determined that $\omega_p, \omega_c = 5\ 4$ was the density-dependent ignition criterion The experimental results are shown to agree with detailed model calculations, which consider the beam-plasma discharge to be produced by large-amplitude electron plasma waves resulting from the beam-plasma interaction

1. INTRODUCTION

A cold electron beam propagating through a weakly ionized plasma will, under proper conditions, produce a modified beam-plasma state known as the beam-plasma discharge (BPD). This discharge state has received considerable attention in recent years as a result of increased interest in mechanisms for vehicle neutralization during spaceborne accelerator experiments [*Bernstein et al*., 1980, *Cambou et al*., 1978; *Galeev et al*., 1976], enhanced beam-plasma ionization processes [*Bernstein et al*., 1978], and, in general, single-particle or collective phenomena initiated by beams injected into neutral gas and charged-particle environments [*Hess et al*., 1971, *Winckler et al*., 1975; *Hendrickson and Winckler*, 1976; *Cambou et al*., 1975; *Monson and Kellogg*, 1978, *Szuszczewicz et al*., 1979; *Jost et al*., 1980, *Winckler*, 1980]

The BPD appears at a critical energetic-electron-beam current I_B^c, with the transition from single-particle behavior ($I_B < I_B^c$, pre-BPD) to collective processes ($I_B > I_B^c$, solid BPD) described as follows for conditions in which the plasma is created by the beam itself

1 As an electron beam linearly interacts with a neutral gas, it collisionally produces a plasma with a density that varies directly with the magnitude of the beam current for a fixed beam energy

2. As the beam current is increased to a critical value I_B^c, a two-stream instability sets in and the electric fields of the excited waves heat the electrons to energies comparable to the ionization energy The 'heated' electrons create an enhanced ionization process, which results in an avalanche breakdown, the BPD

Bernstein et al [1979] have reported the dependence of this critical current I_B^c on various experimental parameters as

$$I_B^c \propto \frac{V_B^{3/2}}{B^{0.7} P L} \tag{1}$$

where V_B, B, P, and L are the beam energy (voltage), the superimposed magnetic field, the ambient neutral pressure, and the beam length (gun-to-collector distance), respectively While the $I_B^c = I_B^c(V_B, B, P, L)$ relationship was established among the controlling system parameters (with the $I_B^c \propto P^{-1}$ behavior applicable at $P \lesssim 10^{-5}$ torr), a clear dependence on plasma density was expected Early thoughts suggested that $\omega_p \geq \omega_c$ satisfied ignition threshold criteria [*Bernstein et al*., 1979; *Getty and Smullin*, 1963]. We have since had the opportunity to test this idea under various beam-plasma conditions Our results include (1) time-delay data and associated analyses indicating that BPD ignition does indeed occur at a critical density, (2) direct measurements of plasma density near ignition threshold with determinations of ω_p/ω_c, and (3) a theoretical analysis that predicts the critical density criterion

In subsequent sections we present the experimental and theoretical details, which establish the density-dependent threshold conditions for BPD at $3\ 5 \lesssim \omega_p/\omega_c \lesssim 6\ 9$

EXPERIMENT CONFIGURATION AND RESULTS

The experiment was conducted in a large vacuum chamber facility at the NASA Johnson Space Center with an experimental configuration similar to those employed in earlier investigations [*Bernstein et al*., 1979] The configuration is illustrated in Figure 1 with specific emphasis on the pulsed plasma probe measurement and the associated procedure for ω_p/ω_c determinations Not shown are the previously described diagnostics [*Bernstein et al*., 1979, *Jost et al* 1980] including the 3914-Å scanning photometer, the segmented current collector, the energetic electron electrostatic analyzer, and the remote wave detection antenna and spectrum analyzer system The beam was generated by a tungsten-cathode Pierce-type diode gun, mounted on a position-controlled cart In all cases the beam was injected parallel to the magnetic field $\vec{B}$ and terminated on a 3 × 3 m target suspended about 20 m above the gun aperture A combination of coil current and the earth's magnetic field established the B field at selected levels up to 1 5 G

In most cases the beam was injected into a neutral gas with no pre-beam plasma, however, the experimental investiga-

[1] Ionospheric Diagnostics Section, E O Hulburt Center for Space Research, Space Science Division Naval Research Laboratory, Washington D C 20375
[2] Science Applications Inc , McLean, Virginia 22102
[3] Center for Space Physics Department of Space Physics and Astronomy, Rice University Houston, Texas 77001
[4] Bendix Field Engineering Corporation, Columbia, Maryland 21045

Paper number 1A1703

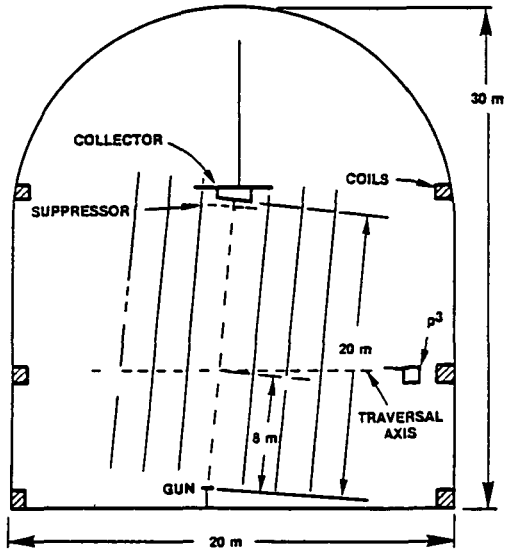

Fig. 1 Experiment configuration

tion included two cases in which the chamber was filled with a plasma created by a Kauffman-type argon ion thruster. In these cases the pre-beam plasma density was lower than the critical density at BPD ignition.

The investigation was conducted in two stages. First, pulsed-gun experiments were carried out to test the concept of a density-dependent threshold condition against the original ideas of *Getty and Smullin* [1963] After the concepts check, a series of direct density measurements was conducted to quantitatively establish the density criteria We describe the results in the order in which the experiments were conducted.

Time Delay Arguments for N_e^c

In pulsed-beam experiments with $I_B \gg I_B^c$, *Getty and Smullin* [1963] identified three sequential phases in the temporal evolution into the BPD (1) a quiescent stable period, (2) an intermediate period during which the gross features of the beam remained unchanged but waves with $f \approx f_{ce}$ were present, and (3) BPD ignition. They suggested that phases 1 and 2 corresponded to the time required for buildup of the ambient density to a critical value a value at which the BPD ignited To test this concept in the space simulation beam-plasma efforts at the JSC facility a series of pulsed-beam measurements were performed to study the temporal evolution of the BPD in the configuration shown in Figure 1 All diagnostics sensitive to the transition to BPD demonstrated identical time delays between beam current initiation and BPD ignition At low pressure ($<4\,(10^{-6})$ torr) the Getty and Smullin phase 2 (characterized by $f \approx f_{ce}$ waves) was clearly evident Figure 2 shows the measured delay times as a function of beam current with values ranging from 0 1 to 20 ms The results in Figure 2 can be understood in terms of a simple time dependent model. If it is assumed that the plasma loss rate is proportional to its density, then the temporal buildup of plasma by electron-neutral collisions is given by

$$\frac{dN_e}{dt} = \gamma - \nu N_e \tag{2}$$

Equation (2) has the solution

$$N_e(t) = \frac{\gamma}{\nu}(1 - e^{-\nu t}) \tag{3}$$

where $\gamma = I_B \sigma N_0/eA$ is the electron-ion pair production rate, ν is the loss rate, σ is the electron impact ionization cross section, N_0 is the neutral density, and A is the beam cross section. At short times, the density will increase linearly with time ($N_e = \gamma t$), and at longer times the density will approach the time independent value $N_e = \gamma/\nu$ If, indeed, there is a critical density N_e^c required for BPD ignition and if we define its relationship to a critical beam current by $N_e^c = (\sigma N_0/eA\nu)I_B^c$, then the time delay t_d until $N_e(t) = N_e^c$ can be obtained from (3) and written as

$$t_d = -\frac{1}{\nu}\ln\left(1 - \frac{I_B^c}{I_B}\right) \tag{4}$$

For $I_B \approx I_B^c$, relatively long delay times should be observed with a rapid decrease in t_d as I_B is increased This is exactly the behavior demonstrated in Figure 2, where the solid curve has been normalized to the data by selecting $I_B^c = 20$ ma and $\nu \approx 400\ s^{-1}$ The good agreement between the simple model calculations and the experimental results supports the concept of a critical density threshold for BPD ignition, but the normalization procedure provides little measure for an absolute value of N_e^c Specific determinations of the critical density threshold criteria are detailed in the next two sections.

Direct Measurements of Critical Density

To establish quantitatively the density dependent threshold criterion for the ignition of a space simulation BPD, emphasis was placed on the direct measurement of plasma density profiles over a range of beam-plasma conditions covering beam currents from 8 to 85 ma, beam energies from 0 8 to 2 0 keV, and magnetic fields at 0 9 and 1 5 G The

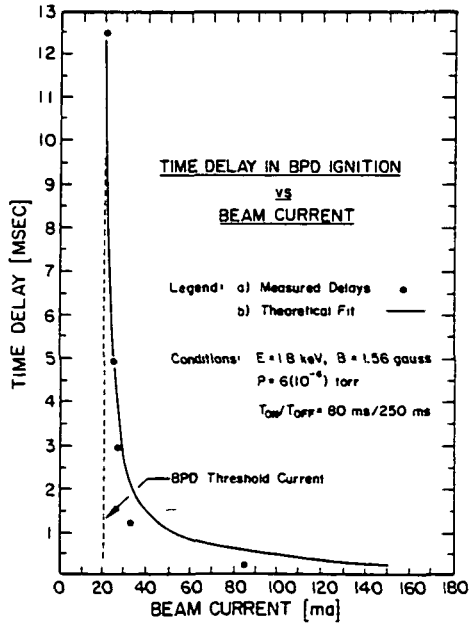

Fig 2 Time delay in the ignition of the beam-plasma discharge with threshold current at 20 ma Electron gun operation was in the pulsed mode with T_{on}/T_{off} = 80 ms/250 ms

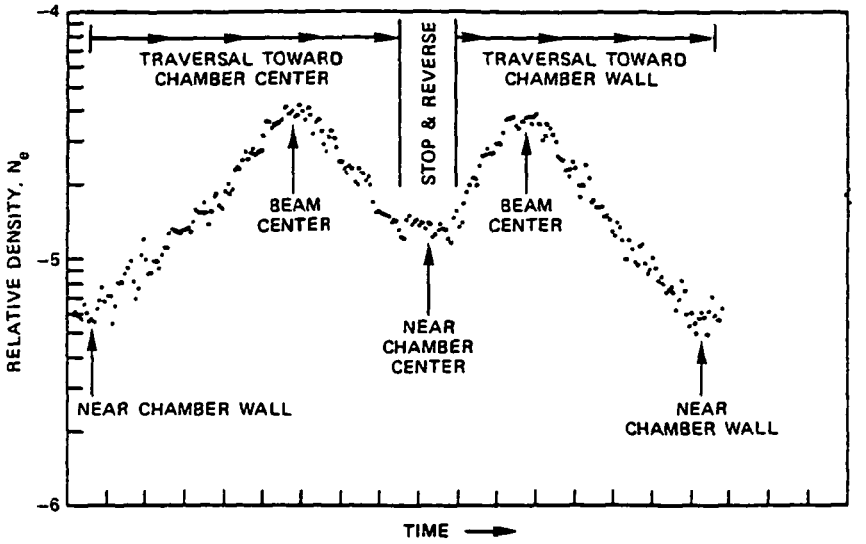

Fig. 3 Radial profile of relative electron density under pre-BPD conditions Run 57 (I_B, V_B, B) = (7 ma, 1 3 keV, 0.9 G) The figure shows two cuts through the beam-plasma profile, as time increases from left to right the plasma density probe moves into and through the beam center, then reverses and passes through the beam a second time The symmetry verifies that beam-plasma conditions were stable during the execution of the radial traversal

procedure involved experimental determinations of radial profiles of electron density for each of the selected conditions extending from a low-density, pre-BPD state to a strong BPD condition. The experimental configuration, illustrated in Figure 1, involved a pair of pulsed-plasma-probes (P^3) mounted on a radial traversal mechanism positioned at approximately 8 m above the injection point of the beam. Each of the probes provided simultaneous measurements of electron density N_e, temperature T_e, plasma potential V_∞, and density fluctuation power spectra $\delta N_e(\rightarrow P_n(k))$ with capabilities for the associated diagnostics in a dynamic plasma environment and under test conditions that could contaminate electrode surfaces [*Holmes and Szuszczewicz*, 1975, 1981, *Szuszczewicz and Holmes*, 1975, 1976].

The plasma density measurements were made for seven different conditions, each identified by preselected values for V_B, B, P and the existence or nonexistence of a pre-beam plasma. For each condition a steady state value for I_B was set, the traversal mechanism was exercised, and an electron density profile was recorded. A sample profile collected under pre-BPD conditions is presented in Figure 3 The abscissa is time relative to the start of the radial traversal, and the ordinate is relative electron density as determined by base line electron-saturation currents collected by the E probe (The second in the two-probe configuration was defined as the I probe because the associated base line currents were collected in the ion-saturation portion of the probe's current-voltage characteristic [*Holmes and Szuszczewicz*, 1975, 1981].) At the start of each traversal the probe was at its outermost position relative to the center of the chamber As time increased, the probe was moved into and through the beam, at maximum penetration toward the chamber center, the traversal system was reversed, allowing a second measurement of the density profile as the probe moved back to its original outermost position. With this procedure the probe's maximum penetration toward the chamber center is identified by the symmetry point in the 'double' profile. The symmetry in the double profile provided confidence that beam-plasma conditions were unchanged during the measurement.

Absolute electron densities were determined by standard P^3 analysis procedures summarized graphically in Figure 4 The technique provides a high-frequency (10^3 Hz in this experiment) determination of relative electron density through the direct measurement of baseline electron-saturation currents. (The baseline currents provide the fundamental data for the relative density profiles presented in Figures 3, 5*a*, and 5*b*) Simultaneously, the technique generates a 'conventional' Langmuir probe characteristic The relative density fluctuations (as indicated by the variations in the base line current) are then unfolded from the raw, uncorrected probe characteristic (Figure 4*a*) yielding a smooth, corrected curve (Figure 4*b*) to which conventional N_e analysis procedures [*Chen*, 1965; *Szuszczewicz and Holmes*, 1977] are applied This procedure, utilized for all beam-plasma conditions included in this investigation, provided a direct scaling of baseline current measurements to absolute electron densities

Complete profile information and associated plasma wave signatures are presented for two independent conditions in Figures 5 and 6 (Note Because of changes in plasma potential, the relative density profiles do not maintain the same scaling to absolute values from run to run) For values of (V_B, B) = (1 3 keV, 0 9 G) and (2 0 keV 1 5 G) in Figures 5 and 6, respectively, the beam current I_B was stepped through a sequence allowing for complete coverage of conditions that encompassed pre-BPD, threshold-BDP, and solid-BPD Because $I_B' = I_B(V_B, B, P, L)$ is known to exhibit hysteresis as I_B is varied about the critical value I_B', the following procedure was utilized in the step-wise selection of beam current levels.

1 With V_B fixed, I_B was steadily increased in a 'search mode to determine an approximate value for I_B'

2 I_B was reset to zero, then increased slowly to I_B' with careful observation of the RF spectrum Threshold was defined as that level at which the RF spectrum was in

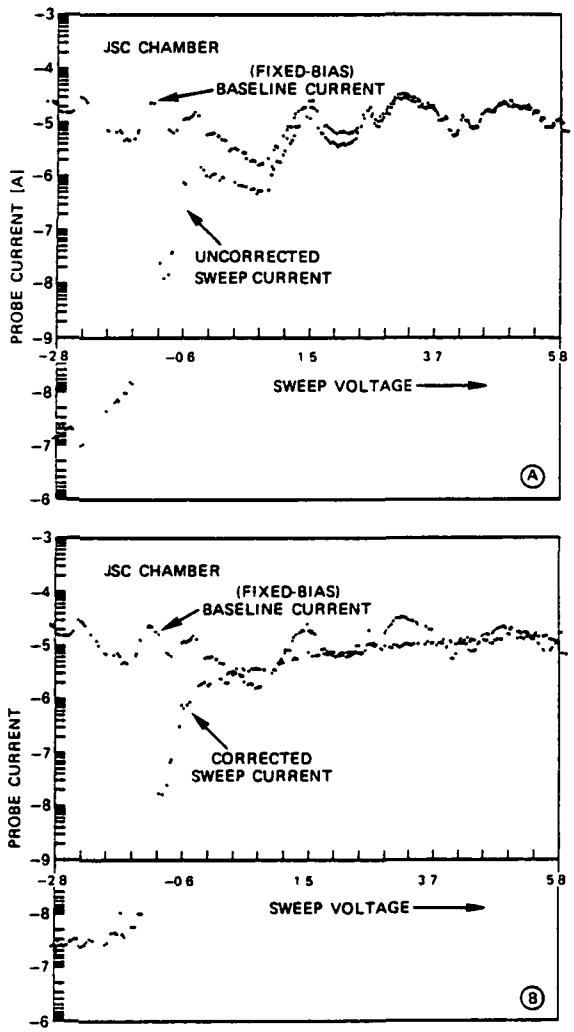

Fig 4 (*a*) Sample of raw probe data showing the effects of density fluctuations (baseline electron-saturation currents) on the probe s current-voltage characteristic (sweep currents) (*b*) The corrected' characteristic that results when density fluctuations have been unfolded The electron saturation portion of the characteristic is then amenable to conventional analyses for determination of N_e (see text)

transition from its pre-BPD signature (flat spectrum at high frequencies, $f \gtrsim f_p$) to its solid BPD characteristic (intense features at $f \gtrsim f_p$) At this transition level (defined here as threshold) the beam-plasma system oscillated between its two states at a repetition frequency generally observed to be no greater than several hertz If the RF spectrum locked up in a characteristically stable RF BPD signature, step 2 was restarted and the previous I_B' level more carefully approached (It is important to note that the time dependent photographs of the threshold RF spectrum, e g., runs 57 and 81, erroneously indicate a solid BPD spectrum and do not reflect the oscillations between the two beam-plasma states) The conditions at threshold and under BPD are summarized in Table 1 where the peak density N_e^{max}, associated plasma frequency $2\pi\omega_p^{max}$, and plasma-to-cyclotron frequency ratio ω_p^{max}/ω_c are also listed. The results can be summarized by $\omega_p/\omega_c = 5.4_{-1.9}^{1.3}$ as the density dependent threshold condition for the BPD As we will show in the next section, this result is consistent with a threshold model, which assumes that BPD is triggered by the onset of a beam plasma instability.

It is proper to introduce one qualification regarding the experimentally determined values for ω_p/ω_c By virtue of the experimental procedure they could represent averages between two beam-plasma states (pre-BPD and solid BPD) The consequence of this in the interpretation of the experimental values is merely one of definition. For example, if threshold were strictly defined as the maximum density under stable pre-BPD conditions (i.e., no oscillations into the solid BPD state), then $(\omega_p/\omega_c) = 5.4$ would represent an upper limit. Extrapolation of complementary sets of data suggests that the associated 'adjustment' in critical density for cases at 0 9 G is inconsequential, while corresponding adjustments at 1 5 G could be as large as a factor of 2–3 The end results would be $\omega_p/\omega_c \approx 4.4$ as compared with the experimentally defined average at 5 4.

Before proceeding to the theoretical treatment, it is appropriate to discuss several of the plasma density and wave-related features in the data presented in Figures 5 and 6

Run 56 (upper left panel Figures 5*a* and 5*b*) is very typical of a pre-BPD environment, in that the beam center (see, e.g., Figure 3) is well defined and of relatively narrow cross section, with an RF signature (upper left panel Figure 5*b*) that is flat in character. At BPD threshold the beam-plasma system intermittently emits RF at and around the plasma frequency, and the plasma expands in cross section (lower left panel, Figure 5*a*) eliminating the narrow beam profile characteristic of the pre-BPD state (Figures 3 and 5*a* upper left). We note that the RF signatures are highly time dependent, generally fluctuating in intensity and in frequency Similarly, the local plasma densities are highly time dependent (see, e.g., I_B fluctuations in Figure 4) with that dependency averaged out over 1-s intervals for the relative density profiles in Figure 5 and 6

As I_B is increased above the threshold level (runs 58 and 59 in Figures 5*a* and 5*b*), the plasma density increases and the radial profiles take on variable configurations. In run 58, for example, the beam center is 'depleted' with an increased density level at its edges This configuration has been observed in a number of cases and is thought to manifest electron heating in the beam core with generally higher diffusion rates and associated losses The profile becomes more complex in run 59, possibly due to higher order diffusion modes

The results in Figure 6 have been selected to present information at a higher applied magnetic field and to illustrate that the description of beam-plasma profiles offered in connection with Figure 5 is by no means considered universally applicable to the various levels of the BPD Our current level of understanding does not allow for a detailed cause-effect description of each and every profile, but at present we would point to Figure 5*a* as the simplest configuration that illustrates the transition from pre-BPD to the solid BPD state

Theoretical Considerations and Discussion of Results

Before presenting the theoretical details of the BPD threshold criteria as applied to the present experiment, it is important to discuss some aspects of our model that play a key role in the interpretation of the experimental results

For all experimental parameters the relevant mean free paths (i e., thermalization, ionization, etc.) were much longer than the system length L. This, as discussed in detail by *Papadopoulos* [1981] for a finite system, leads to a requirement for axial confinement of both the ionizing and the ambient electrons. As shown in the above paper, the required axial confinement can be achieved if the energy deposited by the beam electrons is absorbed by only a few ambient electrons (i.e , 1%), which are accelerated to energies larger than the ionization potential. A fraction of these electrons quickly escapes the system, thereby building potential sheaths at the ends. The sheaths accelerate ambient ions to escape at the rate of the fast electrons, while trapping the cold part of the energetic electron population A detailed description of the process can be found in the work of *Papadopoulos* [1981]. For the purposes of the present paper, we retain the requirement that the collisionless mechanism responsible for BPD should deposit most of its energy in suprathermal tails with energy much larger than the ionization energy while leaving the majority of the electrons cold As discussed in many publications [*Papadopoulos and Coffey*, 1974*a*, *b*, *Papadopoulos and Rowland*, 1978, *Linson and Papadopoulos*, 1980; *Papadopoulos*, 1982], this can be achieved if the frequency of the excited waves is near the

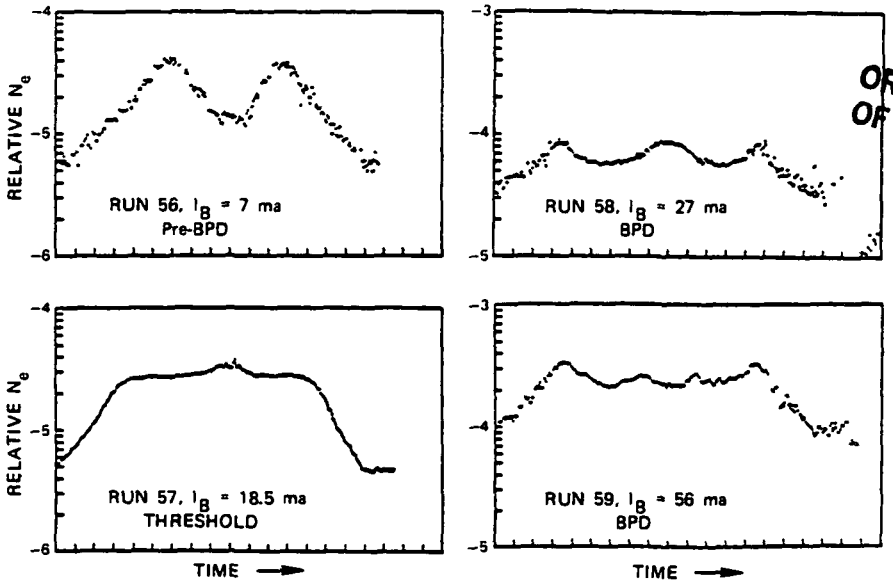

Fig 5*a*

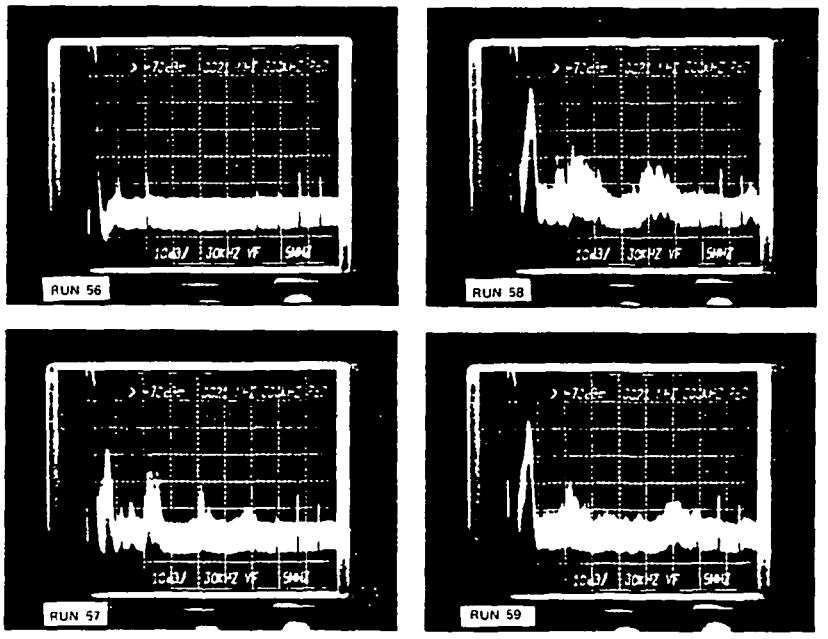

Fig 5*b*

Fig 5 (*a*) Sequence of relative plasma density profiles and (*b*) associated plasma wave signatures for increasing values of beam current I_B at a fixed condition (V_B, B) = (1 3 keV, 0 9 G) encompassing runs 56–59 (pre-BPD through solid BPD)

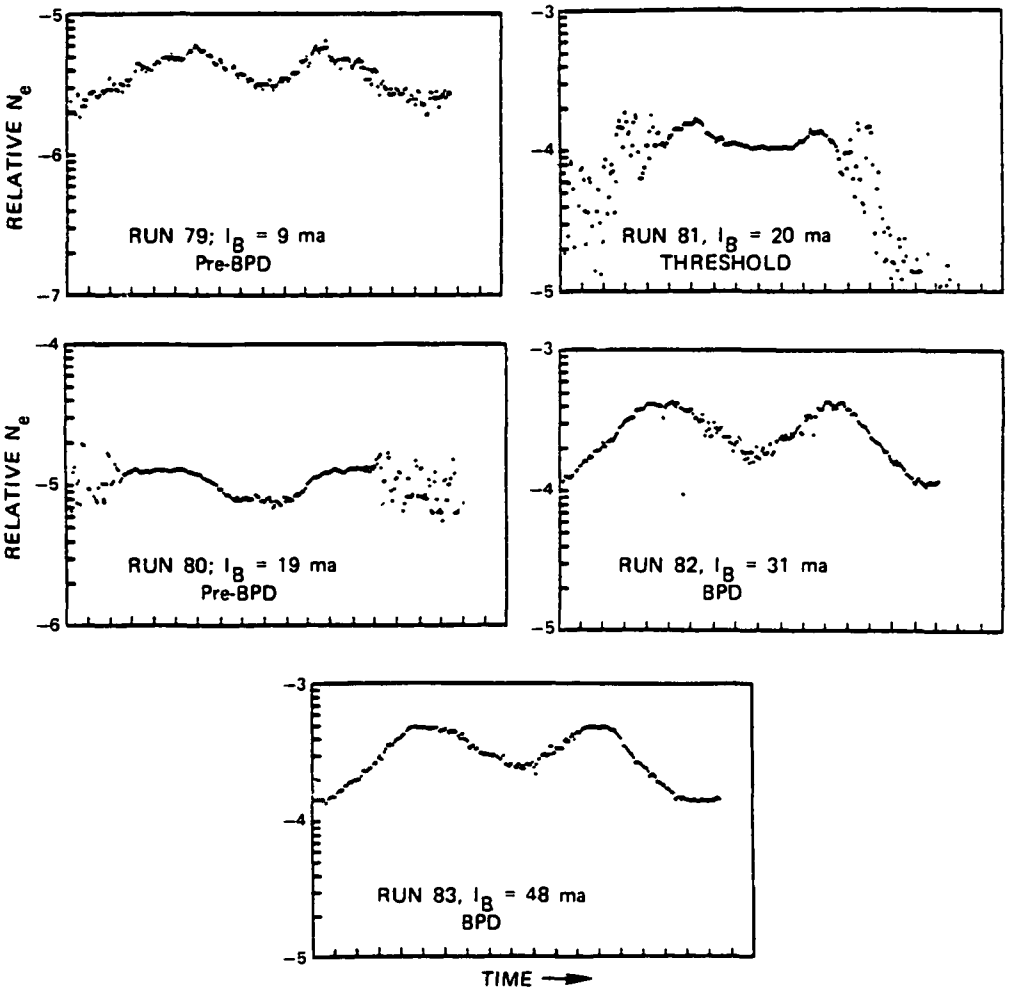

Fig 6*a*

Fig 6 (*a*) Sequence of relative plasma density profiles and (*b*) associated plasma wave signatures for increasing values of beam current I_B at a fixed condition (V_B, B) = (2 0 keV 1 5 G) encompassing runs 79 through 83 (pre-BPD through solid BPD)

electron plasma frequency ω_p and the wave energy $W/(n_e T_e)$ is greater than $k^2\lambda_D^2$, where W is the field energy density, n_e is the ambient electron density, T_e is the electron temperature, k is the wave number of the instability, and λ_D is the Debye length In order for substantial $W/(nT_e)$ to be built in a finite length system, the instability should be almost absolute The dispersion relation for a beam plasma system is [*Linson and Papadopoulos*, 1980, *Rowland et al* , 1981]

$$k_z^2\left(1-\frac{\omega_p^2}{\omega^2}\right)-k_\perp^2\left(1-\frac{\omega_p^2}{\omega^2-\omega_c^2}\right)-k_z^2\frac{\alpha\omega_p^2}{(\omega-k_z v_b)^2}-k_\perp^2\frac{\alpha\omega_p^2}{(\omega-k_z v_b)^2-\omega_c^2}=0 \quad (5)$$

where $k_\perp^2 \equiv \Gamma_{s1}^2/r_0^2$ with Γ_{s1} the roots of the Bessel function $J_1(\Gamma_{s1}) = 0$ and r_0 the beam radius In (5), α is the beam-to-plasma density ratio, ω_p and ω_c are the plasma and electron cyclotron frequencies, v_b is the beam velocity, and k_z is the parallel wave number. On the basis of (5), we can find [*Rowland et al.*, 1981] that an almost absolute instability can be excited near ω_p for

$$\frac{k_\perp^2}{k_z^2} \le 1 \quad (6)$$

Coupling this inequality with $k_z \approx \omega_p/v_b$ and $k_\perp = 2\ 4/r_0$ gives our required threshold condition as

$$\omega_p^2 \ge \frac{(2\ 4)^2 v_b^2 \cos^2\theta_i}{r_0^2} \quad (7)$$

The criterion (7), with θ_i being the beam s angle of injection relative to the magnetic field, can be generalized to the case where the plasma radius R is different from the beam radius r_0 [*Rowland et al* , 1981] In this case, (7) becomes

$$\omega_p^2 \ge 2\frac{v_b^2\cos^2\theta_i}{r_0^2 \ln(R/r_0)} \quad (8)$$

The value of r_0 is given by considering both the Larmor radius as well as the term including space charge beam

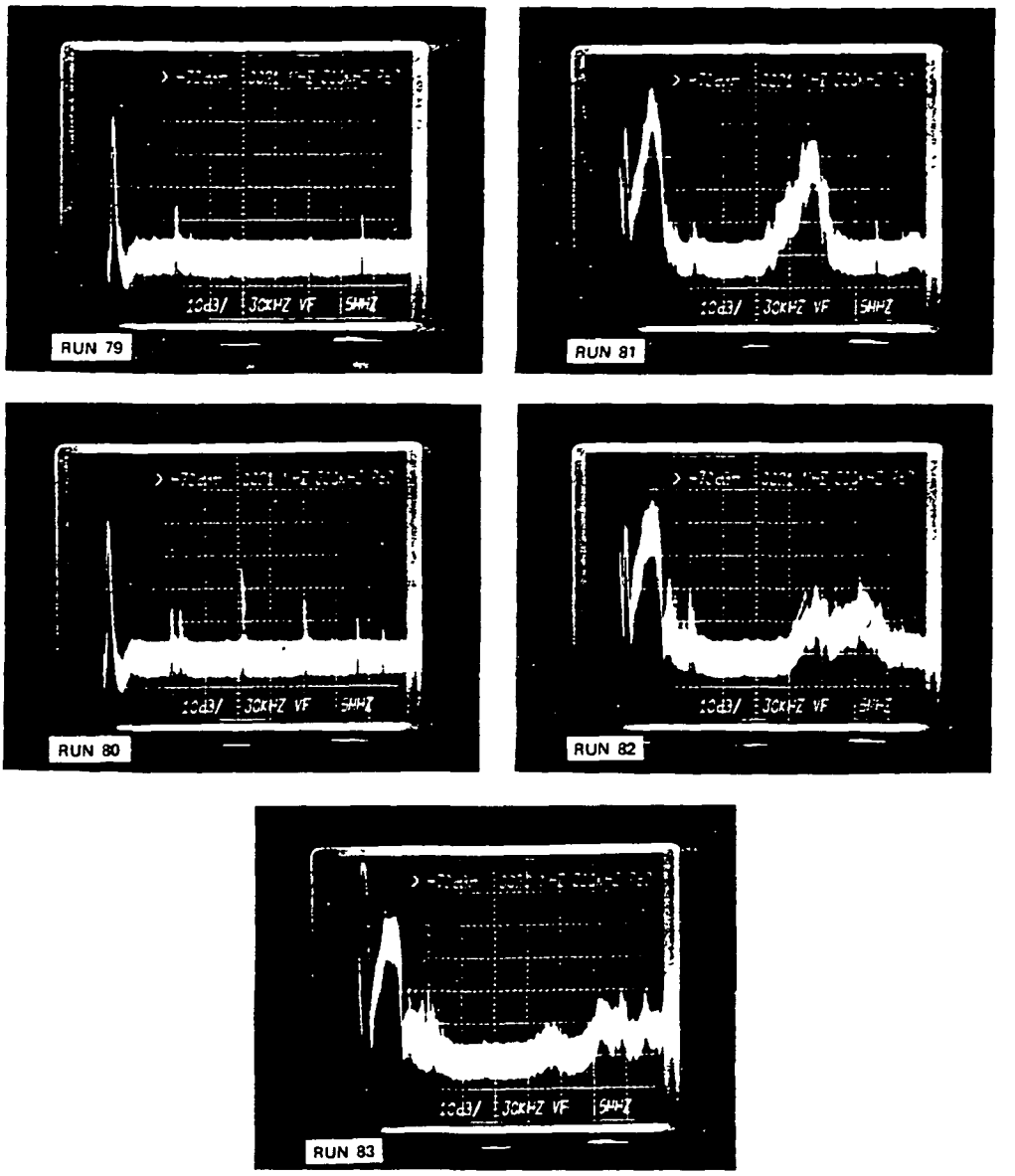

Fig. 6b

TABLE 1 Abbreviated Summary of Beam-Plasma Survey

RUN #	BEAM-PLASMA STATE	ELECTRON GUN		CHAMBER CONDITION			N_e max	f_c	f_p/f_c
		I_B [ma]	V_B [v]	B [g]	P [Torr]	THRUSTER			
40	THRESHOLD	37	1 9 (10^3)	0 9	0 7–1 5 (10^{-5})	ON	3 6 (10^6)	2 5 (10^6)	6 8
41	BPD	47	1 9 (10^3)	0 9	0 7–1 5 (10^{-5})	ON	5 6 (10^6)	2 5 (10^6)	8 4
48	THRESHOLD	34	1 9 (10^3)	0 9	0 7–1 5 (10^{-5})	OFF	3 3 (10^6)	2 5 (10^6)	6 5
49	BPD	45	1 9 (10^3)	0 9	0 7–1 5 (10^{-5})	OFF	5 0 (10^6)	2 5 (10^6)	8 0
57	THRESHOLD	18 5	1 3 (10^3)	0 9	0 7–1 5 (10^{-5})	OFF	1 5 (10^6)	2 5 (10^6)	4 4
58	BPD	28	1 3 (10^3)	0 9	0 7–1 5 (10^{-5})	OFF	4 5 (10^6)	2 5 (10^6)	7 6
63	THRESHOLD	7 8	800	0 9	0 84–1 5 (10^{-5})	OFF	0 98 (10^6)	2 5 (10^6)	3 5
64	BPD	9 9	800	0 9	0 84–1 5 (10^{-5})	OFF	2 6 (10^6)	2 5 (10^6)	5 7
69	THRESHOLD	7 8	800	0 9	0 7 (10^{-5})	ON	3 8 (10^6)	2 5 (10^6)	6 9
70	BPD	10	800	0 9	0 7 (10^{-5})	ON	3 6 (10^6)	2 5 (10^6)	6 8
81	THRESHOLD	20	2 0 (10^3)	1 5	0 6–1 2 (10^{-5})	OFF	7 0 (10^6)	4 2 (10^6)	5 6
82	BPD	30 5	2 0 (10^3)	1 5	0 6–1 2 (10^{-5})	OFF	1 8 (10^7)	4 2 (10^6)	9 1
86	THRESHOLD	12	1 3 (10^3)	1 5	0 6–1 2 (10^{-5})	OFF	3 9 (10^6)	4 2 (10^6)	4 2
87	BPD	18	1 3 (10^3)	1 5	0 6–1 2 (10^{-5})	OFF	1 1 (10^7)	4 2 (10^6)	7 1

C-2

TABLE 2. Comparison Between Theory and Experiment

Run Number	V_B, keV	I_B, ma	ω_p/ω_c (Calculated)	ω_p/ω_c (Observed)
40	1 9	37	4 2	6 8
48	1 9	34	4 4	6 5
57	1 3	18 5	4 5	4 4
63	0.8	7 8	4 7	3 5
69	0 8	6 2	5 37	6.9
81	2	20	5 95	5 6
86	1 3	12	5 55	4 2

expansion [*Linson and Papadopoulos*, 1980] This gives

$$r_0 = 2.1 \frac{I_B^{1/2}}{B V_B^{1/4}} \left(\ln \frac{r_0}{r_g} + \frac{33}{\kappa} \sin^2 \theta_d \right)^{1/2} m \qquad (9)$$

where κ is gun perveance in micropervs, r_g is the gun radius, I_B and V_B are the beam current in amps and energy in keV, the magnetic field B is in gauss, and θ_d is the beam divergence angle. (We note that equation (8) does not include the possibility of beam neutralization by ambient plasma This could result in an overestimate of r_0.) From (8) and (9) and by using $r_g \approx 2$ mm and $r_0/R \approx \frac{1}{2}$ as observed, we find

$$\frac{\omega_p}{\omega_c} \geq \frac{0\ 5\ V_B^{3/4}}{I_B^{1/2}} \frac{\cos \theta_i}{(1 + (8.5/\kappa) \sin^2 \theta_d)^{1/2}} \qquad (10)$$

We can see that the ω_p/ω_c ratio at threshold (with $\kappa \approx 1$ microperv) is rather insensitive to the beam injection angle for $\theta_i \leq 60°$ In Table 2 we present the values of ω_p/ω_c computed on the basis of equation (10) by taking $\cos \theta_i/(1 + (8\ 5/\kappa) \sin^2 \theta_d)^{1/2} \approx 1$ for near parallel injection. From Table 2 we find the average computed value to be $\omega_p/\omega_c = 4\ 95$ This result, while subject to moderate uncertainties in r_0/R, is taken to be in excellent agreement with the experimentally derived conditions (Table 1 and equation (4)) providing complementary arguments that confirm the original suggestion that the ignition of the BPD was coupled to a density-dependent threshold criterion We should mention that the above theory is consistent with the observational facts that the temperature of the plasma electrons is much lower than the ionization potential [*Szuszczewicz et al.*, 1979], and energetic tails are observed within the beam-plasma core [*Szuszczewicz*, 1982]

Acknowledgments The various elements in this investigation were supported in whole or in part by NASA grant NAGW-69 Rice University subcontract NAS 8-33777-1 and NASA/NOAA contract NA79RAE0039 Supplementary funding was also provided by the Office of Naval Research under Program Element 61153N-33 in Task Area RR033-02 We wish to thank J C Holmes for his critical care in electronics design of the P^3 instrumentation, L Kegley for technical assistance in experiment execution, and L Linson for his review and comments on the manuscript

The Editor thanks R J Jost and P J Kellogg for their assistance in evaluating this paper

REFERENCES

Bernstein W, H Leinbach, P Kellogg, S Monson, T Hallinan O K Garriott A Konradi, J McCoy P Daly, B Baker, and H R Anderson Electron beam injection experiments The beam-plasma discharge at low pressures and magnetic field strengths, *Geophys Res Lett*, *5*, 127, 1978.

Bernstein, W, H. Leinbach, P J Kellogg, S J Monson, and T Hallinan, Further laboratory measurements of the beam-plasma discharge, *J Geophys Res*, *84*, 7271, 1979

Bernstein, W, B. A. Whalen, F R Harris, A G McNamara, and A Konradi, Laboratory studies of the charge neutralization of a rocket payload during electron beam emission, *Geophys Res Lett.*, *7*, 93, 1980

Cambou, F, V S Dokoukine, V N Ivchenko, G G Managadze, V V Migulin, O K Nazarenko, A T Nesmyanovich A Kh Pyatsi, R. Z Sagdeev, and I A Zhulin, The Zarnitza rocket experiment on electron injection, *Space Res*, *15*, 491–500, 1975

Cambou, F, J Lavergnat, V V Migulin, A I Morozov B E Paton, R Pellat, A Pvatsi, H Reme, R Z Sagdeev, W R Sheldon, and I A Zhulin, ARAKS-controlled or puzzling experiment?, *Nature*, *271*, 723, 1978

Chen, F F, *Plasma Diagnostic Techniques*, chap 4 edited by R H Huddlestone and S L Leonard, Academic, New York, 1965

Galeev, A A, E V Mishin, R. Z Sagdeev, V D Shapiro, and V I Shevchenko, Discharge in the region around a rocket following the injection of electron beams in the ionosphere, *Sov Phys Dokl*, *21*, 641, 1976

Getty, W D, and L D Smullin, Beam-plasma discharge Buildup of oscillations, *J Appl Phys*, *34*, 3421, 1963

Hendrickson, R A, and J R Winckler, Echo III The study of electric and magnetic fields with conjugate echoes from artificial electron beams injected into the auroral zone ionosphere, *Geophys Res Lett*, *3*, 409, 1976

Hess, W N, M. C Trichel, T N Davis, W C Beggs, G E Kraft, E Strasinopoulos, and E J R Maier, Artificial aurora experiment Experiment and principal results, *J Geophys Res*, *76*, 6067, 1971

Holmes, J C, and E P Szuszczewicz, A versatile plasma probe, *Rev. Sci Instrum.*, *46*, 592, 1975

Holmes, J. C, and E. P Szuszczewicz, A plasma probe system with automatic sweep adjustment, *Rev Sci Instrum*, *52*, 377, 1981

Jost, R. J, H. R Anderson, and J O McGarity, Measured electron energy distributions during electron beam-plasma interactions, *Geophys Res Lett*, *7*, 509, 1980

Linson, L M, and K Papadopoulos, Review of the status of theory and experiment for injection of energetic electron beams in space, *Rep LAPS-69/SAI-D23-459-LJ*, Sci Appl, Inc, LaJolla, Calif, April 1980

Monson, S J, and P J Kellogg, Ground observations of waves at 2 96 MHz generated by an 8- to 40-KEV electron beam in the ionosphere, *J Geophys Res*, *83*, 121, 1978

Papadopoulos, K, Theory of beam plasma discharge in *Proceedings of NATO Advanced Research Institute on Artificial Particle Beams in Space Plasma Physics* Plenum, New York, in press, 1982

Papadopoulos, K, and T Coffey, Nonthermal features of the auroral plasma due to precipitating electrons, *J Geophys Res*, *79*, 674, 1974*a*

Papadopoulos, K, and T Coffey, Anomalous resistivity in the auroral plasma, *J Geophys Res*, *79* 1558, 1974*b*

Papadopoulos, K, and H L Rowland, Collisionless effects on the spectrum of secondary auroral electrons at low altitudes, *J Geophys Res*, *83*, 5768, 1978

Rowland, H L C L Chang, and K Papadopoulos, Scaling of the beam-plasma discharge, *J Geophys Res*, *86* 9215 1981

Szuszczewicz, E P Direct measurements of plasma characteristics in space-simulation beam-plasma interactions, paper presented at 20th Aerospace Sciences Meeting, Am Inst of Aeronaut and Astronaut, Orlando, Fla, Jan 1982

Szuszczewicz, E P, and J C Holmes Surface contamination of active electrodes in plasmas Distortion of conventional Langmuir probe measurements *J Appl Phys* *46*, 5134 1975

Szuszczewicz, E P and J C Holmes, Reentry plasma diagnostics with a pulsed plasma probe, paper presented at 9th Fluid and Plasma Dynamics Conference, Am Inst of Aeronaut and Astronaut, San Diego, Calif July 1976

Szuszczewicz, E P and J C Holmes Observations of electron temperature gradients in mid-latitude E_s layers *J Geophys Res* *82*, 5073, 1977

Szuszczewicz, E P, D N Walker and H Leinbach, Plasma

diffusion in a space simulation beam-plasma discharge, *Geophys Res. Lett*, *6*, 201, 1979

Winckler, J. R., The application of artificial electron beams to magnetospheric research, *Rev Geophys. Space Phys*, *18*, 659, 1980.

Winckler, J R., R L. Arnoldy, and R. A Hendrickson, Echo 2 A study of electron beams injected into the high-latitude ionosphere from a large sounding rocket, *J Geophys. Res.*, *80*, 2083, 1975.

(Received June 29, 1981,
revised October 2, 1981,
accepted October 30, 1981.)

GEOPHYSICAL RESEARCH LETTERS, VOL. 10, NO. 11, PAGES 1124-1127, NOVEMBER 1983

ELECTRON BEAM INJECTION EXPERIMENTS. REPLICATION OF FLIGHT OBSERVATIONS IN A LABORATORY BEAM PLASMA DISCHARGE

W. Bernstein[1], J. O. McGarity[1], and A. Konradi[2]

[1]Department of Space Physics and Astronomy, Rice University, Houston, TX 77251

[2]Solar System Exploration Division, NASA-Johnson Space Center, Houston, TX 77058

Abstract. Recent electron beam injection experiments in the lower ionosphere have produced two perplexing results:

1. At altitudes from 140 km to 220 km, the beam associated 391.4 nm intensity is relatively independent of altitude despite the decreasing N_2 abundance.

2. The radial extent (1B) of the perturbed region populated by beam associated energetic electrons significantly exceeds the nominal gyrodiameter for 90° injection.

A series of laboratory measurements is described in which both of these flight results appear to have been closely reproduced. The laboratory results are reasonably consistent with the transition from a collision dominated to collisionless beam-plasma discharge configuration.

Introduction

Laboratory studies of energetic electron beam-plasma-neutral gas interactions (e.g., the Beam Plasma Discharge) carried out in the large vacuum facility at the Johnson Space Center (Bernstein et al., 1979) have provided a useful framework for the interpretation of data from comparable rocket borne experiments in which energetic electron beams are injected into the lower ionosphere. In two specific cases, however, the laboratory experiments yielded (1) results apparently contradictory to those obtained in the flight experiments or (2) the parameter range accessible in the laboratory experiments did not encompass that encountered in flight. In this letter, we present some new experimental data obtained in the recently operational small BPD device, also located at JSC, which qualitatively reproduces the two specific flight results. Although the new data is not sufficient to provide a physical explanation for the observations, it is anticipated that further study will yield this explanation and place our understanding of electron beam injection experiments on a firmer basis.

Prior Observations

The two particular flight observations include.

(1) Grandal et al. (1980) reported that the measured intensity of beam-associated 391.4 nm emissions in the rocket vicinity decreased exponentially with increasing altitude over the altitude range ~100-140 km; the absolute intensity was reasonably consistent with the estimated N_2 abundance. For altitudes greater than 140 km until apogee at 220 km, the 391.4 nm intensity remained about constant despite the rapidly decreasing N_2 abundance. A similar constancy in the 391.4 nm intensity at altitudes greater than 150 km was reported by Bernstein et al. (1982) and could perhaps be inferred from the data given by Israelson and Winckler (1975). Although it is possible that the neutral gas density in the rocket vicinity was increased by gas evolution from the payload, the particular mother-daughter configuration employed by Grandal et al. (1980) would appear to minimize this effect; furthermore their results indicated no significant difference between the upleg and downleg of the flight. If localized gas evolution did not occur, the constancy of the 391.4 nm intensity above 140 km indicates that the total ionization rate must actually increase with increasing altitude (decreasing total neutral density). In the large vacuum chamber experiments, the steadily deteriorating base pressure limited most photometric measurements to the range $6 \times 10^{-6} - 4 \times 10^{-5}$ torr; therefore measurements in the effective low pressure range were not possible.

(2) Duprat et al. (1983) have reported quantitative measurements of the radial extent (1B) of the region populated by both energetic electrons (suprathermal and primary) and perturbed thermal plasma. Almost identical radial extents were measured for both components and were proportional to the injected beam gyroradius, ρ_{beam1} (90° injection) as

$$d = K(I_B)\,\rho_{beam1} \sin\beta$$

where ρ is the gyroradius for 90° injection, K is a proportionality constant dependent on beam current, and β is the injection pitch angle. Their observations indicated K = 6.0 for 100 ma beams and 3.7 for 10 ma beams. Although the injection pitch angle range studied was limited to 86°-136°, the radial extent of the perturbed region exceeded the nominal gyroradiameter particularly for the largest beam current employed.

Measurements of the dependence of the radial width (FWHM) of the illuminated region on injection pitch angle in the large chamber experiments, using optical techniques, showed a similar dependence on the nominal gyrodiameter but with K = 2. Furthermore, the measured width showed no clear dependence on beam current for currents greater than the ignition threshold, (I_c), up to the space charge limited value (Hallinan et al., submitted, 1983). For large injection pitch angles, a hollow beam configuration centered on the nominal gyroradius was often observed. For small injection pitch angles, $d > 2\rho_{beam1} \sin\beta$.

Paper number 3L1419
0094-8276/83/003L-1419$03.00

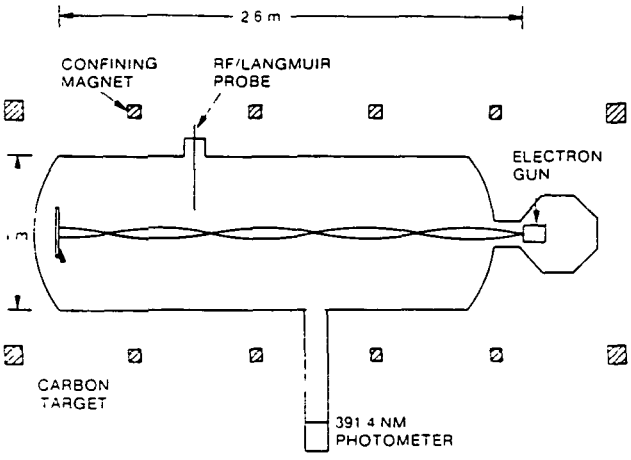

Fig. 1. Schematic representation of the small BPD device.

Experimental Arrangement and Results

The new small BPD device is schematically shown in Figure 1. The magnetic field strength is variable up to 38G, the base pressure is $\approx 5 \times 10^{-7}$ torr and a controlled N_2 leak allows operating pressures up to 5×10^{-4} torr. The same tungsten filament, Pierce geometry electron gun, employed in the large chamber experiments, is used. Injection is parallel to B and operation is steady state (dc).

The reported results were obtained with a scanning photometer which viewed the BPD through the central viewport. The scanning slit (~7.6 cm long and 0.15 cm high) was aligned ∥B. Separation of N_2^+ first negative and N_2 first positive emissions was accomplished by use of a band pass filter centered at 391.4 nm and a second long wavelength filter which transmitted light greater than 618.5 nm, the S-20 cathode photomultiplier (EMI 9558) provided reasonable sensitivity at long wavelengths.. Absolute calibration of the photometer response was not done and all measurements are relative. Parallel radial profiles of probe floating potential were obtained with a conventional moveable Langmuir probe located at a downstream port. Measurements of plasma potential indicated a constant value of ≈ +10 V at large radial distances, because the floating potential becomes increasingly negative with increasing density of the energetic electron component, measurement of the radial position at which the floating potential equals a more negative specific value (0 V was arbitrarily selected) also provides a measure of the radial extent of the active region. Obviously the optically determined width (FWHM) and that given by the probe will only be related to each other but not identical.

Figure 2 shows a set of 391.4 nm photometer scans obtained over the N_2 pressure range $2.5 \times 10^{-5} < P < 5.7 \times 10^{-4}$ torr for a fixed current (40 ma), fixed energy (1.6 keV) beam at 38G. From these curves, we derive the FWHM and total emission intensity (proportional to peak intensity × FWHM). Similar profiles are obtained for the greater than 618.5 nm emissions and for both emissions at 19 and 11G.

Figure 3 shows the dependences of the FWHM and total intensities on pressure for both the 391.4 nm and greater than 618.5 nm emissions for B = 38G and a 40 ma, 1.6 kV beam. Also shown is the amplitude (db above receiver noise) of the whistler mode waves (cutoff at f_{ce}) detected by an RF probe. Several conclusions are evident in these plots

(1) For pressure greater than or equal to 1×10^{-4} torr
   (a) The FWHM is independent of pressure and is greater than the 90° gyrodiameter but less than single particle beam width at the antinode consistent with large chamber observations. The constancy is also apparent in the floating potential measurements.
   (b) The FWHM measured for the greater than 618.5 nm emissions is always ≈ 25% greater than the FWHM of the 391.4 nm emissions.
   (c) The total intensity, $I_L \sim P^{0.6}$ for both emissions
   (d) The amplitude of the whistler mode waves increases very slowly with decreasing P.

(2) For pressures less than 1×10^{-4} torr
   (a) The FWHM increases rapidly with decreasing P as P^{-2} for both emissions, for example at 3.0×10^{-5} torr, the greater than 618.5 nm FWHM is 7.0 cm — about equal to the nominal gyrodiameter for 1.6 kV electrons injected at 90°. This broadening with decreasing pressure is confirmed by the floating potential measurements.
   (b) The total intensity of both emissions falls to a minimum value for pressures near 1×10^{-4} torr but then increases with further decrease in pressure.

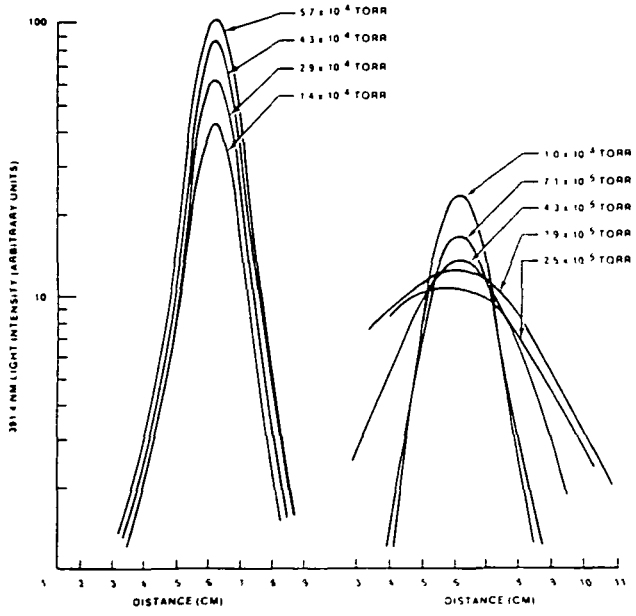

Fig. 2. 391.4 nm photometric scans of the beam-plasma column for different N_2 pressures. The magnetic field strength is 38 G, beam energy is 1.6 keV, beam current is 40 ma DC, and injection is ∥B.

Similar curves are observed for the range of magnetic field strengths employed; no obvious correlation of the pressure minimum with B was observed. Bernstein et al. (1979) also reported the existence of a minimum in the beam current required for ignition (I_c)-pressure relationship in the large chamber experiments, but we believe these two effects to have entirely different origins.

(c) Changes in the ratios of total intensities and FWHMs of the 391.4 nm compared to the greater than 618.5 nm emissions are less than a factor of two from those observed in the higher pressure range.

(d) Although not shown in Figure 3, the total intensity of both the 391.4 nm and greater than 618.5 nm emissions increases slowly with decreasing B.

(e) The amplitude of the whistler mode waves increases rapidly with decreasing P. For example, at P = 5 × 10^{-5} torr, their amplitude is ≈ 40db greater than that observed at 1.4 × 10^{-4} torr.

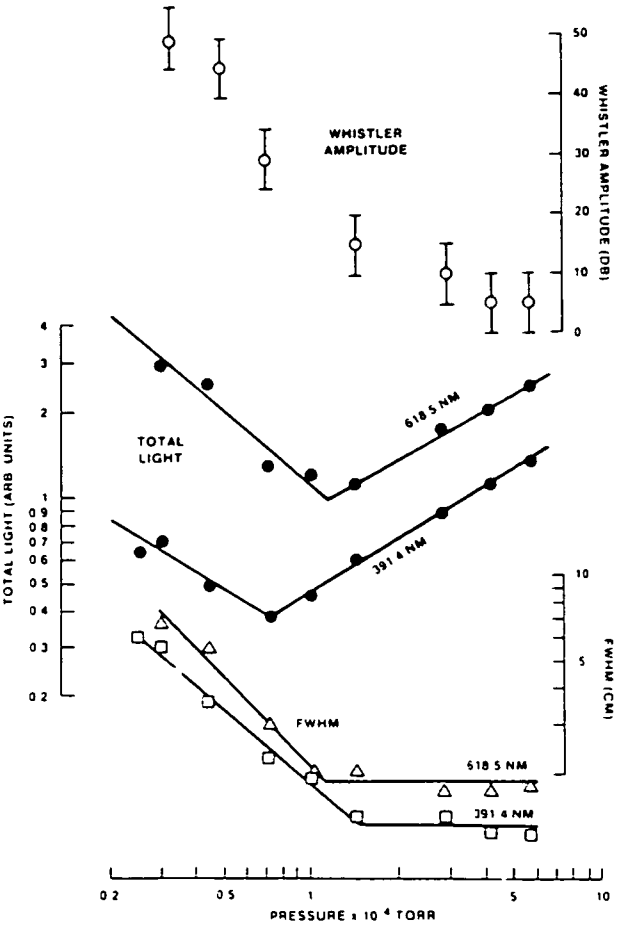

Fig. 3. The variation of the FWHM and total intensity of the 391.4 and greater than 618.5 nm emissions with pressure. Also shown is the simultaneously observed relative whistler wave amplitude greater than receiver noise.

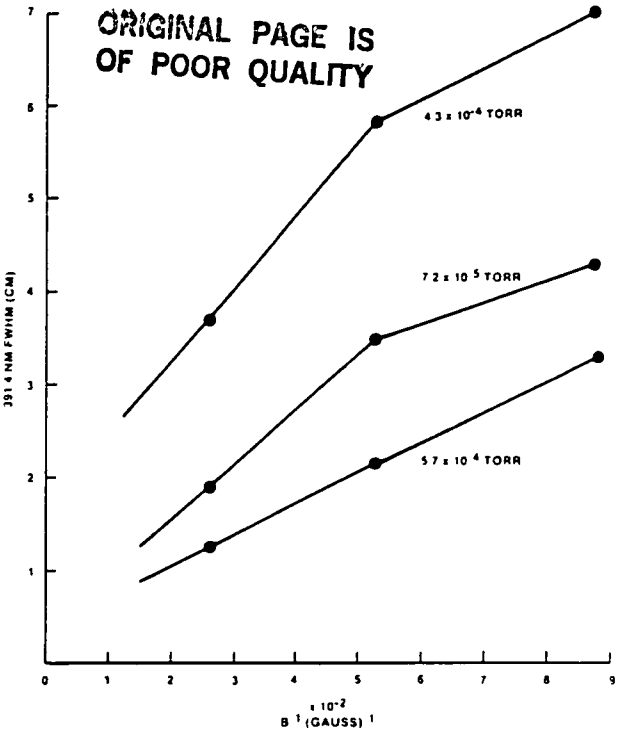

Fig. 4. The dependence of the FWHM of the 391.4 nm emissions on B^{-1} for three N_2 pressures.

Figure 4 shows the dependences of the FWHMs of the 391.4 nm emission on B^{-1} for several pressures. At high pressure (5.7 × 10^{-4} torr) the FWHM show the inverse linear dependence also observed in the large chamber experiments but with a small intercept, which probably results from the finite cathode diameter (0.39 cm). At lower pressures, the FWHM still varies inversely with B, but the linear dependence is questionable and the magnitude of the intercept increases.

Measurement of the dependence of the FWHM on beam current particularly in the pertinent low pressure range (< 1 × 10^{-4} torr) is limited for the following reason. Bernstein et al. (1979) had noted that the ignition current increased with decreasing pressure in the low pressure range. At 38G and 1.6 kV the 40 ma beam current is only about a factor of three greater than I_c, within this limitation, the FWHM is relatively independent of beam current. In the flight described by Duprat et al. (1983), the dependence of width on I_b was studied over a much wider range, a factor of 10, Kellogg (private communication, 1982) has stressed that BPD ignition occurs at much smaller beam currents in the flight experiments than in the laboratory experiments using identical electron beams.

Discussion

It is possible that the change in BPD characteristics near P = 1 × 10^{-4} torr corresponds to the transition between the collisionless (presence of suprathermal electron tails) and collisional (thermalized electron velocity distribution) beam plasma discharges discussed by

Papadopoulos (1982). He suggests that the transition occurs when

$$\omega_p\left(\frac{m}{2M}\right)^{1/2} > \nu_{en}$$

where ν_{en} is the electron-neutral collision frequency.

In these experiments the measured plasma frequency is in the range, $1.3 \times 10^9 < \omega_p < 6.3 \times 10^9$ sec^{-1}. Taking $\omega_p = 1.9 \times 10^9$ sec^{-1} and the thermal plasma $T_e = 1$ eV, the inequality is satisfied for neutral pressures $< 2.4 \times 10^{-3}$ torr compared to the observed transition at $P \approx 1 \times 10^{-4}$ torr. In the large chamber experiments characterized by $\omega_p \approx 1.26 \times 10^8$ sec^{-1}, the inequality is satisfied at $P = 1.9 \times 10^{-4}$ torr. If the scaling were similar in the two experiments, then the low pressure regime was seldom if ever encountered in the more recent large chamber experiments. On the other hand despite the relatively high neutral pressure, suprathermal electrons were clearly observed (Szuszczewicz et al., 1982; Sharp, 1982) in the large chamber experiments.

Therefore, we have not yet formulated a complete explanation for these laboratory and flight results. The new laboratory experiments reproduce two specific flight results at pressures greater than 1×10^{-4} torr: (1) the ionization rate increases with decreasing neutral density and (2) the radial extent $\perp B$ increases with decreasing neutral density and can exceed the nominal gyrodiameter for 90° injection. The patterns must be associated with a gross change in wave-particle configuration at $P \approx 1 \times 10^{-4}$ torr. With the detailed analysis of the wave-particle configuration now being initiated in the laboratory, the desired meaningful explanation should be readily obtained.

Acknowledgments. We acknowledge the assistance of D. Bulgher and useful discussions with Y. Llobet. NSF grant ATM80-22550 and NASA grants NAGW-69 and NGL-44-006-012 provided support for W. Bernstein and J. O. McGarity.

References

Bernstein, W., H. Leinbach, P. J. Kellogg, S. J. Monson, and T. Hallinan, Further laboratory measurements of the beam plasma discharge, J. Geophys. Res., 84, 7271-7278, 1979.

Bernstein, W., P. J. Kellogg, S. J. Monson, R. H. Holzworth, and B. A. Whalen, Recent observations of beam plasma interactions in the ionosphere and a comparison with laboratory studies of the beam plasma discharge, in Artificial Particle Beams in Space Plasma Studies, edited by B. Grandal, pp. 35-63, Plenum Press, New York, 1982.

Duprat, G. R. J., B. A. Whalen, A. G. McNamara, and W. Bernstein, Measurements of the stability of energetic electron beams in the ionosphere, J. Geophys. Res., 88, 3095-3108, 1983.

Grandal, B., E. V. Thrane, and J. Troim, Polar 5: An electron accelerator experiment within an aurora· 4. Measurements of 391.4 nm light produced by an artificial electron beam in the upper atmosphere, Planetary Space Sci., 28, 309-319, 1980.

Israelson, G., and J. R. Winckler, Measurements of 3914 Å light production and electron scattering from electron beams artificially injected into the ionosphere, J. Geophys. Res., 80, 3709-3712, 1975.

Papadopoulos, K., Theory of beam plasma discharge, in Artificial Particle Beams in Space Plasma Studies, edited by B. Grandal, pp. 505-523, Plenum Press, New York, 1982.

Sharp, W. E., Suprathermal electrons produced by a beam-plasma discharge, Geophys. Res. Lett., 9, 869-873, 1982.

Szuszczewicz, E. P., K. Papadopoulos, W. Bernstein, C. S. Lin, and D. N. Walker, Threshold criterion for a beam plasma discharge, J. Geophys. Res., 87, 1565-1573, 1982.

(Received August 11, 1983,
accepted August 17, 1983.)

JOURNAL OF GEOPHYSICAL RESEARCH, VOL. 89, NO. A4, PAGES 2335-2347, APRIL 1, 1984

MEASUREMENTS OF THE OPTICAL EMISSION PRODUCED DURING THE LABORATORY BEAM PLASMA DISCHARGE

T. J. Hallinan

Geophysical Institute

H. Leinbach

National Oceanic and Atmospheric Administration

G. Mantjoukis and W. Bernstein

Rice University

Abstract. Optical observations of a beam-plasma discharge (BPD) in the laboratory showed that the discharge remained confined to a diameter little more than double that of the beam for injection parallel to the magnetic field and approximately equal to that of the beam for injection at large pitch angles. The diameter was independent of beam current but varied linearly with beam velocity and inversely with magnetic field strength. The ionization rate inferred from the total emission of 3914 Å, integrated over the radial extent of the beam, was proportional to the excess beam current above that required for BPD ignition. The proportionality constant $(12 \pm 2) \times 10^{14}$ ions/cm s A was valid over a wide range of pressure and of magnetic field strength. Power loss to ionization in a 20 m path was estimated at up to 44 of the beam power. Evidence is presented for effective confinement of suprathermal electrons (parallel to B) by some unidentified process other than electrostatic confinement.

Introduction

It is now apparent that at least some rocket experiments in which dense, energetic electron beams are injected into the lower ionosphere have produced strong, spatially localized interactions at the injection point [Grandal et al., 1980, Duprat et al., 1983, Galeev et al., 1976]. Galeev et al. first suggested that these interactions might be similar to the beam-plasma discharge (BPD) observed in the laboratory. Other types of interactions, including dc discharges, are discussed by Winckler [1980]. Because of the usual problems associated with active rocketborne experiments, a parallel laboratory investigation of those interactions was initiated using beam parameters (I_b, E_b), magnetic field strengths, and neutral and charged particle densities reasonably similar to those encountered in the space experiments [Bernstein et al., 1978, Bernstein et al., 1979, Szuszczewicz et al., 1982]. It was believed that these laboratory experiments would provide a sensible framework for the interpretation of the flight results together with an understanding of the basic physical processes. This paper reports a series of measurements of the optical emissions produced in the beam-plasma interactions experiments performed in the large SESL vacuum chamber at the Johnson Space Center. These measurements provide evidence for (1) the geometrical configuration of the beam-plasma system, (2) the energy spreading of the energetic beam, (3) heating of the ambient plasma electrons, and (4) the rate of energy transfer from the primary beam to the ambient plasma.

Paper number 3A1873.
0148-0227/84/003A-1873$05.00

Experiment Configuration

The configuration of the experiment was identical to that described by Bernstein et al. [1979] and is shown again schematically in Figure 1. The electron gun was a Pierce diode configuration with perveance (space charge limited operation) approximately equal to 1×10^{-6} A $V^{-3/2}$. A tungsten cathode was employed to minimize contamination effects. Although the gun could be operated in a pulsed mode to allow study of the temporal evolution of the interactions, all data reported here were obtained with steady state (dc) conditions. In addition, although an initial ambient plasma could be introduced by using ion thruster or RF discharge techniques, in these experiments the ambient plasma was entirely self-generated, i.e., through collisional ionization of the ambient neutral gas by the beam itself. The beam was terminated by a segmented collector with an externally biasable grid (for suppression of secondary electrons) located approximately 20 m from the gun along the magnetic field. The set of three coils at the periphery provide a maximum field strength of 2.2 G. Usually, both the collector and gun anode were electrically connected to the chamber ground so that no potentials were applied to the beam-plasma system.

In a later series of measurements, performed in a smaller laboratory device with the same gun, it was found that the measured power supply return current was significantly greater than the beam current arriving at a positively biased collector for currents near the space charge limit of the gun. We have applied the measured corrections to the present data, but certainly the results are more qualitative than had been desired. At beam currents less than 2/3 the space-charge limit, the two measurements are in good agreement, and we believe these data to be reasonably quantitative.

Other diagnostics shown in figure 1 include

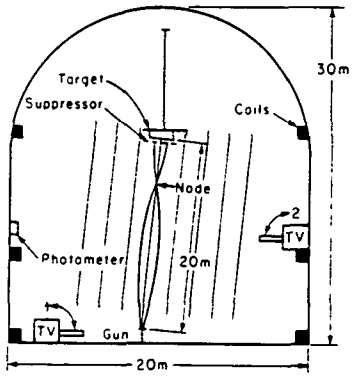

Fig. 1. This schematic illustration shows the approximate positions of the 3914-Å photometer and the low-light-level television cameras relative to the beam.

fixed-position and movable Langmuir probes, several wave detection systems, an electrostatic energy analyzer, and the segmented beam-current collector. The general results have been described by Bernstein et al. [1979]; results from specific diagnostics have been given by Jost et al. [1980], Sharp [1981], Kellogg et al. [1982], and Szuszczewicz et al. [1982].

The ambient gas in the chamber arose primarily from three sources: air from unrepairable leaks (80% N_2), nitrogen backfilled into the chamber to increase the pressure above the base level, and water vapor that slowly evaporated from ice or water trapped on surfaces within the chamber. Although water was a substantial contaminant when the pressure was very low and the chamber had not been evacuated for very long, in most cases the dominant gas was N_2. For the initial runs the base pressure was approximately equal to 1×10^{-6} torr (density of 3.5×10^{10} cm^{-3}), for the later runs the base pressure had increased to approximately 7×10^{-6} torr because of unrepaired leaks.

Photometric data were obtained with a scanning photometer filtered (13 Å bandpass) for the N_2^+ first negative band at 3914 Å.. The photometer had a circular field of view of 0.9° and was scanned horizontally by a motor driven mirror system to provide an intensity profile perpendicular to the beam at a point about midway between the gun and collector. The photometer was mounted at the wall of the vacuum system so that its separation from the nominal beam axis was about 6 m. The projection of the field of view corresponded to about 9-10 cm at the beam. This spatial resolution was adequate to provide radial profiles of intensity for all but the narrowest beams employed.

The photometer used the single-photon detection technique and had an operational dynamic range of about 10^4. A built-in light source was included to check for any long-term drifts in the system. No absolute calibration was available for the photometer and a subsequent malfunction and rework precluded an after-the-fact calibration. However, because the excitation cross section for 3914 Å is well known [Borst and Zipf, 1970], the beam itself (at currents well below the threshold for BPD) served as an approximate calibration standard.

Specifically, the photon-emission rate (arbitrary scale) was measured for 13 combinations of beam current, beam voltage, neutral density and magnetic field strength. In each case the chosen current was sufficiently low that there was no BPD. Hence the emitted light was attributable entirely to collisions of the beam electrons with the ambient gas. These measurements were then compared with calculated values. A scale factor was chosen such that the ratio of observed to calculated intensities had a mean value of unity with an rms deviation of 16%. This scale factor is used as a calibration factor whenever the optical data are given in absolute units.

In all situations encountered in the experiments the density of N_2 exceeded that of N_2^+ by at least four orders of magnitude. Hence direct collisional excitation of ground state N_2^+ was neglected, and all of the measured 3914-Å emission was attributed to the ionization of N_2 followed by the subsequent emission from N_2^+. Because the 3914-Å emission is prompt ($< 10^{-6}$ s), and the emitting ion temperature was low, it is reasonable to assume that the ions were stationary. The geometrical distribution of the 3914-Å emissions thus provides a mapping of the spatial distribution of electrons with energies sufficient to produce ionization (E > IP). The ratio of the ionization rate to the 3914-Å photon production rate is approximately constant at a value of 14 over the range of electron energies encountered in the experiments [Borst and Zipf, 1970]. This value is assumed, and the photometric data are considered throughout the paper as equivalent ion production rates (Q).

Each intensity measurement is a line-of-sight integral of the volume-emission rate. Integrating the signal over a full horizontal scan of the photometer provides a measurement of the total number of photons emitted in a horizontal slab of unit thickness. The equivalent total ionization rate (Q_T) is given in units of ions/cm s.

More general information was provided by two low-light-level television cameras. One camera, located approximately 10 m from the electron gun on the floor of the chamber, had a field of view of 12° x 16°. The other camera, with a 30° x 40° field of view, was located near the photometer. Both cameras were on fully steerable mounts and could view any part of the beam.

The television cameras were image-orthicon systems with extended red (S25) photocathodes sensitive to light in the range 3900-8500 Å. No optical filters were used. For any given setting of the gain control the response to light was linear over a range of approximately 30:1. However, there was no absolute calibration, and the 'zero level' was arbitrary.

The images were recorded on video tape for subsequent viewing and analysis. A recently developed digital image processing system was used in the analysis of the data. This system consists of a Quantex digital image processor and frame store, a Nova minicomputer and disc, and a Tektronix 4010 terminal and hard-copy unit. A special interface card was designed for the Nova to allow direct random access to the Quantex memory.

This system allows the user to obtain horizontal profiles of luminosity through the beam at any location within the TV picture. Where appro-

Fig. 2. A 2000-V, 70-mA beam at a field-strength of 1 G forms a well-defined node below the segmented collector. (Photograph courtesy of R. J. Jost (NASA/JSC) and H. R. Anderson (Science Applications Inc.)

priate, successive TV frames (1/60-s exposures) can be added for an improved signal-to-noise ratio. Similarly, adjacent horizontal scans can be summed, and scans from a 'background' frame in which the beam is off can be subtracted from the data scans to remove TV shading patterns.

The major contributions to the TV signal were from the first negative series of N_2^+ and the first positive series of N_2. An empirical reference comes from the use of one of the television cameras as the detecting element in an auroral spectrograph. In this case the ratio of the integrated signal from the N_2 to that from the N_2^+ emissions was approximately 2.1.

Hence the television image is dominated by excitation of neutral nitrogen and is not necessarily proportional to the ion-production rate. The ratio of N_2 first positive to N_2^+ first negative emissions is approximately constant for electron energies between 1 keV and 300 keV. However, the constancy breaks down at lower energies, e.g., at 100-eV primary energy the ratio is double that produced by 1-keV electrons [Stolarski and Green, 1967].

The television data provide the spatial and temporal distribution of excitation but cannot be used to calculate the ion production rate. Relative intensities of the visible light derived from the video images are designated throughout the paper as VL.

Observations

1. Geometrical Configurations

a. Single particle trajectories. For beam currents significantly less than the critical current required for BPD ignition ($I_b < 0.5\ I_c$), RF activity is undetectable, and the beam geometry is consistent with expectations for single-

particle behavior. Figure 2 illustrates the pattern of optical emissions observed for a 70-mA, 2-keV beam injected parallel to the magnetic field. The noding pattern arises because of the small beam divergence angle α (approximately equal to $\pm 5°$) produced in the gun, ideally, the beam is refocused periodically to the original source size by the magnetic field. The noding length is the ratio of the parallel velocity to the cyclotron frequency and has a value of 6.7 m for $E_b = 1$ KeV and $B = 1$ G.

All the data presented in this paper are limited to combinations of beam voltage (E_b) and magnetic field strength (B) where at least one refocus node was accommodated within the beam path length, i.e., the primary beam electrons experienced at least one gyrorotation. High-voltage breakdown problems limited $E_b < 2.2$ kV, and the gun perveance was too small to produce BPD for $B < 0.89$ G. The finite spread in parallel velocity arising from thermal effects, the finite spread in pitch angle, and perhaps the power supply variations would cause the nodes to disappear at large distances. But the nodes were well defined over the 20-m path length available in the chamber. The presence of the very sharp nodes shown in Figure 2 indicates the monoenergetic character of the primary beam; this has been confirmed by direct measurements of the beam particle energy distribution [Jost et al., 1980]. The beam radius (R) at the antinode is given by

$$R = (2v_b \sin\alpha)/(\omega_c)$$

$$R = 0.186 \text{ m} \quad E_b = 1 \text{ keV} \quad B = 1 \text{ G}$$

Since the source radius is only 0.0025 m, the beam density varied by orders of magnitude along the axial distance traveled. This configuration was grossly different from other laboratory BPD experiments conducted at high magnetic field strengths [e.g., Smullin, 1981] where the beam radius was determined primarily by the source radius.

As a result of the v_b- and B-dependent noding pattern, scans with the fixed axial position 3914Å photometer do not directly yield complete geometric configuration data. Because scans at a constant beam energy showed that the measured beam radius was independent of beam current, it is reasonable to conclude that the beam space charge had been neutralized by collisionally produced ions in steady state [Getty and Smullin, 1963]. Furthermore, the integrated total 3914-Å intensity increased linearly with beam current and N_2 density, was independent of B, and varied inversely with beam energy in accordance with the energy dependence of the ionization cross section given by Borst and Zipf [1970].

The montage shown in Figure 3 shows the trajectory of a beam injected at a pitch angle θ approximately equal to 65°. If there were no spread in the injection pitch angle, the beam would describe a simple helix with the pitch and radius determined by E_b, B, and θ. The injection point is located on the helix periphery with the position of the helix guiding center determined by the injection azimuth. As in the case of parallel injection the finite spread in the angle of injection leads to a noded pattern. In the helical configuration there is one node for each turn of the helix, and the nodes occur on the magnetic field line through the point of injection.

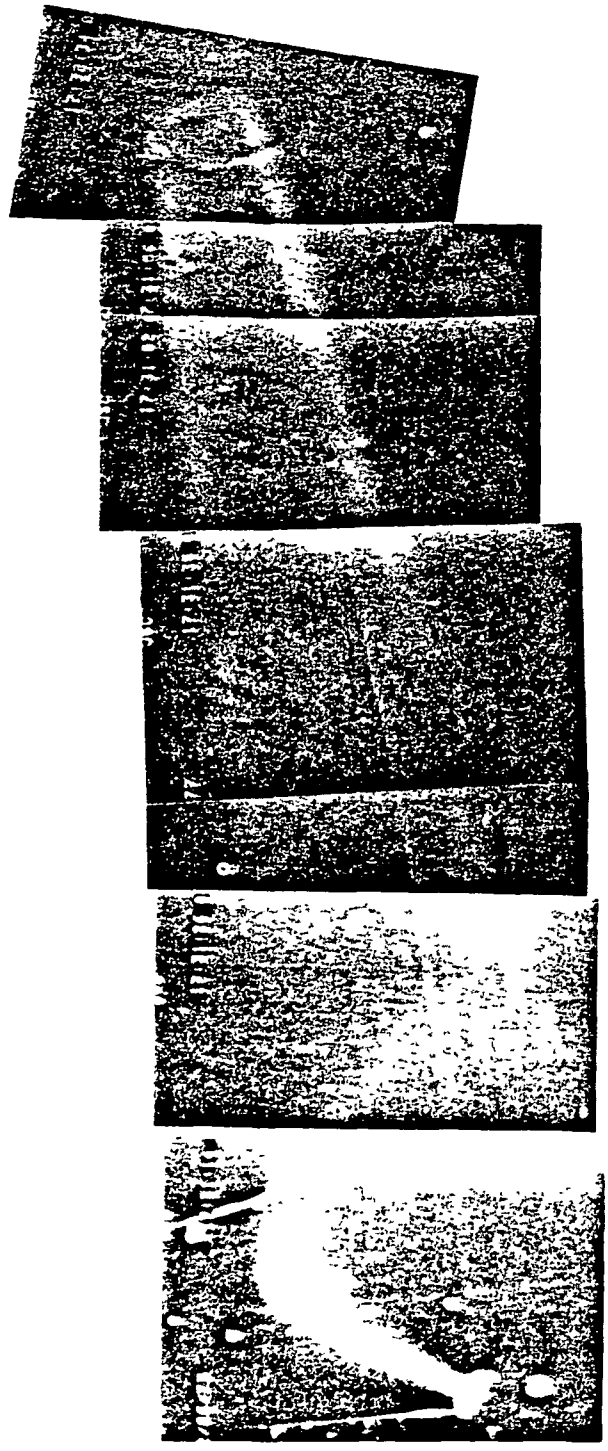

Fig. 3. In this composite TV image a helical beam injected at ~65° is seen to degenerate into a hollow cylinder before reaching the collector at top. There is also a curious black helix, apparently along the path of the unperturbed beam.

The beam shown in Figure 3 was on the verge of BPD as determined by the RF measurements. The smearing in parallel velocity, particularly to-

ward slower velocities, is due in part to the initial spread in the beam but may reflect collective beam-plasma interactions as well. Near the target, the helix has completely degenerated into a hollow cylinder. The concentration of luminosity on the surface of the cylinder implies that even those electrons having parallel velocities well below nominal still retain the nominal gyroradius or, equivalently, the nominal $v_\perp$.

At large distances the only remaining trace of the initial helix is a curious black streak, appearing somewhat like a rope wrapped helically around the luminous hollow cylinder. There appears to be a slight enhancement in the luminosity immediately above and below the black helix. The modulation produced by the black streak was between 10% and 20% of the total luminosity. Since the TV image superposes the front and back of the cylinder, it can be inferred that the true modulation in the volume emission rate was between 20% and 40%.

The photometric measurements showed that, as in the case of parallel injection, the ion production rate as a function of I_b, E_b, and N_o was consistent with simple collisional ionization by the primary beam electrons. In the helical beams the rate of ionization per unit axial distance had, in addition, a $(\cos\theta)^{-1}$ dependence, reflecting the longer spiral path length through the chamber.

b. Intermediate state. Bernstein et al. [1979] had noted that at low neutral densities ($N_o < 1.5 \times 10^{11}$ cm^{-3}) and for beam currents in the range between 0.5 I_c and I_c, strong wave emissions at $f \approx f_c$ appeared, the dependence of the wave frequency on beam current suggested that the wave frequency corresponded to the upper hybrid frequency (f_{UH}) for conditions where $f_c > f_p$. They also reported that this state was associated with the appearance of a low-intensity halo (3914 Å) surrounding the primary beam, which otherwise appeared to maintain its single particle features. Thus some enhanced ionization above that produced by collisional ionization alone occurs in this phase. At neutral densities greater than 1.5×10^{11} cm^{-3} this state is usually absent, and the beam-plasma configuration directly changes from the stable single-particle state to the BPD.

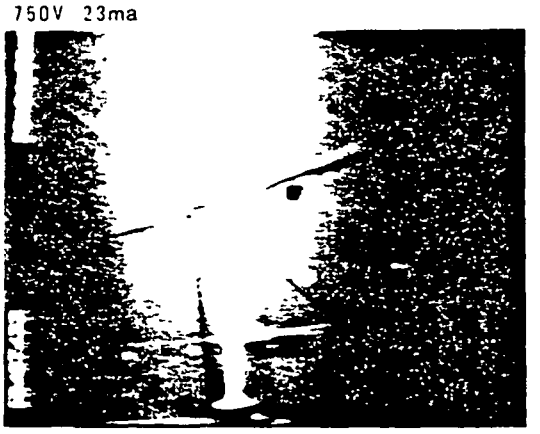

Fig. 4. A 750-V, 23-mA beam emerging from the gun at bottom is quickly lost in the more diffuse glow of the BPD. $P = 2 \times 10^{-6}$ T, B = 1.5 G.

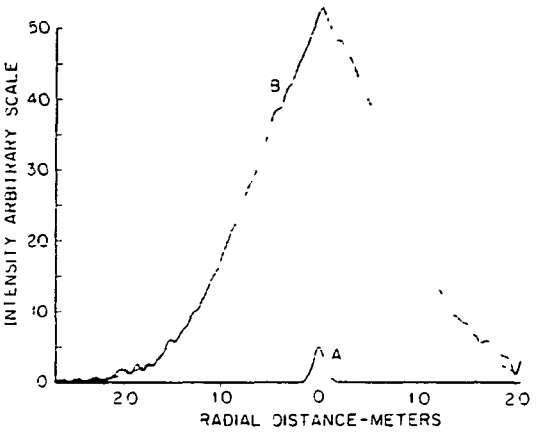

Fig. 5. Scans through the first mode in a TV image of a 1500-V beam at currents just below (A) and just above (B) the BPD ignition current. The dotted line in B is a Gaussian fit to the data. The node is easily seen in the TV image of the BPD and appears as the sharp peak above the Gaussian curve in the intensity scan.

Hallinan et al. [1982] reported that the visible-light intensity of this glow is linear with beam current above a small threshold value. Although the glow is weak compared to the intensity of the beam, it has a large diameter--comparable to that of the BPD at higher currents. From the TV images it was shown that the total emission rate (VL_T), integrated over the entire diameter of the glow, exceeds that of the beam by a factor of 6 or 7. The 3914-Å scan [Bernstein et al., 1979] is similar to the TV data, but there the total intensity (Q_T) of the weak glow is roughly equal to that of the primary beam.

c. Beam-plasma discharge. Ignition of the BPD occurs when the beam current is increased above a critical value. The BPD produced by a 750-V, 23-mA beam injected parallel to B is shown in Figure 4. As noted by Bernstein et al. [1979], ignition is identified by (1) a large change in geometric configuration, (2) a large increase in the intensity of N_2^+ first negative and N_2 first positive emissions, (3) a wave spectrum characterized by strong emissions at the plasma frequency and a lower frequency band extending from a few hertz to f_c, and (4) an increase in ambient electron density and temperature. Subsequently, it was shown that the BPD was characterized by severe beam melting [Post et al., 1980] and the appearance of large electron fluxes in the range 100-400 eV [Sharp, 1981].

In the BPD the primary beam itself is mostly obscured by a bright surrounding glow indicative of anomalous ionization which must be produced by accelerated ambient electrons. Nonetheless, the first and, occasionally, the second node can be seen in the TV images, subsequent nodes are not recognizable. Figure 5 shows horizontal scans through the TV image of the first node at currents below and above the BPD threshold. Although the BPD trace is dominated by the Gaussian profile of the BPD glow, the node is clearly visible as the sharp peak above the Gaussian curve. There is little observable change in the intensity or width of the beam node as compared to the pre-BPD trace.

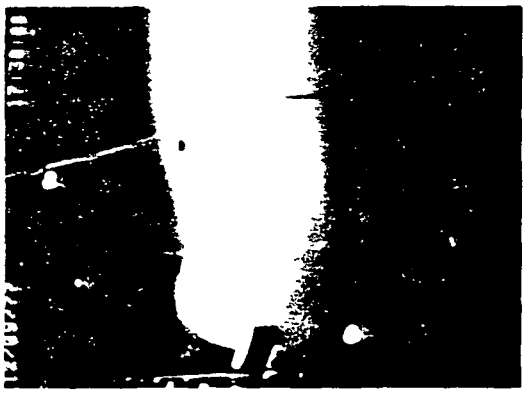

Fig. 6. The BPD glow is seen to extend to the gyroradius of the beam. Apparent variation in the BPD width near the top is due to a real variation in intensity along B. See Figures 9a and 9b.

By digitally subtracting the pre-BPD image from the BPD image, it was found that there was no shift in the position of the node along the beam axis. In most cases the second node is not visually recognizable in the TV images. Nor is it apparent in the scans through the TV image. Occasionally, at low beam voltages (~500 V), two nodes remain visible in the BPD, while the third node disappears. The disappearance of the second node is consistent with the observed heating of the electron beam. The observation of the first node above the BPD glow intensity implies that no significant modification of the beam velocity distribution occurred within the first few meters from the gun.

The Gaussian profile of Figure 5 is typical of both the television scans and the 3914-Å photometer scans. Each intensity measurement is a line-of-sight integral through the emitting volume. Assuming azimuthal symmetry, it can be shown that Gaussian intensity profiles are obtained if the radial dependence of the volume-emission rate is also Gaussian. Hence the average density of electrons having sufficient energy for ionization has the form

$$N \propto e^{-2.8(r/w)^2}$$

where r is the distance from the axis of the beam, and w is the measured full width at half maximum of the intensity profile.

Figure 6 shows the BPD produced by a beam injected at large pitch angle. The beam is recognizable within the BPD glow for one half to three quarters of the first gyrorotation. Beyond that the beam is not recognizable, but it evidently remains within the initial gyroradius. Figure 7 compares 3914-Å scanning photometer radial intensity profiles, normalized in peak intensity, of BPD's produced by 1000-V, 24-mA beams injected parallel to and at $\theta \approx 75°$ to the magnetic field. For parallel injection the measured column width (FWHM) is ~1.1 m, this is approximately 2.5 times the calculated width at the antinode of the stable beam ($\alpha = \pm 5°$). But it is much less than would be expected if the beam electrons were scattered to large pitch angles. For example, it is less than the width at the antinode of a beam having a divergence angle $\alpha = \pm 15°$. Hence the observed expansion of the column width does not imply that the beam is strongly scattered in pitch angle.

For large pitch angle injection the double-peak pattern is indicative of a hollow beam configuration. The distance between the peaks corresponds to the expected width of the helical orbit ($2V_b \sin \theta/\omega_c$). The hollow beam configuration is most marked for beam currents near I_c and gradually disappears with increasing beam current. However, the FWHM remains unchanged with increasing I_b so that, for $I_b >> I_c$, beams injected at high pitch angle also produce a more uniform cyclindrical BPD. The radial intensity distribution is Gaussian for beams injected parallel to B but is more flat-topped for large injection pitch angle.

Figure 8a shows the inverse dependence on magnetic field strength of the width (FWHM) of the BPD produced by a 1600-V, 40-mA beam injected parallel to B. Figure 8b shows the dependence on beam velocity of the BPD width (FWHM) produced by a fixed current ($I_b >> I_c$) beam injected parallel to B. The BPD width increases linearly with increasing beam velocity but extrapolates to a finite value at zero beam velocity. The finite intercept suggests that the width is determined by two parameters: the primary beam electrons (v_b) alone and the energetic electrons (v_e) which produce the enhanced ionization. Rather similar results are obtained for the various injection pitch angles studied where the width is primarily determined by the beam parameters $v_b \sin \theta/\omega_c$.

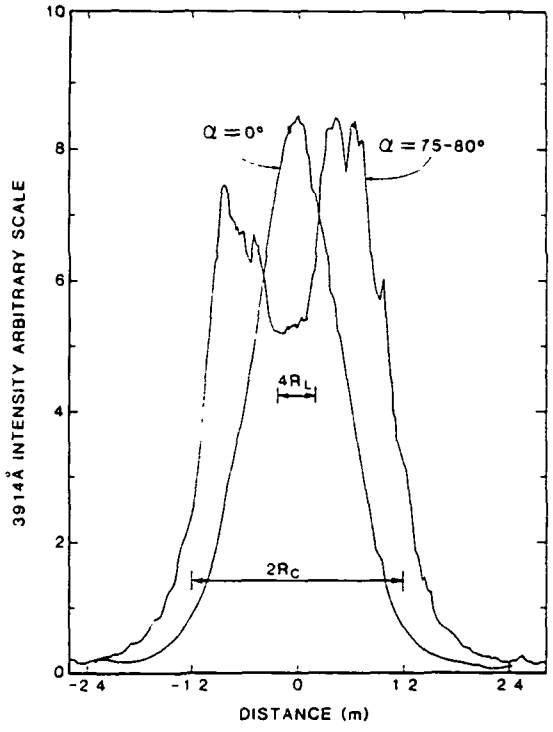

Fig. 7. Relative intensity profiles (3914 Å) through the BPD for beams injected parallel (α = 0) and at large angle (α = 75-80°) to B. The profiles are normalized to the same peak value; 2 R_c is the diameter of the helical beam and 4 R_L is the antinode diameter of a beam having a spread in pitch angle of ±5°. E = 1 keV, B = 0.9 G, I = 24 mA.

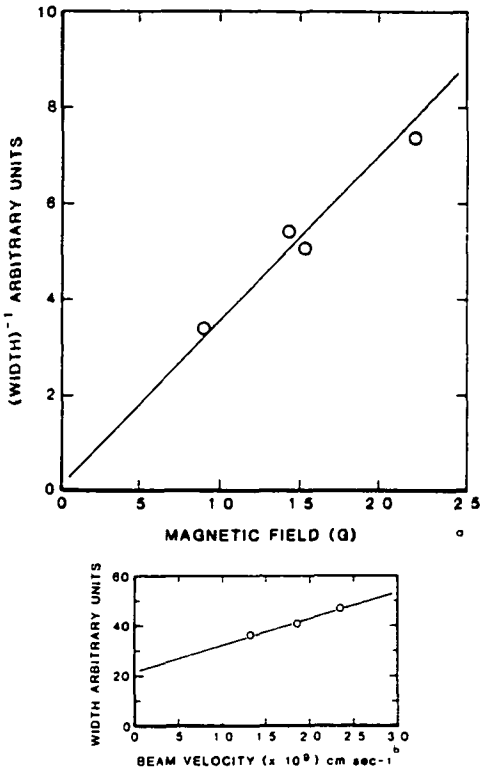

Fig. 8. (a) The inverse width of the BPD glow for a 1600-V, 40-mA beam varies linearly with magnetic field strength. (b) The width of the BPD at constant current, field strength, and pressure varies linearly with the velocity of the beam electrons.

Clearly, stong pitch angle diffusion of the primary beam was not observed for either parallel or nearly perpendicular injection. Similarly, although Szuszczewicz et al. [1978] reported observations of fast (Bohm) radial diffusion of the cool ambient plasma, the present observations indicate that the energetic suprathermal electron component remains well confined by the magnetic field. The geometric configuration of the BPD thus consists of the cylindrical primary beam that is immersed in a wider halo of suprathermal electrons, which in turn are immersed in a very broad thermal plasma arising from radial diffusion processes.

All the experiments have been performed at low neutral densities so that the electron (suprathermal and primary) collision mean free path is greater than 20-m path length. Electrons are free to move along the field lines and may even perform multiple transits because of electrostatic reflections at the boundaries, one would therefore expect the BPD intensity to be independent of the axial distance z, even if the region of electron energization (large wave amplitudes) were spatially localized. Similarly, even if the radius of the active region increased with increasing Z, one would expect the optically measured radius to be independent of Z and to be given by the maximum radius produced in the 20-m path length.

The existence of axially uniform light emission is difficult to test. The photometer scanned in a fixed plane and therefore provides no data. Variation in background and in aspect angle (optical path length through the beam) make it impossible to use the TV for an accurate survey of the intensity along the entire length of the beam. Visual observations through a window in the chamber, as well as the TV images, provided an overall impression of uniformity along B.

However, there seem to be exceptions to this general uniformity. The BPD glow in Figure 6 extends below the gun as expected. But it is noticeably brighter near the top of the picture. This appearance is confirmed by scans through the image just above the gun and near the top of the image (Figures 9a and 9b).

The other case of an intensity gradient parallel to B was somewhat of a special situation. On several occasions during one series of tests, an electric field probe was suspended in the beam at the last node below the target. A cable from the probe was hanging down in a loop so that a portion of it ran nearly parallel to the beam. The discharge (Figure 10) was considerably brighter above the probe than below. Figure 11 shows the peak intensity (taken from individual TV scan lines through the glow) as a function of distance above the node. The rate of increase is nearly linear. Below the node, intensity measurements are complicated by the fact that the beam is brighter than the BPD glow. The glow intensity is roughly uniform at a value of approximately 1.0 units from the node all the way to the floor. (Visually, the diameter of the glow seems less near the node than near the target. However, this is an illusion caused by the tendency of the

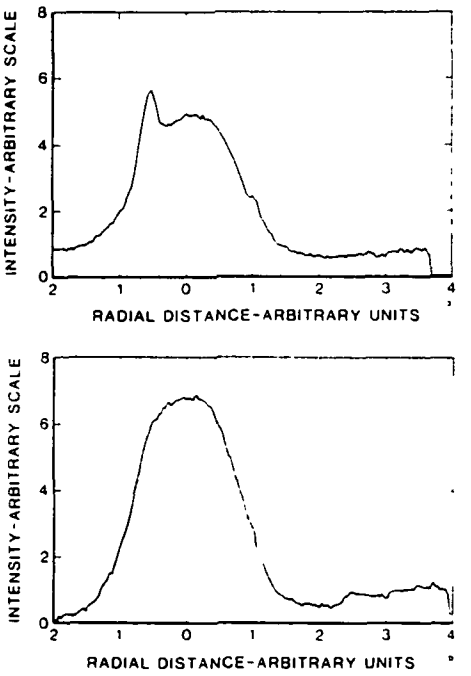

Fig. 9. Intensity scans through the image shown in Figure 6 of a BPD at a large injection angle. The scan in (a) is from the region just above the gun while that of (b) is taken near the top of the picture. The assymetry in (a) is due to the mixture of the BPD glow and the beam itself (left edge).

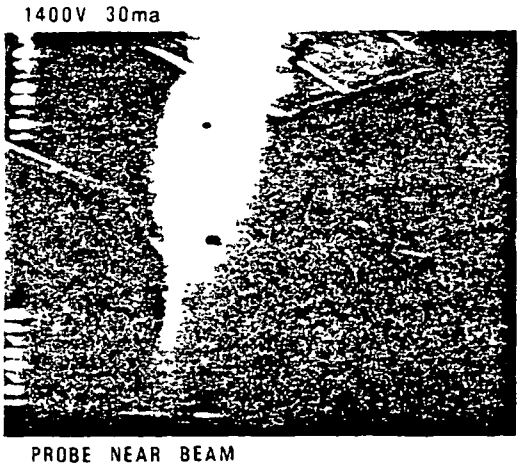

Fig. 10. Under some circumstances, placement of a probe near the last node of the beam suppressed the BPD below the node. The apparent variation in BPD diameter above the node is due to a real variation in intensity along B. See Figure 11.

eye to follow contours of constant intensity. Actually, the glow has a Gaussian cross section with a constant diameter (FWHM) of ~1.2 m in the entire region above the node and below the node as well).

It should be noted that both of these examples of intensity gradients parallel to B pertain to the total visible light rather than to the emission at 3914 Å. Hence they imply gradients in the density of electrons sufficiently energetic to excite visible emissions. But they do not necessarily imply gradients in the density of electrons exceeding the ionization potential.

2. 3914-Å Emission Rates in the BPD

Figure 12 shows the dependence of the total 3914-Å light intensity on beam current ($I_b > I_c$) for E_b = 1.0 kV and B = 1.52 G at approximate injection pitch angles of 0°, 45°, 65°, and 75°. Two features are apparent: (1) the light intensity increases approximately linearly with increasing beam current, and (2) although the intensities observed for 45° injection are somewhat lower than at other angles, the relative intensities at constant I_b ($> I_c$) appear to be rather insensitive to large variations in injection pitch angle. Thus despite the large changes in geometric con-

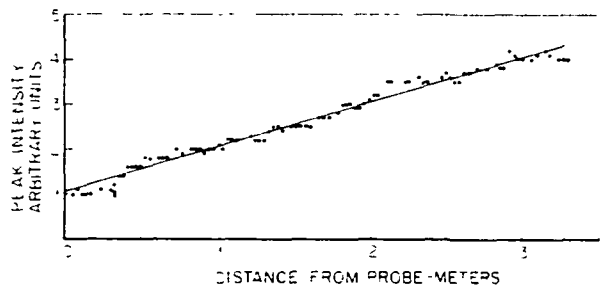

Fig. 11. The relative intensity of the BPD in Figure 11 increases linearly with distance above the probe. The intensity is constant at 1.0 unit below the probe.

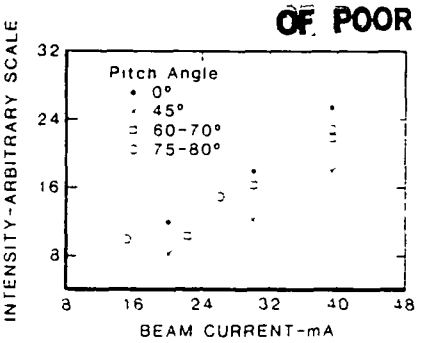

Fig. 12. The intensity of the BPD varies linearly with beam current. Varying the pitch angle changes the absolute intensity but not the slope of the line. E_b = 1000 V, B = 1.5 G, P = 8 × 10^{-9} T.

figuration and primary beam total path length, the total rate of ion production per centimeter of axial path length remains about constant.

Figure 13 shows the dependence of the total ionization rate on beam current for 500-, 1.0-kV, and 1.5-kV beams, B was 1.4 G and $\alpha \sim 0°$. As in Figure 12 the ionization rate varies linearly with the beam current. The three plots have a common slope but are offset by the differences in the voltage-dependent critical current. From plots similar to those of Figure 13 the slopes were determined for nine sets of conditions covering voltages from 500 to 2000 V, magnetic fields from 0.9 to 2.2 G, and pressures from 3.8 × 10^{-9} to 9 × 10^{-6} Torr (density between 1.3 × 10^{11} cm^{-3} and 3.2 × 10^{11} cm^{-3}). Eight of the nine determinations fell within the range

$$\partial N_T / \partial L = (12 \pm 2) \times 10^{14} \text{ ions/cm s}$$

3. Observations at Pressures Below 4 × 10⁻⁹ Torr

It has already been noted that below 4 × 10^{-9} Torr (density of 1 × 10^{11} cm^{-3}) there are strong emissions (below the critical current) related to

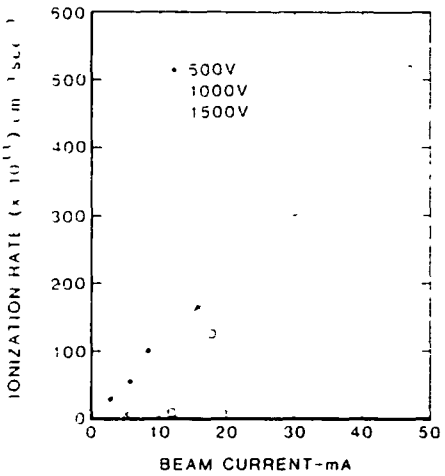

Fig. 13. The ionization rate per centimeter of beam path length in the BPD (calculated from the measurements of 3914-Å intensity) varies linearly with beam current. Varying the beam voltage changes the critical current (I_c) but not the slope of the line. B = 1.4 G, P = 4.6 × 10^{-9} T.

the electron cyclotron frequency and its harmonics and that these emissions are accompanied by a significant anomalous glow. The dependence of the BPD luminosity on beam current is also different than that at higher pressures. Although, because of the difficulty in reaching the lowest pressures, systematic photometric data were not obtained, a few individual photometer scans are available, and these are supplemented by the video imagery.

The ignition curves at very low neutral density are noticeably different from those obtained at higher pressure in two respects. First, at 2 × 10^{-6} torr, ignition of the BPD is indicated by a large jump in the luminosity, while at higher pressures it shows simply as a breakpoint in the slope of the luminosity curve. The resolution provided by the data points is typically a few milliamperes. However, the TV camera was running while the beam current was slowly changing in a continuous manner between fixed settings. The jump in luminosity always occurred within one TV field (1/60 s), presumably corresponding to a small fraction of a milliampere change in current.

A second characteristic of all the low density runs was a definite hysteresis in the Q vs. I_b curves [Bernstein et al., 1978]. Typically, the current I_e at which the BPD extinguished was approximately half the critical current required for ignition. Hysteresis was not observed at pressures above 4 × 10^{-6} torr. For currents between I_e and I_c it was possible to shock the system into BPD by temporarily applying a negative voltage to the target or by temporarily applying an RF signal to a loop antenna to induce an RF discharge near the beam.

The abrupt jump in intensity is characteristic of the BPD at very low pressure. Sometimes, there is a second jump, of about 20%, coupled with a slight reduction in the diameter of the glow [Hallinan et al., 1982]. Under other circumstances there is just a single jump. The differences in circumstances are not clear.

The two steps of the transition to BPD are displaced slightly in either time or current [Hallinan et al., 1982]. The experimental setup did not allow a clear distinction since the current was changing during the transition. The two states of the BPD are similar but differ measurably in the peak intensity and in the diameter of the glow. The final state is the brighter and narrower of the two. The hysteresis region preserves the distinction between the two states of the BPD. As the beam current is reduced, there is a well-defined current at which the glow switches to the wider state. At a still lower current, the BPD is extinguished.

For the purposes of this paper we will ignore the subtlety of the double jump and consider only the total change in optical intensity between the beam-only case and the full BPD. This jump is most easily characterized by the ratio (R) of the total luminosity at a current just above I_c to that at a current just below I_c. This differs from the ratio of peak intensities, particularly for scans taken near a beam node, since both the peak intensity and the glow width can change at BPD ignition.

For a low neutral density BPD the value of R derived from the 3914-Å photometer scans (R_Q) is ~20. At a somewhat higher pressure and magnetic field strength the TV scans yielded visible-light ratios (R_{VL}) of 92 at 1000 V and 128 at 1500 V. The values of R determined from the TV data are five to six times that of the single available photometric determination. Similarly, the cyclotron-associated glow discussed earlier was approximately six times as intense (relative to the beam's intensity) in the TV images as in the published photometer scan. This discrepancy between R_Q (3914 Å) and R_{VL} (integrated visible light dominated by N_2 first positive emissions) is most plausibly explained as resulting from the relatively low energy of the electrons in the glow regions, e.g., for 100 eV electrons, R_{VL} should be roughly 1.5 times R_Q. This takes into account the relative contributions of N_2^+ and N_2 emissions in the TV data as well as the energy dependence of the corresponding collision cross sections. Most likely, the average electron energy is well below 100 eV, leading to values of R_{VL} that are much larger than R_Q.

4. Efficiency of Power Transfer From the Beam to the Plasma

Although some one-dimensional beam particle energy distribution measurements have been made, they have not been complete enough to provide a quantitative estimate of the beam energy loss in transit of the 20-m path length. The 3914-Å total intensity measurements provide a lower estimate of the beam energy loss as manifested by the enhanced ionization rate, provided that the assumptions of uniform axial light emission and of approximate proportionality between 3914-Å emission rate and the ionization rate are reasonably valid.

A convenient starting point is the slope $\Delta Q/\Delta I$ from the curves of luminosity vs. current. As described earlier this slope was found to have a value of (12 ± 2) × 10^{14} ions/cm s A over a wide variety of conditions. The energy lost per ion formed is usually taken to be around 35 eV for energetic electrons. However, the loss is greater for electrons that have energies much less than 1 kV [Stolarski and Green, 1967]. A conservative value is 50 eV per ion.

The total power dissipated is

$$\Delta P = (\Delta Q_T/\Delta I)\ 50\ e\ L\ \Delta I$$

where I is in amperes and L is the path length in centimeters.

$$\Delta P/\Delta I = 19\ W/A$$

Since this value pertains to beams having energies from 500 to 2000 V, the power lost to ionizing collisions is between 1% and 4% of the beam power. It is tempting to express the 19 W/A as 19 V. However, except for calculations of energy dissipation, it is not clear that any particular meaning can be attached to this 'voltage.'

One can also calculate the flux of suprathermal electrons necessary to produce the observed luminosity

$$\Delta F_s/\Delta I = \Delta Q_T/2\ \sigma_s N \Delta I\ e/s\ A$$

where σ_s is the ionization cross section for the suprathermal electrons and N is the nitrogen

density. The factor of 2 results from the presumption that there are equal fluxes in both directions, both contributing to the ionization. The energy flux is

$$\Delta P_s / \Delta I = e\ T_s\ \Delta Q_T / 2\sigma_s N \Delta I$$

where T_s is the typical energy of the suprathermal electrons. The ratio T/σ has a minimum value for energies near 40 eV. Thus the minimum energy flux per ampere of beam current is

$$\Delta P_s / \Delta I = 40\ e\ (\Delta Q_T / \Delta I) / 2\sigma_{40} N$$

At a pressure of 4×10^{-6} torr this reduces to

$$\Delta P_s / \Delta I = 150\ W/A$$

Since there are suprathermal electrons traveling in both directions, there is no net energy flux. However, if the electrons are lost at the ends of the chamber, there would be a net loss of 150 W/A at each end or a total of 300 W/A. For a 500-V beam this would be 60% of the total beam power. This is clearly unreasonable, especially since it does not include additional losses caused by the escape of waves and of heated thermal electrons below the ionization potential.

5. Temporal Variations

The HF Langmuir wave absolute instability occurs typically in random bursts with duration of 10-100 f_p periods [Boyd et al., 1973]. Because of the relatively long lifetime of the plasma and the superthermal electrons (several milliseconds), these temporal variations would not be observable (even with adequate diagnostics) in the optical emissions. Therefore, we have tended to view the BPD as a steady state phenomenon. However, from time to time, various periodic lower-frequency variations (Hz-kHz) in light intensity have been observed in both the TV and photometer displays. These were highly complex in their behavior and could not be repeatedly induced. Sometimes they appeared to be alternations between the single particle beam configuration and the BPD. More often, the BPD glow simply fluctuated in intensity (~20%).

Only those oscillations with frequencies below 60 Hz could be fully examined with the TV systems. When the frequency exceeds 60 Hz, it is aliased by the TV frame rate. This appears in the TV image as a series of horizontal bands that modulate the BPD intensity and drift vertically through the picture. (If the frequency is an exact multiple of 60 Hz, the bands appear stationary). Because of the aliasing, the vertical dimension of the TV picture provides primarily temporal rather than spatial information. The higher the frquency, the closer the bands. The horizontal dimension still provides spatial data.

Frequencies of up to several kilohertz were detected by observing the aliased TV images. These fluctuations were horizontally coherent, i.e., the intensity fluctuations at the center of the column were in phase with those at the edge. Because of the aliasing, the range of vertical coherence cannot be determined with this technique. The fluctuations are occasionally sinusoidal but are more often burstlike with a broad range of frequencies.

Some situations that seem to have induced flickering are (1) setting the beam current just above the threshold current, (2) applying a positive voltage to the collecting target or allowing an isolated electron gun to charge positively, (3) hitting the edge of the target with the beam so that some portions of the glow are on longer flux tubes than others, (4) operating active probes in or near the beam.

Summary of Observations

The major features of the optical observations are as follows:

(1) At current far below the BPD threshold the beam is described by single-particle trajectories of the beam electrons. The luminosity and the ionization rate are given by the appropriate collision cross sections, the beam current, and the neutral density. An intriguing exception to the simple behavior occurs when, owing to the finite spread in $v_\parallel$, a helical beam degenerates into a hollow cylinder. A well-defined dark helix shows that electrons are systematically deterred from entering regions where they would mix with those electrons remaining on the nominal beam helix.

(2) At pressures below 4 μtorr ($n = 1.4 \times 10^{11}$ cm^{-3}) there is sometimes a weak glow surrounding the beam in the absence of BPD. The appearance of this glow is apparently coincident with the onset of narrow-band emissions at frequencies above the electron cyclotron frequency. The intensity (VL) of the glow is proportional to the beam current above a small threshold, and the total light of the glow (VLT) can exceed that produced by the beam itself.

(3) In BPD the beam retains its first node with no measurable alteration, but subsequent nodes are usually undetectable. The beam does not appear to change diameter, although it becomes impossible to differentiate the beam image from that of the brighter BPD glow. Even the glow is usually not much wider than the diameter of the beam at its antinode. In the case of large-angle (helical) injection the BPD glow is almost entirely contained within the helix.

(4) At pressures below 4 μtorr there is a pronounced hysteresis in the curves of ionization rate vs. beam current. The current at which BPD extinguishes (I_e) is about half the value at which it ignites (I_c). When the beam current has a value between I_e and I_c, the system can be shocked into BPD by externally increasing the plasma density. This can be done by inducing an RF discharge near the beam or by reducing the plasma loss rate by applying a negative voltage to the beam collector.

(5) On occasion, at pressures below 4 μtorr, there are two recognizable states of the BPD characterized by somewhat different half-widths for the glow region. The two appear in rapid succession at BPD ignition, and it is unclear whether they are separated by an inherent time delay or simply have slightly different beam current thresholds. In the hysteresis region the BPD switches abruptly between the two states at a well-defined current.

(6) The BPD glow is more or less uniform over most of the length of the beam. But there are gradients in the intensity (VLT) near the gun and also near an immersed probe that interfered with the BPD. (The BPD was suppressed below the probe.) In these regions the intensity increased linearly with z, i.e., in the direction of travel of the beam electrons. The BPD reached full intensity in approximately 2-3 m.

(7) The BPD glow is not always steady. A variety of flicker modes have been observed optically and, in at least one case, with particle counters [Jost et al., 1980]. Optically observed frequencies range from a few hertz to several kilohertz. Optical frequencies above the TV line rate (15.75 kHz) could not be observed. The oscillations were occasionally sinusoidal but were more often burstlike and incoherent. The largest intensity variations were observed for beam currents near I_c; these intensity variations are consistent with a periodic relaxation between the BPD and stable single particle states. Other intensity variations could be produced by a nonuniform termination caused either by placing large probes in the beam or by missing target with part of the beam.

(8) At pressures above 4 μtorr the ionization rate is proportional to the excess of beam current above the critical current. The rate of increase with beam current, $\Delta Q_T/\Delta I$, is approximately 12 x 10^{14} ionization/cm s A. This value holds within ±20% for all combinations of pressure (above 4 μT), magnetic field strength, beam voltage, and pitch angle encountered in the series of experiments. The dependence of Q_T on beam current above I_c was not measured at pressures below 4 μT. The rate of increase in power dissipation associated with the ionization is

$$\Delta P/\Delta I = 19 \text{ W/A}$$

(9) The flux (in each direction) of suprathermal electrons necessary to account for the observed luminosity is

$$\Delta F_s/\Delta I = 2.3 \times 10^{19} \text{ e/s A}$$

If these suprathermal electrons are allowed to escape at the ends of the flux tube (chamber floor and target), they would carry a current of 7.4 A for each ampere of beam current. The power lost would be 300 W for each ampere of beam current.

Discussion

Although the results reported here pertain to investigations of the BPD in the laboratory, a major motivation for the research was to obtain a better understanding of electron beams injected from rocketborne accelerators. Several ionospheric electron accelerator experiments have provided evidence for the occurrence of processes apparently similar to those comprising the beam plasma discharge. Examples include ARAKS [Mishin and Ruzhin, 1978, 1980], $E_\parallel B$ [Bernstein et al., 1982], NVB-06 [Duprat et al., 1983], and Polar V [Grandal et al., 1980]. On the other hand, the abrupt onset of BPD ignition with increasing beam current or neutral density, so characteristic of the laboratory experiments, has not been observed in the rocket experiments except perhaps on the G-60-8 flight [Managadze et al., 1983].

The laboratory experiments do not completely duplicate the space environment. The presence of conducting boundaries and the absence of a homogeneous background plasma are two obvious limitations of the laboratory. Moreover, it is very difficult to maintain in the laboratory the low neutral density appropriate to altitude greater than ~150 km. One cannot expect that the complex of processes referred to collectively as the BPD would occur in space in a manner completely analogous to their occurrence in the laboratory. Nonetheless, the essential plasma physics of a monoenergetic electron beam flowing through a dilute magnetized plasma should be common to the two classes of experiments.

In the present experiments the lower limit to the beam energy loss in the 20-m path length is ~2%. If the energy loss increased linearly with path length, the beam would totally disappear in a 1-km path length. Yet downward injections during the Hess experiment [Davis et al., 1971] and the Echo experiments [Hallinan et al., 1978] produced optically detectable auroral streaks, indicating that beams could be transmitted more than 100 km without any major loss in beam power. Davis et al. [1980] reported the optical detection of a streak produced in the atmosphere conjugate to an upward injection of electrons (L = 1.2). The distance traveled was approximately 7000 km. Estimates of the optical intensity, based on the limiting stellar magnitudes in the video image, indicated that there was no gross dissipation of beam power during its transit. The height-luminosity profiles were suggestive of only a mild spreading in the velocity distribution of the beam.

Quasi-linear theory indicates that the hydrodynamic and kinetic stages of the beam-plasma interaction persist until the beam plasma system is driven to a stable plateau velocity distribution. In their treatments of the hot, dilute beams, which (1) traverse the interplanetary medium to produce type III radio bursts and (2) traverse the ionosphere to produce visible auroral arcs, Papadopoulos [1975] and Matthews et al. [1976] have suggested a stabilization mechanism that allows propagation of a linearly unstable hot beam over large distances without further modification. Hence it is unclear whether the atmospheric optical streaks observed in these rocket experiments imply that the BPD did not occur or simply that the process is stabilized before it destroys the beam.

The laboratory experiments indicate that, for large injection pitch angle, the radial extent of the BPD is limited to the region bounded by the single particle helix; at small injection pitch angle the radial extent is larger than the maximum single particle beam width but is much less than the gyrodiameter for 90° injection. The radial extent is relatively independent of beam current. In their flight, Duprat et al. [1983] have measured the radial extent of the region of strong interaction as characterized by the suprathermal electron and back-scattered primary beam particle fluxes and by the perturbations of the ambient plasma. They suggest that the radial extent is well described by the relationship

$$d = K(I_b)\ \rho_{beams\ \perp}\ \sin\beta_{gun}$$

where $\rho_{beam\ \perp}$ is the nominal gyroradius for 90° injection, and K is a proportionality constant that is 6 for 100-mA and 3.7 for 10-mA beams, and β_{gun} is the injection pitch angle. Thus, in this flight experiment, the radial extent of the interaction region was current dependent and was proportional to but much greater than the nominal gyroradius.

At the present time it is somewhat difficult to reconcile these laboratory and flight results. It is possible that slow radial diffusion of the beam occurs with increasing path length , but that a relatively large path length (hundreds of meters) would be required for significant increases in radius to be apparent. Second, it has been noted that, qualitatively, the BPD diameter in the laboratory increases with decreasing neutral density; however, the data are insufficient to permit an extrapolation to the neutral density of 10^9–10^{10} that surrounds the rocket at 200-km altitude.

Another important issue in comparing laboratory and flight results is the question of axial confinement of suprathermal electrons. It was shown earlier that, if these electrons are free to leave the system, the power necessary to replace them is as much as 60% of the beam power. This is clearly unrealistic. Moreover, the ion current would be unable to match the electron current. In a typical example (I_b = 50 mA, $N_1 = 2 \times 10^7$ cm^{-3}, and $A_b = 3 \times 10^4$ cm^2) the ion velocity required to produce an ion flux equal to the suprathermal electron flux is 2×10^6 cm/s. This would correspond to an ion energy of 53 eV. Obviously, there must be confinement of suprathermal electrons.

The apparently severe beam energy loss, derived on the assumption of free axial escape of the suprathermal electrons, arises because the mean free path for ionization is much greater than the finite system length. Almost all the suprathermal energy is lost to the boundaries rather than expended in ionization. An alternate description can be formulated in terms of the Townsend condition [$T_1 < 1$] necessary for the occurrence of a discharge. This condition can be restated as $L_1 \sigma/2 > 1$, for our experimental conditions, and assuming free suprathermal escape, $L_1 \sigma/2 < 3 \times 10^{-2}$, so that a discharge would not be possible.

Papadopoulos [1982] recognized the need for axial confinement of the suprathermal electrons, confinement is the equivalent of a large increase in L. He suggested that the confinement must be provided by the naturally arising electrostatic sheaths at the boundaries which equalize the ion and electron loss rates to maintain charge neutrality. Reduction of the suprathermal loss rate to the ambipolar rate would simultaneously greatly reduce the estimated beam energy loss and allow the Townsend condition to be satisfied.

Estimation of sheath potential drop is uncertain because both the suprathermal electron velocity distribution and the abundance relative to the thermal plasma are only poorly known. However, in order to affect ionization probabilities the potential barrier must exceed the ionization potential (≈ 16 V), because of the small values of the ionization cross section near threshold, more likely +30–50 V potentials should be required. The BPD column should therefore be at a positive potential with respect to the ends, with a maximum value of +30–50 V midway between gun and collector. A sheath of this magnitude would totally confine the thermal electrons while allowing the escape of just enough suprathermals to balance the ion current at the boundaries. The loss of one suprathermal for each ion lost implies an energy flow to the boundaries roughly equal to the power dissipated by ionizations in the BPD. Hence the total power lost from the beam would be approximately 40 W/A.

However, measurements of the plasma potential in the laboratory do not support such a large sheath potential (>20 V). At the midpoint of the chamber, Szuszczewicz [1982] measured a maximum potential of 3.1 V with a movable Langmuir probe. In the cooler plasma outside the BPD column the potential was 2.5 V. The optical observations reported here are consistent with a relatively low plasma potential. There is no observable change in the location of the first node at the transition to BPD. With a 1-kV beam a change of ~6 V would produce an observable shift. Hence the plasma potential during BPD differs from that of the beam alone by less than 6 V.

It can be speculated that the BPD turbulence could inhibit the free escape of suprathermal electrons (K. Papadopoulos, personal communication, 1982). In this case the optical intensity would maximize where the suprathermals are produced. This would be consistent with the spatial gradients (Figures 6, 9, 10, and 11) in luminosity. Additional support comes from measurements of the HF wave amplitudes by Jost et al. [1982]. The amplitudes were found to increase by 5–10 dB between locations 1 m and 4 m above the accelerator. The observed gradients in optical intensity and in electric field strength are similar.

The question of confinement of suprathermal electrons is important in attempting to apply the laboratory results to the space environment. If the confinement in the laboratory is due to sheaths at the boundaries, there is no precise analog in free space. However, if the same wave turbulence that creates the suprathermals also confines them, the laboratory results may be more relevant to space. It should be noted that the path length was 20 m, while the observed spatial gradients were ~3–4 m.

Acknowledgements. We wish to acknowledge support from the National Science Foundation (grant ATM80-22550), the National Aeronautics and Space Administration (grant NAGW-69) and the National Oceanic and Atmospheric Administration (grant NA-83RAA01238). We also thank Y. Llobet and C. Deehr for their helpful discussions. The digital video analysis capability was developed by J. Baldridge and P. Wagner. The Editor thanks J. R. Winckler and G. R. J. Duprat for their assistance in evaluating this paper.

References

Bernstein, W., et al., Electron beam experiments: The beam plasma discharge at low pressures and magnetic field strengths, Geophys. Res. Lett., 5, 127, 1978.

Bernstein, W., H. Leinbach, P. J. Kellogg, S. J.

Monson, and T. Hallinan, Further laboratory measurements of the beam plasma discharge, J. Geophys. Res., 84, 7271, 1979.

Bernstein, W., P. J. Kellogg, S. J. Monson, R. H. Holzworth, and B. A. Whalen, Recent observations of beam plasma interactions in the ionosphere, in Artifical Particle Beams in Space Plasma Studies, edited by B. Grandal, Plenum, New York, 1982.

Borst, N. L., and E. C. Zipf, Cross-section for electron-impact excitation of the (0, 0) first negative band of N_2^+ from the threshold to 3 keV, Phys. Rev. A., 1, 834, 1970.

Boyd, D., W. Carr, J. Marrickam, B. Rosen, and M. Seidel, Transition from absolute to convective instability in a beam-plasma system, Phys. Rev. Lett., 30, 1296, 1973.

Davis, T. N., T. J. Hallinan, G. D. Mead, J. M. Mead, M. C. Trichel, and W. N. Hess, Artificial aurora experiment: Ground-based optical observations, J. Geophys. Res., 76, 6082-6092, 1971.

Davis, T. N., W. N. Hess, M. C. Trichel, E. M. Wescott, T. J. Hallinan, H. C. Stenbaek-Nielsen, and E. J. R. Maier, Artificial aurora conjugate to a rocket-borne electron accelerator, J. Geophys. Res., 85, 1722-1728, 1980.

Duprat, G. R. J., B. A. Whalen, A. G. McNamara, and W. Bernstein, Measurements of the stability of energetic electron beams in the ionosphere, J. Geophys. Res., 88, 3095, 1983.

Galeev, A. A., E. V. Mishin, R. Z. Sagdeev, V. D. Shapiro, and I. V. Shevchenko, Discharge in the region around a rocket following injection of electron beams in the ionosphere, Sov. Phys. Dokl., 21, 641, 1976.

Getty, W. D., and L. D. Smullin, Beam plasma discharge· Buildup of oscillations, J. Appl. Phys., 34, 3421, 1963.

Grandal, B., E. V. Thrane, and J. Troim, Measurement of the 391.4 nm light produced by an artificial electron beam in the upper atmosphere, Planet. Space Sci., 28, 291, 1980.

Hallinan, T. J., H. C. Stenbaek-Nielsen, and J. R. Winckler, The Echo 4 electron beam experiment: Television observation of auroral streaks indicating strong beam interactions in the high-latitude magnetosphere, J. Geophys. Res., 83, 3263-3271, 1978.

Hallinan, T. J., F. H. Leinbach, and W. Bernstein, Visible signatures of the multi-step transition to a beam-plasma-discharge, in Artificial Particle Beams in Space Plasma Studies, edited by B. Grandal, Plenum, New York, 1982.

Jost, R. J., H. R. Anderson, and J. O. McGarity, Electron energy distributions measured during electron beam-plasma interactions, Geophys. Res. Lett., 7, 509, 1980.

Jost, R. J., H. R. Anderson, W. Bernstein, and P. J. Kellogg, Radial dependence of the HF wave field strength in the BPD column, in Artificial Particle Beams in Space Plasma Studies, edited by B. Grandal, Plenum, New York, 1982.

Kellogg, P. J., H. R. Anderson, W. Bernstein, T. J. Hallinan, R. W. Holzworth, R. J. Jost, F. H. Leinbach, and E. P. Szuszczewicz, Laboratory simulation of injection of particle beams in the ionosphere, in Artificial Particle Beams in Space Plasma Studies, edited by B. Grandal, Plenum, New York, 1982.

Matthews, D. L., M. Pongratz, and K. Papadopoulos, Nonlinear production of suprathermal tails in auroral electrons, J. Geophys. Res., 81, 123, 1976.

Mishin, E. V., and Yu. Ya. Ruzhin, Beam plasma discharge during electron beam injection in the ionosphere; dynamics of the region in rocket environment in ARAKS and ZARNITZA-2 experiments, Rep. 21a, b, Acad. Sci. USSR, Inst. Terr. Mag. Ionos. Radio Propag., Moscow, 1978.

Mishin, E. V., and Yu. Ya. Ruzhin, The model of beam-plasma discharge in the rocket environment during an electron beam injection in the ionosphere, Ann. Geophys., 36, 423, 1980.

Managadze, G. G., S. B. Lyakhov, B. M. Balabanov, T. I. Gagua, A. A. Martinson, A. D. Mayorov, M. F. Friedrich, W. K. Reidler, Z. Klos, N. A. Laliashvili, and N. A. Leonov, Plasma processes caused by an electron beam injected from a high altitude rocket probe; Studies of beam-plasma discharge, Rep. IWF 8303, Tech. Univ. Graz, Austria, 1983.

Papadopolous, K., Non-linear stabilization of beam-plasma interactions by parametric effect, Phys. Fluids, 18, 1769, 1975.

Papadopoulos, K., Theory of beam-plasma discharge, in Artificial Particle Beams in Space Plasma Studies, edited by B. Grandal, Plenum, New York, 1982.

Sharp, W. E., Low energy distribution produced by a beam-plasma discharge, Eos Trans. AGU, 62, 1001, 1981.

Smullin, L. D., A review of the beam plasma discharge, in Relation Between Laboratory and Space Plasma, edited by H. Kikuchi, D. Reidel, Hingham, Mass., 1981.

Stolarski, R. S., and A. E. S. Green, Calculations of auroral intensities from electron impact, J. Geophys. Res., 72, 3967-3974, 1967.

Szuszczewicz, E. P., Direction measurements of plasma characteristics in space simulation beam-plasma interactions, paper presented at 20th Aerospace Science Meeting, Am. Inst. Aeronaut. Astronaut., Orlando, Florida, January 11-14, 1982.

Szuszczewicz, E. P., D. N. Walker and H. Leinbach, Plasma diffusion in a space simulation beam-plasma discharge, Geophys. Res. Lett., 6, 201, 1978.

Szuszczewicz, E. P., K. Papadopoulos, W. Bernstein, C. S. Lin, and D. N. Walker, Threshold criterion for a beam plasma discharge, J. Geophys. Res., 87, 1565, 1982.

Winckler, J. R., The application of electron beams to magnetospheric research, Rev. Geophys. Space Phys., 18, 659, 1980.

T. J. Hallinan, Geophysical Institute, Fairbanks, AK 99701.

H. Leinbach, National Oceanic and Atmospheric Administration, Boulder, CO 80302.

G. Mantjoukis and W. Bernstein, Rice University, Houston, TX 77001.

(Received August 9, 1983,
revised November 7, 1983,
accepted November 22, 1983.)

JOURNAL OF GEOPHYSICAL RESEARCH, VOL 90, NO A6, PAGES 5187-5196, JUNE 1, 1985

The Spatial Evolution of Energetic Electrons and Plasma Waves During the Steady State Beam Plasma Discharge

X. LLOBET[1] AND W BERNSTEIN

Department of Space Physics and Astronomy, Rice University, Houston, Texas

A. KONRADI

Solar System Exploration Division, NASA Johnson Space Center, Houston, Texas

Changes in the characteristics of the electron beam and the associated wave spectrum as a function of axial distance from the electron gun have been studied in a steady state laboratory beam plasma discharge. The beam energy distribution evolves from a monoenergetic beam to a heated beam (characteristic of trapping) and then to an almost flat (plateau) distribution with increasing distance from the gun. The wave spectrum evolves similarly from a small amplitude single band at the upper hybrid frequency $f_{UHF} = (f_p^2 + f_c^2)^{1/2}$ to a much larger amplitude, harmonic rich spectrum with increasing distance Accompanying the degraded energy spectrum, the valleys between the harmonic peaks disappear to produce a continuous spectrum greater than f_{UHF} with reduced amplitude Very little spatial diffusion or pitch angle scattering of the beam is observed, indicating that the interaction is predominantly one-dimensional The axial positions, where these different wave-beam electron configurations appear, depend upon the experiment parameters, beam current I_b, beam energy E_b, and neutral density The described results clearly indicate the occurrence of the absolute rather than the convective instability and confirm that the beam plasma discharge (avalanche ionization) is a particular manifestation of the well-studied strong beam-plasma interaction (avalanche ionization absent)

INTRODUCTION

Experiments, in which energetic (keV) electron beams have been injected into the ionosphere–upper atmosphere system from rocket-borne electron guns, have provided reasonably clear evidence for the occurrence of strong beam-plasma interactions (BPI) both near to and remote from the injection point [*Galeev et al.*, 1976, *Maehlum et al.*, 1980; *Duprat et al.*, 1983, *Managadze et al.*, 1983; *Arnoldy et al*, 1984, *Wilhelm et al*, 1985] On the other hand, the flight experiments have not provided clear and unambiguous evidence for the basic physical processes which produce the very wide variety of confusing signatures. Some shortcomings of the flight experiments arise from both the very limited capabilities of the diagnostics employed to date and the difficulties in arranging the proper spatial location of these diagnostics.

In an effort to clarify some of these ambiguities, a laboratory experimental program was initiated which simulated (1) the long pathlength, (2) low neutral density, (3) low magnetic field strength, and (4) the small beam–large ambient plasma radial configuration present in the ionosphere It must be emphasized that, unlike the ionosphere, the initial ambient plasma in these experiments was self-produced (i e., by collisional ionization of the ambient neutral gas by the beam) rather than by an alternative (not beam related) source. These experiments were initially carried out in the very large (26 5 m path length) vacuum chamber at the Johnson Space Center (JSC), following its deactivation in 1982, scaled experiments were continued in a smaller (2.6 m path length) chamber also located at JSC. These earlier experiments, which identified ignition of the beam plasma discharge (BPD) and some of the gross characteristics of the steady state BPD, were reported by *Bernstein et al.* [1979, 1983] and *Hallinan et al* [1984] This work stimulated the recent theoretical analyses of BPD ignition by K Papadopoulos (unpublished manuscript, 1984) and *Llobet* [1984]

In this paper we describe some new experimental studies of the evolution of both the beam energy spectrum and the local wave amplitude-frequency spectrum at increasing axial distances from the electron gun for a variety of experiment conditions (E_b, I_b, and neutral density) Measurements of this type have been an intrinsic part of all earlier studies of the beam-plasma interaction [*Shustin et al*, 1969, *Levitskii and Shashurin*, 1967, *Gentle and Lohr*, 1973, *Jones et al*, 1976, *Seidl et al*, 1976, *Whelan and Stenzel*, 1983, *Wong and Cheung*, 1984] Areas of agreement and inconsistency with these earlier experiments will be described

Incomplete and isolated measurements of this type were carried out in the early large chamber experiments For instance, *Jost et al* [1980] reported modest beam heating during the steady state BPD with their energy analyzer located just in front of the beam termination and at the radial periphery of the beam region In another series of measurements, *Jost et al.* [1982] observed the severe radial confinement of large amplitude plasma waves to the radial extent occupied by the beam, but the measurements only extended over a small axial distance

EXPERIMENTAL ARRANGEMENT

These experiments were performed in the small laboratory BPD device, schematically shown in Figure 1 [*Konradi et al*, 1983], the important diagnostics included directional retarding potential analyzers and RF probes A positioning system was installed near the gun end of the device to allow quantitative motion of the diagnostics (axial, radial, and pitch angle) over the limited range 26 cm to 52 cm from the gun A second radially movable but axially fixed diagnostic probe could be inserted 191 cm from the gun, rotation of this probe provided

[1] Now at Institute for Fusion Studies, University of Texas, Austin.

Paper number 4A8391
0148-0227/85/004A-8391$05 00

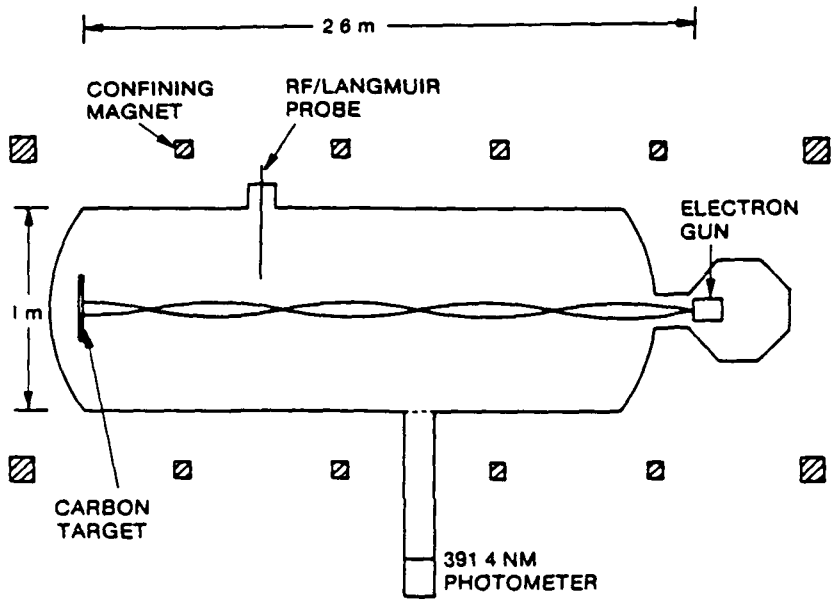

Fig. 1 Schematic representation of the experimental configuration

a very qualitative scan in pitch angle. The RF probes were interchanged with the two energy analyzers to provide the accompanying wave measurements. Thus the particle and wave data were obtained sequentially rather than simultaneously

The Pierce type tungsten cathode electron gun was the same gun employed in the large chamber experiments and had a perveance of $\sim 1.3 \times 10^{-6}$ A $V^{-3/2}$ and a divergence angle of $\sim \pm 5°$ Because of the divergence angle and the small anode aperture (0.25 cm diameter), alignment of the beam with the solenoidal magnetic field resulted in the familiar noded pattern when the beam-plasma configuration was stable ($I_b < I_c$) The beam was terminated in a carbon collector Both the electron gun and the collector were electrically grounded All the described measurements employed beam injection nominally parallel to the 19-G field, although the facility allowed field strengths up to 38 G. The positioning system provided axial motion parallel to the axis of the vacuum chamber However, because the axes of the solenoidal magnetic field and of the chamber were not exactly parallel and the beam was also injected at a small pitch angle, this axial motion actually produced a radial displacement of the detectors from the beam axis Therefore it was necessary to readjust the radial position at each axial location, it was assumed that the maximum flux was observed at the beam axis for each position, but certainly comparisons of the fluxes observed at different axial positions are qualitative. The beam noding patterns introduced similar problems The chamber base pressure was usually less than 1×10^{-6} torr and could be increased to 4×10^{-4} torr by addition of dry nitrogen, this upper limit was set by the possibility of breakdown within the gun

The directional retarding potential energy analyzer was based on the retarding potential analyzer concepts described by *Stenzel et al* [1983] It basically consisted of a multihole collimator system, retarding and isolating grids, and a collector electrode biased at +30 V to reduce secondary electron emission and ion collection effects In order to reduce interference with the beam-plasma system and magnetic field effects, both the diameter and the total length of the system were small, ~0.4 cm. Rather than employing the μ channel collimating plate described by Stenzel et al, we followed their suggestion of using a set of very small drilled holes giving a circular field of view with an $\sim \pm 5°$ full acceptance angle and a total geometric factor of $\sim 10^{-3}$ cm^2 sr. The typical energy resolution ($\Delta E/E$ at full width at half maximum (FWHM)) for a stable "single particle" beam was ~7% Because the voltage applied to the retarding grid equaled the energy of the particles to be analyzed, we found it necessary to limit the beam energy to $\lesssim 1000$ V Even at low beam energies and modest beam currents we encountered severe breakdown problems which appeared to be associated with heating of the detector by the dc beam. The retarding potential analyzer had been operated as an integral detector, the differential energy spectrum was obtained later by differentiation of the integral curve. The usual time required for a complete energy scan was 20 s. Typical detector currents ranged from 5×10^{-5} to 10^{-8} A, current fluctuations were assumed to be temporal in origin and were ignored.

The RF probe was a simple coaxial system with the inner conductor extending ~5 mm beyond the grounded outer conductor Measurements showed the frequency response to have been reasonably flat up to 1 GHz. These wave measurements provide only frequency and relative amplitude data, we have not obtained absolute field strength measurements to date Tests with an external oscillator indicated that harmonics were not introduced by the probe-cable-spectrum analyzer system. However, we have not determined whether the probe-plasma coupling might have introduced harmonic distortion

We have made two important assumptions in this work

1. The idealized objective was the study of the interaction during both the steady state BPD (avalanche ionization present) and the steady state BPI (avalanche ionization absent) The theoretical treatments of K. Papadopoulos (unpublished manuscript, 1984) and *Llobet* [1984] indicate that BPD ignition and the threshold for the BPI occur at the same ambient plasma density n_a and beam density n_b values for a self-generated plasma. The ambient neutral density must be sufficiently high and the plasma lifetime sufficiently long to allow accumulation of the required n_a by collisions, this neutral den-

sity is high enough that BPD ignition and the steady state BPD are almost always observed once the interaction thresholds are achieved. Therefore it has not been possible to produce steady state BPI in our device using only the self-generated ambient plasma.

We have assumed that the enhanced ionization during the BPD simply results in a somewhat, though not quantitatively, controllable ambient plasma density, but that the basic plasma physics of the BPD and BPI are the same. The variable avalanche ionization rate is also associated with a variety of LF (<1 kHz) variations which somewhat confuse but do not preclude meaningful wave and particle measurements.

2. The insertion of probes into the active region could produce both gross and subtle modifications in the plasma physics. To study these effects, we determined the modifications in the current required for BPD ignition I_c produced by the insertion of large and small objects at different axial and radial positions. If the object was sufficiently large to effectively terminate the beam, the $I_c \sim 1/L$ (where L is the pathlength) scaling given by *Bernstein et al.* [1979] was observed. When the intercepted current was only a small fraction of the beam current, I_c increased about inversely with the reduction in the calculated total volume ionization rate (and therefore ambient density) consistent with the ignition model given by K. Papadopoulos (unpublished manuscript, 1984). Remember that the insertion of the obstacle only modifies the beam cross-sectional area, not beam density, provided radial diffusion of the beam electrons is slow Certainly, a gross modification in I_c would be expected if the small obstacle were located at a node, and we have made some effort to select parameters where this did not occur. The antinode diameter for a stable 1-keV, 5° divergence half-angle beam is ~2 cm, compared with the 0.4-cm diameter detector, so that the detector is effectively a small obstacle. Second, the measurements were carried out during the steady state BPD where the nodes have broadened or disappeared and the beam diameter more closely equals that of the antinode.

On the other hand, we have some evidence that the presence of obstacles does modify the configuration For example, insertion of a probe at 191 cm produced both large changes in the low frequency variation pattern and small changes in the energy spectrum recorded by the probe located at 56 cm from the gun. Not surprisingly, insertion of a probe near the gun produced similar modifications in the data recorded by the downstream probe. In fact, when the two probes were aligned on axis, the LF variations were in phase, but when one probe was on axis and the other at the radial boundary, the variations were markedly out of phase. Because of these effects, only single, rather than simultaneous, probe measurements have been made. We neglect these physically unimportant modifications produced by probe insertion in our analysis.

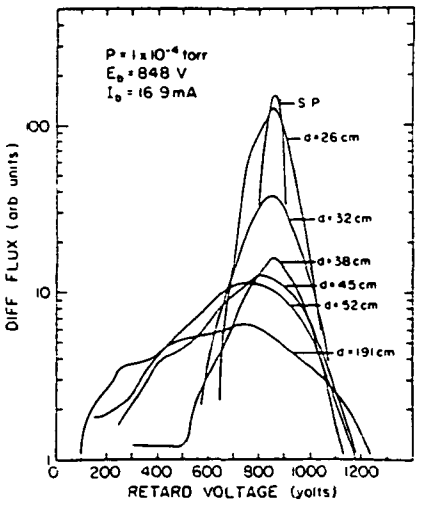

Fig. 2*a* Energy spectra (0° detector pitch angle) measured at 26, 32, 38 45, 52, and 191 cm from the gun for an 848-V, 16 9-mA beam at $p = 1 \times 10^{-4}$ torr, the energy spectrum observed for this energy beam under stable conditions (SP) is also shown

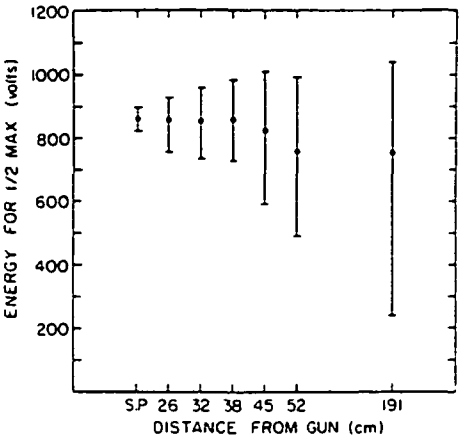

Fig. 2*b* FWHM in volts for the various spectra shown in Figure 2*a*; the solid circles indicate the energy at which the maximum flux is observed. Note the nonlinear axial distance scale, the single particle spectrum was obtained for $I_b < I_c$ and is shown for reference only Obviously, the single particle spectrum should be present for all beam currents at the injection point

Experimental Results

Figure 2*a* shows the differential energy spectra during a steady state BPD observed at various axial distances from the electron gun for the following experiment conditions: $I_b =$ 16 9 mA, $E_b = 848$ V, $P = 1 \times 10^{-4}$ torr N_2, and detector pitch angle of 0° A typical measured single particle (stable) spectrum is included for reference, supplementary measurements indicate that the measured width of the spectrum represents the resolution of the detector. Even at the shortest distance (26 cm), significant broadening of the energy distribution is present. This initial broadening appears to be symmetric in the sense that equal fluxes are accelerated to $E > E_b$ and decelerated to $E < E_b$ while the energy of the peak remains relatively constant The width of the energy distribution increases with increasing distance Then at distances beyond 45 cm the accelerated component remains unchanged while the low energy cutoff continues to decrease to lower energies, so that the average particle energy decreases This behavior is summarized in Figure 2*b*, which shows the dependence of the energy width (measured at half maximum) on distance; the solid circles indicate the energy at which the maximum differential flux occurs.

Figure 3 shows the dependence of the wave spectra on axial distance for somewhat different experiment conditions $I_b =$ 27 4 mA, $E_b = 850$ V, and $P = 3 \times 10^{-5}$ torr N_2, accompanying energy spectra observed at each position are sketched on the right side At 26 cm a narrow peak is observed at 170 MHz with relatively small amplitude harmonics, if we assume that the fundamental corresponded to the ambient plasma frequency ($f_{UHF} \approx f_p$ for $f_p \gg f_c$), $n_a = 3\,6 \times 10^8$ cm^{-3}. At 52 cm the amplitude has increased by approximately 34 dB, and

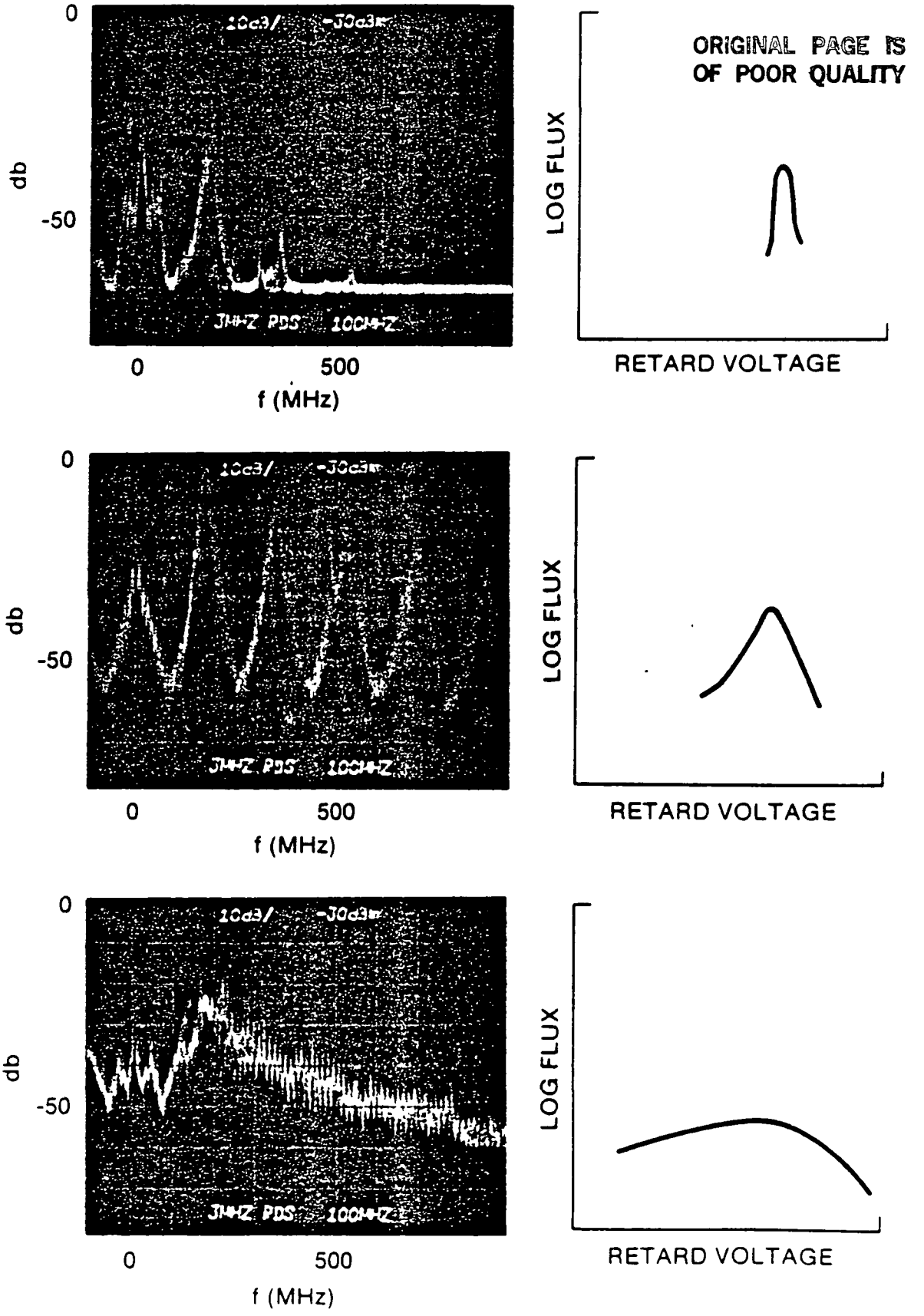

Fig. 3. RF spectra observed at 26, 52, and 191 cm (top to bottom) from the gun for an 850-V, 27.4-mA beam; the corresponding energy spectra are shown schematically. $P \approx 3.5 \times 10^{-4}$ torr.

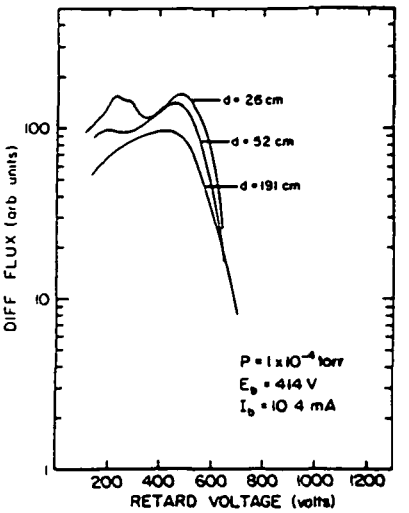

Fig. 4 Energy spectra (0° detector pitch angle) measured at 26, 52, and 191 cm from the gun for a 414-V, 10.4-mA space charge limited beam ($K = 1.23 \times 10^{-6}$ A $V^{-3/2}$) at $p = 1 \times 10^{-4}$ torr

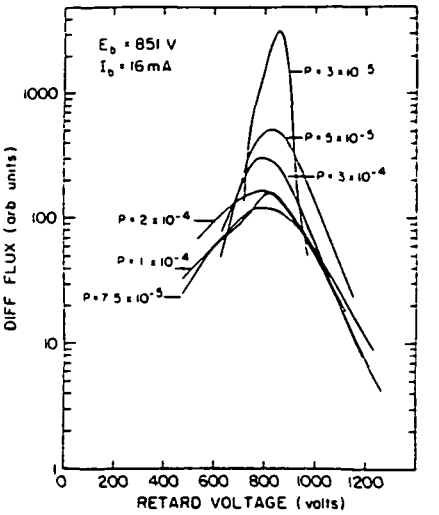

Fig 6a The variation of the energy spectra (0° detector pitch angle) measured 52 cm from the gun with pressure measured in torrs (neutral density) for a constant energy (851 V), constant current (16 mA) beam.

the fundamental frequency remains 170 MHz, but the relative harmonic amplitude ($n = 2$–5) has increased significantly Finally, at 191 cm the frequency spectrum has greatly broadened, extending up to 0 9 GHz, with only the slightest trace of the harmonic pattern present at 52 cm. The amplitude has decreased by approximately 20 dB, with the maximum amplitude still appearing at 170 MHz. Energy spectra at 26 cm show slight beam heating, at 52 cm show severe beam heating (still symmetric), and at 191 cm show the very broad, degraded energy spectrum Clearly, the axial variations of the wave patterns and of the beam energy distribution are intimately related

Figures 4 and 5 show the axial distance variation of the beam energy spectrum for almost space charge limited beams ($K = IV^{-3/2} = \text{const}$) at 414 V ($K = 1\,23 \times 10^{-6}$ A $V^{-3/2}$) and 855 V ($K = 1.06 \times 10^{-6}$ A $V^{-3/2}$), respectively; $P = 1 \times 10^{-4}$ torr N_2, and the detector pitch angle is 0°. Not shown are measurements for $E_b = 604$ V and 748 V Because of the beam divergence angle, space charge limited operation implies approximately constant beam density at the antinodes At 414 V the broad degraded spectrum is already observed at 26 cm from the gun, implying that the severe modifications occurred at shorter distances. At 855 V the heated but not degraded spectrum is observed at 26 cm, the degraded spectrum is present at distances of ≥ 52 cm. These results, together with those obtained at the intermediate voltages, show that interaction regions tend to move further from the gun with increasing beam energy at constant perveance It should be noted, however, that the ambient plasma production rate and therefore the ambient plasma density increases with increasing beam power during BPD [*Hallinan et al*, 1984], although the gun perveance remains constant

Figure 6a shows the energy spectra observed at 52 cm for different neutral densities, experiment conditions were $I_b = 16$ mA, $E_b = 851$ V, and detector pitch angle of 0° Clearly, even at low neutral densities the symmetric heated beam is observed The beam width (FWHM) increases with increasing neutral density up to $\sim 1 \times 10^{-4}$ torr N_2, but the width is significantly reduced at 3×10^{-4} torr N_2 The dependence of the energy width (FWHM) on neutral density is summarized in Figure 6b These data imply that the interaction regions move closer to the gun with increasing neutral density but

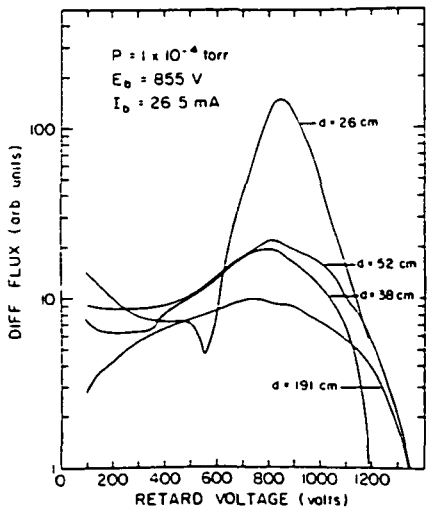

Fig 5 Energy spectra (0° detector pitch angle) measured at 26, 38, 52, and 191 cm from the gun for an 855-V, 26 5-mA, almost space charged limited ($K = 1\,06 \times 10^{-6}$ A $V^{-3/2}$) beam at $p = 1 \times 10^{-4}$ torr

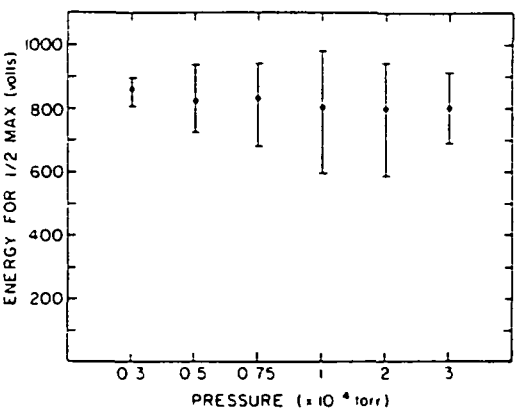

Fig 6b FWHM in volts for the various spectra shown in Figure 6a Again note the nonlinear pressure scale

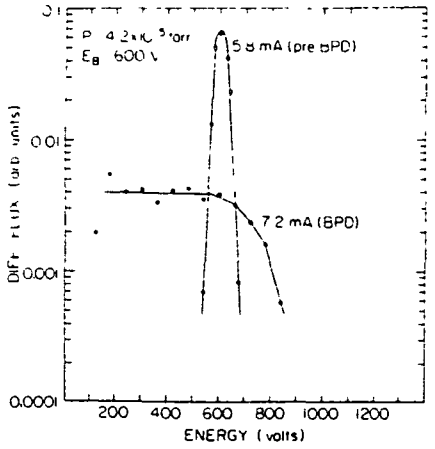

Fig 7 Energy spectra measured with the detector (0° detector pitch angle) located at 191 cm from the gun for pre-BPD (I_b = 5 8 mA) and BPD (I_b = 7 2 mA), E_b = 600 V and $P = 4\,2 \times 10^{-5}$ torr

that at pressures greater than 1×10^{-4} torr N_2 the interaction process is modified Wave measurements indicate that the ambient plasma density is proportional to the neutral density up to $\sim 1 \times 10^{-4}$ torr N_2 but then increases more slowly with further increases in neutral density Prior measurements of the optical emissions and whistler wave amplitude ($f < f_c$) show that major changes in these features also occur at neutral pressures of $1\text{–}2 \times 10^{-4}$ torr [*Bernstein et al.*, 1983]

The abrupt transition from the stable (pre-BPD) state to the BPD at the critical beam current I_c is also apparent in the gross changes in the energy spectra measured by the detector located at 191 cm from the gun, as shown in Figure 7. As a general rule, only the final evolutionary state is observed during BPD for all values of $I_b > I_c$ by the detector located near the beam termination, none of the intermediate evolutionary states described earlier are detected at that position The corresponding integral curves for the stable and BPD cases give agreement in total beam fluxes to better than a factor of 2 Figure 8 shows the dependences of the energy spectra measured at 191 cm on beam current for beam currents of $> I_c$ For this case, I_c was $\sim$6–7 mA Note the constant spectral shape and the scaling of the differential flux with beam current

The dependence of the beam energy spectra on both the radial position and the detector pitch angle at different axial positions has also been studied Figure 9 shows the dependence of the integral flux at $E > 300$ V on radial position and the differential energy spectra measured on axis at 52 and 191 cm, the experiment conditions were I_b = 27 4 mA, E_b = 862 V, $P = 3 \times 10^{-5}$ torr N_2, and detector pitch angle of 0° The two energy spectra are consistent with the previously described results, at 52 cm the symmetric heated beam distribution is observed, whereas at 191 cm the very broad, degraded spectrum is present The radial widths at the $1/e$ flux level are $\sim$0 4 cm at 52 cm and $\sim$1 2 cm at 191 The narrow width at 52 cm is less than the estimated antinode radius, 0 91 cm, but this could be the result of the persistence of the beam noding pattern at 52 cm. The 1 2-cm radial width measured at 191 cm is more consistent with the antinode width Therefore the increased radius observed at 191 cm may not necessarily be indicative of radial diffusion of the beam with increased path length. In general, however, these radial widths are very small in comparison to the 90° gyroradius of an 862-V electron, 5 2 cm.

Spectra measured at different radial positions indicate that the FWHM increases slowly with increasing radial distance However, as noted earlier, these small variations might be attributed to a modification of the BPD characteristics produced by the presence of the analyzer

Figure 10 presents some initial measurements of the pitch angle dependence of the energy spectra The data shown are for an 850-V, 25-mA beam at $P = 5 \times 10^{-5}$ torr, the axial position of the detector was 52 cm from the gun As noted earlier, the detector full field of view was $\sim \pm 5°$ circular The spectra at 0° and 12° (center) are very similar, but the spectrum at 24° (center) shows a gross shift toward lower energies with a decrease of about a factor of 50 in the detected flux at nominal beam energy Comparison of the integral fluxes at $E > 300$ V shows a reduction of $\sim$30 as the detected pitch angle is shifted from 0° to 24° Although the 0° energy spectrum shown here is broad, it remains symmetric, and there is no good evidence for gross energy degradation However,

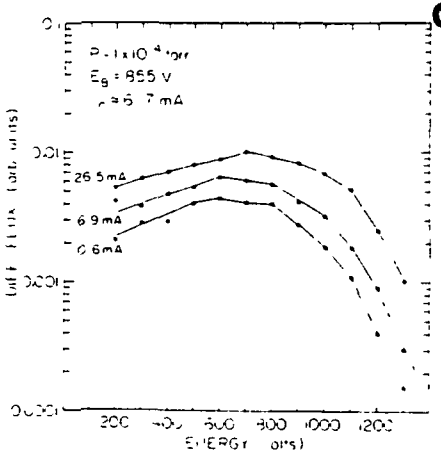

Fig 8 Energy spectra measured with the detector (0° detector pitch angle) located at 191 cm from the gun for various $I_b > I_c$, E_b = 855 V, and $P = 1 \times 10^{-4}$ torr For these conditions, $I_c \approx$ 6–7 mA

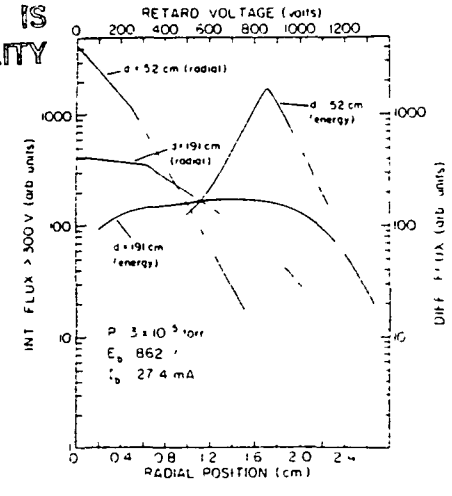

Fig 9 Energy spectra (on axis and 0 detector pitch angle) and the dependence of the integrated flux of > 300 V on radial position (0° detector pitch angle) measured at 52 and 191 cm from the gun The beam energy was 862 V beam current 27 4 mA, and $p = 3 \times 10^{-5}$ torr

qualitatively very similar pitch angle dependences were observed using the detector located at 191 cm, where energy degradation was apparent.

SUMMARY OF RESULTS

The beam energy and wave frequency spectra show important correlated changes with increasing distance from the electron gun for constant experiment conditions (E_b, I_b, neutral density)

1 At short distances the initially monoenergetic electron beam is heated; the heating is symmetric in the sense that the average (peak) energy remains unchanged. The wave spectrum is characterized by a single narrow band emission at f_p with small amplitude higher harmonics

2. At larger distances the beam heating is increased, but the distribution is still symmetric; the peak energy is unchanged. The wave amplitude increases, and the amplitude of the higher frequency harmonics ($n = 2$–5) increases more rapidly than that of the fundamental.

3 At still larger distances, severe energy diffusion to lower energies is apparent, so that the average energy is decreased to $\sim 0.6E_b$, however, further energization to $E > E_b$ does not occur. All the narrow band wave features (fundamental and higher harmonics) disappear; the featureless spectrum extends to frequencies much greater than f_p. The maximum amplitude still occurs at the nominal f_p, but the relative amplitude is decreased from that observed at the intermediate position

The experimental data indicate that relatively smooth transitions occur between these different states. The interaction regions move closer to the gun with increasing beam density and ambient plasma density and farther from the gun with increasing beam energy It is not possible to further quantify these dependences during BPD, because the rate of ambient plasma production by the suprathermal electrons depends on beam density (gun perveance), ambient plasma density, and neutral density (see discussion section)

Measurements made outside the beam provide only the grossest evidence for the interaction processes. The radial extent of the active region is primarily determined by that of the primary beam, not that of the light-emitting region. These differ significantly for the lowest neutral density BPD configurations [*Bernstein et al.*, 1983] Also, the characteristics of the beam-plasma system vary greatly with distance from the gun.

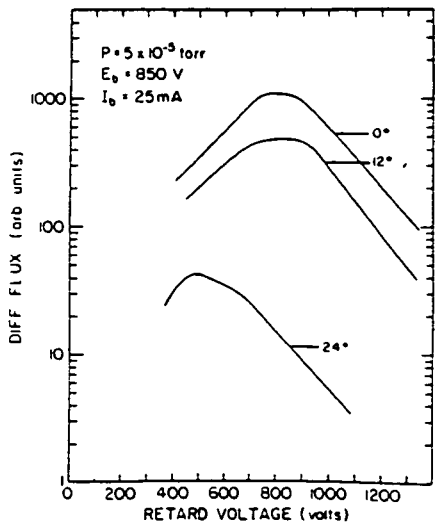

Fig 10 Energy spectra (on axis) measured at 0°, 12°, and 24° to the beam at 52 cm from the gun for an 850-V, 25-mA beam at $p = 5 \times 10^{-5}$ torr

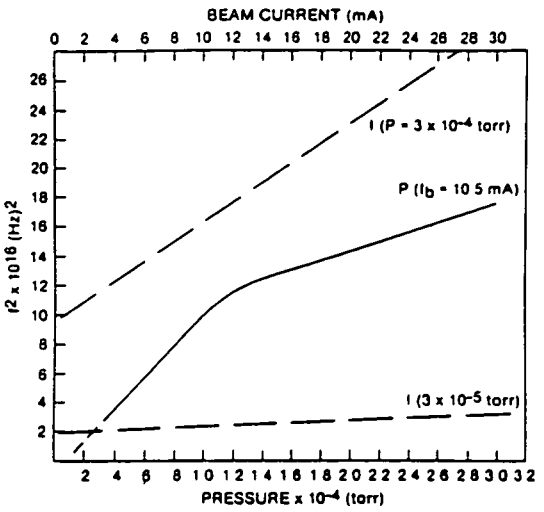

Fig. 11 The dependence of f_p^2 (where f_p is the fundamental RF frequency) on beam current (constant pressure) and pressure (constant beam current)

4 The energy diffusion processes appear to be one-dimensional despite the weak magnetic field strength The energy diffusion is not associated with significant pitch angle diffusion over the available path length (191 cm) Also, the rate at which the beam diffuses radially is small, so that significant changes in radius are not observed in the available 2.5-m path length Similar conclusions were made by *Hallinan et al* [1984] from their television and photometric observations of light emissions from a steady state BPD Any backward directed energetic electron flux is below the sensitivity limits of the detectors Similarly, electrons with $E \gg E_b$ [*Smullin*, 1980; *Wilhelm et al.*, 1984] are not observed here, which is consistent with other BPD measurements in a short path length solenoidal geometry [*Smullin*, 1980]

DISCUSSION

The general spatial evolution of the electron energy and wave spectra seen in the present experiment is completly consistent with those reported from the earlier theoretical and experimental studies of absolute and convective instabilities in strong beam-plasma interactions [*Seidl et al.*, 1976; *Jones et al.*, 1976] in which the initial linear instability has been saturated by trapping [*O'Neill et al.*, 1971] These earlier experiments had been conducted in much stronger magnetic fields (> 1 kG), which eliminated the variable beam density inherent in the noding patterns and produced a more one-dimensional wave-particle configuration Furthermore, the present experiments were conducted in a steady state BPD, whereas some of the earlier experiments were conducted in systems which used an externally produced plasma and employed a low neutral density, a very short pulse duration, or low beam power so that BPD ignition did not occur It seems evident that the BPD is simply the manifestation of the strong BPI when ignition is not suppressed by the imposed experiment conditions

A direct comparison of the BPD and the earlier BPI experiments can be, at best, qualitative In the BPD case, the various important experiment parameters are coupled because of the avalanche ionization process Typically, the ambient density is dependent upon (1) the neutral density, (2) the beam density,

(3) the beam energy, and (4) the magnetic field strength The dependences of f_p^2 ($\sim n_a$) on I_b at constant neutral density and neutral density at constant I_b are shown in Figure 11 Therefore it is not possible to determine quantitatively the dependence of the interaction characteristics on each of these variables

The evidence for initial stabilization by trapping [*Chen*, 1974] is reasonably strong and includes the following

1 There is moderate beam heating, particularly the presence of electrons with $E \approx 1.3$–$1.5E_b$ While not directly predicted by the trapping theory per se, such heating is a general feature of all experiments designed to demonstrate trapping [*Gentle and Lohr*, 1973] and computer simulations of beam-plasma interactions [*Kainer et al*, 1972]

2 Although possibly arising from the probe-plasma coupling, the intense harmonic content shown in Figure 3 at 52 cm is consistent with the theroetical predictions of *O'Neill et al.* [1971] and the measurements of *Gentle and Lohr* [1973] The harmonic content of the wave power obeys the power law, $\epsilon^2 \propto n^{-\alpha}$ ($n = 2$–5), but with $\alpha \approx 5$ rather than the predicted 3–3.5 It should be noted, however, that these measurements were only qualitative, because of the poorly known probe frequency response and the qualitative nature of the frequency spectrum display

3 The initially narrow band (single wave) spectrum gradually broadens with increasing distance from the gun, indicating growth of waves not predicted by the linear single wave model

We have not observed the cyclic interchange of wave energy density and particle energy characteristic of trapping [*O'Neill et al*, 1971], rather we only observe beam heating However, this obvious cyclic energy interchange is, in general, characteristic of weak beam interactions Here we estimate $n_b/n_a > 1 \times 10^{-2}$, so that strong beam conditions are applicable with the more rapid disappearance of these idealized features In addition, the variable (axial) beam and ambient (radial) plasma density distribution could smear such features completely

It is difficult, from only the spatial measurements presented here, to distinguish between the occurrence of the absolute and convective instabilities As noted by *Jones et al* [1976] and *Seidl et al* [1976], both modes can be saturated by trapping, and each shows axial wave growth prior to saturation but with different rates The wave growth and correlated beam heating dependence on the experiment parameters (E_b, I_b, and neutral density) seem more consistent with the convective instability [*Smullin*, 1980]

In fact, both *Jones et al* [1976] and *Seidl et al* [1976] attribute the appearance of rapid wave growth at a relatively large axial distance from the gun during the absolute instability to the presence of a measured density gradient in that region. Rapid wave growth occurs once the beam enters the uniform density region The axial ambient plasma density gradient probably arises because of the location of the end boundary of the experiment configuration near the gun Because this density gradient should be relatively independent of the experimental parameters (E_b, I_b, and neutral density), the location of the rapid wave growth region should be insensitive to these parameters

The primary evidence for the absolute instability lies in the abrupt threshold (beam current, pressure, etc) of BPD ignition and the correlated change in the energy spectra measured by a detector located at or near the beam termination In this respect it is useful to compare our results with those of *Shustin et al* [1969] and *Levitskii and Shashurin* [1967], which were also performed with a self-made plasma and in a solenoidal magnetic field configuration However, the magnetic field strengths employed there ranged from several hundred gauss to 1.5 kG so that $\omega_p < \omega_c$, whereas in the present experiments at 19 G, $\omega_p \gg \omega_c$ The energy spectra in the earlier experiments were only measured at the beam termination Variation of beam current or pressure allowed observation of all the evolutionary states at the termination, whereas in the present experiment, only either the unperturbed (pre-BPD) or final (BPD) states were present at that position However, as has been shown earlier, when the waves and beam electrons are measured at intermediate locations, their characteristics appear to be identical to those measured at the beam termination in the earlier work, the complete evolution is observed with variation in I_b or pressure This different behavior between the two configurations leads to the conclusion that the convective instability occurred in the earlier experiments and that the absolute instability occurred in the low magnetic field strength experiments described here, which is consistent with theoretical expectations for conditions $\omega_p > \omega_c$, $\omega_p \neq n\omega_c$, and $L > L_{crit}$ (K. Papadopoulos, unpublished manuscript, 1984) From the present data it appears that for BPD ignition associated with the absolute instability, the accommodation of the total beam-plasma interaction process (energy deposition length) within the available path length is required

There are some supplementary observations which also imply occurrence of the absolute instability

1 From Figure 3 the wave amplitude grows by ~ 34 dB as the RF probe is moved from 26 cm to 52 cm from the gun. If we assume that the growth remains exponential over this distance, then the growth length, $l \approx 6$ cm, is consistent with but less than the simple estimated convective growth length, $l \approx v_b/[(n_b/n_a)^{1/3}\omega_p]$ The small radial beam dimension compared to that of the ambient plasma would further increase the calculated growth length More importantly, for almost all conditions the wave amplitude at 26 cm from the gun has grown sufficiently large that observable modifications of the beam energy distribution have occurred at that point It does not seem reasonable that four convective growth lengths would allow sufficient wave growth from thermal noise to allow occurrence of these modifications, therefore existence of a much larger wave amplitude than thermal noise at the injection point appears to be required

2 Wave measurements in the large chamber BPD experiments, using a fast filter bank spectrum analyzer, showed that the high frequency waves occurred in bursts with a typical duration of a few microseconds Typical values of plasma density there were $\sim 5 \times 10^9$ cm^{-3}, corresponding to $f_p = 20$ MHz *Seidl et al* [1976] have shown that such a burst pattern is characteristic of the quenched absolute instability when strong beams ($n_b/n_a > 10^{-2}$) are employed.

Following wave saturation, the present results and those of *Jones et al* [1976] show that the beam undergoes energy diffusion toward lower energies together with a gross smearing of the wave spectrum It is not clear, however, whether the beam velocity distribution function at large distances is actually driven to a "plateau" (stable) configuration Even in Figure 10 (measured at 52 cm where the 0° spectrum is heated but not degraded) it is evident that the angular distribution of the lower energy electrons is significantly different (tending toward isotropy) from that of the almost one-dimensional

higher energy electrons This tendency toward isotropy of the lower energy electrons is more apparent at 191 cm, where the 0 spectrum is degraded With increasing isotropy, derivation of the one-dimensional velocity distribution [$f(v_{\parallel})$] function requires integration over the perpendicular component However because of the small low energy fluxes and the qualitative nature of the angular measurements at 191 cm, our present instrumentation has not allowed accurate measurement of the total (over all pitch angles) energy distribution with sufficient accuracy to determine whether $f(v_{\parallel})$ has indeed reached a plateau distribution

Figures 7 and 8 also provide some evidence for the one-dimensional nature of the modification of the beam energy distribution to the final evolutionary state In Figure 7 the total fluxes measured for the pre-BPD and BPD states are in agreement to within a factor of 2. In Figure 8 the measured fluxes scale directly with the injected beam current. Because of the selective angular response of the detectors, pitch angle scattering or radial diffusion of the beam electrons would be expected to be evidenced in the gross nonconservation of the beam flux for the different conditions.

One of the very clear and perhaps surprising results of the flight experiments has been the detection of large fluxes of energetic electrons, with $E \leq E_b$, which return to the injection altitude whenever detectors are placed on or near the injection line of force [*Wilhelm et al*, 1985] These fluxes have been detected with delay times as long as 0.4 s after beam injection has ceased One reasonable, but not the only, cited explanation for these observations is that the injected beam is always unstable in its transit of the ionosphere and continuously generates this backward directed energetic electron flux A delay time of 0 4 s corresponds to a round trip distance of $\sim 10^4$ km for 2-keV electrons injected parallel to B Thus the beam should not have been driven tc a stable plateau distribution in the near vicinity of the injection point Although velocity dispersion effects would tend to regenerate the unstable velocity distribution, it is more reasonable to conclude that the broad velocity distribution is stabilized prior to plateau formation so that the hot beam propagates over large distances while remaining linearly unstable [*Papadopoulos*, 1975] Thus the strong interaction near the injection point should not have produced the stable plateau velocity distribution

Wilhelm et al [1985] also estimate that the radial dimensions of the backward directed energetic electron flux are approximately one gyrodiameter (90° injection) when they originate near the injection point and that the dimensions increase slowly as the distance from the gun (time after injection) increases Furthermore, the backward directed flux appears to be relatively isotropic and independent of the injection pitch angle These results imply that the continuous instability is associated with both slow pitch angle and radial diffusion of the injected beam with increasing distance Given the one-dimensional nature of the propagating beam interaction in the laboratory experiment, the ratio of the propagating and returning fluxes near the gun is probably greater than 10^7 In the flight experiments the detector parameters have been optimized for the detection of the return fluxes, whereas in the present laboratory experiments the detectors have been optimized for study of the primary beam It is therefore not surprising that we have not been able to detect any backward directed flux in the present experiments, in all likelihood such a flux, if detected, would be dominated by collisional backscattering from the beam termination It seems clear that the immense path length available in the flight experiments provides a gross difference from the laboratory configuration with a 2 5-m path length

Conclusions

The following conclusions appear evident

1 The most important process is the high frequency beam-plasma interaction. This configuration has been studied experimentally and theoretically and is now well understood Associated low frequency waves (ion acoustic and ion cyclotron) have been observed in both laboratory [*Shustin et al*, 1969] and flight [*Winckler et al*, 1984] experiments These are probably produced by parametric decay of the large amplitude Langmuir waves [*Parker and Throop*, 1973] produced in the high frequency process

2. For low magnetic field strengths and sufficient beam path lengths the beam-plasma interaction is an absolute instability The energy deposition length varies directly with E_b and inversely with n_a and n_b Because of the coupling arising from the avalanche ionization process we have not been able to establish the quantitative dependence of the energy deposition length on the individual parameters

3 Although the energy deposition length is much shorter and is located much closer to the gun for the absolute instability than for the convective case, it can still extend over a reasonably large distance for certain experimental conditions

4 Because of the low magnetic field strength, the long path length, and the usual ionospheric condition $\omega_p > \omega_c$ at typical flight altitudes (100–500 km) we anticipate occurrence of the absolute instability there At lower altitudes, collisional beam ionization of the atmospheric neutral gas should also satisfy the requirements for the absolute instability analogous to the laboratory experiments However, even if the absolute instability does not occur for a variety of reasons, the convective instability should still occur because of the long path length The variety of cited laboratory experiments indicate that the same end results appear for either interaction mode only the axial location and extent of the energy deposition length are modified

5 Comparison of our described BPD results with those from prior non-BPD (BPI) investigations indicates that the same physical processes occur in both cases

Acknowledgments We wish to thank J O McGarity, K R Caldwell and J L Winkler Jr for development of the retarding potential analyzer and positioning system and for their invaluable assistance in the performance of the experiments We have had many useful discussions with K Papadopoulos X Llobet and W Bernstein acknowledge support by NASA grant NAGW-69 and National Science Foundation grant ATM80-22550

The Editor thanks K Wilhelm and H R Anderson for their assistance in evaluating this paper

References

Arnoldy R L C Pollock and J R Winckler, The energization of electrons and ions by electron beams injected into the ionosphere, paper presented at the Conference on Beam-Plasma Interactions in Space, NASA and Sci Appl, Inc Eastsound, Wash, Aug 12–16 1984

Bernstein, W H Leinbach P J Kellogg S J Monson, and T Hallinan Further laboratory measurements of the beam-plasma discharge *J Geophys Res* 84 7271-7278 1979

Bernstein, W J O McGarity and A Konradi Electron beam injection experiments Replication of flight observations in a laboratory beam plasma discharge *Geophys Res Lett*, 10 1124 1127 1983

Chen, F F *Introduction to Plasma Physics* p 209, Plenum, New York, 1974

Duprat, G R J B A Whalen, A G McNamara, and W Bernstein, Measurements of the stability of energetic electron beams in the ionosphere, *J Geophys Res*, *88*, 3095–3108, 1983

Galeev, A A, E V Mishin, R Z Sagdeev V D Shapiro, and V I Shevchenko, Discharge in the region around a rocket following injection of electron beams into the ionosphere, *Sov Phys Dokl*, Engl Transl, *21*, 641, 1976

Gentle, K W, and J Lohr, Experimental determination of the nonlinear interaction in a one-dimensional beam-plasma system, *Phys Fluids*, *16*, 1464–1471, 1973

Hallinan, T J, H Leinbach, G Mantjoukis, and W Bernstein, Measurements of the optical emission produced during the laboratory beam plasma discharge, *J Geophys Res*, *89*, 2335–2347 1984

Jones, J, W Carr, and M Seidl, Transition from particle trapping to a quasilinear-like beam-plasma system, *Phys Fluids*, *19*, 548–553, 1976

Jost, R J, H R Anderson, and J O McGarity, Electron energy distribution measured during electron beam/plasma interactions, *Geophys Res Lett*, *7*, 509–513, 1980

Jost, R J, H R Anderson, W Bernstein, and P J Kellogg, Radial dependence of the HF field strength in the BPD column, in *Artificial Particle Beams Utilized in Space Plasma Studies*, edited by B Grandal, pp 431–437, Plenum, New York, 1982

Kainer, S, J Dawson, R Shany, and T Coffey, Interaction of a highly energetic electron beam with a dense plasma, *Phys Fluids*, *15*, 493–502, 1972

Konradi, A, W Bernstein, D L Bulgher, J O McGarity, and J L Winkler, Jr, Initial experimental results from a laboratory size beam-plasma discharge device, Active Experiments in Space, *European Space Agency Spec Publ ESA SP-195* 185–188, 1983

Levitskii, S M, and I P Shashurin, Spatial development of the plasma-beam instability, *Sov Phys JETP*, Engl Transl, *25*, 227–231 1967

Llobet, X, A model of the beam-plasma discharge, thesis, Rice Univ, Houston, Tex, 1984

Maehlum, B N, B Grandal T A Jacobsen, and J Troim, Polar 5—An electron accelerator experiment within an aurora, *Planet Space Sci*, *28*, 279–289, 1980

Managadze, G G, W K Riedler, B M Balebanov, T I Gagua, M F Friedrich, Z Klos, N A Lahashvili N A Leonov, S B Lvakhov, A A Martinson, and A D Mayorov Plasma processes in the region of electron beam injection from a high altitude payload, Active Experiments in Space *European Space Agency Spec Publ*, *ESA SP-195*, 161–169, 1983

O Neill, T M, J H Winfrey, and J H Malmberg, Nonlinear interaction of a small cold beam and a plasma, *Phys Fluids 14* 1204–1212, 1971

Papadopoulos, K, Nonlinear stabilization of beam plasma interaction by parametric effects, *Phys Fluids*, *18*, 1769–1777 1975

Parker, R R, and A L Throop, Observation of parametric instability induced by beam-plasma interaction, *Phys Rev Lett*, *31* 1549–1552, 1973

Seidl, M, W Carr, D Boyd, and R Jones, Nonlinear development of absolute and convective instabilities, *Phys Fluids*, *19*, 78–92, 1976

Shustin, E G, V P Popovich, and I F Kharchenko Distribution function of an electron beam in a beam-plasma discharge *Sov Phys Tech Phys*, Engl Transl, *14*, 745–750, 1969

Smullin, L D, A review of the beam plasma discharge, in *Relation Between Laboratory and Space Plasmas*, edited by H Kikuchi, pp 45–65, D Reidel, Hingham, Mass, 1980

Stenzel, R L, W Gekelman, N Wild, J M Urrutia, and D Whelan Directional velocity analyzer for measuring electron distribution functions in plasmas, *Rev Sci Instrum*, *54*, 1302–1310, 1983

Whelan, D A, and R L Stenzel, Nonlinear energy flow in a beam-plasma system, *Phys Rev Lett*, *50*, 1133–1136, 1983

Wilhelm, K, W Bernstein, P J Kellogg, and B A Whalen, Acceleration of electrons in strong beam-plasma interactions, *Geophys Res Lett*, *11*, 1176–1179, 1984

Wilhelm, K, W Bernstein, P J Kellogg, and B A Whalen, Fast magnetospheric echoes of energetic electron beams, *J Geophys Res*, *90*, 491–50, 1985

Winckler, J R, J E Steffen, P R Malcolm, K N Erickson, Y Abe, and R L Swanson, Ion resonances and ELF wave production by an electron beam injected into the ionosphere Echo 6, *J Geophys Res*, *89*, 7565–7571, 1984

Wong, A Y, and P Y Cheung, Three dimensional self-collapse of Langmuir waves, *Phys Rev Lett*, *52*, 1222–1225, 1984

W Bernstein, Department of Space Physics and Astronomy, Rice University, Houston, TX 77251

A Konradi, Solar System Exploration Division, NASA Johnson Space Center, Houston, TX 77058

X Llobet, Institute for Fusion Studies, University of Texas, Austin, TX 78712

(Received October 24, 1984
revised January 21, 1985,
accepted February 8, 1985)

Section IV - Flight Experiments

Wilhelm, K., W. Bernstein and B. A. Whalen, "Study of electric fields parallel to the magnetic lines of force using artificially injected electron beams," Geophys. Rev. Letters, 7, 117, 1980.

Duprat, G. R. J., B. A. Whalen, A. G. McNamara and W. Bernstein, "Measurements of the stability of energetic electron beams in the ionosphere, J. Geophys. Res., 88, 3095-3108, 1983.

Wilhelm, K., W. Bernstein, P. J. Kellogg, and B. A. Whalen, "Acceleration of electrons in strong beam-plasma interactions," Geophys. Res. Letters, 11, 1170-1179, 1984.

Wilhelm, K., W. Bernstein, P. J. Kellogg and B. A. Whalen, "Fast magnetospheric echoes of energetic electron beams," J. Geophys. Res., 90, 491-504, 195.

Llobet, X., W. Bernstein and K. Wilhelm, "Strong interaction of low power electron beams with the ionosphere," accepted for publication Journal AIEE - Plasma Science, 1985.

JOURNAL OF GEOPHYSICAL RESEARCH VOL 88, NO A4, PAGES 3095-3108, APRIL 1, 1983

Measurements of the Stability of Energetic Electron Beams in the Ionosphere

G. R. J. DUPRAT, B. A. WHALEN, AND A. G. MCNAMARA

Herzberg Institute of Astrophysics, National Research Council of Canada Ottawa, Ontario K1A OR6 Canada

W BERNSTEIN

Department of Space Astronomy, Rice University, Houston, Texas 77001

A Nike Black Brant V rocket was launched from the Churchill Research Range (Manitoba) on December 3, 1979, into a bright east-west oriented auroral arc The rocket payload consisted of two separable sections, each containing its own telemetry and a full set of wave and charged particle detectors An electron gun, carried in the main payload, produced a pulsed electron beam with energies of 1 9, 4, and 8 keV at 1, 10, and approximately 100 mA in a programed format Charged particle observations from the flight are used to define the spatial distribution of perturbed volume surrounding the accelerator during gun firing The radial dimensions of the perturbation were found to scale with the primary electron beam gyroradius and current and were also dependent on the beam injection angle On magnetic field lines near the gun, the induced return electron energy spectrum is characterized by a monotonically decreasing intensity with increasing energy out to the approximate beam energy At increasing distances across field lines the energy spectrum takes on a monoenergetic appearance peaked near the beam energy All beam-induced electron fluxes drop rapidly to background at the edge of the perturbed volume The intense flux of low-energy electrons observed on field lines near the rocket are shown to be accelerated ambients, whereas the particles at or near the beam energy and at large radial distances are presumably beam primaries The ambient thermal ion plasma was not measurably affected by the beam while the local electron temperature increased during gun pulses Results from this flight are compared with the corresponding observations made in a large vacuum tank simulation, and it is concluded that certain features in the data are consistent with the beam-plasma instability observed in the laboratory

1. INTRODUCTION

During the last decade, interest in the use of electron accelerators as a tool for controlled investigation of the upper atmosphere has increased considerably The diversity of the possible uses of the technique is demonstrated by experiments such as the 'Echo' series by the University of Minnesota group [*Winckler*, 1981, 1982], the Norwegian 'Polar' series [*Maehlum et al*, 1980*a*, *b*], the Franco-Soviet Artificial Radiation and Auroras Between Kerguelen and the Soviet Union (ARAKS) projects [*Cambou et al*, 1980], and others All these active experiments have recently been reviewed by *Winckler* [1980]

Here we report on a joint NASA/National Research Council of Canada (NRCC) project the use of an electron gun as a magnetospheric probe to search for the occurrence of electric fields parallel to the local magnetic field ($E\|B$) as well as to study local beam-plasma interactions The results presented here were derived from the third in a series of four rocket flights

In the first flight, the seal on the front of the electron gun failed to deploy properly, and no useful data were collected for our purposes During the second flight, the electron gun system operated properly, however, some interference with the gun program was encountered Beam pulses generated during this flight were used to probe auroral field lines for magnetospheric $E\|B$ as was described by *Wilhelm et al* [1980]. *Bernstein et al* [1982] also presented results from this flight and identified some features in the data which were consistent with the ignition of the beam plasma discharge at high altitudes Because of these results and the laboratory simulations [*Bernstein et al*, 1979] the scientific objectives of the third flight were expanded to include (1) a more detailed investigation of the electron beam dynamics near the rocket and (2) the study of vehicle neutralization during electron beam emissions The use of electron beams, modulated at very low frequencies, as antennas for VLF waves [*Holzworth and Koons*, 1981] was also investigated.

A brief description of the payload instrumentation is given in section 2, and in section 3 the flight and auroral conditions are discussed. Section 4 is devoted to the presentation of the results from the flight, and these observations are summarized and discussed in sections 5 and 6

2 INSTRUMENTATION

The rocket payload consisted of two separable sections (a 'mother'-'daughter' configuration), each containing its own telemetry and a full set of particle and wave detectors The mother payload, which was attached to the rocket motor, also carried the programed electron accelerator This configuration, and a low mother-daughter separation velocity, were chosen so that the characteristics of the beam could be studied as a function of radial distance from the gun. The probability of successful echo detection from remote $E\|B$ structures was also improved on the daughter payload since it does not suffer from severe vehicle charging effects during gun firings A schematic diagram of the payload configuration at the time of release is shown in Figure 1

The electron accelerator consisted of a power converter

Paper number 3A0125
0148-0227/83/003A-0125$05 00

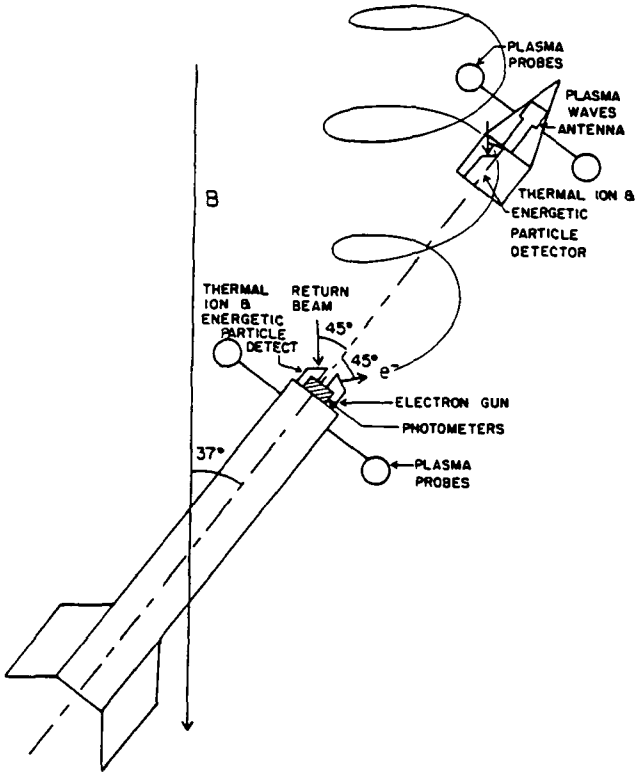

Fig 1 Flight configuration after payload separation

and two Machlett EE-65 triode guns, mounted at 45° to the rocket spin axis. Each gun had a perveance of $\approx 2 \times 10^{-7}$ A/V$^{3/2}$ and a beam divergence angle of less than 10° for all energies. This divergence angle was minimized by selecting the optimum voltage (≈90% of the cathode voltage) for the focusing element in the gun. A planar grid system was used to control the cathode current to an accuracy of better than 10% at all currents Both guns were operated in parallel and were programed to produce 50-ms bursts of electrons at varying currents and voltages Two different sequences were employed. The primary sequence (A) called for three different voltage steps (at 1 9, 4, and 8 kV) and three different current steps (1, 10, and 100 mA) at each voltage The gun perveance limited the maximum current I_{max} emitted by both guns at 2 kV and 4 kV to 60 mA and 90 mA, respectively, and at 8 kV, the gun current was regulated at 100 mA A schematic diagram of three A sequences is shown in the bottom two panels in Figure 2. The second sequence (B) called for the emission of a 100-mA square wave modulated (at 3 kHz) beam current at 8 and 4 kV

The NRCC instrumentation on each section of the rocket payload included charged particle detector sets and plasma probes The charged particle detectors consisted of collimators, cylindrical plate electrostatic analyzers, and channel electron multiplier sensors Solid state detectors were also used in both packages to detect energetic particle fluxes Details of this instrumentation are listed in Table 1 for the mother payload and in Table 2 for the daughter

The plasma diagnostic instrumentation consisted of two Langmuir probes carried in the mother payload and one Langmuir probe and a retarding potential analyzer (RPA) in the daughter payload The four instruments were extended perpendicular to the rocket spin axis, 30 cm from the vehicle surface, as shown in Figure 1 The probe in the mother payload was a 0 635-cm diameter spherical Langmuir probe and was designed to measure the ambient electron density and temperature. The current amplifier was operated in a linear gain switched mode with the probe bias fixed at −2.96 V for 0.4 s, then swept to +4 86 V in 0.5 s, and held fixed at +4.86 V for 1 2 s. The other probe was a cylindrical Langmuir probe, 3 cm long, and was designed to follow plasma density variations and effects of vehicle potential variations with very fast transient response. The amplifier was logarithmic and had a dynamic range of 10^6 The probe bias was alternated between fixed bias levels of −4 02 and +4 94 V, every 2 s, to examine the electron and ion collection behavior.

The Langmuir probe carried in the daughter payload was identical to the spherical probe described previously The voltage on the probe was programed to remain fixed at −2.96 V bias for 0.6 s, then to sweep up to +6 18 V, and to remain fixed at this voltage for 1 4 s

The RPA was constructed in the form of a hemisphere and consisted of an inner electrode biased at +22 V and an outer grid whose bias voltage tracked the Langmuir probe voltage but had a voltage range from −3.47 V up to +5 81 V When biased at −3 47 V, the probe collected electrons with energies of >4 eV

In addition to this, the mother payload also carried two pairs of 'ram sensors' (J A. Koehler, University of Saskatchewan) and a bank of photometers (F R Harris, NRCC, Ottawa) for optical measurements, and the daughter payload a plasma wave detector (P J Kellogg, University of Minnesota).

On-board magnetometers were used to derive the magnetic attitude of the mother and the daughter payloads, and

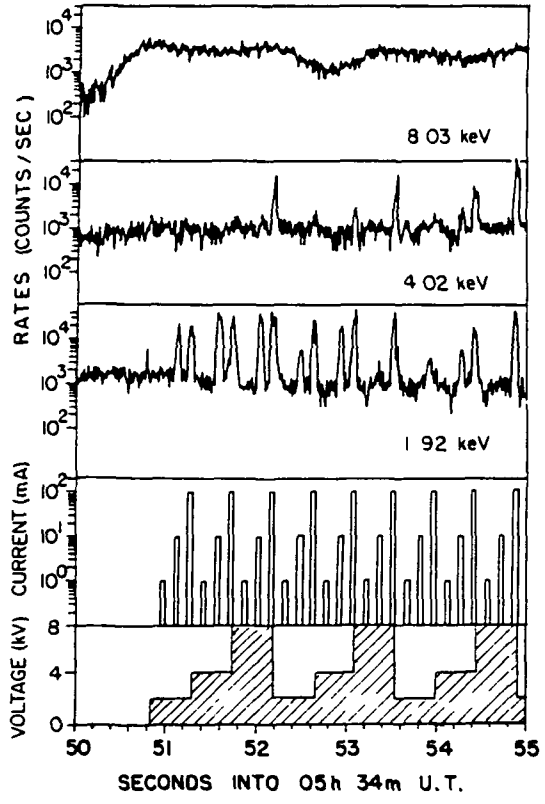

Fig 2 Energetic particle detector count rates and gun program for first sequence of gun pulses

TABLE 1 Charged Particle Instrumentation in the Mother Payload

Instrument	Energy Range	Look Angle, deg	Geometric Factor	$\Delta E/E$, %
low-energy electron detector	energy fixed at 60 eV	45	9.43×10^{-6}	4
high-energy electron detector	energy fixed at 1.43 keV	45	2.25×10^{-4}	4
electron spectrometer	16 steps from 132 eV to 17.6 keV every 3.7 s	45	$1.57 \times 10^{-4} E$	4
proton spectrometer	16 steps from 179 eV to 23.9 keV every 3.7 s	45	$5.30 \times 10^{-3} E$	10
two thermal ion spectrometers	swept from 1.65 eV to 8.95 eV every 180 ms*	45	$6.36 \times 10^{-8} E$	3.5
		90	$6.36 \times 10^{-8} E$	3.5
two high-energy electron solid state detectors	$E > 22$ keV	60	5.45×10^{-3}	
	$E > 38$ keV	60	5.45×10^{-3}	

The geometric factors are in units of cm^2 sr eV except for solid state detectors, which have units of cm^2 sr

* The ions were preaccelerated by 2 V before reaching the sensor; therefore the corresponding ion energy in the plasma varied between 0 and 6.95 eV

these data were combined with the output of lunar sensors to determine the absolute attitude of both payload sections

3. Flight and Auroral Conditions

The Black Brant V rocket AAF-NVB06 was launched from the Churchill Research Range (Manitoba, Canada) on December 3, 1979, at 0532 47.0 UT (2332 47.0 LT) into a bright east-west oriented auroral arc and reached an apogee of 338 km. The ground-based (λ = 5577 Å) photometers recorded intensities up to 40 kR in the arc The rocket was launched on an azimuth of 4.3° west of north. Despin occurred at T + 57.9 s (0533 44.9 UT), and the resulting spin period was 2.8 s

The daughter payload was ejected forward of the mother payload at T + 119.6 s (0534 46.6 UT) when the rocket was at an altitude of 193 km The mother-daughter separation speed was measured using a linear displacement transducer (LDT) which was composed of a 76.2-cm-long string wound on a constant tension drum which in turn was connected to a potentiometer The LDT was mounted on the mother, and the end of the string was connected to the daughter As the payload separated during flight, the string was pulled off the drum, and the potentiometer indicated the instantaneous separation distance When the full extension of the string was reached, the string was pulled free of the snap connector and was rewound onto the spool The error in the LDT measurement of the relative separation speed was estimated to be less than 1%

The direction of the relative velocity vector was assumed to coincide with the instantaneous spin axis direction of the rocket at separation time The separation system manufacturer (Bristol Aerospace Ltd., Winnipeg, Manitoba) estimated that the 'tip-off' error should be less than ±1° The instantaneous spin axis orientation was determined from onboard magnetometers and moon sensors which provide absolute attitude to within 1° Therefore the total error in ejection direction should be less than 2° The spin axis elevation and azimuth were measured to be 37° and 37° west of north, respectively, in the frame of reference of the mother section (see Figure 1). This implies that the daughter payload preceded the mother payload after separation The relative mother-daughter separation velocity in the ejection direction was 1.62 ± 0.02 m/s which produced an across–magnetic field line velocity of 0.97 ± 0.05 m/s

TABLE 2 Charged Particle Instrumentation in the Daughter Payload

Instrument	Energy Range	Look Angle deg	Geometric Factor	$\Delta E/E$ %
three electron detectors at the nominal beam energies	energy fixed at 1.92 keV	45	1.13×10^{-2}	10
	energy fixed at 4.02 keV	45	2.37×10^{-2}	10
	energy fixed at 8.03 keV	45	4.73×10^{-2}	10
electron spectrometer	16 steps from 160 eV to 20 keV every 2.9 s	45	$5.89 \times 10^{-4} E$	10
two thermal ion spectrometers	swept from 1.9 eV to 6.52 eV every 170 ms*	45	$6.36 \times 10^{-8} E$	3.5
		90	$6.36 \times 10^{-8} E$	3.5
two high-energy electron solid state detectors	$E > 20$ keV	60	5.45×10^{-3}	
	$E > 36$ keV	60	5.45×10^{-3}	

The geometric factors are in units of cm^2 sr eV except for solid state detectors which have units of cm^2 sr

* The ions were preaccelerated by 2 V before reaching the sensor therefore the corresponding ion energy in the plasma varied between 0 and 4.52 eV

Separation induced a tumbling motion of the daughter payload, which was characterized by a coning half angle of 45°, a cone axis angle of 18° with respect to the local magnetic field line, and a coning period of 7 5 s The daughter spin period was 2.8 s. At T + 123.8 s (0534 50.8 UT) a tumble gun produced a coning motion of the mother payload with a period of 256 4 s The half cone angle was 62° inclined at 18° with respect to the local magnetic field lines The combined coning and spin motion of the payload sections provided a wide range of injected and detected particle pitch angles throughout the flight The gun injected particles with pitch angles between 80° and 180°, and the detected particle pitch angles were limited to values of less than 105° therefore the beam was directed almost exclusively into the hemisphere away from the ionosphere, and the particle detectors viewed mostly reflected or backscattered beam particles

4 Results

4 1 *Energetic Particles*

The following results were derived mainly from the daughter payload, although some data from the mother payload were used to confirm these observations

The gun was turned on 4 2 s after payload separation, when the mother-daughter total separation distance was 6 8 m (4.1 m $\perp B$) The first sequence of pulses, starting at 0534·50.8 UT (201 km altitude), are displayed in Figure 2 along with the count rates observed in the three fixed energy detectors carried by the daughter payload The 10-mA and I_{max} pulses were easily observable in the 1 92-keV detector above the background due to auroral precipitation No response was observed in any channel in coincidence with the 1-mA pulse Note that the response in the energetic particle detectors was not linear with beam current, the 10-mA and I_{max} intensities were comparable for the first sequence A, and the 1-mA response was not apparent, which it would have been if the response were linear Note also the sharp rise and fall of the count rate in the 1 92-keV and 4 02-keV detectors in coincidence with the gun pulses This effect was confirmed by detectors on the mother payload The response time was estimated to be less than 1 25 ms

Only the normal spin-modulated auroral background was observed in the 8 03-keV channel at any time during the flight This lack of response to beam pulses could be due to two effects At the time shown in Figure 2 the converter system was loaded by the 8-kV, I_{max} pulses, and as a result the gun emitted particles with energies slightly (≈10%) less than the programed beam energy E_B of 8 keV In addition, data from the mother section indicate that at high altitudes the mother charged positively during 10-mA and I_{max} pulses, which would have the net effect of reducing the free space beam energy Thus the absence of an I_{max} response at 8 03 keV could be due to a combination of these two effects Only spacecraft charging could account for the lack of a response to a 10-mA pulse since no significant converter loading was present during these pulses We will discuss later a more likely source of this response (or lack thereof) in terms of electron beam dynamics

Variations in the energetic particle detector (EPD) pulse amplitudes, which are clearly visible over the 4 s displayed in Figure 2, indicate that the response is dependent on parameters other than simply the beam current I_B and energy For example, in Figure 2, the 10-mA pulses decreased in amplitude to the auroral background level (for a few seconds), while the I_{max} pulses remain relatively constant throughout this time interval Energetic particle responses to beam pulses were observed for 31 s after payload separation, the last detectable pulse being the 8-kV I_{max} pulse injected at 90° to the magnetic field line

To investigate the source of the modulation in the detected fluxes at specific gun energies and currents responses were plotted in a polar coordinate system where the polar angle was the gun azimuth and the radius was the mother-daughter payload separation distance across magnetic field lines ($d_\perp$) Figure 3*a* displays these results for the 8-kV, I_{max} beam pulses for the first 31 s after payload separation Large open circles indicate that responses were observed in the 4 02-keV detector channel, and large solid circles indicate no measurable response A small solid circle is used to signify when a response was also observed in the 1 92-keV channel Rectangles correspond to periods when the beam was modulated at 3 kHz The spatial coordinate of each point is defined by the instantaneous gun azimuth at a distance $d_\perp$ measured in units of $\rho_{beam\perp}$, the gyroradius of the electron beam injected at 90° to the field line Note that $\rho_{beam\perp}$ refers to the beam energy, 8 keV in the case of Figure 3*a* Also shown in the figure is the azimuth of the daughter payload as viewed from the mother (D_S) and the azimuth of rocket velocity (D_R) as viewed from the ground

Similar plots were made for the 8-kV, 10-mA, 4-kV, I_{max}, and 4-kV, 10-mA beams, and these are displayed in Figures 3*b*, 3*c*, and 3*d* Only one response was observed in coincidence with the 8-kV, 10-mA pulses, that being the one on the first sequence A in the 1 92-keV channel shown in Figure 2

Comparison of these figures indicates that the returning beam particles are confined to $d_\perp$ distances of less than $6\rho_{beam\perp}$ and that the perturbed volume occupied by energetic particles decreases with decreasing current It also seems that certain azimuths are favored for producing responses, however, it will be shown later that the controlling factor is probably the gun elevation which has a one-to-one correlation with beam azimuth

Table 3 lists $d_\perp$(max), the distance at which all beam-induced energetic electron fluxes drop rapidly to background Also listed is the value of the gun injection angle β_{gun} (where β_{gun} = 180° for electrons injected upward) for that pulse and the value of $d_\perp$(max) normalized to the beam gyroradius ($\rho_{beam\perp}$ = 5 2 m for 8-keV 3 7 m for 4-keV, and 2 6 m for 1 9-keV particles) Although a considerable amount of scatter is evident in the table, probably because the injected and detected particle pitch angles are not identical for the different conditions, it is seen that $d_\perp$(max) increases with increasing beam energy E_B and current I_B Generalizing somewhat, it appears that $d_\perp$(max) is $5\rho_{beam\perp}$ or $6\rho_{beam\perp}$ for I_{max} beams and approximately 3 for the 10-mA beams Of course no responses due to the 1-mA beams were detected, therefore $d_\perp$(max) for the 1-mA beams was less than or of the order of 2 beam gyroradii

This table indicates that the 1 9-kV pulses do not appear at the same normalized distance from the gun For example, the last response in the EPD's occurred for $d_\perp = 2.3\rho_{beam\perp}$ This discrepancy may be associated with the fact that the guns were capable of producing only 60 mA current at 1 9 kV Thus if $d_\perp$(max) were dependent on beam current only, then the beam spreading for the 1 9-keV maximum current

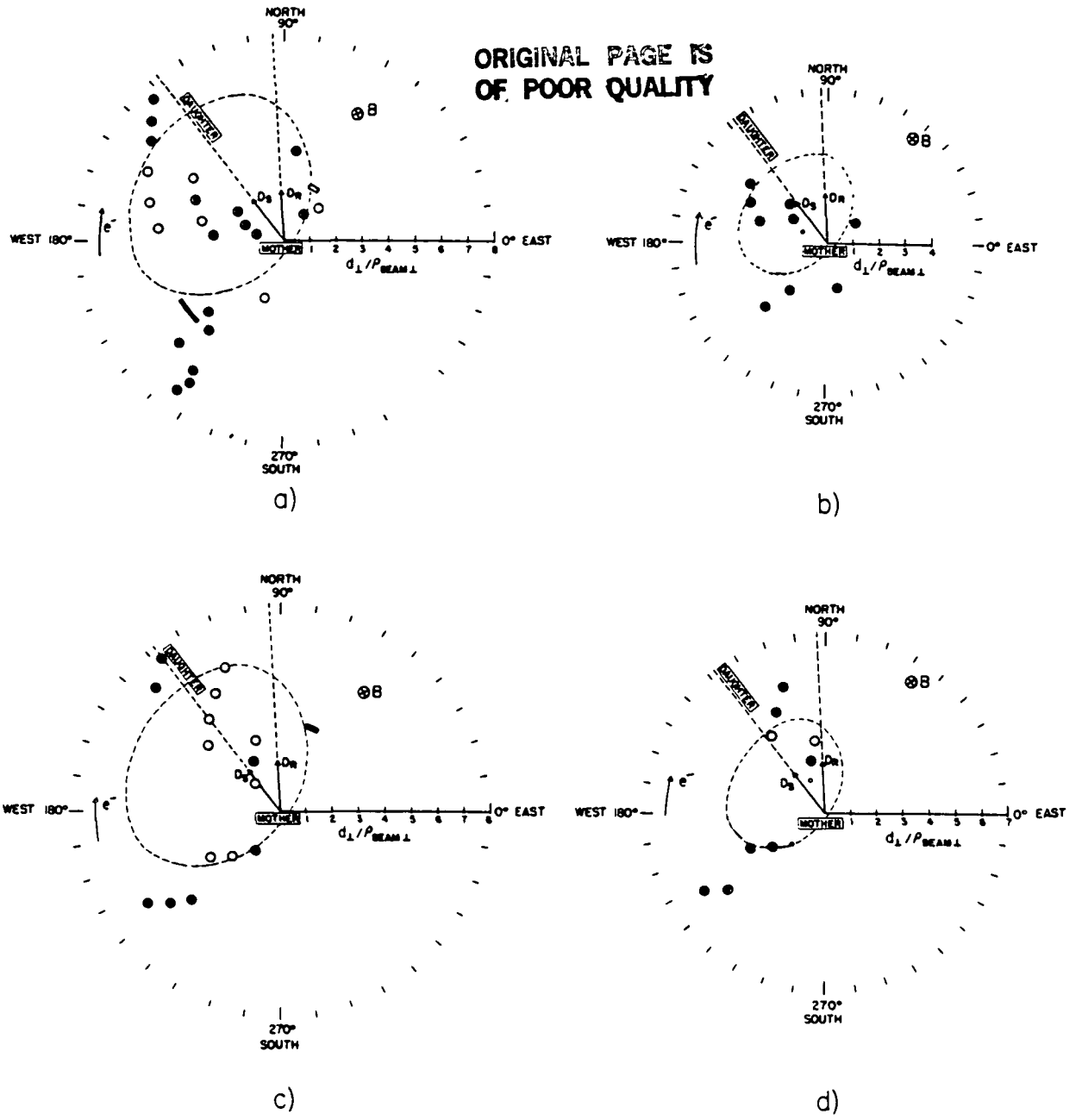

Fig 3 Spatial distribution of energetic particle detector responses to beam pulses The coordinate system used is the gun azimuth and perpendicular 'mother - daughter payload separation distance normalized to perpendicular beam gyroradii Responses in the 1 92- and 4 02-keV detectors are indicated by small solid circles and open circles respectively Large solid circles indicate no response in either sensor A response in the 4 02-keV detector to a modulated beam pulse is indicated by an open rectangle, while no response is indicated by a solid rectangle D_R represents the rocket flight azimuth, and D_S represents the azimuth of the daughter payload as viewed from the mother (*a*) 8-kV, I_{max}, (*b*) 8-kV 10-mA, (*c*) 4-kV I_{max}, and (*d*) 4-kV 10-mA beams

would be less than for the other two energies The spreading as a function of current would, however, have to be highly nonlinear to account for this difference

The normalized beam spreading $d_\perp(\max)/\rho_{beam\perp}$ for constant (10 mA) current is also energy dependent For example, as shown in Figure 3*b*, only the first 8-kV, 10-mA gun pulses produced a measurable response in the energetic particle detector, whereas responses were observed at $d_\perp$ greater than 13 m for 4-kV, 10-mA pulses (Figure 3*d*) Similar normalized spreading was observed for the 1 9-kV and 4-kV, 10-mA pulses (Table 3) This suggests that the dynamics of a 10-mA beam injected into the ionospheric plasma is energy dependent, with the normalized spreading decreasing sharply with increasing energy

Two sources of the azimuthal asymmetry, apparent in Figure 3, were considered. First, the perturbed region could be limited to one side of the rocket, as is the case with single-particle trajectories However, since beam particles were observed up to over 6 beam gyroradii from the rocket, which implies strong collective interactions, this interpretation seems unlikely Second, the perturbed volume could be symmetric about the rocket with the radial extent controlled

TABLE 3 Last Observable Response in Energetic Particle Detector Array

E_B, keV	I_B, mA	$d_\perp$(max), m	$d_\perp$(max)/$\rho_{\text{beam}\perp}$	β_{gun}, deg
1 9	10	5 9	2 3	122 9
1 9	$I_{\max}$	6 0	2 3	130 6
4	10	13 4	3 6	95 9
4	$I_{\max}$	22 8	6 2	117 3
8	10	5 5	1 1	98 2
8	$I_{\max}$	30 2	5 8	86 4

by the gun injection pitch angle β_{gun}. Then the correlation between gun azimuth and elevation could be the source of the apparent azimuthal asymmetry

To test the second hypothesis, it was assumed that the perturbed volume was symmetric about the rocket and extended across field lines a distance d proportional to the injected beam gyroradius, that is,

$$d = K(I_B)\rho_{\text{beam}\perp} \sin \beta_{\text{gun}}(\phi)$$

where K is a proportionality constant dependent on I_B and ϕ is the azimuthal angle.

Assuming that $K = 6.0$ for $I_{\max}$ pulses and 3 7 for 10-mA pulses, the predicted perturbation regions were calculated at each azimuth and are plotted in Figure 3 as dashed lines It is seen that to a good approximation, with the exception of the 8-kV, 10-mA pulses (Figure 3*b*), responses are observed out to the predicted boundary of the perturbed region. The lack of responses to 8-kV, 10-mA pulses, as discussed previously, is in clear disagreement with the model and appears to be a special case.

The energy spectrum and pitch angle distribution of the energetic electron population induced by beam firings was also investigated as a function of radial distance from the rocket.

Responses to $I_{\max}$ pulses at 4 and 8 kV in two detector channels as a function of particle pitch angles and perpendicular distance $d_\perp$ are shown in Figure 4. As indicated in the figure, the maximum pitch angle (β_{det}) detected was 104°, therefore these data concern mostly the return flux from the beam The responses to both the 8-kV and 4-kV beams indicated by open rectangles and circles, crosses, and small solid circles are seen to be randomly distributed in pitch angle as are the lack of responses at large $d_\perp$ These data, along with the corresponding intensity measurements indicate that the return flux was isotropic

The responses of the charged particle detectors on the daughter section during periods when the beam was injected at $\beta_{\text{gun}} = 90°$ were investigated for effects due to collisions of the primary beam with the mother payload (as observed, for example, by *Israelson and Winckler* [1975]) Aside from the systematic increase in the radial dimensions of the perturbed volume d reported previously, no unusual response was observed in the daughter sensors at injection angles near 90°

This lack of response may be attributed to the fact that because at the angular divergence of the beam, only ≈10% of the beam would strike the mother section at any one time Also, since the average energy of secondary electrons from beam impacts would be much lower than the primary beam energy, the impact-produced secondaries would be expected to be confined to field lines passing near the mother and would thus be undetectable at the daughter section

Another (more speculative) effect may also play a role in reducing the response due to beam impacts on the mother payload As will be discussed later, if the beam is highly unstable, it may not even be able to complete one cyclotron orbit as a single-particle system Any such beam-plasma instability could spatially diffuse the beam and thus reduce the effects due to beam impacts on the payload.

Four-point energy spectra derived from the three fixed energy detectors and the electron spectrometer, for a few selected 8-kV, $I_{\max}$ and 4-kV, $I_{\max}$ beam pulses (injection pitch angle near 90°), are displayed in Figures 5 and 6, respectively, as a function of $d_\perp$ (or time) The solid state detectors which were sensitive to electrons with energies greater than 20 keV did not respond to any beam pulses Referring to Figure 5, we see that near the gun (sample 1) the spectrum is characterized by a monotonically decreasing intensity with increasing energy out to the approximate beam energy where the intensity drops rapidly to background levels. At increasing distances from the mother (samples 2 to 6) the intensity near E_B remains relatively constant while at lower energies the flux rapidly decreases, resulting in an energy distribution peaked near the beam energy As mentioned previously, E_B was slightly less than 8 keV at this time, and particles at this energy would be below the bandpass of the 8 03-keV detector This last effect implies that the real location of the peak is between 4 and 8 keV All beam-induced electron fluxes drop rapidly to background at $d_\perp$(max) (see Table 3)

In Figure 6 the corresponding results for 4-kV, $I_{\max}$ pulses are presented. Similar, although less systematic, responses are observed here. Near the gun, intense fluxes of low-energy electrons are observed, while at larger distances the beam-induced electron distributions take on a monoenergetic appearance with a maximum flux at or near E_B. A similar spectral variation is observed for the 4-kV, 10-mA gun pulses.

Because of poor sampling statistics (only the first two pulses produced measurable responses), very little is known of the spectrum during 2-kV, $I_{\max}$ and 2-kV, 10-mA gun firings It is clear, however, after a similar study, that no significant fluxes of electrons above E_B were observed and a large flux was present near E_B

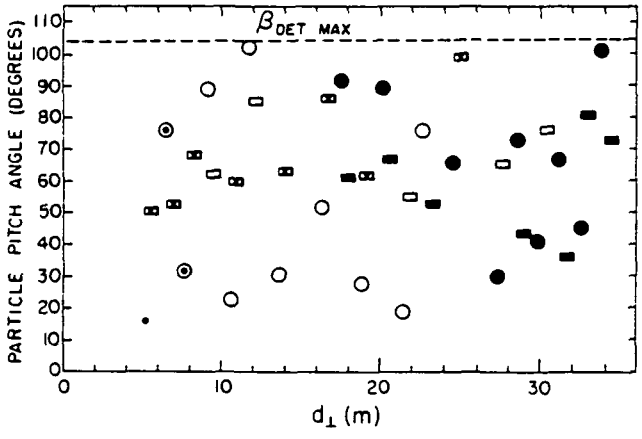

Fig 4 Daughter payload energetic particle pitch angle distributions as a function of the perpendicular separation distance for $I_{\max}$ pulses The crosses and open rectangles correspond to responses to 8-kV pulses in the 1 92-keV and 4 02-keV channels, respectively The small solid circles and the open circles correspond to 4-kV pulses in the 1 92-keV and 4 02-keV channels Solid rectangles and circles correspond to no responses in either detector to 8-kV and 4-kV pulses

The source of the systematic reduction in low-energy electron intensities as a function of $d_\perp$ evident in Figures 5 and 6 is not clearly understood, since these observations apply to a radial diffusion system in which the diffusion coefficients may change significantly over distances comparable to an electron gyroradius. Although no exact theoretical treatment exists which describes this situation, certain features are expected to appear in any model For example, if the last scattering occurs for each electron at the same radial distance from the center of the beam, one would expect to observe electrons with the largest gyrodiameter (highest energy) at maximum radial distances. These electrons should also have an azimuthally asymmetric distribution consistent with their gyrocenters being inside the perturbed region. The appearance of a monoenergetic spectrum at the outer boundary of this region (Figures 5 and 6) is clearly consistent with this model

The azimuthally asymmetric (monodirectional) beam expected at the edge of this volume is more difficult to verify because of the limited sampling. However, the last few pulses observed near the beam energy (for 8-kV, I_{max} pulses) were detected coming from the southwest quadrant, which is consistent with this model.

4 2 *Thermal Plasma Observations*

The response of the ionospheric plasma to the injected electron beam is investigated in this section using measurements from both the Langmuir probes and the thermal ion sensors. First, data from the daughter payload relating to vehicle charging and the spatial extent of beam-induced perturbations are presented, and then observations from the mother are used to corroborate these results Plasma heating effects associated with beam firings are discussed in section 4 2.3.

4 2.1 *Daughter payload* The Langmuir probe responses during a portion of the first two sequence A routines are shown in Figure 7 The suprathermal electron flux (STEF) is shown in the top panel, while the thermal electron flux (TEF) and gun program are shown below The TEF signal was telemetered on a continuous channel with good (1 kHz) frequency response The STEF was telemetered via a channel with a sampling period of 50 ms which produced an apparent delay in these data As can be seen in the top panel,

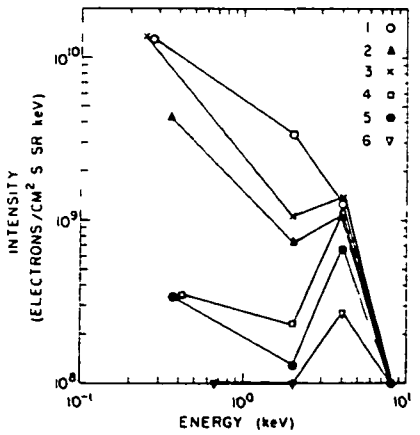

Fig 5 Spatial distribution of induced electron energy spectra for 8-kV I_{max} pulses Spectra 1, 2 3 4 5, and 6 were measured when the two payloads were separated, in the plane perpendicular to the magnetic field, by distances of 8 2, 10 9, 14 0, 19 3, 25 0, and 30 2 m, respectively

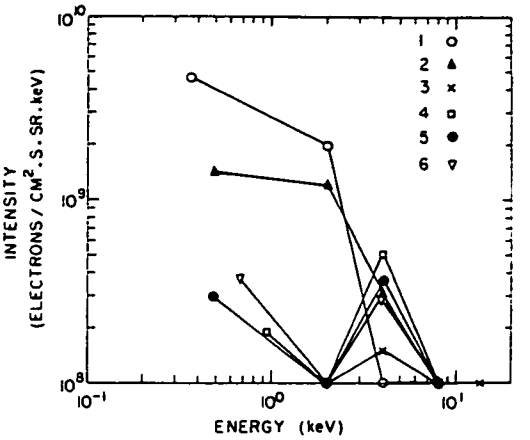

Fig. 6 Spatial distribution of induced electron energy spectra for 4-kV, I_{max} pulses Spectra 1, 2, 3, 4, 5, and 6 were measured at perpendicular payload separation distances of 5 2, 7 8, 9 1, 10 4 13 6, and 16.2 m, respectively

when the RPA was biased to measure the STEF (bias voltage = −3.47 V), a logarithmically increasing flux was observed for the 1-mA, 10-mA, and I_{max}, 4-kV beam pulses Thus the STEF increased approximately linearly with beam current On the next series of gun pulses with E_B = 8 keV, no response is observed at 1 mA. No further clearly identifiable responses to 1-mA pulses were observed thereafter. The STEF went into a sweeping mode after the 8-kV, 1-mA pulse and reached a thermal electron collection mode at the beginning of the next sequence A.

The STEF response in the suprathermal mode was investigated as a function of $d_\perp$ and found to be similar to that in the EPD array Except for a few instances, every pulse in the STEF was accompanied by a response in the EPD array The $d_\perp$(max) for the last observable response in the STEF sensor is listed in Table 4 for 10-mA and I_{max} pulses at all energies. Also tabulated is the gun injection pitch angle β_{gun}

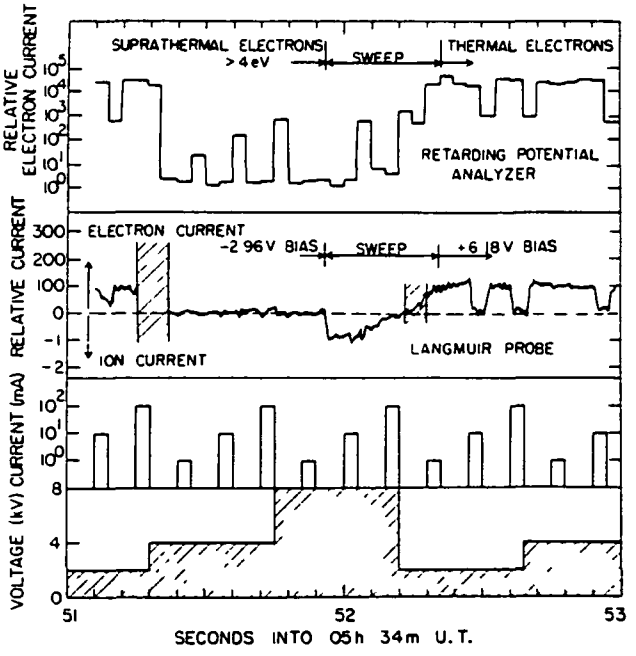

Fig 7 Suprathermal electron and thermal electron fluxes observed immediately after payload separation Also shown is the corresponding gun program.

TABLE 4 Last Observable Response in the Suprathermal Electron Flux

E_B, keV	I_B, mA	$d_\perp$(max), m	$d_\perp$(max)/$\rho_{beam\perp}$	β_{gun}, deg
1 9	10	9 9	3 8	143 9
1 9	I_{max}	10.0	3 8	132.0
4	10	13 4	3 6	95 9
4	I_{max}	22 8	6 2	117 3
8	10	5 5	1 1	98 2
8	I_{max}	30 2	5 8	86 4

for the corresponding last pulse Except for the 2-kV pulses the $d_\perp$(max) values are identical to those found in the EPD array (Table 3). In the 2-kV beam case, $d_\perp$(max) is larger in the STEF than in the EPD One response was also observed in the STEF to the 1-mA beam while none was observed in the EPD.

Referring once again to Figure 7, the STEF in the thermal electron mode and the TEF in the electron collection mode (+6.18-V bias) had similar responses to beam injections. The TEF, while in the ion collection mode (−2.96-V bias), had no measurable response The shaded areas in the TEF corresponded to times when amplifier gain changes were occurring. The step in the TEF current coincident with the sweep start was due to a simultaneous change in amplifier gain and should be ignored.

During the second sequence A, 10-mA and I_{max} beam pulses caused drastic decreases in the thermal electron flux to the probes. To account for the TEF decrease observed, a rocket potential shift of about 4 V is required, and this shift would have to be associated with an increase in average electron energy (equivalent to a temperature increase). Confirmation of this rocket potential shift was provided by the thermal ion sensor on the daughter section.

A characteristic thermal ion energy spectrum detected at 0534:48.2 UT just after payload separation but just before the first sequence of gun pulses is shown in Figure 8 These data were gathered when the sensor was viewing ions near the 'ram' direction and then fitted to a drifting Maxwellian distribution preaccelerated by the 'rocket potential' V_R [see *Green and Whalen*, 1974, *Yau et al*, 1981] V_R is evaluated at −3 V, and the rocket potential in this case includes the 2-V preacceleration applied to the ions before analysis The best fit ion temperature T_i was 1200°K, and the fitted distribution is shown in Figure 8 as a solid curve

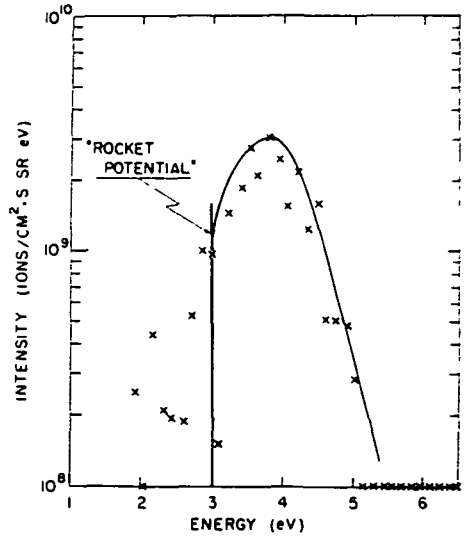

Fig. 8 Unperturbed thermal ion energy spectrum measured at 0534 48 2 UT, before gun turn-on, by the daughter payload detector

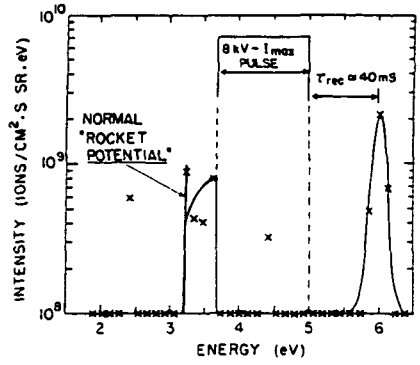

Fig 9 Perturbed thermal ion energy spectrum measured at 0534 54 9 UT by the daughter payload detector, during an 8-kV, I_{max} gun pulse

During beam firings a different response is observed in these sensors as demonstrated in Figure 9 This spectrum was measured at 0534 54 9 UT The linear sweep started at approximately 2 V and began to sweep out the unperturbed distribution just above the normal V_R The count rate dropped to zero in coincidence with the start of the 8-kV, I_{max} pulse, and 40 ms after the end of the pulse a burst of counts was observed well above the normal thermal energy The interpretation is as follows the gun pulse induces a rapid negative shift in the floating potential, and therefore ions arriving at the sensor have fallen through a much larger potential and have energies well above the instrument limit When the pulse ends, the rocket recovers to its original potential, and during the recovery the peak in the ion energy distribution sweeps past the energy bandpass of the instrument, giving rise to a burst of counts In Figure 9 we see that the peak in the energy spectrum was near 6 eV, 40 ms after the end of the pulse, which is an energy shift of 2 1 V from the normal (Figure 8)

If we let τ_{rec} (the recovery time) be the time between the end of the pulse and the time when a burst of counts is observed in the sensor, and let ΔV_R be the shift in peak ion energy (the rocket potential shift), then τ_{rec} should clearly be a function of ΔV_R The recovery time τ_{rec} was measured as a function of ΔV_R on those occasions when the thermal ion

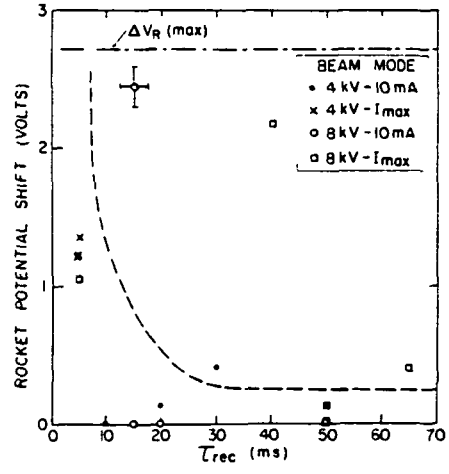

Fig 10 Daughter rocket potential shift (ΔV_R) induced by electron beam pulses as a function of the time after 4- and 8-kV, 10-mA and I_{max} pulses

detector energy sweeps were properly phased with respect to the gun pulses, and these measurements are displayed in Figure 10 Indicated here is the maximum detectable potential shift ΔV_R (max) and the observed shifts for 8-kV and 4-kV, 10-mA and I_{max} pulses. Most of the data points lie near the dashed curve, which is included to guide the reader's eye, except for one 8-kV, I_{max} pulse. The source of the scatter in data points shown here will be discussed further in the next section The rapid (10–20 ms) recovery of the rocket potential following beam pulses is clearly illustrated in this figure

The time required for the rocket potential to recover to near normal values was also investigated using the Langmuir probes Two TEF responses to 8-kV, I_{max} pulses are shown in Figure 11 In both cases, β_{gun} was approximately 90°, however, the lower profile was observed to be close to the mother ($d_\perp$ = 8.2 m) at 0534·55 0, and the upper was close to $d_\perp$ (max) ($d_\perp$ = 27 5 m) at 0535 14.8. The time required for the signal to recover to within 10% of its original level (τ_{rec}') was estimated as shown in this figure

Assuming that the recovery time was related to the time required for the daughter to move out of the perturbed volume, then the distance across this region is given by $d_\perp$(rec) = $\tau_{rec}' v_{R\perp}$, $v_{R\perp}$ being the rocket velocity component perpendicular to the field line. Assuming the ionospheric drift velocity equals zero in the earth's frame of reference, which is consistent with preliminary analysis of the ion drift data, $v_{R\perp}$ is found to be 310 m/s Similar responses to other

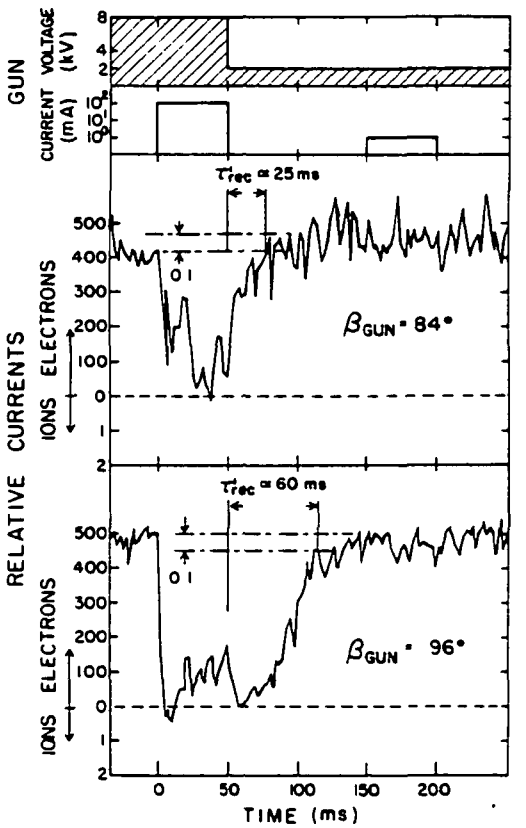

Fig 11 Thermal electron flux measured by the Langmuir probe on the daughter payload during an 8-kV, I_{max} gun pulse Shown here in the top panel is the gun program, in the middle panel the probe response for the sequence starting at 0535 14 8 UT and in the bottom panel the probe response for the sequence starting at 0534 55 0 UT

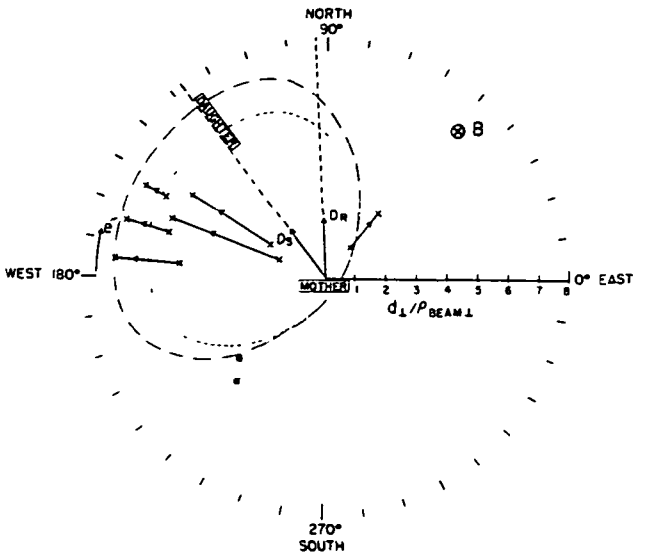

Fig 12 Perpendicular distance traveled by the daughter payload during 8-kV, I_{max} gun pulse recovery time The spatial coordinates used are gun azimuth and distance traveled across field lines Also shown is the azimuth of the daughter payload as viewed from the mother (D_S) and the rocket azimuth in the earth frame of reference (D_R) The predicted radial extent of the perturbation is plotted as a function of beam injection azimuth (elevation) assuming scaling constants of 6 (dotted curve) and 7 (dashed-dotted curve) beam gyroradii

8-kV, I_{max} pulses were analyzed for the first 31 s after payload separation, and the $d_\perp$(rec) estimates for all these pulses are plotted in Figure 12 These results are displayed in the polar coordinate system similar to that used for the EPD data where the azimuth is defined by the electron gun and the distances are measured from the instantaneous position of the mother package Each sample is represented by two crosses joined by a solid line The cross closest to the mother defines the position of the daughter at the end of the pulse, and the distance between the crosses is $d_\perp$(rec) The arrow indicates direction of travel The dashed, egg-shaped curves are the estimated boundaries of the region in which perturbed plasma occurs for K = 6 (inner curve) and K = 7 (outer curve)

These results demonstrate that τ_{rec}' is shortest for pulses where the daughter is near the boundary and increases to a maximum for those cases where the daughter has the longest travel time through the estimated perturbed volume It is also apparent that perturbations to the ambient plasma were observed out to 7 beam gyroradii, which is 1 gyroradius beyond the perturbed region defined by the energetic electrons

The response of the thermal ion sensor to beam injections was also investigated as a function of $d_\perp$ and found to be in agreement with the TEF results shown in Table 4

4 2 2. *Mother payload* To confirm that the perturbed volume was symmetric about the rocket and that the radial dimensions across B scaled as the injected beam gyroradius for a fixed beam current, profiles from the TEF sensor on the mother were investigated

Two typical TEF profiles at different beam injection pitch angles are shown in Figure 13 During the 8-kV, I_{max} pulses (illustrated in the top panel), the TEF signals (bottom two panels) oscillated about the normal level and then dropped abruptly to near zero at the end of the pulse The TEF

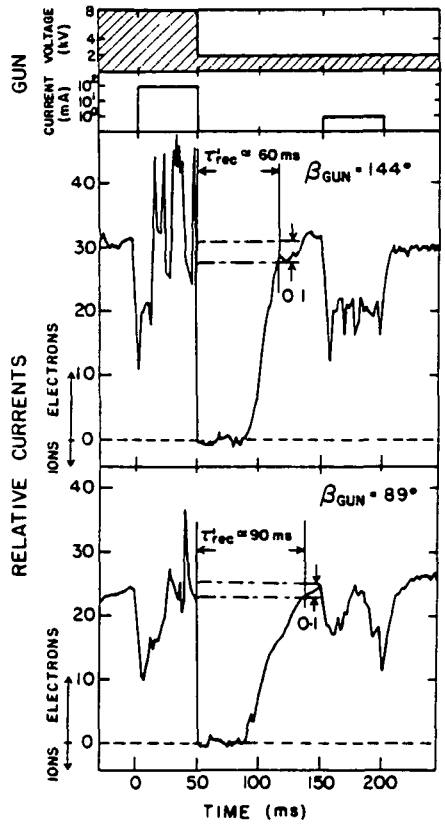

Fig 13 Thermal electron flux, measured by the Langmuir probe on the mother payload, during 8-kV, I_{max} gun pulses as a function of beam injection pitch angle Displayed in the top panel is the gun program while the middle panel shows the probe response for an injection pitch angle of 144° (at 0535 27 4 UT), and the bottom panel shows the probe response for an 89° injection pitch angle (at 0535 8 9 UT)

remained near zero for a few tens of milliseconds and then recovered to the previous level

The model used to interpret the daughter thermal plasma observations was also applied to these profiles When the gun is turned on, it heats the plasma in the vicinity of the rocket, however, during this period the mother floating potential is driven to a relatively high positive value (10 V) At this time no thermal ions are observable on the mother, and the TEF signal is dominated by the electron return flux When the beam is turned off, the payload potential rapidly goes negative in response to the hot ambient plasma surrounding the vehicle This response was previously reported by *Arnoldy and Winckler* [1981] The vehicle then moves out of the perturbed volume in 50 to 100 ms

Nine TEF responses during 8-kV, I_{max} pulses were selected between 0535 00 0 UT and 0535 43 0 UT, and the recovery time τ_{rec}' defined in the previous section was estimated for each pulse The distance traveled across field lines during this time interval ($v_{R\perp}\tau_{rec}'$) is plotted in Figure 14 as a function of the injected beam gyroradius $\rho_{beam} = \rho_{beam} \sin \beta_{gun}$ The dashed line represents the boundary of the perturbed region predicted from the EPD results These data indicate that perturbations are observed in the TEF until the mother exits the predefined perturbed volume which has a radius of approximately 6 beam gyroradii

The discrepancy between predicted and observed response at small $\rho_{beam}(\beta_{gun} \gtrsim 160°)$ evident in Figure 14 can be explained by the gun characteristics The angular divergence of the injected electron beam is typically ≈10°, thus the spread in initial beam injection angle plus further spreading due to space charge effects [*Gendrin*, 1974] will limit the average ρ_{beam} to 1–2 m in this figure, independent of the central injection angle (β_{gun})

A similar study of τ_{rec} as a function of beam injection azimuth was also made during a time period when the spin axis of the mother section was near the magnetic field line With this orientation, β_{gun} remained relatively fixed near 135° for the full rotation about the spin axis. No obvious azimuthal variation was noted, which once again indicated that the perturbed region surrounding the gun was symmetric about the vehicle

Returning now to Figure 10, it is apparent that the scatter in the data shown here is related to geometrical effects associated with the mother-daughter separation distance and gun injection pitch angle

A characteristic thermal ion energy spectrum measured on the mother at 0541 03 3 UT (altitude = 167 km) during an 8-kV, I_{max} pulse is shown in Figure 15 The initial rocket potential is found to be around −2.2 to −2 4 V (the ions are still preaccelerated by 2 V) The detected intensity dropped to zero as soon as the gun was turned on, which is consistent with the rocket potential being driven positive during gun pulses When the gun is turned off, the rocket potential is driven negative in less than 6.25 ms (the time interval between two samples in the ion sensor) and then recovers to the original potential, as indicated by the enhancement in the ion intensity at energies near 6 eV, after 19 ms for this example.

During the 1-mA pulses the rocket potential shifted positively but remained within the limit of the detectability for the ion sensor. The average rocket potential change was found to be approximately 0.7 V during all 1-mA pulses A second interesting feature observed from the mother payload during 1-mA pulses is shown in Figure 13 We note that the TEF decreases in coincidence with the 1-mA pulse, which can only be explained by either a decrease in n_e (the electron density) or an increase in T_e Since we know from the ion sensor that n_i remains unchanged during these pulses, T_e

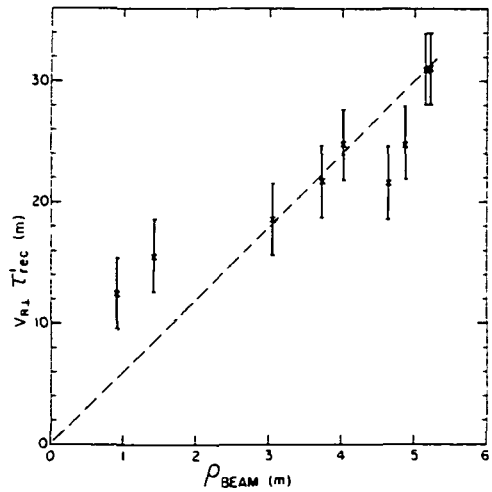

Fig 14 Distance traveled by the mother payload during recovery time (τ_{rec}') as a function of the beam gyroradius ρ_{beam} The dotted line is the predicted response assuming a scaling constant of 6 gyroradii

must have increased significantly even during the 1-mA pulse.

An upper limit on the mother vehicle charging during I_{max} pulses may be set from inspection of Figure 6. These data clearly show that electrons near (within 90% of) the initial beam energy are detected at the daughter vehicle during 4-kV, I_{max} and 2-kV, I_{max} pulses This in turn implies that the potential difference between the mother and daughter vehicles ΔV_{md} is less than 10% of the beam energy (200 eV) while the daughter was in the perturbed volume No signatures of a large potential difference across the boundary of the perturbed volume were observable in either thermal or energetic plasma particles; therefore it is reasonable to assume that ΔV_{md} is a valid estimate of the maximum potential difference between the mother package and the ambient ionosphere during I_{max} pulses

4.2.3 *Plasma heating* A certain level of ambient electron heating, or energization, is clearly evident in the EPD observations during beam pulses (see discussion). Temperature measurements near thermal (electron volts) energies are, however, complicated by vehicle charging effects. As discussed previously, the mother section charged to a large positive potential during beam pulses, which made ion and electron temperature measurements impossible on this section. The daughter section charged negatively during beam pulses while in the perturbed volume surrounding the gun; however, a few examples were found where the floating potential shift was small enough to allow for temperature measurements. An example of an ion distribution observed during one of these events at 0534 56 7 and $d_\perp$ = 9 8 m is shown in Figure 16. A normal distribution with a −3 V effective floating potential was being swept out by the analyzer until the start of the 2-kV, I_{max} pulse, at which time the peak in the distribution shifted upward by 0 8 V No change in the distribution function, other than the floating potential shift, was apparent in the data. Upper limits on the ion temperature and density changes ΔT_i and Δn_i, respectively, during this pulse were set at

$$\Delta n_i/n_i \leq 30\%$$

$$\Delta T_i/T_i \leq 30\%$$

Similar results were obtained for the two other examples when ΔV_R remained small enough to allow for density and ion temperature measurements

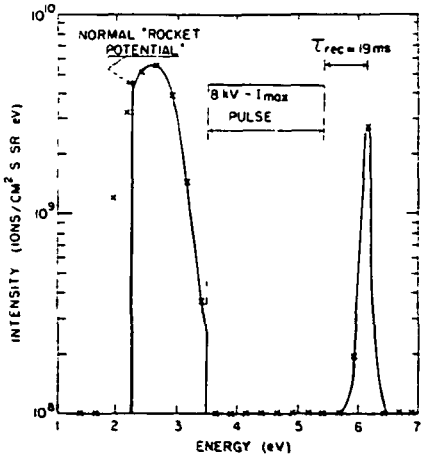

Fig 15 Thermal ion energy spectrum measured at 0541 03 3 UT on the mother payload during an 8-kV, I_{max} gun pulse

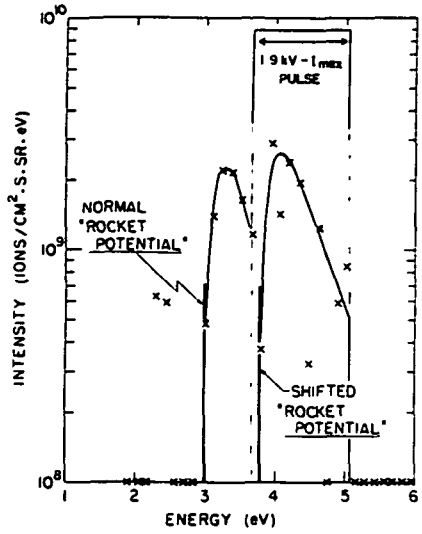

Fig 16 Thermal ion energy spectrum measured on 0534 56 7 UT on the daughter payload during a 2-kV, I_{max} gun pulse

It should be remembered that since these events were selected by the requirement that ΔV_R be small, they may not be representative of all I_{max} and 10-mA pulses. However, these estimates are consistent with the TEF results in the ion collection mode (section 4 2.1)

The electron temperature and density were also estimated during one of these events using the rocket potential shift defined by the thermal ion sensors and the output from the TEF probe. Assuming the electron distribution was Maxwellian, which may not be a good assumption during beam pulses, an electron temperature $T_e \approx 6200$°K was estimated for the 4-kV, 10-mA pulse at 0535 00 2 UT, while the electron temperature just before this gun pulse was 2400°K The ambient electron density was estimated to be 1 5 × 10^5 cm^{-3}

5 Summary

The high-altitude (>200 km) charged particle observations presented here clearly show an electron beam behavior which is inconsistent with single-particle motion For example, the return (or downward directed) energetic electron flux associated with the upward directed beam pulses was observed to have the following characteristic

1 The volume occupied by energetic electrons and perturbed ionospheric plasma induced by the beam is symmetric about the magnetic field line passing through the electron gun. The perpendicular dimension of the perturbed volume scales as the primary electron beam gyroradius, and the scaling factor increases with increasing current The typical radial extent across field lines is $6\rho_{beam}$ for 100-mA pulses, 3 7ρ_{beam} for 10-mA pulses (with the exception of the 8-kV pulses), and less than $2\rho_{beam}$ for 1-mA pulses

2. The pitch angle distribution of energetic electrons was isotropic over the upper (return flux) hemisphere

3 The intensity of the energetic electron return flux was not linearly dependent on beam current for a fixed energy For example, when observable, the response to 10-mA and I_{max} beams was approximately independent of current

4 The energy spectra of beam-induced electrons observed near the rocket are strongly dependent on the distance across field lines ($d_\perp$) from the gun Close to the

rocket, large fluxes of low-energy ($E < 1$ keV) electrons are observed, and the energy spectra (Figures 5 and 6) show monotonically decreasing intensities with increasing energies out to approximately the beam energy where the intensities drop rapidly to background The low-energy electron flux decreases with increasing $d_\perp$ while the flux near the beam energy remains relatively constant, resulting in a monoenergetic spectrum peaked at E_B at large $d_\perp$ The energetic flux drops rapidly to background at the edge of the perturbed region.

5 The volume in which perturbations to the ambient plasma were observed overlapped and extended to slightly larger $d_\perp$

6. Only very limited information on thermal plasma heating during beam firings was available, because of spacecraft charging effects, however, in those few examples where measurements were possible, the ion temperature was not measurably affected by the beam ($\Delta T_i/T_i \leq 30\%$) Electron temperatures, however, increased from a normal value of $T_e = 2400°K$ up to $T_e \geq 6000°K$ This observation is consistent with the observations presented in section 4 and with the measurement of large negative floating potentials on the mother directly after beam pulses which indicates that the rocket was surrounded by a hot electron gas during and for some tens of milliseconds after the gun was turned off Also, assuming that the rocket floating potential varies linearly with KT_e, an increase in floating potential of the daughter payload from the normal value of -1 V to more than -5 V, during and directly after gun firings, implies a perturbed temperature of T_e of 10,000°K

Estimates of the plasma density during beam firings were also hampered by vehicle charging effects on both payloads, however, a few examples were found where the daughter vehicle charged to only a few volts, and in these instances the plasma density was observed to be unaffected (increased by less than 30%) by the beam Estimates of the plasma density were also made directly after beam pulses when the rocket was immersed in the perturbed plasma, and these data once again indicated that the density changed by less than 30%

The positive potential shift of the vehicle carrying the accelerator during beam pulses was measured to be 0 7 V for 1-mA pulses and less than 200 V for I_{max} beams

6 Discussion

Many of the observations summarized above are consistent with those previously reported in the literature For example, the dense cloud of low-energy electrons (5–2000 eV) accompanying beam firings has been reported on nearly all previous flights (see, for example, *Maehlum et al* [1980*b*] and *Winckler* [1982]) The spatial extent of the perturbation in the ionospheric plasma and the temporal response of the energetic and thermal plasma after beam firings are also consistent with many previous reports [*Cartwright et al* 1978 *Jacobsen et al* 1981] The scaling of this volume with beam current energy, and injection pitch angle is more clearly defined here

In a previous flight, using a similar accelerator and detector configuration, return beam profiles were measured as a function of separation distance, and these results were reported by *Bernstein et al* [1982] Their measurements at energies less than the beam energy are consistent with those presented here, however, no particles at or near the beam energy were detected The intense flux of auroral electrons present during the previous flight could be responsible for masking this response

Maehlum et al [1980*b*] also measured the energetic electron distributions near an electron accelerator which operated at slightly higher energies and currents (10 keV and 130 mA) They observed a dense 'core' of energetic electrons near (within 2 beam gyroradii of) the accelerator, presumably the primary beam, and a weak 'halo' of energetic electrons, at and below the beam energy, which exponentially decreased in intensity with distance across B and extended to several gyroadiameters The intensity of the halo was 1 to 2 orders of magnitude below the limit of detectability for the results presented here and was several orders of magnitude less intense than the return flux reported in section 4 The source of this discrepancy remains unclear at this time since the experimental conditions were similar for both measurements

The observations summarized above suggest that the electron beam was severely modified over a short path length through the high-altitude auroral ionosphere This is most easily demonstrated by calculating the return (downward directed) energetic electron number and energy flux and comparing them with the upward injected primary beam values

The return number flux for 8-kV, I_{max} pulses was estimated by integrating the measured energy distributions (Figure 5) over energy and area out to d(max), the maximum radial distance where beam-induced energetic electrons were observed. The number flux N and energy flux ζ were evaluated between 100 eV and 2 keV and from 2 to 7 keV, assuming an isotropic distribution over the upper hemisphere (see section 5, characteristic 2), with the following result

$$(2 - 0.8) \times 10^{17} \leq N_L \leq (2 + 1\,2) \times 10^{17}$$

$$(1 - 0\,4) \times 10^{17} \leq \zeta_L \leq (1 + 0\,6) \times 10^{17}$$

for 100 eV $\leq E \leq$ 2 keV, and

$$(3 - 1\,2) \times 10^{17} \leq N_H \leq (3 + 1\,8) \times 10^{17}$$

$$(7 - 2\,8) \times 10^{17} \leq \zeta_H \leq (7 + 4\,2) \times 10^{17}$$

for $2 \leq E \leq 7$ keV The injected beam values (N_B and ζ_B) were $N_B = 6 \times 10^{17}$ electrons/s and $\zeta_B = 4 \times 10^{18}$ keV/s

We see immediately that the sum of the downward directed low- and high-energy electron fluxes is at least 50% of or significantly larger than the original beam flux Since at least an equal number are expected to be injected upward into the magnetosphere, a substantial fraction of the downward directed electrons must be accelerated ambient electrons We note that if the energetic electrons ($E > 2$ keV) are degraded beam particles, then half the original beam particles are scattered into the return hemisphere Also, a substantial fraction of the initial beam energy is carried by the energetic return particles

The above estimates refer to beam injection pitch angles β_{gun} near 90° At smaller or larger β_{gun} the radius of the perturbed volume decreases, and, since the magnitude of the energetic particle intensities was not strongly dependent on β_{gun}, the return flux decreases Because the radius of the perturbed region scales as $\sin \beta_{gun}$, the return flux scales roughly as $\sin^2 \beta_{gun}$ The scaling applies only at large angle to the magnetic field since the minimum for this angle is limited by the gun divergence characteristics and space charge considerations

To determine the relative contributions of collective processes and 'normal' single-particle scattering to the intense low-energy return flux, the following single-particle estimate was made. Using the U.S. Standard Atmosphere (1976, p. 211) to define the neutral density and the *Banks et al.* [1974] ionization cross sections, the total number of secondaries produced above the rocket by an 8-kV, I_{max} beam, in the 200- to 500-eV energy range, was estimated to be 4×10^{13} electrons/s This may be compared with the measured return flux of $\approx 10^{16}$ electrons/s, which is several orders of magnitude larger than the maximum due to secondaries. Thus even assuming that all the secondaries returned to the area surrounding the gun, this source is insufficient to account for the measured return flux.

The spatial distribution of the electrons near the beam energy is not consistent with simple radial diffusion models Data presented here indicate a spatial intensity profile which is more or less constant out to 4 or 5 gyroradii, followed by a sharp decrease in intensity over approximately 2 gyroradii. A diffusion coefficient independent of radial distance from the beam would be expected to produce a more or less constant radial gradient. The data suggest that the diffusion coefficient for these electrons is dependent on the radial distance from the beam, diffusion being strongest in the perturbed volume and dropping to a small value near the boundary.

Support for this model can be found in the plasma wave observations from the same flight reported by *Kellogg and Monson* [1981]. They show that the intensities of broadband plasma wave emissions, presumably the waves involved in the radial diffusion process, have a profile similar to the energetic electrons. That is, they see a large steplike decrease in the plasma wave intensity at the energetic electron boundary which in turn could produce the required rapid decrease in the radial diffusion.

It should be noted that *Kellogg and Monson* [1981] also observed high-frequency waves at 13 MHz which were interpreted as plasma frequency emissions This implies a local plasma density of 2×10^6 cm^{-3} during gun firings, which is in apparent disagreement with the observations reported here (section 4). Since the Langmuir probes measured the local density averaged over several milliseconds, one possible explanation is that remote spatially confined enhancements in the local plasma density were produced by the beam or that transient plasma density fluctuations were present which met the conditions for wave emission without inducing a measurable response in the other plasma sensors

Measurements of the temporal response of the energetic electrons to beam injections may be used to set an upper limit on the longitudinal extent of the region in which strong energetic electron scattering effects occurred Induced energetic (200 eV $< E <$ 8 keV) electron enhancements were observed simultaneously at all energies in coincidence with beam pulses and had rise and fall times of less than 1.25 ms, the detector sampling time This implies a maximum source distance of <10 km for 200-eV electrons.

Also, perturbed ionospheric plasma was observed for up to $\approx$100 ms after gun pulses, which implies that the longitudinal extent of the perturbed volume was greater than 100 m if we assume that the longitudinal ambipolar plasma diffusion [*Krall and Trivelpiece*, 1973], at 200 km altitude, was responsible for the replenishment of the ambient plasma. We note that the perturbation must extend 100 m in both directions along the field lines and that this is only a lower limit since the 100-ms delay was consistent with the flight time of instruments through the perturbation and does not necessarily represent the plasma recovery time.

These data therefore demonstrate that the high-current (10 mA and I_{max}) electron beams were severely modified after traveling a short (<10 km) distance through the ionospheric plasma. Charged particle observations during low current (1 mA at 1.9, 4, and 8 kV) and the 8-kV, 10-mA pulses were consistent with the single-particle motion for the beam particles with no strong local interactions. The process responsible for the beam modification also produced large fluxes of low-energy electrons (hundreds of electron volts), presumably by accelerating ambient ionospheric particles

Some features in the data are consistent with observations of the configuration known as the beam plasma discharge (BPD) which can occur when a strong energetic electron beam traverses a poorly ionized ambient plasma [*Bernstein et al.*, 1979]. During tests of the same electron accelerator system in the large vacuum chamber at the Johnson Space Center in Houston [*Bernstein et al.*, 1980], the 2-kV, I_{max} and sometimes the 4-kV, I_{max} beams produced the BPD while 8-kV, I_{max} and all 10-mA and 1-mA beams demonstrated single particle behavior. In the present flight experiment, all I_{max} beams and 2- and 4-kV, 10-mA beams produced collective effects which were not present for 8-kV, 10-mA and all 1-mA beams. Therefore, assuming that the BPD was responsible for the observed collective effects, it seems that it is somewhat easier to excite the BPD in the ionosphere than in the laboratory, which is consistent with the conclusion of *Kellogg and Monson* [1981] from a preceding flight.

Another obvious discrepancy exists between the laboratory and space measurements of the spatial extent of the instability. In the laboratory, for injections at pitch angle $\leq$150°, the maximum radial extent $d_\perp$(max) of the active region is limited approximately to the diameter of the stable single-particle helix independent of beam current (I_B), whereas in the ionosphere, $d_\perp$(max) increased with I_B reaching 3 gyrodiameters for I_{max} pulses

No reasonable comparisons between the longitudinal or temporal characteristics of the process can be made, since in the laboratory these considerations are dominated by the presence of finite axial and radial boundaries (the walls of the vacuum tank)

Finally, the energy spectrum measured in space at high beam currents and on field lines near the gun (Figures 5 and 6) is flat or monotonically decreasing in intensity out to the beam energy where it falls rapidly to zero Similar spectra were recorded in the laboratory when the beam was in the BPD mode [*Jost et al.*, 1980]

In the Echo experiments the data demonstrated that the energetic electron beam displayed single-particle behavior over several hundreds of kilometers, which appears to be in conflict with the results presented here However, this may be related to I_c (the critical current required for local ignition of the BPD), which is approximately dependent on beam energy As pointed out by *Winckler* [1982], the electron gun current in the Echo series was below the critical current for the BPD, and therefore single-particle behavior is expected.

Vehicle charging effects were also clearly evident in the charged particle observations. The conclusion that the rocket potential did not exceed 200 V at maximum (I_{max}) current is in agreement with previous reports [e.g., *Gringauz and Shutte*, 1980] and with vehicle charging calculations such as those of *Linson* [1969] Linson shows that with an ambient

density of $\approx 10^5$ cm^{-3} and assuming a temperature of 10^4 °K, the ambient current density,

$$J_0 = \frac{e}{4} n_e \left(\frac{2kT_e}{m_e}\right)^{1/2}$$

is 2 mA/m^2, where e and m_e are the electron elementary charge and mass, respectively Assuming a cross-sectional area, projected perpendicular to B, of 5 m^2 for the rocket collection surface area, we estimate the current intercepted by the vehicle (I_0) to be 10 mA, resulting in an I_B/I_0 ratio of 10 during 100-mA pulses Referring to *Linson* [1969, Figure 3], we see that a vehicle potential of 200 V is expected from the $q_c = \frac{1}{4}$ model and for the *Beard and Johnson* [1961] model, the two models that place limits on the maximum possible return current. These data suggest that the increased vehicle neutralization currents required to balance the beam currents are provided by the increased electron temperature and by the increase in collection area due to the expanded sheath around the vehicle.

It is interesting to note that in the absence of electron heating, I_0 would be decreased by a factor of 2 or 3, and the predicted vehicle potential would increase to several kilovolts, which is of the order of the beam energy Thus the electron heating, presumably due to the energetic electron beam interaction with the ambient plasma, seems to be instrumental in providing the required return current to the vehicle

To summarize, these high-density electron beams, which in this case were intended to be used as single-particle probes of magnetospheric processes, were grossly modified by their interaction with the ionospheric plasma Local ionospheric electron heating and strong pitch angle, energy, and spatial diffusion of the beam were observed after the beam had traveled only a short distance (10 km) Many of these features in the induced charged particle distributions were similar to those observed in laboratory simulations of the experiment where a beam-plasma instability, referred to as the beam plasma discharge, was initiated by beam pulses However, serious discrepancies between measurements made in the laboratory and those made in space still exist

Clearly, before this technique can be effectively used to probe magnetospheric processes, a better understanding of the electron beam dynamics in the ionosphere is required Continued investigation of the stability of artificial electron beams in the ionosphere and magnetosphere may also lead to an improved understanding of the dynamics of naturally occurring electron beams in the magnetosphere (e g , auroral electron beams) and in more remote astrophysical systems

Acknowledgments The authors gratefully acknowledge the extensive contribution made by P J Kellogg to the interpretation and discussion of the results which appear in this paper The participation of W Bernstein in this investigation was supported by NASA grant NAGW-69

The Editor thanks B N Maehlum and J R Winckler for their assistance in evaluating this paper

REFERENCES

Arnoldy R L , and J R Winckler The hot plasma environment and floating potentials of an electron-beam-emitting rocket in the ionosphere, *J Geophys Res* , *86*, 575 1981

Banks, P M, C R Chappell and A F Nagy, A new model for the interaction of auroral electrons with the atmosphere Spectral degradation, backscatter optical emission, and ionization, *J Geophys Res* , *79* 1459 1974

Beard, D B , and F S Johnson, Ionospheric limitations on attainable satellite potential, *J Geophys Res* , *66*, 4113, 1961

Bernstein, W , H Leinbach, P J Kellogg, S J Monson, and T Hallinan, Further laboratory measurements of the beam-plasma discharge, *J Geophys Res* , *84*, 7271, 1979

Bernstein, W , B. A Whalen, F R Harris, A G McNamara, and A Konradi, Laboratory studies of the charge neutralization of a rocket payload during electron beam emission, *Geophys Res Lett* , *7*, 93, 1980

Bernstein, W , P J Kellogg, S J Monson R H Holzworth and B A Whalen, Recent observations of injected beam plasma interactions in the ionosphere and a comparison with laboratory studies of beam plasma discharge, in *Artificial Particle Beams Utilized in Space Plasma Physics, Proceedings of a NATO Advanced Research Institute, April 21–26, 1981, Geilo, Norway* edited by B Grandal, p 35, Plenum, New York 1982

Cambou, F , V S Dokoukine, J Lavergnat, R Pellat, H Reme, A Saint-Marc, R Z Sagdeev, and I A Zhulin, General description of the ARAKS experiment, *Ann Geophys* , *36*, 271, 1980

Cartwright, D G , S J Monson, and P J Kellogg, Heating of the ambient ionosphere by an artificially injected electron beam, *J Geophys Res* , *83*, 16, 1978

Gendrin, R , Initial expansion phase of an artificially injected electron beam, *Planet Space Sci* , *22*, 633, 1974

Green, D W , and B A Whalen, Ionospheric ion flow velocities from measurements of the ion distribution function technique, *J Geophys Res* , *79*, 2829, 1974

Gringauz, K I , and N M Shutte, The study of electron fluxes with energy 3 keV in the ARAKS experiment of January 26, 1975, *Ann Geophys* , *36*, 381, 1980

Holzworth, R H , and H C Koons, VLF emissions from a modulated electron beam in the auroral ionosphere, *J Geophys Res* , *86*, 853, 1981

Israelson, G , and J R Winckler, Measurements of 3914-Å light production and electron scattering from electron beams artificially injected into the ionosphere, *J Geophys Res* , *80*, 3709, 1975

Jacobsen, T A , J Troim, B N Maehlum, and M. Friedrich, Ionospheric electron heating by a rocket borne electron accelerator, *Adv Space Res* , *1*, 123, 1981

Jost, R J , H R Anderson, and J O McGarity, Electron energy measured during electron beam-plasma interactions, *Geophys Res Lett* , *7*, 509, 1980

Kellogg, P J , and S J Monson, Rocket borne electron accelerator results pertaining to the beam plasma discharge, *Adv Space Res* *1*, 61, 1981

Krall, N A , and A W Trivelpiece, *Principles of Plasma Physics*, p 321, McGraw-Hill, New York, 1973

Linson, L M , Current-voltage characteristics of an electron-emitting satellite in the ionosphere, *J Geophys Res* , *74* 2368 1969

Maehlum, B N , K Maseide, K Aarsnes, A Egeland, B Grandal, J Holtet, T A Jacobsen, N C Maynard, F Soraas, J Stadsnes, E V Thrane, and J Troim, Polar 5—An electron accelerator experiment within an aurora 1, Instrumentation and geophysical condition, *Planet Space Sci* , *28*, 259, 1980*a*

Maehlum, B N , B Grandal, T A Jacobsen, and J Troim, Polar 5—An electron accelerator experiment within an aurora, 2, Scattering of an artificially produced electron beam in the ionosphere, *Planet Space Sci* *28* 279, 1980*b*

Wilhelm K , W Bernstein, and B A Whalen, Study of electric fields parallel to the magnetic lines of force using artificially injected energetic electrons, *Geophys Res Lett* , *7*, 117, 1980

Winckler, J R The application of artificial electron beams to magnetospheric research *Rev Geophys Space Phys* , *18*, 659 1980

Winckler, J R , Probing the magnetosphere with artificial electron beams *Adv Space Res* , *1*, 17 1981

Winckler, J R , The use of artificial electron beams as probes of the distant magnetosphere, in *Artificial Particle Beams Utilized in Space Plasma Physics, Proceedings of a NATO Advanced Research Institute April 21–26 1981 Geilo Norway*, edited by B Grandal, p 3, Plenum, New York 1982

Yau, A W , B A Whalen and F Creutzberg, Rocket-borne observations of the ion convection and electric fields in dayside and nightside visual auroral arcs, *J Geophys Res* , *86*, 6899 1981

(Received July 15 1982,
revised January 17 1983
accepted January 19 1983)

JOURNAL OF GEOPHYSICAL RESEARCH, VOL 90, NO A1, PAGES 491–504, JANUARY 1, 1985

Fast Magnetospheric Echoes of Energetic Electron Beams

KLAUS WILHELM,[1] WILLIAM BERNSTEIN,[2] PAUL J. KELLOGG,[3] AND BRIAN A. WHALEN[4]

Electron beam experiments using rocketborne instrumentation have confirmed earlier observations of fast magnetospheric echoes of artificially injected energetic electrons A total of 234 echoes have been observed in a pitch angle range from 9° to 110° at energies of 1 87 and 3 90 keV Out of this number, 95 echoes could unambiguously be identified with known accelerator operations at 2-, 4-, or 8-keV energy and highest current levels resulting in the determination of transit times of typically 300 to 400 ms In most cases, when echoes were present in both energy channels, the higher-energy electrons led the lower-energy ones by 50 to 70 ms Adiabatic theory applied to these observations yields a reflection height of 3000 to 4000 km An alternative interpretation is briefly examined, and its relative merit in describing the observations is evaluated The injection process is discussed in some detail as the strong beam-plasma interaction that occurred near the electron accelerator appears to be instrumental in generating the source of heated electrons required for successful echo detection for both processes

1 Introduction

The importance of electric fields parallel to the geomagnetic field lines ($E \| B$) in the context of modern auroral theories prompted the attempt, described in this paper, to use artificially injected energetic electron beams, injected from a low-altitude (~ 200 km) vehicle, as remote probes of such fields If successful, this technique would provide important estimates of critical features of the $E \| B$ configuration, i e, the total potential drop, field strength, altitude dependence, spatial extent, and correlation with the energetic particle precipitation. In an earlier related experiment an ion beam produced in a shaped charge release had also been used for the study of propagation effects in the magnetosphere and led to the determination of an acceleration potential of several kilovolts [*Haerendel et al*, 1976]

In a series of sounding rocket experiments, *Winckler* [1980, *Winckler et al*, 1975] pioneered the use of electron beams as remote probes for magnetospheric configuration studies Two distinct echo delay time patterns were observed for the injected 20–40 keV beams (1) delay times of several seconds arising from reflection at the conjugate points (magnetospheric echoes) and (2) delay times of 10–20 ms attributed to reflections (either mirrored or collisionally backscattered) from altitudes below the rocket payload (quick echoes) In the present experiment, using lower-energy (2–8 keV) beams, the reflection of injected electrons at an electric potential drop located at several thousand kilometers altitude should result in delay times of approximately 0 5 s termed fast echoes in this report

The experiment to be discussed here was carried out by the University of Minnesota, the National Research Council of Canada, and the Max-Planck-Institut fur Aeronomie in the framework of the project SCEX (Several Compatible EXperiments to utilize an electron accelerator, NASA flight 27 045) The results obtained qualitatively support the existence of parallel electric fields and can be consistently interpreted by assuming that the $E \| B$ configurations that supposedly provide the acceleration of auroral electrons above discrete arcs also cause the reflection of the artificially injected beams Although this consistency is a strong argument, certain more quantitative aspects of the data suggest that other processes may play an important, if not the dominant, role in producing the observations A comparison is therefore made with an alternative explanation The main goal of this report is, however, to present the observations and to describe the conditions under which the data have been obtained

The original $E \| B$ experiment was first planned for a sounding rocket flight in 1978, when it was thought that the energetic electrons could be considered as single particles during the injection, transit, and detection phases [*Wilhelm et al*, 1980] As a consequence, echo detection was only expected to be possible if the injection parameters (energy, pitch angle, and azimuth) would closely coincide with the corresponding detection parameters In addition, the payload velocity across the magnetic field and the electric field drift would place constraints on the locus of an eventual echo The probability of finding an echo under these conditions was considered to be very small In the meantime it has become clear that a strong beam-plasma interaction (BPI) probably occurs near the injection point (at least for large beam currents) and that this interaction would substantially enhance the probability of echo detection by diffusing the injected velocity and pitch angle distributions

2 Concept of the Experiment

2 1 *Transit Time Observations*

Parallel electric fields above auroral arcs capable of accelerating magnetospheric electrons downward should also be able to decelerate and eventually reflect artificially injected energetic electrons travelling upward. The task at hand is to observe such reflected electrons and to measure the transit time as a function of the injection parameters In order to apply adiabatic theory the transit time T has to be determined as function of the magnetic moment of the injected electrons and their energy according to

$$T = T(\mu, W) \tag{1}$$

[1]Max-Planck-Institut fur Aeronomie, Katlenburg-Lindau, Federal Republic of Germany
[2]Department of Space Physics and Astronomy Wiess School of Natural Sciences, Rice University, Houston, Texas
[3]School of Physics and Astronomy University of Minnesota, Minneapolis
[4]National Research Council Canada, Herzberg Institute of Astrophysics Ottawa, Ontario

Paper number 4A8147
0148-0227 85 004A-8147505 00

TABLE 1 Instrument Parameters of Electron Spectrometer Channels

Channels	Angular Resolution, deg		Electron Energy		Electron Velocity, m/s	Conversion Factor, cm^2 sr eV cts/e^-
	Elevation	Azimuth	Center,* eV	Resolution (FWHM), %		
TAD 2/FU 1/SB 1/2	6 9	3 3	1870	12.8	2.56×10^7	$2\,13 \times 10^{-1}$
/4	8 0	3 3	3930	15 6	$3\,72 \times 10^7$	$6\,99 \times 10^{-1}$
/SB 2/4̄	9 2	2 8	3940	13 6	$3\,72 \times 10^7$	$6\,53 \times 10^{-1}$
/8̄	6 6	2 9	7860	13 7	$5\,26 \times 10^7$	1 22
TAD 4/FU 2/SB 1/2	7 1	3 2	1870	15 6	$2\,56 \times 10^7$	$2\,57 \times 10^{-1}$
/4	8 7	3 7	3930	16 5	$3\,72 \times 10^7$	$5\,52 \times 10^{-1}$
SB 2/4̄	8 5	3 8	3830	16 5	$3\,67 \times 10^7$	$7\,41 \times 10^{-1}$
/8̄	6 5	3 1	7890	14 8	$5\,27 \times 10^7$	1 52

*Analyzer constant 9 5 eV/V

where $\mu = W(s_0)B^{-1}(s_0) \sin^2 \alpha(s_0)$ is the magnetic moment, s_0 the injection point measured from the earth's surface along the geomagnetic field, $W(s_0)$ the injection energy, $B(s_0)$ the magnetic field induction at s_0, and $\alpha(s_0)$ the electron injection pitch angle In the presence of a parallel electric field $E_\parallel(s)$ and consequently of an electric potential

$$\phi(s) = -\int_{s_0}^{s} E_\parallel(s)\, ds \tag{2}$$

the longitudinal electron velocity is

$$v_\parallel(s) = \pm\left[\frac{2}{m}\left[W(s_0) - q\phi(s) - \mu B(s)\right]\right]^{1/2} \tag{3}$$

with m and q the mass and electric charge of an electron, respectively Hence the transit or echo time at s_0 can be expressed by

$$T(\mu, W) = 2\int_{s_0}^{s_m} \frac{ds}{v_\parallel(s)} \tag{4}$$

where s_m is the mirror point determined by $v_\parallel(s_m) = 0$ If $T(\mu, W)$ could be measured and $B(s)$ assumed as earth's magnetic field, the solution of (4) should provide $\phi(s)$ and thus a profile of the electric field along the magnetic field

In the SCEX project the attempt to measure electron transit times was only one aspect among others Nevertheless, it required some elaborate experimental conditions if a reasonable probability of success was to be achieved Besides the electron accelerator on the main payload, energetic electron detectors with very high time resolution were a basic requirement They had to be mounted on throwaway packages (TAD's) because of the payload velocity perpendicular to the magnetic field and the unpredictable $\mathbf{E} \times \mathbf{B}$ drift motion of the electron beam As controlled ejection of the TAD's was beyond the financial scope of the project, several subpayloads were released at random in order to enhance the area where echoes could be detected Measurements made on two of them form the basis of this analysis

Also, for financial reasons it was necessary to rely on the uncontrolled tumbling motion of the TAD's for pitch angle coverage of the detectors The TAD's therefore were designed with three unequal moments of inertia and were released with their angular velocity around the intermediate axis Trajectory and attitude measurements both on the main payload and on the TAD's were a prerequisite for a meaningful data interpretation Finally, a careful launch time selection in relation to the geophysical conditions was required in order to encounter potential parallel electric field conditions

2 2. *Injection Processes*

One of the problems in devising this experiment was the fact that little was known about the actual injection mechanism The simplest assumption would be that the beam particles follow single particle trajectories and behave adiabatically Although easy to treat theoretically, this case would require minute planning of the experimental configuration as close correspondence of the accelerator and detector parameters in energy, pitch angle, and azimuth is a necessary but not a sufficient condition for echo identification In addition, the separation distance between the injection and reception points has to be matched to both the payload movement across the magnetic field and the drift motion of the particles caused mainly by perpendicular electric fields

Earlier observations indicated that the assumption of a collective interaction of the beam particles with the surrounding plasma near the injection point would be more appropriate in arriving at a consistent interpretation [*Wilhelm et al*, 1980] Laboratory work also demonstrated that high-current electron beams (with a beam current I_b greater than the critical current I_c) interact strongly with the local ambient plasma-neutral gas environment [*Bernstein et al*, 1978, 1979, *Szuszczewicz et al*, 1982] One consequence of this interaction, as observed in the laboratory, is the heating and pitch angle scattering of the injected beam [*Jost et al*, 1981] Values of $\Delta W/W$ for the modified beam range from ~0 13 to 1 (W Bernstein, private communication, 1983) for different experimental conditions, typically electrons with energies greater than the injection energies, are also produced It is important to emphasize that, to date, all energetic electron measurements performed in flight experiments have been limited to electrons which have returned to the injection altitude, (i e, backscattered electrons) and that no measurements of the propagating beam spectrum have been made In all cases the return fluxes show severe energy diffusion [*Arnoldy and Winckler*, 1981, *Duprat et al*, 1982, *Grandal*, 1982] Because of these findings it was assumed for the reflection experiment that electron beams above a certain current threshold would lead to strong interaction processes, resulting in energy as well as pitch angle diffusion near the accelerator The heated electron beam would then constitute the source of energetic electrons to which adiabatic theory could be applied. This concept, if it were correct, would substantially increase the probability of finding echo pulses because electrons would be injected into wide energy, pitch angle, and azimuth ranges In other words the space and time windows in which returning electrons could be detected would be greatly enlarged This would at the same time alleviate the horizontal coincidence requirement considerably If it is as-

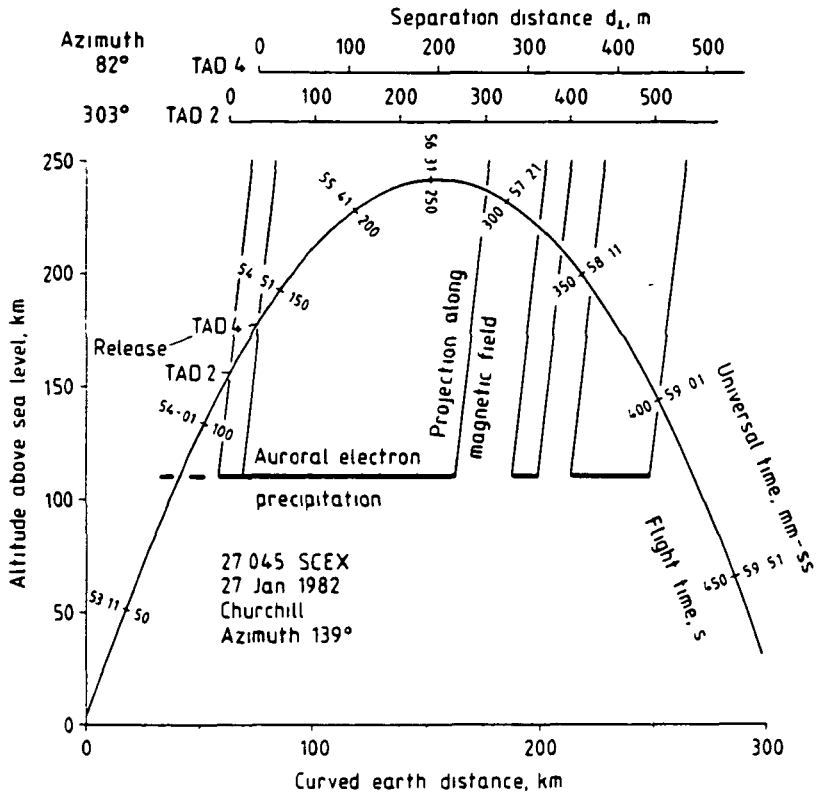

Fig 1 SCEX trajectory plotted as altitude over curved earth distance in an azimuth of 139° Flight time is indicated every 50 s in relative and universal time after 03-00 UTC Releases of TAD 2 and 4 are shown together with the transverse separation distances and azimuths of the TAD's for the remainder of the flight Based on the energetic electron observations of the TAD's (to be presented below), the approximate locations and times of the auroral arc crossings are also sketched

sumed that the strong perturbations of the electron beam occur within a comparatively short distance from the accelerator, the detected energetic electrons (echoes) can still be completely characterized by the receiver settings in energy, pitch angle, azimuth, and separation distance, making a controlled experiment possible

Any further limitation of the application of adiabatic theory can, of course, not be ruled out a priori It would lead, however, to an increase in experimental and theoretical difficulties up to a point where controlled experimentation breaks down The observations of prompt responses to accelerator operations in the near environment of the main payload to be presented in this report support the assumption of a strong beam-plasma interaction during high current modes of the accelerator and provide some insight into the spatial structure and temporal development of the disturbed region

3 Instrumentation

3 1 *Electron Accelerator*

The maximum perveance of the accelerator system was approximately 1×10^{-6} IU$^{-3/2}$ (AV$^{-3/2}$) The triode electron gun was mounted in the front section of the main payload and injected electrons at an angle of 45° with respect to the payload axis The accelerator operation was initiated 117 s after liftoff at an altitude of 156 km and functioned nominally until approximately 355 s elapsed time when some degradation of the highest current pulses occurred The accelerator continued to function in this fashion for another 70 s before reentry

The accelerator emitted electrons at three energy levels of approximately 2, 4, and 8 keV with currents of 1, 10, or 100 mA The large range in injection beam current was included for two reasons (1) the occurrence of the strong beam-plasma interaction is critically dependent on both the beam and ambient plasma density, and (2) it was feared that the injection of high-density beams into an $E \| B$ configuration might modify the electric field configuration itself The pulses were 50 ms long interrupted by off times of 100 ms Interspersed with seven normal accelerator cycles of nine pulses were a 3-kHz modulation period at 8 and 4 kV and 100 mA and a cycle with no pulse injection A normal cycle consisted of nine pulses with the following designation 1 2 keV, 1 mA, 2 2 keV, 10 mA, 3 2 keV, 100 mA, 4 4 keV, 1 mA, 5 4 keV, 10 mA, 6 4 keV, 100 mA, 7 8 keV, 1 mA, 8 8 keV, 10 mA, and 9 8 keV, 100 mA Every accelerator pulse during flight 27 045 was identified by a code of the form XX-X-X giving sequence, cycle, and pulse numbers

Measurements of the direction of the ambient thermal ion drift velocity ($\mathbf{E} \times \mathbf{B}$ drift) were made with ion drift meters included in the payload of the accelerator section Although such measurements could not be made during and immediately after accelerator operation because of vehicle charging effects, we believe the detectors provided consistent measurement of the ion drift direction when no particle beam was emitted Unfortunately, quantitative measurements of the magnitude of the drift velocity could not be obtained

3 2 *Electron Detectors on Throwaway Packages (TAD's)*

TAD 2 and TAD 4 each carried four fixed-energy electron detectors with electrostatic deflection systems followed by

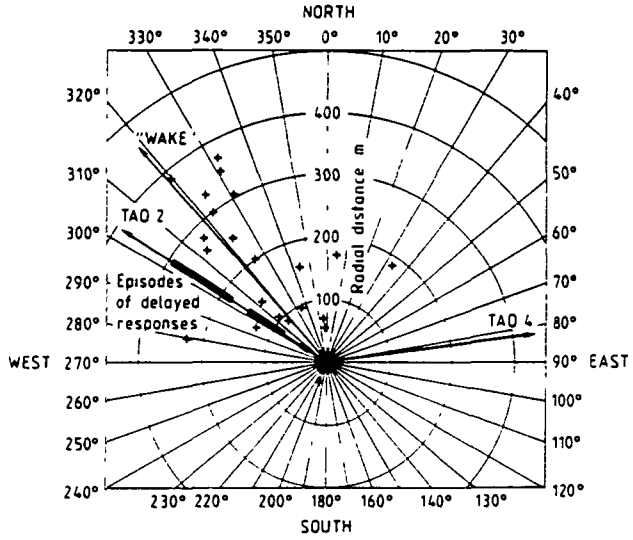

Fig 2 Ion drift direction measurements in the frame of reference moving with the main payload The azimuths of the flow are given at distances equal to the TAD 2-mother payload separation distance Also shown are the TAD 2 and 4 trajectories as well as the wake direction In general the ion drift measurements are clustered around the "wake" direction, which in turn is close to the TAD 2 trajectory No delayed responses were observed when the flow azimuth was far removed from the trajectory

channel electron multipliers (CEM) Channels 2 and 4 looked into the same direction out of the TAD's, whereas channels $\overline{4}$ and $\overline{8}$ were mounted with their view angles in the opposite direction Other characteristics of the channels have been compiled in Table 1

The output of the CEM, after suitable amplification, was counted in a nine-bit register for each of the four channels The registers in turn were interrogated by the telemetry system every 0 76 ms without reset As the timing of the TAD channels with respect to the link of the main payload carrying the accelerator is of great importance for the echo experiment, it was fortunate that the accuracy could be checked while the TAD's were very near to the main payloads It was found that the timing errors did not exceed ± 3 ms

4 Flight Characteristics

4 1 *Geophysical Conditions*

The launch of payload 27 045 (SCEX) took place on January 27 1982, at 03-52-20 850 UTC from the Churchill Research Range, Canada The geomagnetic activity at Churchill was not very pronounced before the launch, except for some positive disturbances in the X (north) component of the field in the local afternoon Shortly before the launch, the X component decreased slightly with a slope of 200 nT/h followed by substorm activity at approximately 04-30 UTC, 28 min after liftoff of the rocket

A thin, uniform cloud cover prevented detailed observations of the auroral displays An auroral arc formed or brightened at approximately 03-37 UTC near the launch gate from 35° to 56 elevation in southeast direction The arc extended from WNW to ESE and had an apparent width of $\approx 10°$ The photometer reading for the oxygen line at 557 7 nm was 4 8 kR, which can only be considered as a relative measure as the attenuation of the cloud cover is not known The arc brightened to 6 3 kR at launch and split into two bands in the aiming area, followed by a decline in intensity until 100 s after launch when the arc brightened again while forming a spiral of about 200-km diameter The auroral arc configuration was relatively stable during the flight with some variations in intensity The payload flew into the arc near its northern boundary and followed it nearly parallel in ESE direction for the first portion of the flight The arc was crossed near 250 s elapsed time At 300 s the southern boundary of the main arc was reached Although details could not be seen through the cloud cover, it appears as if some additional faint activity was located south of the main arc

4 2 *Trajectory and Attitude*

The SCEX payload was launched by a Nike/Black Brant V motor at an azimuth of 139° and reached a peak altitude of 240 6 km at 254 s elapsed time and a ground range of 154 km The release and switch on times of TAD 2 and TAD 4 were +118 440 and +135 310 s after launch, respectively The radial velocities of the TAD's have been determined with the help of potentiometer encoders to be $v_2' = (1\ 20 \pm 0\ 17)$ m/s and $v_4' = (1\ 49 \pm 0\ 18)$ m/s The total release velocities could then be calculated to amount to $v_2 = 1\ 87$ m/s and $v_4 = 1\ 93$ m/s, taking into account the tangential velocities at separation The attitude information on the main payload, which was measured by a gyro system, an earth sensor, and a magnetometer, allowed the determination of the ejection direction of the TAD's and thus the evaluation of the velocities perpen-

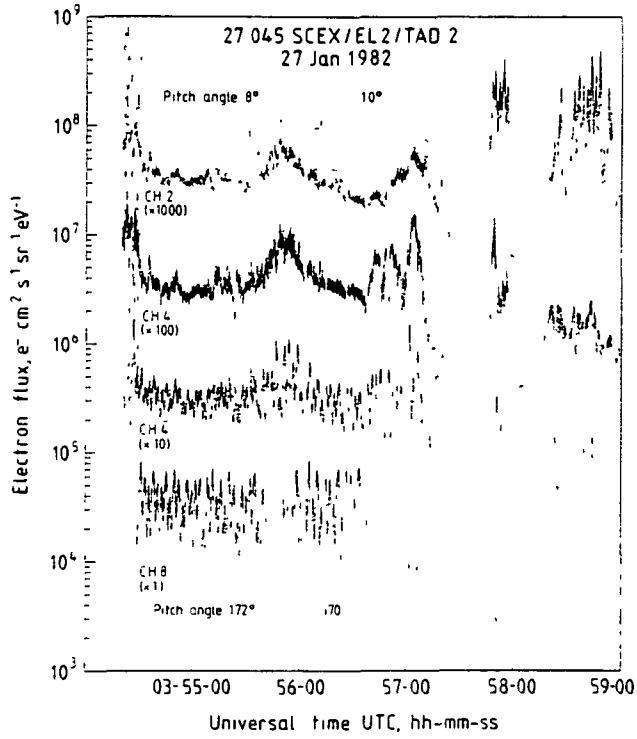

Fig 3 The auroral electron flux observed by the four fixed-energy channels on TAD 2 is plotted versus flight time The channels are displaced by factors of 10 as indicated The first 15 s of data in this figure are dominated by prompt responses to accelerator operations Echoes could, in particular, be observed in channel 2 around 03-56 UTC Pitch angle anisotropy combined with the tumbling motion of the TAD led to the modulation in the high-energy channels Some extreme values of detector viewing directions are given as pitch angles for the upper and lower traces Each data point was computed from the time required to sample 400 electron counts giving a uniform statistical error of $\pm 5\%$ irrespective of the flux level

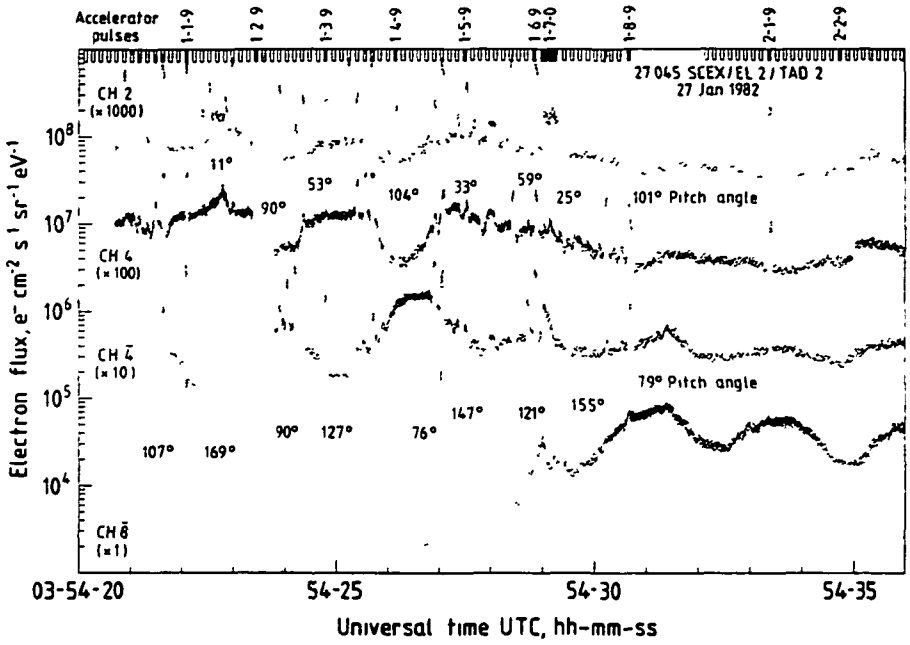

Fig 4 Electron flux data measured by four detectors on TAD 2 immediately after its release from the main payload at 03-54-19 290 The format is similar to that of Figure 3 with an enlarged time scale For comparison the times of the accelerator pulses have been added in the upper margin Only the 8-keV, 100-mA pulses have been labeled for reasons of legibility For details of the pulse program, see section 3 1 Prompt responses can be seen for the first 15 s after ejection The natural flux in the 8-keV channel and to a lesser degree in the 4-keV channel was strongly anisotropic before 54-29 The statistical error is ± 10%, resulting from a sampling scheme of 100 counts per data point

dicular to the magnetic field as 1 75 m/s for TAD 2 and 1 67 m/s for TAD 4 Confirmation of the release directions could be obtained by a flashlight system on the main payload and light detectors on the TAD's The payload trajectory and the TAD's ejection parameters are shown in Figure 1 together with a schematic indication of the regions of intense natural auroral electron precipitation Figure 2 shows a polar representation of the azimuthal configuration of the TAD's with respect to the main payload. Note that TAD 2 was released almost antiparallel to the horizontal payload velocity vector, whereas that of TAD 4 was aligned at a large angle Provided **E** × **B** drifts were small, TAD 2 would therefore transit the injection line of force at linearly increasing times after its release with respect to the beam injection payload Conversely, TAD 4 could only be located near the injection line of force for a short period of time after release, only a fortuitous combination of **E** × **B** magnitude and direction would allow interception at later times

The attitude knowledge of the main payload also permitted the determination of the injection pitch angle and azimuth of the beam electrons with respect to the magnetic field In line with the common definition of pitch angle, small values refer to downward firings in the northern hemisphere The attitudes of the TAD's with respect to the magnetic field are of importance in interpreting the observed electron fluxes in the framework of the earth's magnetic field This information was obtained by measuring the three magnetic field components and transmitting the information to the ground station every 0 76 ms

The various measurements were performed over a relatively large altitude range. For example, TAD 2 was released at an altitude of ≈157 km, prompt responses (with delay times of less than 50 ms) were observed over the injection altitude range 157–180 km, and fast echoes (with delay times of more than 50 ms) were first clearly identified at an injection altitude of ≈190 km According to the estimates of *Mishin and Ruzhin* [1980], ignition of the beam-plasma discharge (BPD) at the injection point would only occur at altitudes < 180 km unless the vehicle were surrounded by its own enhanced neutral density cloud arising from off-gassing and out-gassing processes On the other hand, although both the injected beam and ionospheric plasma densities were probably sufficient for occurrence of the strong interaction at the higher altitudes, the BPD would not be ignited It is not clear whether these altitude-dependent effects had significant impact on the experiment

5 Observations

5 1 *Auroral Electron Flux Measurements*

The study of the natural auroral electron flux was not an objective with high priority in the context of the fast electron echo experiment, and consequently, the instruments were not optimized for these observations The main limitation, in this respect, stems from the very restricted spectral resolution provided by three different fixed-energy bands Nevertheless, the measurements are of importance in characterizing the auroral conditions under which the artificial electron fluxes to be discussed below have been observed Figure 3 summarizes the data obtained from TAD 2 It was within an intense electron precipitation region when it was switched on after release TAD 2 left this precipitation region near 57-10 but encountered two more auroral structures between 57-44 and 57-57 and 58-16 and 59-12 Large flux increases, notably in channels 2 and 4 near 55-30, appear to be correlated with viewing directions near 180° with respect to the magnetic field and are, therefore, indicative for strongly field-aligned electron beams into the ionosphere with energies of at least 4 keV

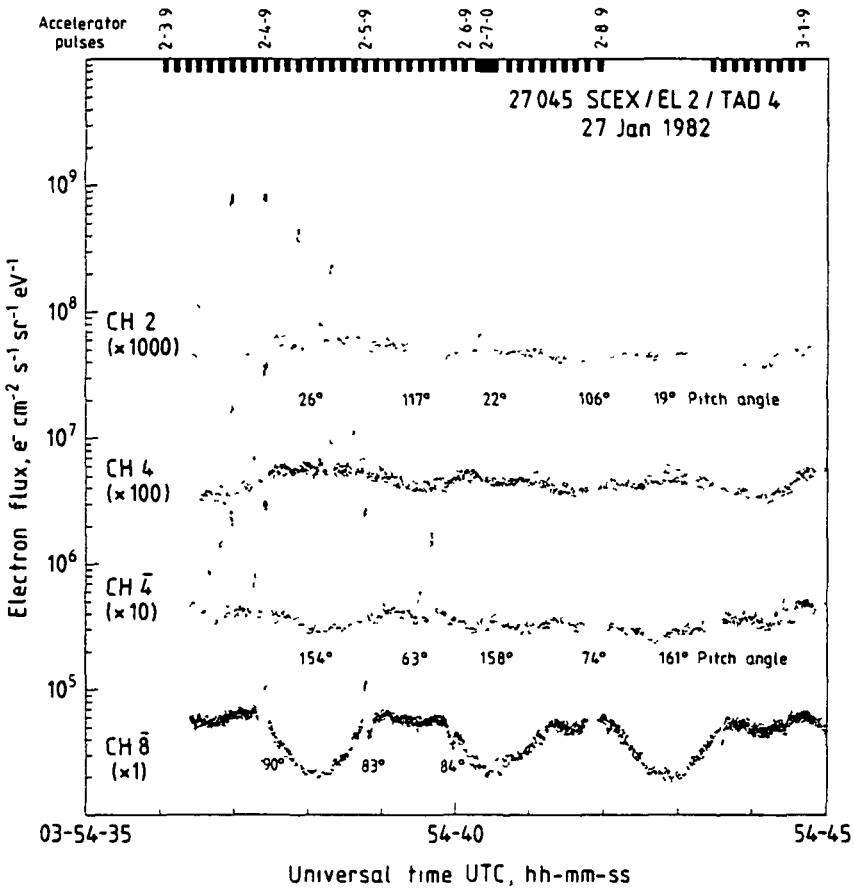

Fig 5 Same as Figure 4 for TAD 4 Compared to TAD 2 observations, prompt responses to accelerator pulses can only be seen for a short time interval after the release at 03-54-36 160 Note that channel 4̄ reacted longer than channel 2

5 2 *Artificial Electron Fluxes*

Prompt responses Both TAD's were released after switch-on of the electron accelerator and obtained data on the energetic electron flux distribution in the neighborhood of the main payload An overview of these measurements is given in Figure 4 for TAD 2 and in Figure 5 for TAD 4 It should be noted that all the observations on artificial electron fluxes to be discussed here have been obtained in the presence of a very intense natural background flux

Figure 4 depicts prompt responses superimposed on the natural electron flux in all four channels for about 15 s after release of TAD 2 Only every ninth pulse of a cycle has been labeled in the upper margin, although the full pulse program as detailed in section 3 1 was executed and indicated by tick marks Peak flux values in channel 2 for 100-mA emissions are remarkably stable at about 10^9 $e^- cm^{-2}s^{-1}sr^{-1}eV^{-1}$ during the first 10 s Thereafter they rapidly drop in intensity Besides most of the 10-mA operations, three 1-mA pulses also led to prompt responses near 03-54-20 8, 24 0 and 25 4 The last clear prompt response was observed near 54-35 6 with a delay time of ~40 ms in channel 2 followed by a response near 54-37 4 with a delay time of 74 ms The first signal showing a substantially different shape was observed in channel 2 at 54-44 350 with a duration at FWHM (full width at half maximum) of 90 ms and a delay with respect to a 4-kV 100-mA pulse of 180 ms

In marked contrast to the TAD 2 measurements, TAD 4 observations shown in Figure 5 exhibit prompt responses only for a short time period after release One 1-mA pulse triggered a response in channel 4 at 03-54-36 7 Note that three out of four signals received in both TAD's during 1-mA emissions could only be observed at the energy of the primary beam

Figure 6 shows a compilation of response times with respect to the corresponding accelerator pulse onsets Plotted were the times of the rising and falling edges at half maximum for all prompt signals observed There is a tendency of retardation with increased separation distance of TAD 2 This could be substantiated by calculating the regression lines for channel 2 It appears as if the signals had a FWHM of about 60 ms and were retarded according to the slope of the regression lines No trend could be observed on TAD 4 The large scatter of data points may partly be introduced by pitch angle and azimuth variations of the injection device which have not been taken into account

Delayed responses The identification of delayed signals was done by plotting all sensor channels on a time scale of 10 cm/s and marking spikes above the statistical error Enhancements resulting from natural field-aligned fluxes could easily be excluded by noting their pitch angle dependence and their symmetrical form with respect to the minimum pitch angle attained Proper identification of artificial electron enhancements has only been considered possible if the accelerator operation sequence could be seen in the TAD data In that case the signals were classified as "good" and included in Table 2 under the corresponding columns Other signals with characteristics similar to those described above but occurring in isolation have been grouped together under the heading "poor " In this class there are also a number of responses included that were distorted by short telemetry blackouts The

poor signals have been mentioned here to demonstrate the approximate total number of artificial electron flux enhancements They will, however, not be used in the following analysis, which will be based on the 95 "good" events originating from 100-mA operations The high number of 43 "good" echoes resulting from 10-mA emissions was biased and caused by the fact that even small precursors to 100-mA events could unambiguously be determined as response signal Yet it should be mentioned here that no systematic variation could be found in the delay times between 100- and 10-mA pulses No echoes from 1-mA emissions were detected

As an example, Figure 7 shows a series of delayed responses in channel 2 of TAD 2, some of which can also be seen in channels 4 and $\bar{4}$. In channel 2, nearly all 100-mA pulses of this series can be detected, some of them with small amplitudes at large pitch angles. The time delay can be determined unambiguously by evaluating the sequence of events for pulse 10-7-0, the modulation period The off-time following pulse 10-8-9 is reflected by the absence of any flux enhancements in that time interval, although channels 2 and 4 were looking at pitch angles between 20° and 40° The pulse assignment is indicated by oblique lines. In some cases, when signals in channels 2 and 4 occurred in response to the same accelerator pulse, vertical lines have been drawn in order to show that events in channel 4 led those in channel 2. Several enhancements recorded during this echo episode originated from 10-mA pulses, namely from 10-4-2, 10-4-5, 10-4-8, 10-5-2, and 10-5-5. At least one of them, corresponding to 10-4-8, can be seen in channel 4 as well. No delayed response is present in channel $\bar{8}$ in this figure, nor was there any response detected at all during the flight.

Even if the relationship of the observed electron flux enhancements with beam injections is beyond any doubt, it may be useful to consult simultaneous measurements taken on TAD 4 This is done in Figure 8 with the result that, with the exception of two events, no delayed responses can be detected It thus is established that the spatial extent of the electron flux enhancements under discussion is limited to dimensions comparable or smaller than the mutual separation distance of the TAD's This distance was approximately 300 m during this sequence of events Observations earlier in the flight would allow observations of a much smaller upper limit of the echo extension It should also be pointed out that the echoes were much wider than the 50 ms accelerator pulses An average width at half maximum of 180 ms was measured for the channel 2 echoes, 200 ms for the channel 4 echoes

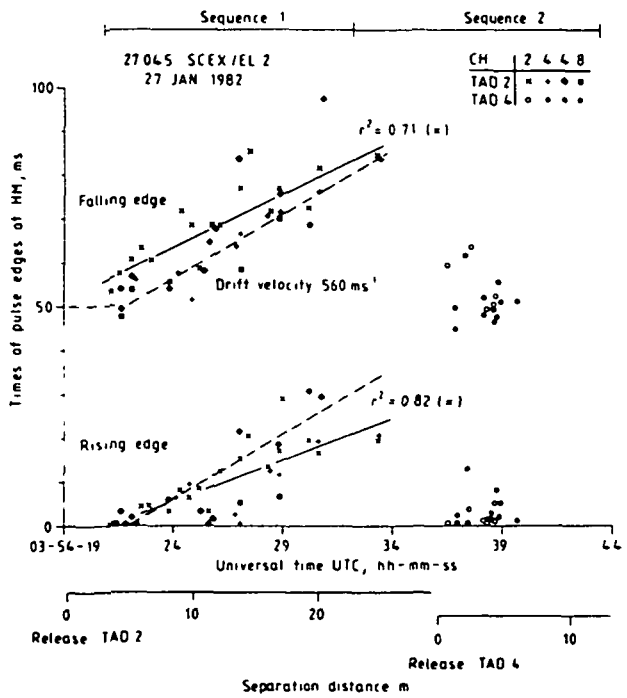

Fig 6 Occurrence times of rising and falling edges at half maximum (HM) of response pulses as function of universal time and/or separation distances The times are given in ms after beginning of corresponding accelerator pulse TAD 2 data exhibit a clear trend, as demonstrated by the linear regression lines and their correlation coefficients calculated for the channel 2. The dashed lines will be referred to in the text

TABLE 2 Number of Detected Delayed Responses

Accelerator Pulse Quality	100 mA		10 mA		1 mA	
	Good	Poor	Good	Poor	Good	Poor
TAD 2 Channel 2	61	30	30	3	–	
4	24	15	3	2	—	—
$\bar{4}$	2	7	1			
$\bar{8}$	—	—	—	—	—	—
TAD 4 Channel 2	6	22	5	–	—	—
4	2	13	4	–	—	—
$\bar{4}$	—	4	—		–	—
$\bar{8}$	—	—	—	—	–	—
TOTAL	95	91	43	5	—	—
GRAND TOTAL						234

An overview of the occurrence of echo responses to 100-mA pulses is given in Figure 9 The transit time is taken to be the delay between the middle of the accelerator pulse and the middle of the response signal at FWHM Pitch angle information has not been taken into account in this figure. It is, however, worthwhile mentioning that all echoes on TAD 2 were observed in the pitch angle range from 9° to 94° (accuracy ± 8°) It is important to note that the regression lines for each of the total 2- and 4-keV echo sets (upper solid line marked (×) and lower solid line marked (+), respectively) show (1) the delay time increases slowly with increasing flight time (separation distance), (2) the regression lines extrapolate to finite large delay times at the TAD release time, and (3) the measured delay times are consistently smaller for channel 4 (3 9 keV) than for channel 2 (1 9 keV) Surprisingly, however, the separate regression lines (dashed lines) for the 1 9-keV electrons in each of the echo groups show a much more rapid increase in delay time with increasing flight time and appear to extrapolate to nearly zero time delay at the TAD release time

The directions of the **E** × **B** drifts are shown in Figure 2, which shows instantaneous measurements of the thermal ion drift velocity direction for the entire period during which delayed echoes were detected The individual points are plotted at the radial distance equal to the accelerator-TAD separation distance at the time of the measurement Superimposed on the TAD 2 trajectory are the specific time intervals when echoes were detected Echoes are detected when the ion drift velocity direction is reasonably aligned with the vehicle and TAD 2 azimuths. Specifically, the absence of echoes between the two groups described earlier is well correlated with the gross change in ion drift direction at that time

Under adiabatic conditions the dependence of the transit time on the magnetic moments and thus the pitch angles of

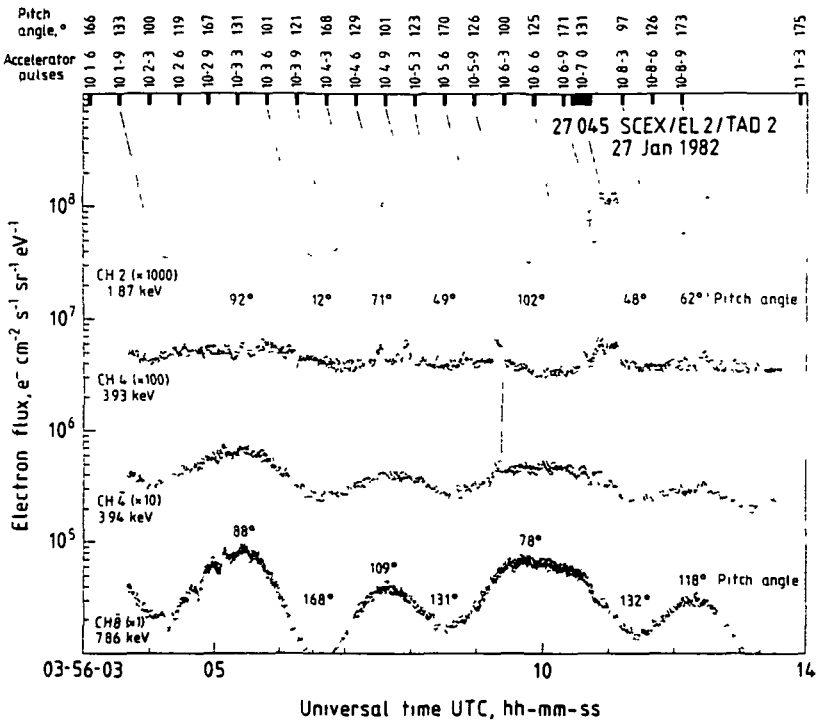

Fig 7 Time interval of TAD 2 observations with distinct responses to accelerator pulses with delay times of several hundred milliseconds Most of the flux enhancements can be seen in channel 2 only When concurrent responses occurred in channel 4, however, they were advanced with respect to channel 2 The accelerator sequence is shown in the upper part of the diagram together with the injection pitch angle Comparison shows that the prominent responses originate from 100-mA pulses Only a few 10-mA injections led to significant flux increases at the detector location and none of the 1-mA pulses Note that 2-keV responses can be attributed to 2, 4, and 8-keV pulses The long response pulse near 56-11 stemmed from a modulation period of the accelerator and allows an unambiguous determination of the delay time

the moving electrons should be a critical input for calculating the reflection height The transit times of intervals 1 and 2 for channel 2 and of channel 4 have, therefore, been plotted as functions of pitch angle in Figure 10 The regression lines and their small correlation coefficients reflect the large scatter of the data points It is, however, obvious that there was no strong dependence of the transit times on the pitch angle of the electrons The regression lines were then used as input functions for the conversion procedure described in section 6 3

5 3 *Summary of Flight Observations*

The following conclusions can be drawn from the energetic electron flux enhancements observed in response to electron beam injections into the ionosphere

The experiment was performed with a high natural auroral electron flux as background

Field-aligned natural electron fluxes could be identified at energies of 1 9 and 3 9 keV but not at 7 9 keV

Prompt echo signals could be observed in the neighborhood of the accelerator for up to 15 s and approximately 4 s after separation of TAD 2 and TAD 4, respectively

The prompt signals indicate a considerable energy spread and pitch angle diffusion

The energetic electron flux on the disturbed field lines appeared to have a surprisingly long lifetime

More than 200 delayed signals could be identified in channels 2 and 4 ($\bar{4}$) up to separation distances of 350 m perpendicular to the magnetic field direction in response to 10- and 100-mA current emissions

No delayed echoes could be found for 1-mA pulses

No delayed echoes were detected in channel $\bar{8}$ for any beam current

The delay times are typically 300 to 400 ms for 1 9-keV electrons and 50 ms less for 3 9-keV electrons

The pulse widths of the observed echo signals were approximately 130 ms wider than the source pulse

The pitch angle dependence of the echo transit time was not very strong

6 INTERPRETATIONS

6 1 *Analysis of Prompt Responses*

Although investigations of the beam injection processes were not the prime objective of the experiment discussed here, some of the observations appear to be of importance for the fast echo experiment and are thus pertinent to the following discussion

In the first place it should be noted that during all 100-mA, some of the 10-mA, and four of the 1-mA pulses studied in the neighborhood of the accelerator, large electron fluxes were detected in the energy channels less than or equal to the nominal beam energy Thus, 2-keV injection produced a response in channel 2, 4-keV injection produced responses in channels 2 and 4, and 8-keV injection produced responses in channels 2, 4, and 8 As noted earlier, energy spreading has been observed in the propagating beam in laboratory experiments and in the return fluxes in flight experiments Because of the absence of optical, wave, and plasma density data it was not possible to identify independently whether BPD ignition had occurred for these injections

An explanation for the retardation at half maximum may be

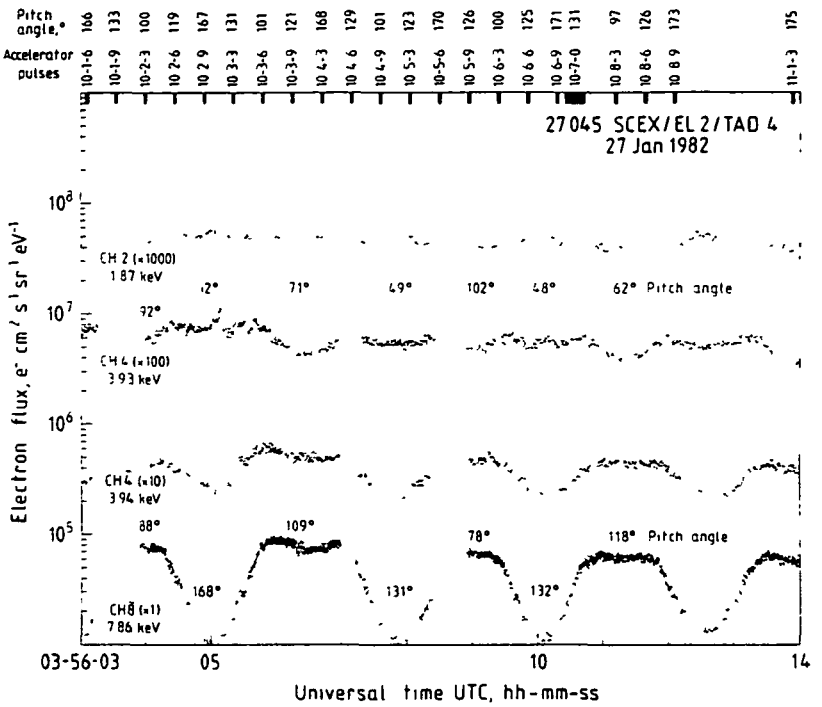

Fig 8 Same as Figure 7 for TAD 4, showing that only marginally significant responses occurred on this throwaway detector The data gaps in this and the previous figure result from telemetry losses during the tumbling motion of the TAD's The number of electron counts sampled was 100 providing a statistical error of ±10%

found by analyzing the flight configuration of the main payload with respect to TAD's 2 and 4 near the times of release The rocket system crossed magnetic field lines at a speed of approximately $v_\perp$ = 560 m/s at this time and was flying in an azimuth of 139° TAD 2 was ejected at an azimuth of 303°, only 16 off the direction opposite to the flight azimuth It was therefore nearly trailing the main payload TAD 2 should consequently encounter retarded echo phenomena that are fixed on a particular field line This requires no or small electric fields perpendicular to the magnetic field, an assumption which can be justified by observations made in similar auroral arcs [cf *de la Beaujardiere and Vondrak*, 1982] and is supported by the ion drift measurements on this flight for most of the time The retardation would be determined by the ratio of the separation distance normal to the magnetic field and $v_\perp$ This interpretation can be seen to conform with the observations by a comparison of the regression lines with the dashed lines of Figure 6 which reflect the ratio mentioned above together with a prompt response within the first 5-m separation For the rising edge the agreement is almost perfect. In evaluating the situation for the falling edge one has to take into account that the injection process was indeed instantaneous (on the time scale considered here) over a full gyrodiameter and cannot be approximated by a point source TAD 2 trailing the main payload thus had to travel a distance of 50 ms × 560 m/s + 5 m = 33 m in the disturbed region This requires 59 ms at a speed of 560 m/s in striking accord with the observations

It should also be noted that immediate reactions to accelerator pulses were detected up to about 23-m separation This can be seen for instance, in Figure 11, where first indications of flux increases can be noticed almost simultaneously with the beam onset times, even though the high natural background flux might conceal the true start time This is in qualitative agreement with the halo observations reported by *Maehlum et al* [1980] and *Duprat et al* [1983]

The explanation presented for the prompt responses observed on TAD 2 must, of course, also provide an interpretation of the TAD 4 situation, where prompt signals could only be detected up to separation distances of 6 m The decisive parameter in creating the different behavior is the different ejection azimuth of 82°, which is about 60° away from the flight direction The core of the disturbed region thus has a cross-section normal to the magnetic field direction of typically 33 m in length and presumably approximately 12 m in width (a more detailed study of the disturbed region near the payload is in preparation) This is comparable to the region accessible to the primary beam particles during a 50-ms pulse

Another question concerns the temporal development of the perturbed beam In principle two ways of discussing this problem are available The first describes the development of the perturbed region as seen from an earth-fixed system As the beam injections lasted 50 ms, their state of development depends on the location relative to the main payload The second description is given in a system traveling with TAD 2 For each accelerator pulse the observing platform has a nearly constant separation from the main payload and encounters the plasma disturbance at a certain phase The second scheme is obviously closely related to the method of observation in the SCEX experiment and was therefore adopted in presenting the data in Figure 12 Representations of four intense 100-mA, 8-kV pulse responses have been plotted as flux levels above background over a plane defined by separation distance and relative time The most prominent feature in this diagram is the plateau reaching out to separation distances of 15 m The slopes of the responses show a definite tendency of flattening with increased separation distance Since an enhanced flux of

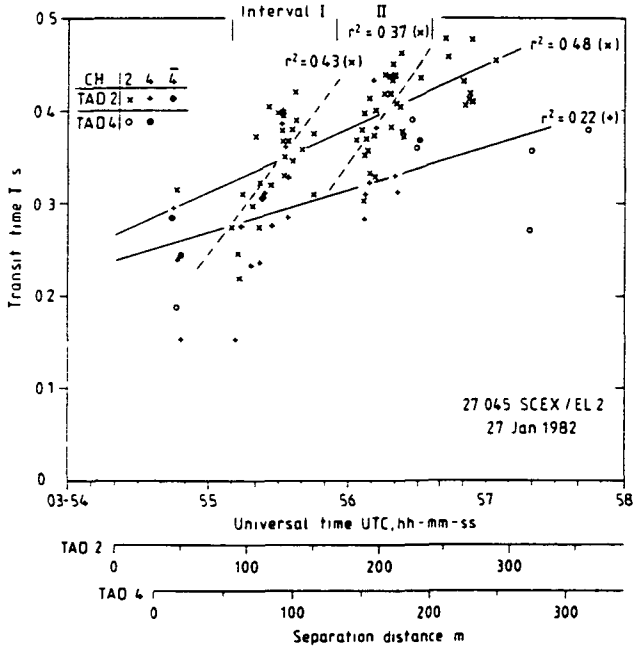

Fig 9 Transit times of echoes originating from 100-mA accelerator operations over flight time Regression lines for channel 2 (×) and channel 4 (+) observations are given In intervals 1 and 2, echoes appear to be lumped together, and separate regression lines have also been calculated for TAD 2 channel 2 data in these intervals

energetic electrons could be observed by TAD 2 trailing the accelerator by up to 32 m, a minimum lifetime of 57 ms for the disturbed region after cessation of injection has to be assumed These results are in substantial agreement with the findings of *Jacobsen* [1982] for low-energy (< 5 eV) suprathermal electrons The phenomelogical description of the prompt echo observations given so far obviously has to be complemented by a physical explanation of how the high-energy electrons could be seen near the TAD for such a comparatively long time With a collision frequency of approximately 10^3 s^{-1} for 2-keV electrons with neutrals at 200-km altitude, both axial and radial confinement for more than 50 ms appears difficult to accomplish The persistence of the energetic electrons thus seems to imply the presence of a continuous generation mechanism The only source for this production seems to be the heated electron beam propagating away from the injection region

6 2 *Analysis of the Delayed Echo Results*

Three features of the experimental results appear to be inconsistent with the modified $E \| B$ concept described in sections 2 1 and 2 2, i e, that the beam electrons are diffused in velocity near the injection point, then travel without significant further perturbation to a reflection point at a height of several thousand kilometers and return These are (1) echo durations approximately 130 ms longer than the injected pulse duration, (2) a consistent increase of delay times with increasing separation distance, for each observed energy, and for each set of echoes (Figure 9), (3) the presence of prompt responses, which persisted for at least 50 ms after the accelerator had been turned off In addition, the delayed echoes were observed over a time period of > 2 min This seems excessively long given the highly selective nature of the echo detection configuration

Some of the aspects related to the injection and detection processes are sketched in Figure 13 The upper part summarizes in a somewhat simplified manner the configuration of the injection process. The diagram can best be understood by considering the position of the perturbed beam resulting from an accelerator operation in an earth-fixed system represented by the abscissa as distance perpendicular to magnetic field and the ordinate as injection time Both of them are referred to time T_0 as the middle of the accelerator operation The approximate effect of the finite gyrodiameter is indicated by the asymmetry It represents an instantaneous injection (on the time scale considered here) within one gyrodiameter The finite lifetime of the energetic electron population of at least 50 ms is represented by the vertical extension of the perturbed region This region is shown as hatched area for a lifetime of 50 ms As this value was only established as a lower limit, a longer lifetime could not be excluded In such a case the dotted regime would also belong to the perturbed environment The velocity of the payload system $v_\perp$ = 620 m/s perpendicular to the magnetic field at this time was used in converting the distance coordinate into a relative flight time. The paths of TAD's at four different separation distances are shown as well A TAD in position d of the upper panel should in principle provide the information to settle the question of the maximum lifetime of the disturbance There is, however, the possibility (and indeed some evidence) that TAD 2 was not exactly trailing the main payload and was thus drifting out of the perturbed region perpendicularly The perturbed beam will move upward along the field lines Under favorable conditions it will be reflected, and electrons with certain energy and pitch angle will cross the interception plane of the TAD's after some time $T_0^* - T_0$ This situation is shown in the lower panel of the figure

All coordinates defined in analogy to the injection process are now referenced to T_0^* The characteristics of the detector

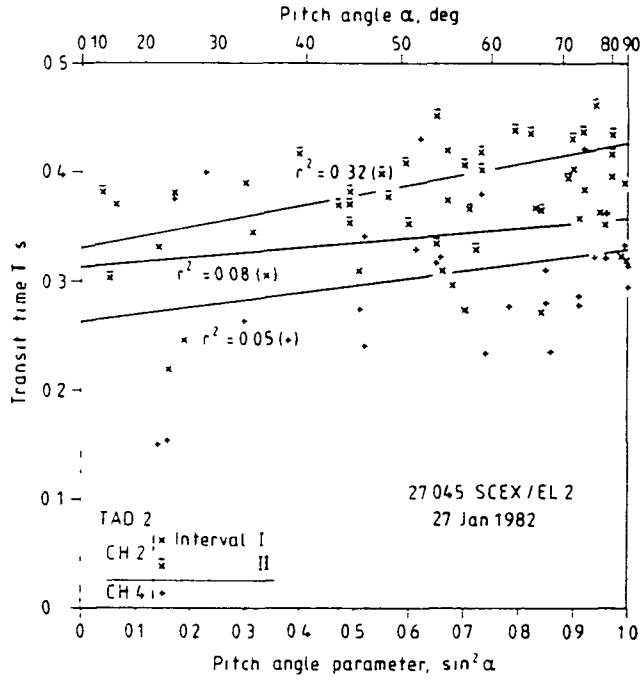

Fig 10 Pitch angle dependence of transit times plotted for three groups of echo data points together with the corresponding linear regression lines and correlation coefficients Intervals 1 and 2 refer to the two bunches of echoes identified in Figure 9

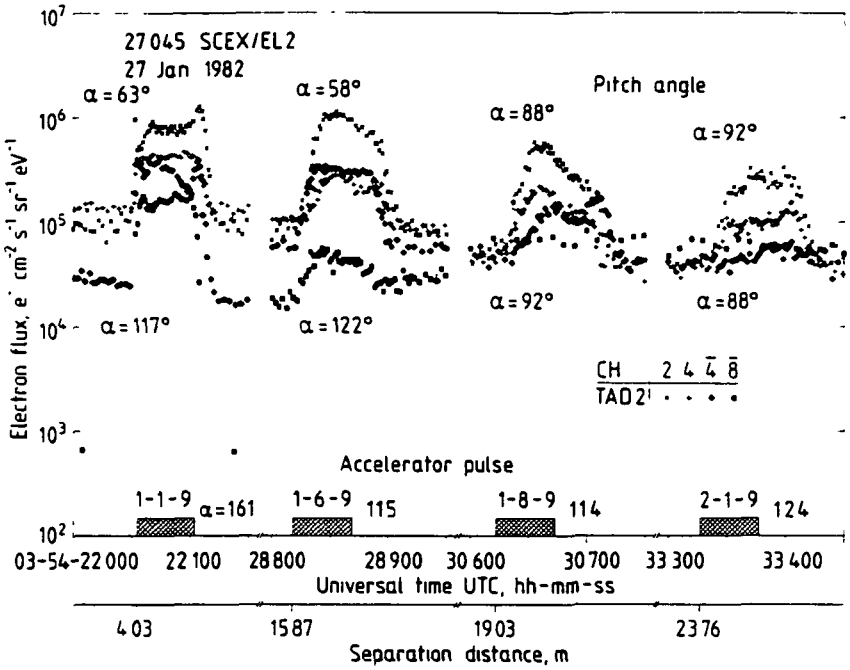

Fig 11 Detailed response functions of TAD 2 detectors to 8-keV, 100-mA electron pulses at various separation distances from the accelerator transverse to the magnetic field In order to achieve a high time resolution in this and the following figures the number of counts sampled has been reduced to 40, resulting in a statistical error of ±16% Also indicated are the pitch angles under which the observations were performed Important observations resulting from this diagram are the increased delay of the response pulse plateaus with respect to the accelerator pulse and the flattened slopes of the leading and falling edges with increasing separation distances. There is also a tendency of diminishing flux levels at longer range Note the different flux levels of channels 4 and $\bar{4}$ near 90° pitch angle for pulse 2-1-9

devices determine certain energy and pitch angle ranges in which the signal was observed Under adiabatic conditions the energy band effect would contribute ±15 ms and the detector pitch angle range about ±5 ms to the relative injection time The contributions have been schematically indicated by a downward extension of the direct echo regime by 20 ms in the relative injection time scale The influence of the changing pitch angle on the delay time during the tumbling motion of the TAD's is strongly model dependent and could therefore not be considered here So far we have discussed the adiabatic reflection model Should the lifetime of the disturbance be very long, the leading edge in the lower panel might not be existing at all or not be detectable (referred to by the question mark) Again four sample paths of TAD's have been included in the lower panel Path a intersects the point T_0* and therefore should be in the best position for observing this particular accelerator pulse The echo signal pulse width would be determined by the cross section of the TAD paths with the echo regime measured in relative flight time As we noted above, the average width was 180 ms, a value that was used to draw the vertical dashed lines in the lower panel

From Figure 13 it is evident that a linear increase in delay time for each group of echoes results from increased separation distances with flight time At large separation distances the **E** × **B** velocity must be very small or aligned parallel or antiparallel to the directed velocity for interception as shown in Figure 2 A slowly varying **E** × **B** velocity magnitude could produce the different slopes observed for the regression lines of the two echo groups This implies that, although the detector only selects particles distributed over a small range in energy and pitch angle, the spread in transit times is very large so that the field line is populated by echo electrons for long times Again referring to Figure 13, the long echo pulse duration requires not only the long time duration of the echo flux but also significant spatial expansion of the echo footprint traversed by the TAD Thus the pulse duration is determined by the transit time of the TAD across the footprint (at detection altitude). Pitch angle diffusion of the propagating electrons could account for the required spread in transit times, and the accompanying radial diffusion would produce the increase in footprint dimensions

Therefore it seems possible to explain the experimental results with two grossly different models First, we may assume that the original concept of hot beam injection, stable (adiabatic) propagation, reflection by the $E \| B$ potential drop and final detection of a selected component of the echo beam remains valid Conversely, we may extrapolate the indicated nonadiabatic behavior to the extreme conditions where the propagating beam remains unstable over large distances after leaving the strong interaction region at the injection point The continuous in-flight instability (kinetic phase) produces a continuous backscatter flux together with radial diffusion of the propagating beam until the beam density relative to the ambient density is reduced to the stable value a schematic representation of the inflight beam configuration is shown in Figure 14 The consequences for the diagram in Figure 13 would be that there should be no leading edge in the lower panel as the energetic electron flux would be present until the beam configuration became stable In a sense the phase simply represents a continuation of the strong interaction at injection but with modified growth rates and features Thus the detected echo flux is not produced by reflection at a potential drop but is observed when the TAD enters the wake of the injected unstable beam, that is, "apparent" pulses are produced here by a spatial rather than temporal effect The column of returning energetic electrons will, of course, undergo the **E** × **B** drifts

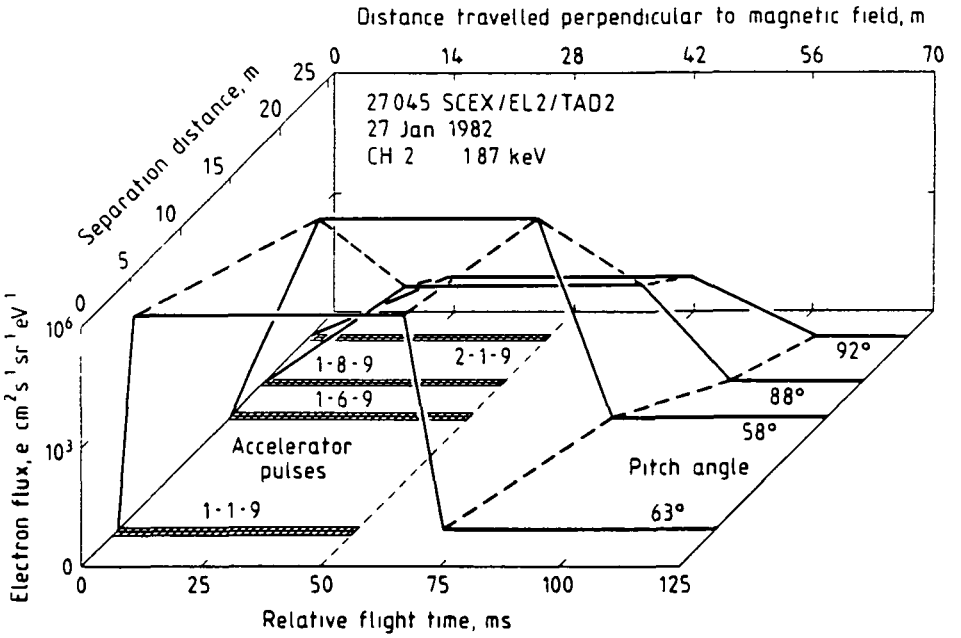

Fig 12 Schematic presentation of prompt response characteristics at maximal levels observed for 8-keV, 100-mA pulses by channel 2 on TAD 2 Electron flux levels above background are shown on a linear scale as a function of relative flight time starting at the beginning of the corresponding accelerator pulse The separation distances transverse to the magnetic field between the TAD and the main payload are given on the left scale

Because the observations are insufficient to produce any clear-cut distinction between the two models, we believe it worthwhile to discuss the conclusions of each model further

The main deficiency in the observations lies in the area of energy resolution both concerning the near payload environment and the delayed response regime Any future investigations should aim at improving this aspect Also of great importance would be a detailed study of the exact dimensions and temporal developments of the perturbed region This is particularly true for the forward direction of the beam emission This appears to be a difficult task and probably would require a multiple payload concept with sophisticated release arrangements Confirmation of the continuous backscatter model could also be obtained by selecting launch criteria which definitely rule out $\mathbf{E} \times \mathbf{B}$ conditions to be prevailing A negative result would, however, still give ambiguous information as delayed echoes could have been missed for geometrical reasons, although they were present at other locations

6 3 $E \| B$ Model

Based on the $E \| B$ model, two independent and complementary methods of analyzing the data will be introduced The first method utilizes equations (2), (3), and (4) to calculate expected transit times for model distributions of the parallel electric field By comparing the calculated functions with observed transit times and executing suitable iterations it should be possible to match the calculated transit time functions to the observed ones For the purpose of these calculations the geomagnetic field was assumed to follow the relation

$$B(s) = B_0 R_E^3 (R_E + s)^{-3} \tag{5}$$

with R_E the earth's radius and $B_0 = B(0)$ the magnetic field on the surface of earth

The question whether the results thus obtained are unambiguous or whether the same transit time function could be modeled by more than one electric field distribution is beyond the scope of this study

The second method relies on evaluating equation (4) Solutions can be obtained both for $T = T(W)$, μ = constant and $T = T(\mu)$, W = constant under very general assumptions by solving an integral equation of Abel's type [*Wilhelm*, 1977, 1982] Solving $T = T(\mu)$, W = constant is more adapted to space experimentation as electron injection and detection with constant particle energy and variable magnetic moment is much easier to achieve than vice versa The main problem with this concept is that the function $T = T(\mu)$ for W = constant has to be measured in a wide range before the integral equation can be solved The range required is wider than is achievable from a fixed altitude because of the limitation in injecting electrons with

$$\mu > \frac{W(s_0)}{B(s_0)} \tag{6}$$

It could, however be demonstrated that the electric field profiles calculated for the reflection region do not critically depend on the exact function $T(\mu)$ in the missing inteval of μ A suitable extrapolation will thus not introduce substantial errors

In order to generate a realistic extrapolation beyond the range of observation, model calculations were performed as a first step The model electric field was constructed of two contributions (1) a constant field above 2000 km and (2) a field with Gaussian distribution with maximum at s and a width specified by σ By adjusting these parameters and computing several iterations, a reasonable fit could be obtained for small pitch angles At larger pitch angles however, there remained a substantial discrepancy, indicating that a more sophisticated model field would be required As these electrons mirror at low altitudes, a modification toward smaller field strength would be needed there

We will not attempt to improve on the model assumptions

but rather perform the conversion of the transit time function as a next step The results of the model calculations will be utilized in this conversion procedure insofar as the required extrapolation is based on the model fields The calculations were carried out for the three transit time functions in Figure 10 and resulted in parallel electric field structures shown in Figure 15 together with the model assumptions It can be seen that the electric field is characterized by a steep increase at about 3000-km altitude The agreement between the three computations is quite acceptable Fields derived from interval 2 data occur at higher altitudes, as would be expected from the increase of the transit times with flight time The model fields shown by dashed curves fit the calculated fields very well at high altitudes, while a more complicated structure is present at lower heights

The conversion field for 3 9-keV electrons ends near 3500 km at a field strength of about 2.7 mV/m. The reason clearly is that electrons of this energy and 180° injection pitch angle will mirror at that point under the prevailing conditions. Information on fields at greater altitudes would require observations at higher electron energies A careful search for any echo signature in channel 8 was performed without conclusive result It should, however, be mentioned that the tumbling motion of the TAD's caused an uneven coverage of pitch angles in the sense that the 8-keV channels viewed into the downward direction more often than upward The profiles, therefore, cannot be extended to greater altitudes with the observations available The poor altitude resolution of the profiles does not allow us to draw any definite conclusions on the fine structure of the parallel electric field at this stage

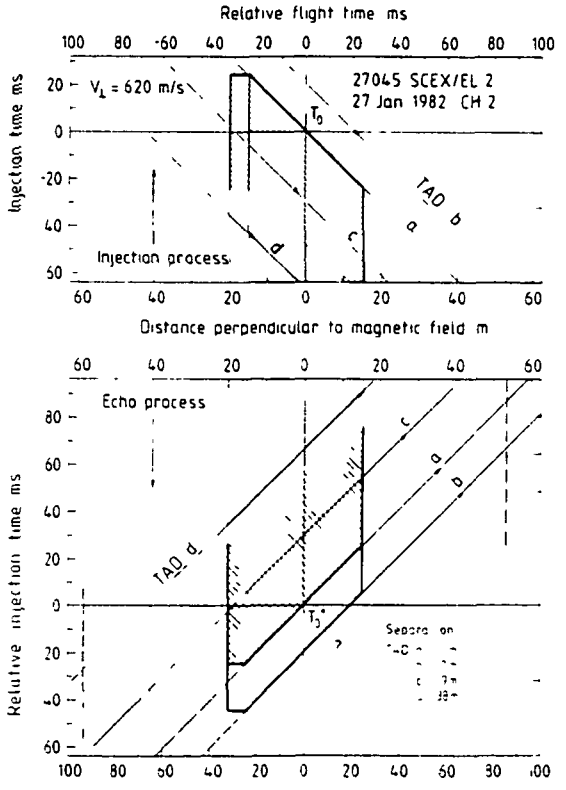

Fig 13 Schematic presentation of the injection and detection characteristics In the upper panel the disturbed region near the accelerator is shown for $E_\perp = 0$ In the lower panel the corresponding echo has been given after a time delay of $T_0^* - T_0$ Magnetic field lines are vertical lines in this figure The trajectories of TAD's at various separation distances transverse to the magnetic field are also plotted in order to demonstrate their intersections with the disturbed region and the locus of the echoes For more details, refer to the text The important question is whether the leading edge in the lower panel exists or whether the flux tube is permanently filled with energetic electrons for a long time after the injection process

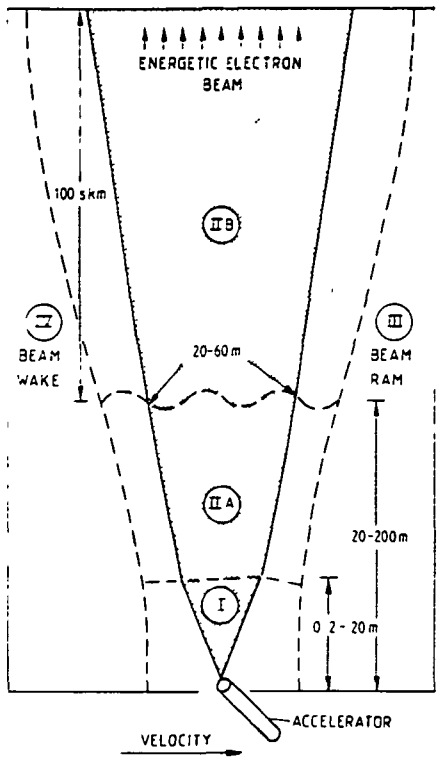

Fig 14 Beam-plasma interaction phases in the neighborhood of an electron accelerator In the near-accelerator region 1, beam expansion, neutralization, and sheath potential come into play, in region 2*a*, strong interaction with energy spread and plasma turbulence is of importance, while region 2*b*, the kinetic regime, is characterized by its long extension and the production of low-energy electrons (after K Papadopoulos, private communication, 1983)

6 4 *Continuous Backscatter Model*

The continuous backscatter model has two requirements (1) the beam-plasma system must retain its linearly unstable features over the flight path, and (2) the total time integrated backward directed energy flux cannot exceed the total injected energy As a consequence of the strong local interaction produced by the monoenergetic injected beam the beam is strongly heated and the instability is transformed into the smaller growth rate kinetic instability However it seems unlikely that the hot beam will ever be driven totally to a stable plateau velocity distribution [*Papadopoulos*, 1975, K Papadopoulos, private communication, 1983) Furthermore, time-of-flight velocity dispersion effects will always tend to regenerate the linearly unstable velocity distribution at the forward edge of the beam

A crude estimate of the total number of echo electrons is 7.5×10^{16} electrons, assuming (1) 0 5-s time delay, (2) the echo flux is uniformly distributed over the 50-m-radius footprint and (3) a flat energy spectrum extending to 8 keV Although this is larger than the total number injected (100 mA for 50 ms = 3.13×10^{16} electrons), the very crude assumptions do not totally invalidate a reasonable particle balance In addi-

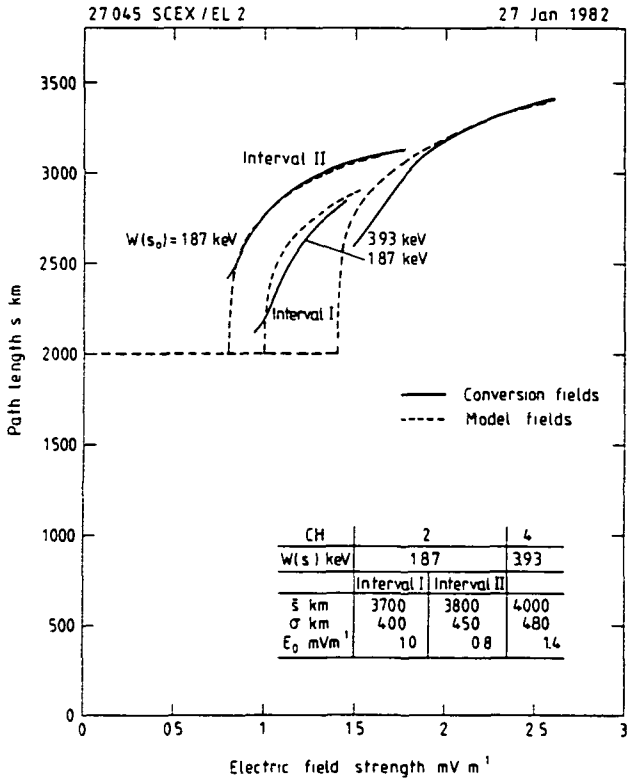

Fig 15 Parallel electric field profiles deduced from the transit time measurements taken during intervals 1 and 2 of channel 2 and over the whole observation time for channel 4 The profiles are shown together with model fields (indicated by dashed lines) constructed in such a way as to match the calculated transit time functions to the observations (see section 2 2) The resulting model assumptions are given in the insert No error bars are given but the large scatter in the input data presented in Figure 13 shows that the resolution of the profiles is rather poor

tion, it is of course impossible to distinguish whether the detected echoes are produced by backscattered degraded primary (injected) electrons or by newly accelerated (by wave-particle interactions) ambient electrons (suprathermal electrons)

The measured shorter delay times of the 4-keV echoes are difficult to explain with this model Because of the criterion used in defining the delay time (the delay between the midpoint of the injection pulse and the midpoint of the echo pulse at FWHM) a simple energy-dependent footprint radius cannot explain the observation A spatial displacement of the 4-keV echo pattern relative to the 2-keV footprint is required for which no explanation can be offered in this model Should this model represent the correct interpretation of the observations, the echo characteristics provide a simple remote diagnostic for distant beam-plasma interactions

Acknowledgments The design construction and testing of this payload was carried out by personnel from the Goddard Space Flight Center and General Electric Matsco Major contributions were made by C Campbell J Stephenson and J Hanamian S J Monson of the University of Minnesota was responsible for coordination and integration of the various instruments The contributions of C Becker R Schmidt E Frank and H Lindner to the success of the MPAE experiment are greatly appreciated Many stimulating discussions with C K Goertz took place during the evaluation phase The project was financially supported by NASA NRC and the German Bundesministerium fur Forschung und Technologie through DFVLR-PT under grant 0 0M 030-ZA/WF WRK 275 3-1 2 W Bernstein was supported by the NASA grant NAGW-69

The Editor thanks B N Maehlum and R L Arnoldy for their assistance in evaluating this paper

REFERENCES

Arnoldy, R L, and J R Winckler The hot plasma environment and floating potentials of an electron-beam-emitting rocket in the ionosphere, *J Geophys Res 86* 575, 1981

Bernstein, W et al, Electron beam experiments The beam plasma discharge at low pressures and magnetic field strengths, *Geophys Res Lett*, *5*, 127 1978

Bernstein, W, H Leinbach P J Kellogg, S J Monson, and T Hallinan, Further laboratory measurements of the beam plasma discharge, *J Geophys Res*, *84* 7271, 1979

de la Beaujardiere, O, and R Vondrak, Chatanika radar observations of the electrostatic potential distributions of an auroral arc *J Geophys Res*, *87*, 797, 1982

Duprat, G R J, A G McNamara, and B A Whalen, Charged particle measurements from a rocket-borne electron accelerator experiment, in *Artificial Particle Beams in Space Plasma Studies 79* edited by B Grandal, p 65, Plenum, New York, 1982

Duprat, G R J, B A Whalen, A G McNamara, and W Bernstein Measurements of the stability of energetic electron beams in the ionosphere, *J Geophys Res*, *88*, 3095, 1983

Grandal, B, Highlights of the observations in the Polar 5 electron accelerator rocket experiment, in *Artificial Particle Beams in Space Plasma Studies 79*, edited by B Grandal, p 159, Plenum, New York, 1982

Haerendel, G, E Rieger, A Valenzuela, H Foppl, H C Stenbaek-Nielsen, and E M Wescott, First observation of electrostatic acceleration of Barium ions into the magnetosphere, *Proceedings of the Symposium on European Programmes on Sounding-Rocket and Balloon Research in the Auroral Zone, Rep ESA SP-115*, p 203 Eur Space Agency, Paris, 1976

Jacobsen, T A, Observations of plasma heating effects in the ionosphere by a rocket borne electron accelerator, in *Artificial Particle Beams in Space Plasma Studies 79* edited by B Grandal, p 175 Plenum, New York, 1982

Jost, R J, H R Anderson, and J O McGarrity, Electron energy distributions measured during electron beam/plasma interactions, *Geophys Res Lett*, *7*, 509, 1980

Maehlum, B N, B Grandal, T A Jacobsen, and J Troim, Polar-5 An electron accelerator experiment within an aurora, 2, Scattering of an artificially produced electron beam in the atmosphere *Planet Space Sci*, *28*, 279 1980

Mishin, E V, and Yu Ya Ruzhin, The model of the beam plasma discharge in the rocket environment during an electron beam injection in the ionosphere, *Ann Geophys*, *36*, 423 1980

Papadopoulos K Non-linear stabilisation of beam-plasma interaction by parametric effects *Phys Fluids 18*, 1769 1975

Szuszczewicz E P K Papadopoulos W Bernstein, C S Lin and D N Walker Threshold criterion for a space simulation beam-plasma discharge, *J Geophys Res*, *87* 1565 1982

Wilhelm K Remote sensing experiment for magnetospheric electric fields parallel to the magnetic field *J Geophys 43* 731 1977

Wilhelm K W Bernstein and B A Whalen Study of electric fields parallel to the magnetic lines of force using artificially injected energetic electrons *Geophys Res Lett 7*, 117 1980

Wilhelm K On the use of artificially injected energetic electrons as indicators of magnetospheric electric fields parallel to the magnetic lines of force, in *Artificial Particle Beams in Space Plasma Studies 79* edited by B Grandal p 75 Plenum New York 1982

Winckler J R R L Arnoldy, and R A Hendrickson Echo II A study of electron beams injected into the high-latitude ionosphere from a large sounding rocket, *J Geophys Res 80* 2083 1975

Winckler J R The application of artificial electron beams to magnetospheric research, *Rev Geophys Space Phys*, *18* 575 1980

W Bernstein Department of Space Physics and Astronomy Wiess School of Natural Sciences Rice University Houston TX 77001

P J Kellogg, School of Physics and Astronomy University of Minnesota Minneapolis MN 55455

B A Whalen, Herzberg Institute of Astrophysics National Research Council of Canada, Ottawa Ontario Canada

K Wilhelm Max-Planck-Institut fur Aeronomie D-3411 Katlenburg-Lindau, Federal Republic of Germany

(Received May 9, 1984
revised July 9 1984
accepted July 23, 1984)

GEOPHYSICAL RESEARCH LETTERS, VOL. 11, NO. 12, PAGES 1176-1179, DECEMBER 1984

ACCELERATION OF ELECTRONS IN STRONG BEAM-PLASMA INTERACTIONS

Klaus Wilhelm

Max-Planck-Institut für Aeronomie

William Bernstein

Department of Space Physics and Astronomy, Wiess School of Natural Sciences, Rice University

Paul J. Kellogg

School of Physics and Astronomy, University of Minnesota

Brian A. Whalen

National Research Council Canada, Herzberg Institute of Astrophysics

Abstract. The sounding rocket payload SCEX (Several Compatible EXperiments to utilize an electron accelerator; NASA flight 27.045) launched on January 27, 1982 from the Churchill Research Range provided an opportunity to observe the effects of strong beam-plasma interactions on the electron population in a region of space remote from the main payload carrying the accelerator. We present observations demonstrating that electron energies of up to four times the injection energy occurred during accelerator operations in high-current mode. Detailed instrumental performance characteristics in flight and in the laboratory will be discussed. The acceleration events occurred at reception pitch angles between 54° and 126°. Long confinement times seem to be a necessary condition for generating the energetic electrons. It is proposed that they result from the length of the interaction region.

Introduction

The SCEX rocket flight, described in detail by Wilhelm et al. [in press, 1984], allowed the study of the prompt (during electron beam injection) and delayed electron fluxes returning to the injection altitude (echoes). The prompt echoes could be explained by the occurrence of a strong beam-plasma interaction near the injection point. However the experimental data were insufficient to distinguish whether the delayed echoes resulted from (1) the reflection of the modified beam by a field-aligned potential drop located at high altitude or (2) the continuous generation of the return flux by an unstable beam-plasma configuration extending over distances as long as 3000 km. Clear evidence for the gross degradation of the initially monoenergetic electron beam with energy E_b was obtained because echoes at much lower energies E than E_b were produced (8-keV injected beams produced prompt echoes at 1.9, 3.9, and 7.9 keV). The above analysis of prompt and delayed echoes was limited to energies $E \leq E_b$.

In this letter, we wish to describe some infrequent observations not discussed in the earlier paper: the detection of returning fluxes (echoes) with energy up to 4 times greater than E_b (i.e., injection of a 2-keV beam produced a response at 7.9 keV). It should be emphasized that although several hundred prompt and delayed echoes with $E \leq E_b$ were detected, only a few cases of such superenergization were observed.

Paper number 4L6358.
0094-8276/84/004L-6358$03.00

Experimental Configuration and Observations

The electron detectors (1.9-, 3.9-, and 7.9-keV fixed-energy, curved-plate electrostatic analysers) were carried by two subsidiary payload sections (ThrowAway Detectors, TAD's); these were released from the main payload at altitudes of 157 and 178 km, respectively. A stepped electron energy analyser was included on the main payload section which also carried the electron accelerator. The payload was launched over an auroral arc and encountered intense natural auroral electron fluxes. A summary diagram of the geometry of the main payload and the TAD's is shown in Figure 1 together with a schematic representation of the interval in which prompt responses ($E \leq E_b$) to accelerator operations were observed on TAD 2 or TAD 4. The dots indicate locations where echoes with $E >> E_b$ were detected. Perpendicular to the magnetic field, the acceleration thus appears to be observable only near the injection point in the region of strong beam-plasma interactions (one exception will be discussed later).

Examples with enhancements in channels set at twice the injection energy are shown in Figures 2 and 3. The TAD 2 observations resulted from a 4 keV, 100 mA accelerator pulse, while the TAD 4 event was recorded in response to a 2 keV, 100 mA beam injection. The 7.9-keV channel response to a 2 keV, 100 mA pulse is shown in the lower trace of Figure 4. Channels 2 and 4 looked in opposite directions as $\bar{4}$ and $\bar{8}$. The pitch angle α_D refers to channels 2 and 4. Channels $\bar{4}$ and $\bar{8}$ thus measured at $180°-\alpha_D$. Each data point in the diagrams represents 40 electron counts resulting in a statistical fluctuation of ± 16 %. All of these increases are therefore statistically significant. Similar enhancements at $E >> E_b$ were not observed with the stepped analyser carried on the main payload. It showed, instead, a sharp cut-off of the return electron spectrum at $E \simeq E_b$. However, this instrument had a significantly smaller geometric factor so that it would not respond to the $E >> E_b$ fluxes indicated in Figures 2 to 4.

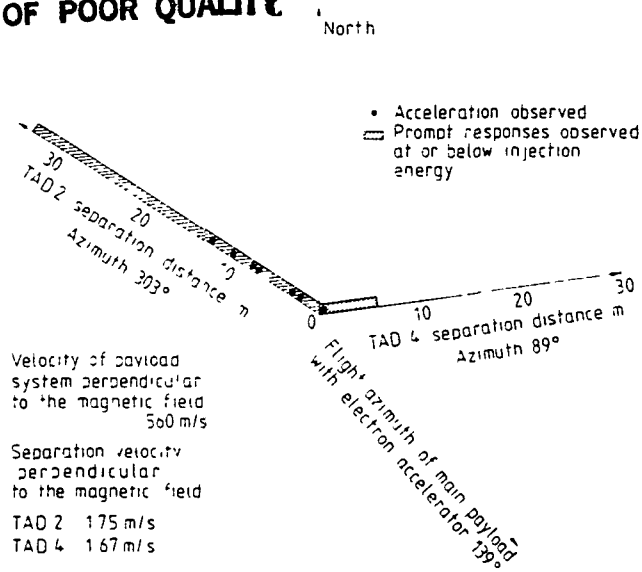

Fig. 1. Plot of the SCEX flight azimuth and the TAD release azimuths shown in a plane perpendicular to the magnetic field. Also shown are the regions where prompt responses during accelerator operations could be detected by the electron spectrometers mounted on the TAD's. The dots indicate the occurrences of acceleration events.

The original concept of the experiment was to detect delayed echoes, of which several hundred were found [Wilhelm et al., in press, 1984]. In Figure 5 we show that one of those observed in the 3.9-keV channel on TAD 2 originated from a 2 keV, 100 mA pulse (pulse no. 7-6-3) with a delay time of 340 ms. As two 8-keV pulses (7-4-9 and 7-5-9) preceding the 2-keV pulse and one 4-keV pulse (7-6-6) following it could also be identified, there is little doubt that the accelerated electrons have also been detected far from the injection point.

The total number of acceleration events observed was too small and the spectral resolution was too poor to allow a systematic study with a view to identifying the causes of the acceleration and the processes involved. For instance, it could not be determined whether the energetic electrons were a heated plasma population or accelerated beam particles. In Figure 6 we show, however, that the acceleration events occurred in the pitch angle range from 54° to 126°. The result is of importance as acceleration effects at high pitch angles have subsequently been observed on Spacelab 1, while no energetic flux could be found in directions parallel to the magnetic field [Wilhelm et al., 1984].

The important question is whether the indicated $E >> E_b$ fluxes were real or the consequence of possible spurious effects produced by the very intense low energy return fluxes associated with beam injection. Prior observations by Winckler [1980], Bernstein et al. [1982], and Duprat et al. [1983] showed that the return fluxes with $E < 1$ keV were typically in the range $10^7 - 10^9$ cm^{-2} s^{-1}sr^{-1}eV^{-1}, where the lower limit was observed on throwaway packages. To resolve this question, a spare flight unit was tested in the laboratory. The highest electron flux levels that could be produced in the test facility at 650 eV were of the order of 10^7 cm^{-2}s^{-1}. Bombardment of the instruments from all directions did not increase the count rate above the background rate of approximately 0.3 counts s^{-1}. When the electron beam was directed toward the aperture within the viewing cone of the instrument more than 10^7 e$^-$s^{-1} entered the inner part of the system but did not raise the rate above 1 count s^{-1}. Spurious effects in channel 8 with rates of more than 2 x 10^5 counts s^{-1} as observed during the events under discussion would thus require an electron bombardment of the instrument by at least 10^{12} cm^{-2} s^{-1}. Taking a flux level of 10^7 cm^{-2}s^{-1}sr^{-1}eV^{-1} below 1 keV as point of departure, we would, however, not expect more than 10^{10} to 10^{11} cm^{-2}s^{-1} during the flight. The striking difference of the pulse pattern observed in the various energy channels is another argument against spurious signals in response to suprathermal background electrons

Discussion

The data presented and the supporting laboratory measurements show that electrons with energies of at least two and probably four times the injection energy were observed during some strong

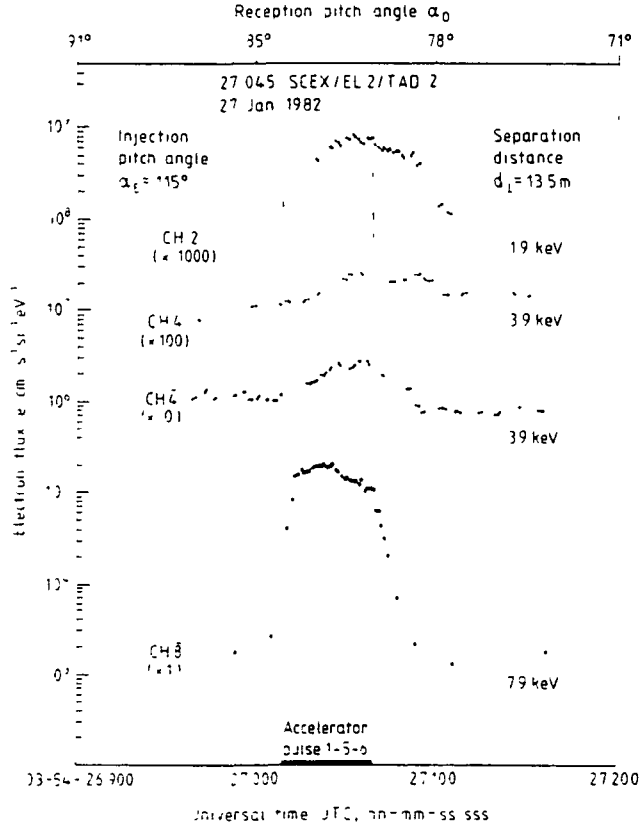

Fig. 2. TAD 2 observations during accelerator pulse no. 1-5-6 (4 keV, 100 mA) showing a pronounced effect in the 7.9-keV channel. All spectrometer channels had an energy resolution of approximately 14 % and were set at the energy levels indicated. The logarithmic flux intensity scale is valid for the lowest curve. The other curves are displaced for reasons of presentation.

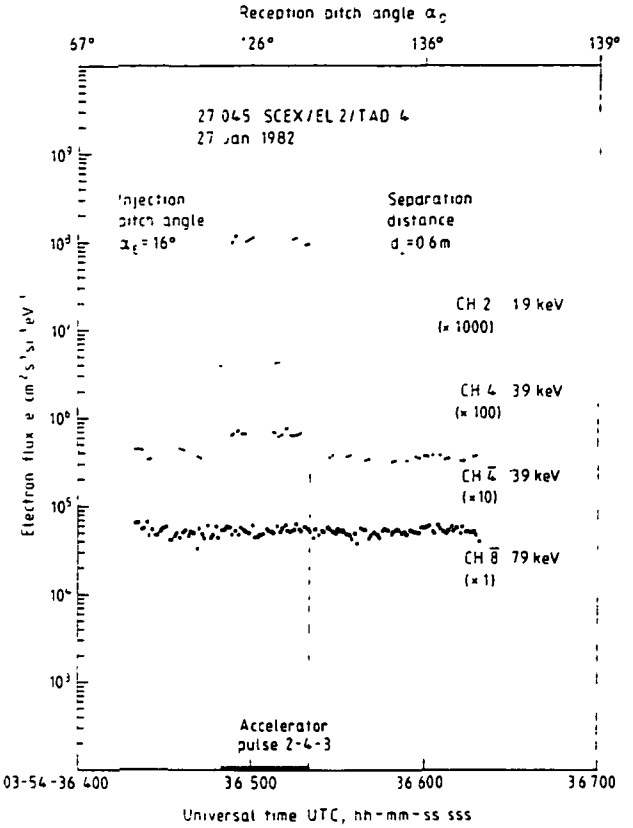

Fig. 3. TAD 4 measurements during accelerator pulse 2-4-3 (2 keV, 100 mA) at very close range from the main payload. A slight, however, statistically significant increase can be found in both 3.9-keV channels. The auroral background flux in channel $\bar{8}$ was very low before 03-54-29 UTC when it increased to the level shown here.

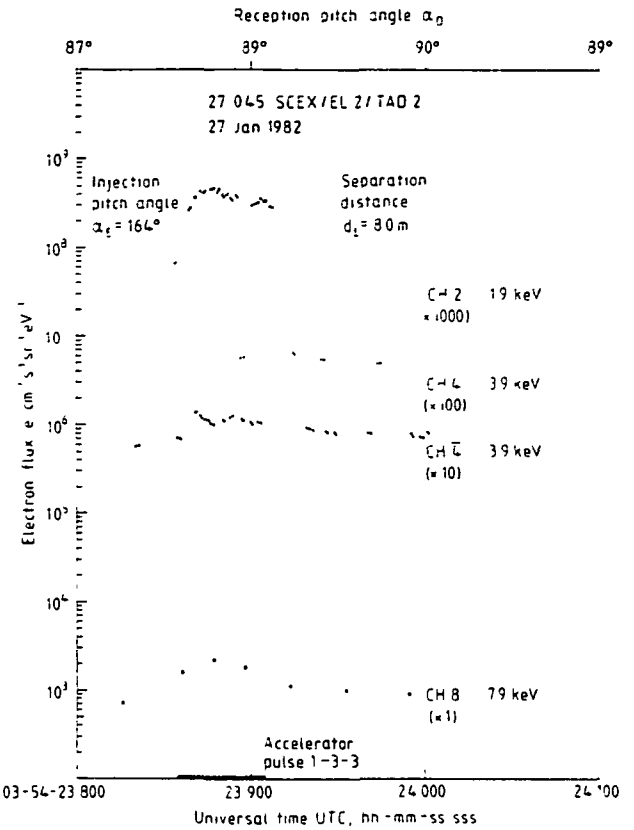

Fig. 4. Reactions of the 3.9- and 7.9-keV channels to a 2 keV, 100 mA pulse (1-3-3).

beam-plasma interaction events (prompt echoes occurring near the injection point); the presence of these particles was also observed in one delayed event. The energized electrons are detected at high pitch angles indicating the acceleration to be perpendicular to the magnetic field B.

In many respects, these observations are very similar to those reported by Smullin and Getty [1966] in their studies of the beam-plasma discharge. When the discharge was ignited in a mirror geometry (mirror ratio > 3), the injection of a monoenergetic 10-keV beam produced large fluxes of 50- to 100-keV X rays indicating the presence of an electron component with corresponding high energy. Such X-ray fluxes decreased with decreasing mirror ratio and were not detected in a solenoidal configuration. In more detailed studies of the electron distribution in a solenoidal beam-plasma discharge, Jost et al. [1980] and Anderson et al. [1982] reported the presence of electron fluxes with energy extending up to 1.3 E_b. These results suggest that the acceleration process must be stochastic and perpendicular to B; the mirror configuration provides sufficient confinement to allow the acceleration to occur.

It is of course valid to question the relevance of the laboratory experiments to the space observations for two reasons: (1) despite the many beam injection flights, the presence of a beam-plasma discharge has not yet been unambiguously identified above 200 km and (2) the magnetic field configuration in space is at best an open ended mirror so that rapid particle escape from an active region along the field lines will occur.

The application of the laboratory results to the flight data can, however, be justified The evolution of the beam particle energy distribution

Fig. 5. Delayed echoes observed in channel 4 of TAD 2 in response to accelerator operations. The separation of the detector from the accelerator was approximately 130 m perpendicular to the magnetic field during this interval.

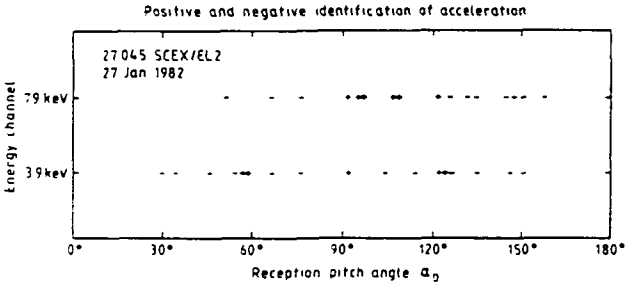

Fig. 6. Positive and negative identifications of electron acceleration on TAD 2 and TAD 4 have been plotted versus the reception pitch angle. The 3.9- and 7.9-keV channels are shown separately. The acceleration events seem to be concentrated at high pitch angles.

and local plasma wave spectrum have been measured as a function of increasing axial and radial distance from the electron accelerator in laboratory beam-plasma discharge experiments (X. Llobet, unpublished data, 1984). Jones et al. [1976] studied the convective and absolute beam-plasma interactions under conditions where the ambient plasma was produced by auxiliary means. In the latter case, the ambient neutral density was sufficiently low to preclude a discharge ignition. The great similarity in the two experimental results implies that the basic plasma physics is the same for the beam-plasma interaction and the discharge; the avalanche ionization characteristic of the discharge simply serves to modify the ambient plasma density conditions in a somewhat uncontrolled fashion. Almost every rocket flight has returned evidence for the beam-plasma interaction.

The available interaction length is the most critical difference between the space and laboratory configurations. If we make the assumption that the maximum length along the magnetic field is determined by the time the injection persists on a particular field line (up to 10 ms) and the longitudinal velocity of the electrons, we obtain a length between 50 and 130 km for a 2-keV injected beam, except for injections very near 0° and 90°. This length increases linearly with beam energy. An analogy to a mirror configuration can be made if it is further assumed that the entire region is active as had been proposed by Wilhelm et al. [in press, 1984]. Here the length of the active region provides the required confinement.

Possible acceleration mechanisms have been discussed in an enlightening interchange between Stix [1965] and Smullin [1965] but have not been definitively identified to date. However, the observation of superaccelerated electrons in flight experiments represents additional evidence for the occurrence of strong beam-plasma interactions when energetic electrons are injected into the ionospheric plasma.

Acknowledgments. The development of this payload was carried out by personnel from GSFC and General Electric Matsco. Major contributions were made by C. Campbell, J. Stephenson and J. Hananian. S.J. Monson of the University of Minnesota was responsible for co-ordination and integration of the various instruments. The contributions of C. Becker, R. Schmidt, E. Frank and H. Lindner of the MPAE are greatly appreciated. The project was financially supported by NASA, NRC and the German BMFT through DFVLR-PT grant 0 OM 030-ZA/WF/WRK 275/3-1.2. W. B. was supported by the NASA grant NAGW-69.

References

Anderson, H.R., R.J. Jost, and J.G. Gordeuk, Electron energy distribution produced by beam-plasma discharge, in Artificial Particle Beams in Space Plasma Studies, edited by B. Grandal, pp. 351-359, Plenum, New York, 1982.

Bernstein, W., P.J. Kellogg, S.J. Monson, R.H. Holzworth, and B.A. Whalen, Recent observations of beam plasma interactions in the ionosphere and a comparison with laboratory studies of the beam plasma discharge, in Artificial Particle Beams in Space Plasma Studies, edited by B. Grandal, pp. 35-64, Plenum, New York, 1982.

Duprat, G.R.J., A.G. McNamara, and B.A. Whalen, Charged particle measurements from a rocket-borne electron accelerator experiment, in Artificial Particle Beams in Space Plasma Studies, edited by B. Grandal, pp. 65-73, Plenum, New York, 1982.

Jones, R., W. Carr, and M. Seidl, Transition from particle trapping to a quasi-linear beam-plasma system, Phys. Fluids, 19, 548-553, 1976.

Jost, R.J., H.R. Anderson, and J.O. McGarity, Electron energy distributions measured during electron beam/plasma interactions, Geophys. Res. Lett., 7, 509-512, 1980.

Smullin, L.D., Comments on 'Energetic electrons from a beam plasma overstability', Phys. Fluids, 8, 1412-1415, 1965.

Smullin, L.D., and W.D. Getty, Characteristics of the beam plasma discharge, Proc. International Conf. Plasma Physics and Controlled Nuclear Fusion, 2, 815, 1966.

Stix, T.H., Reply to comments by L.D. Smullin, Phys. Fluids, 8, 1415-1416, 1965.

Wilhelm, K., W. Bernstein, P.J. Kellogg, and B.A. Whalen, Fast magnetospheric echoes of energetic electron beams, J. Geophys. Res., in press, 1984.

Wilhelm, K., W. Studemann, and W. Riedler, Electron flux intensity distributions observed in response to particle beam emissions from Spacelab 1, Science, 225, 186-188, 1984.

Winckler, J.R., The application of artificial electron beams to magnetospheric research, Rev. Geophys. Space Phys., 18, 659-682, 1980.

W. Bernstein, Department of Space Physics and Astronomy, Wiess School of Natural Sciences, Rice University, Houston, TX 77001.

P.J. Kellogg, School of Physics and Astronomy, University of Minnesota, Minneapolis, MN 55455.

B.A. Whalen, Herzberg Institute of Astrophysics, National Research Council of Canada, Ottawa, Ontario, Canada.

K. Wilhelm, Max-Planck-Institut fur Aeronomie, D-3411 Katlenburg-Lindau, Federal Republic of Germany.

(Received September 10, 1984;
revised October 18, 1984;
accepted October 19, 1984.)

Section V - (Non-Refereed Publications)

Bernstein, W., "Laboratory simulation of the injection of energetic electron beams into the ionosphere-ignition of the beam plasma discharge," in Relation Between Laboratory and Space Plasmas, ed. by H. Kikuchi, pp. 45-60, D. Reidel and Company, Dordrecht, Holland, 1981.

Bernstein, W. and P. J. Kellogg, "Laboratory simulation of the injection of energetic electron beams into the ionosphere - ignition of the beam plasma discharge," in Adv. Space Res., 1, 347-360, COSPAR, 1981.

Konradi, A., W. Bernstein and X. Llobet, "Linear and nonlinear effects in the beam plasma discharge," presented at Conference on Beam-Plasma Interactions in Space Eastsound, WA, Aug. 12-16, 184 and EOS, 65, 1054, 1984.

Papers in Artificial Particle Beams in Space Plasma Studies

Edited by B. Grandal, Plenum Press, New York, 1982

Bernstein, W., P. J. Kellogg, S. J. Monson, R. H. Holzworth, and B. A. Whalen, "Observations of beam-plasma interactions in the ionosphere and a comparison with laboratory studies of the beam plasma discharge, pp. 35-64.

Kellogg, P. J., H. R. Anderson, W. Bernstein, T. J. Hallinan, R. H. Holzworth, R. J. Jost, H. Leinbach and E. P. Suszczewicz, "Laboratory simulation of injection of particle beam in the ionosphere," pp. 289-330.

Hallinan, T. J., H. Leinbach and W. Bernstein, "Visible signatures of the multi-step transition to a beam plasma discharge," pp. 351-360.

Jost, R. J., H. R. Anderson, W. Bernstein and P. J. Kellogg, "Radial dependence of the HF wave field strength in the BPD column, pp. 431-438.

Papers in Active Experiments in Space

Edited by W. R. Burke, ESA Sp-195, European Space Agency, Paris 1983

Bernstein, W., G. Mantjoukis, H. Leinbach and T. J. Hallinan, "Optical measurements of a large-scale laboratory BPD," pp. 177-180.

Konradi, A., W. Bernstein, D. L. Bulgher, J. O. McGarity and J. L. Winkler, Jr., "Initial experimental results from a laboratory size beam plasma discharge device," pp. 185-188.

Wilhelm, K., W. Bernstein, P. J. Kellogg, and B. A. Whalen, "Fast magnetospheric echoes of energetic electron beams," pp. 113-119.

Section VI (Ph.D. and M.S. Theses)

*X. Llobet, "A Model of the Beam Plasma Discharge," Ph.D. Thesis, Dept. of Space Physics and Astronomy, Rice University, May, 1984.

X. Llobet, "The Beam-Plasma Discharge Revisited (A New Theoretical Model), M.S. Thesis, Dept. of Space Physics and Astonomy, Rice University, May 1, 1982.

G. A. Mantjoukis, "Optical Emission Measurements during Beam Plasma Interactions," M.S. Thesis, Dept. of Space Physics and Astronomy, Rice University, Aug., 1984.

R. Mesli, "RF Wave Observation in the Beam Plasma Discharge," M.S. Thesis, Dept. of Space Physics and Astronomy, Rice University, May, 1982.

*This thesis was selected as the outstanding thesis in the Physical Sciences by the Rice University-Texas Medical Center Chapter of Sigma Xi for the academic year 1983-84.

Abstract

A Model of the Beam-Plasma Discharge

by

Xavier Llobet

The beam-plasma instability is one of the most basic and general situations in plasma physics. Under suitable conditions, it gives rise to strong electrostatic waves, which interact with the plasma electrons and ions. If the neutral density is high enough, a charge is ignited, the Beam-Plasma Discharge. In this thesis, the onset of the strong beam-plasma instability is studied, and scaling laws of the discharge ignition are obtained for different configurations. The mechanism responsible for the discharge, i.e., the energization of plasma electrons by the plasma waves, is also studied. The model proposed here is consistent with the experimental data, is free from the contradictions present in other models, and explains the observed discharge signatures (wave, light and particle characteristics). The agreement with the experimental scalling law is remarkably good.

OPTICAL EMISSION MEASUREMENTS DURING BEAM PLASMA INTERACTIONS

by

George Mantjoukis

ABSTRACT

3914 Å (N_2^+: $B^2\Sigma_u^+ \rightarrow X^2\Sigma_g^+$) light intensity profiles were measured with a geometrically scanning photometer during interactions of an energetic electron beam with a weakly ionized plasma. Mass spectrometric measurements indicated N_2 to be the dominant neutral constituent. The experiments were carried in the very large SESL vacuum facility at the Johnson Space Center which allowed an interaction length of ~ 20 m. Variable current (1-70 ma) and variable energy (500-1600 V) beams were injected over a large pitch angle range (0 to ~ 75°) for several applied magnetic field strengths (0.89, 1.52, and 2.22 Gauss) over the pressure range (0.6-3.0 x 10^{-5} Torr) to allow study of the light intensity dependence on the experiment parameters. The photometer measurements were made at a fixed axial position (~ midway between the electron gun and the collector); overall measurements of the complete beam emission patterns (total light) were made with several low light level TV cameras. The measured 3914 Å intensity profile gives the radial distribution of the ionization rate while its integral gives the total ionization rate independent of geometry.

The following important results were obtained

1) At low beam currents ($I_b < I_c$, the beam current required for BPD ignition) the relative light intensity and beam geometric configuration were consistent with single particle behavior.

2) At $I_b = I_c$ (ignition) the total relative ionization rates were reasonably consistent with the theoretical predictions of the critical density model of Rowland et al.

3) For $I_b > I_c$ (BPD) the geometry of the illuminated region changes drastically and the 3914 Å total intensity increases by factors of 10-20 indicating the presence of new ionization sources (suprathermal electrons).

(a) For beam injection parallel to the magnetic field (zero pitch angle), the radial width (FWHM) of the illuminated region is ~ twice the maximum (anti-node) width for pre-BPD conditions; it scales approximately as $1/B$ and $E^{1/2}$.

(b) For non-zero pitch angle injection, the full width of the illuminated region is ~ equal to the diameter of the single particle helix; at large pitch angle injection, the BPD shows significant limb brightening indicating a somewhat hollow configuration. Significant ionization outside the helical dimensions is not observed.

(c) For all conditions the total 3914 Å light intensity during BPD can be fitted to the parabolic relationship

$$Q_T \sim K\, I_c^{1/2}\, (I_b - I_c)^{1/2}$$

Thus the total ionization rate increases nonlinearly with I_b and

remains proportional to the square root of the threshold current during BPD although $I_b >> I_c$. The consistency of this scaling over the large injection pitch angle range implies that the important plasma processes are independent of injection pitch angle.

(d) The maximum efficiency of energy transfer from the beam to the plasma (as measured by the total ionization rate) occurs when $I_b = 2\ I_c$. Typical estimates of this maximum efficiency range from 3-12% for the 20 meter path length.

ABSTRACT

RF Wave Observations in Beam-Plasma Discharge

The Beam Plasma Discharge (BPD) has been produced in the large vacuum chamber at Johnson Space Center (20 × 30 m) using an energetic electron beam of moderately high perveance ($K \sim 1.4 \times 10^{-6}$ A $V^{-3/2}$).

A more complete expression of the threshold current I_c taking into account the pitch angle injection dependence is given.

Ambient plasma density inferred from wave measurements under various beam conditions are reported. It is observed that the maximum frequency of the excited RF band behaves differently than the frequency of the peak amplitude. The latter shows signs of parabolic saturation consistent with the light data. It is found that the beam plasma state (pre-BPD or BPD) does not affect the pitch angle dependence.

Unexpected strong modulation of the RF spectrum at half odd integer of the electron cyclotron frequency $(n + 1/2)f_{ce}$ is reported ($5 < n < 10$). Another new feature, the presence of wave emission around $3/2\ f_{ce}$ for $I_b = I_c$ is reported.